

**University of Alberta**

Functional Magnetic Resonance Imaging of Schizophrenia

by

David Paul McAllindon



A thesis submitted to the Faculty of Graduate Studies and Research  
in partial fulfillment of the requirements for the degree of

Master of Science

Department of Biomedical Engineering

Edmonton, Alberta

Fall 2008



Library and  
Archives Canada

Bibliothèque et  
Archives Canada

Published Heritage  
Branch

Direction du  
Patrimoine de l'édition

395 Wellington Street  
Ottawa ON K1A 0N4  
Canada

395, rue Wellington  
Ottawa ON K1A 0N4  
Canada

*Your file* *Votre référence*

*ISBN: 978-0-494-47304-7*

*Our file* *Notre référence*

*ISBN: 978-0-494-47304-7*

**NOTICE:**

The author has granted a non-exclusive license allowing Library and Archives Canada to reproduce, publish, archive, preserve, conserve, communicate to the public by telecommunication or on the Internet, loan, distribute and sell theses worldwide, for commercial or non-commercial purposes, in microform, paper, electronic and/or any other formats.

The author retains copyright ownership and moral rights in this thesis. Neither the thesis nor substantial extracts from it may be printed or otherwise reproduced without the author's permission.

**AVIS:**

L'auteur a accordé une licence non exclusive permettant à la Bibliothèque et Archives Canada de reproduire, publier, archiver, sauvegarder, conserver, transmettre au public par télécommunication ou par l'Internet, prêter, distribuer et vendre des thèses partout dans le monde, à des fins commerciales ou autres, sur support microforme, papier, électronique et/ou autres formats.

L'auteur conserve la propriété du droit d'auteur et des droits moraux qui protègent cette thèse. Ni la thèse ni des extraits substantiels de celle-ci ne doivent être imprimés ou autrement reproduits sans son autorisation.

---

In compliance with the Canadian Privacy Act some supporting forms may have been removed from this thesis.

Conformément à la loi canadienne sur la protection de la vie privée, quelques formulaires secondaires ont été enlevés de cette thèse.

While these forms may be included in the document page count, their removal does not represent any loss of content from the thesis.

Bien que ces formulaires aient inclus dans la pagination, il n'y aura aucun contenu manquant.

■+■  
**Canada**

## **Dedication**

I dedicate this thesis to Yordanos, Mom and Dad. Thanks Yordanos for putting up with me during my studies and being willing to live frugally. Thanks Mom and Dad for all your support and encouragement through the years, including well past the age when you shouldn't have to worry about me.

## **Abstract**

Functional magnetic resonance imaging is a form of magnetic resonance imaging that has rapidly become a standard tool in cognitive neuroscience and psychiatry. In this thesis, fMRI is applied to schizophrenia. After preliminary discussions of schizophrenia, MRI and fMRI, an fMRI study of schizophrenia is described. 15 people with chronic schizophrenia were compared with 25 healthy volunteers and 11 first-degree relatives during performance of a visual 2-choice reaction time task using block and event-related paradigms. People with chronic schizophrenia were found to have activation deficits in bilateral putamen, thalamus, R cingulate gyrus and R insula compared to healthy volunteers. First-degree relatives were found to have greater activation than healthy volunteers in R medial frontal gyrus, L cingulate gyrus, R inferior parietal lobule, R precuneus and R inferior temporal gyrus. Finding greater activity in first-degree relatives compared to lower activity in people with schizophrenia is unexpected and deserves further study.

## **Acknowledgements**

Back in 2003 when I was still pondering my next stage, I had contacted Dr. Alan Wilman about graduate studies using fMRI and he was enthusiastic in offering me an opportunity. Although I didn't take it at that time, when I returned from my adventure in Ethiopia I went back to ask him again. Although he didn't have funding himself, he was generous in finding another professor with funding and interest. My thanks go to Alan and to Dr. Philip Tibbo for giving me a chance.

# Table of Contents

Chapter 1 Introduction .....	1
Chapter 2 Schizophrenia .....	2
2.1 Description .....	2
2.1.1 Etiology and Epidemiology .....	2
2.1.2 Symptoms and Signs .....	6
2.1.2.1 Positive Symptoms .....	7
2.1.2.2 Negative Symptoms .....	8
2.1.2.3 Differential Diagnosis .....	8
2.1.3 Pharmacotherapy .....	9
2.2 Cognitive and Neurophysiological Testing .....	10
2.2.1 Cognitive Tests .....	10
2.2.2 Neurophysiological Tests .....	12
2.2.3 Functional Magnetic Resonance Imaging in Schizophrenia .....	13
2.3 Summary .....	17
References: .....	18
Chapter 3 Magnetic Resonance Imaging .....	25
3.1 Magnetic Resonance Imaging .....	25
3.1.1 Imaging Stages .....	25
3.1.2 Spatial Encoding .....	26
3.1.3 K space .....	32
3.1.4 Imaging Parameters .....	33
3.2 Echo Planar Imaging .....	34

3.2.1 Echo Planar Imaging Sequence.....	35
3.2.2 Echo Planar Imaging Artifacts.....	36
3.2.3 Echo Planar Imaging in Practice.....	41
3.2.4 Variations in Echo Planar Imaging .....	43
References:.....	45
Chapter 4 Functional MRI .....	47
4.1 BOLD contrast mechanism.....	47
4.1.1 Measuring Blood Oxygen Changes with MRI.....	48
4.1.2 Physiological Changes .....	54
4.1.3 Hemodynamic Response.....	58
4.2 Design of fMRI Experiments.....	61
4.2.1 Paradigms.....	61
4.2.2 Block Design.....	63
4.2.3 Event-Related.....	64
4.2.4 Comparison of Designs.....	65
4.3 Analysis of fMRI Experiments .....	69
4.3.1 Noise .....	69
4.3.2 Pre-Processing.....	70
4.3.3 Conventional Statistical Analysis .....	73
4.3.4 Event-Related Analysis Options .....	75
4.3.5 Other Analysis Options.....	75
References:.....	77

## Chapter 5: Investigation of Functional and Structural Abnormalities in the Anterior

Cingulate Cortex in Recent-Onset and Chronic Schizophrenia.....	85
5.1 Background/Motivation .....	85
5.1.1 Reaction Time in Schizophrenia.....	85
5.1.2 Neuroimaging Studies of Reaction Time.....	87
5.1.3 Heritability of Reaction Time .....	91
5.1.4 Structural Abnormalities.....	92
5.1.5 Models of Reaction Time.....	92
5.2 Objectives and Hypotheses:.....	94
5.3 Research Procedures .....	94
5.3.1 Recruitment.....	94
5.3.2 Paradigm .....	98
5.4 Method of Data Analysis .....	102
5.4.1 Behavioural Data.....	102
5.4.2 fMRI Data .....	103
5.5 Results.....	111
5.5.1 Demographic Data .....	111
5.5.2 Behavioural Data.....	112
5.5.3 Volumetric Data.....	114
5.5.4 Functional Data for Block Design .....	120
5.5.5 Functional Data for Event-Related Design.....	125
5.6 Discussion.....	130
5.6.1 Behavioural Results .....	130

5.6.2 Volumetric and VBM Results.....	131
5.6.3 Functional Results.....	132
5.6.4 Other Functional Results.....	135
References:.....	139
Chapter 6: Conclusions.....	147
6.1 Summary.....	147
6.1.1 Behavioural Results.....	147
6.1.2 Volumetric and VBM Results.....	147
6.1.3 Block Design Results.....	148
6.1.4 Event-Related Design Results.....	148
6.2 Limitations.....	149
6.2.1 Paradigm Design.....	149
6.2.2 Behavioural.....	149
6.2.3 Volumetric and VBM Study.....	150
6.2.4 Functional Results.....	151
6.2.5 Homogeneity of Groups.....	153
6.3 Future Directions.....	155
References:.....	157
APPENDIX A SUMMARY of fMRI PAPERS in SCHIZOPHRENIA.....	160
APPENDIX B DEVELOPMENT OF HTML VERSION OF THE SCID.....	166
APPENDIX C CHOICE vs SIMPLE PARADIGM RESULTS.....	168
APPENDIX D EVENT-RELATED ANALYSIS of FAST versus SLOW.....	171
APPENDIX E ANALYSIS of FLASHING CHECKERBOARD.....	173

## List of Tables

Table 2-1 Cognitive Tests Showing Greatest Ability to Detect Schizophrenia .....	11
Table 2-2 Effect Sizes of Neurophysiological Tests .....	12
Table 5-1 Demographic Data .....	112
Table 5-2 Behavioural Data Summary .....	112
Table 5-3 Correlation Coefficients .....	112
Table 5-4 Gray and White Matter Volumes in Litres .....	114
Table 5-5 Summary of VBM Results - Gray Matter .....	115
Table 5-6 Summary of VBM Results - White Matter .....	117
Table 5-7 Correlation With RT Analysis Results .....	123
Table 5-8 ACC ROI Analysis Summary .....	123
Table 5-9 HV2 > CH Group Comparison Results .....	123
Table 5-10 CH > HV2 Group Comparison Results .....	124
Table 5-11 FR > HV1 Group Comparison Results .....	124
Table 5-12 FR > CH Group Comparison Results .....	124
Table 5-13 HV2 > CH Event-Related Group Comparison Results .....	128
Table 5-14 CH > HV2 Event-Related Group Comparison Results .....	128
Table 5-15 FR > HV1 Event-Related Group Comparison Results .....	128
Table 5-16 HV1 > FR Event-Related Group Comparison Results .....	128
Table 5-17 HV1 > HV2 Event-Related Group Comparison Results .....	129
Table 6-1 Median Versus Average Group RTs .....	150

## List of Figures

Figure 2-1. Neurodevelopmental Model of Schizophrenia .....	4
Figure 2-2. Interaction Between Glutamate, GABA and Dopamine Neurotransmitters ...	6
Figure 2-3. Profile of Cognitive Deficit in Schizophrenia Versus Other Disorders .....	10
Figure 2-4. Cluster analysis of 15 peak activation areas during working memory tasks. Above: simple storage, Below: executive functions .....	14
Figure 2-5. Relation of dorsolateral prefrontal cortex (DLPFC) activation to working memory load (squares show measured activation, asterisks are unmeasured) .....	15
Figure 3-1. Encoding Spatial Information in Frequency Using a Linear Magnetic Field Gradient .....	27
Figure 3-2. Slice Selection .....	28
Figure 3-3. Practical rf Pulse and Slice Profile .....	29
Figure 3-4. Frequency and Phase Encode Steps .....	30
Figure 3-5. Example Sequence .....	31
Figure 3-6. K-Space View of Basic Sequence .....	33
Figure 3-7. Comparison of k-space Traversal for Gradient Echo and Echo Planar Imaging Sequence .....	35
Figure 3-8. Idealized Echo planar imaging pulse sequence .....	36
Figure 3-9. Variation in Signal Over Acquisition Time .....	38
Figure 3-10. Effect of Gradient Ramps on K-Space Sampling .....	38
Figure 3-11. Example of Ghosting .....	39
Figure 3-12. Example of Distortion in an EPI Image a) EPI image of phantom with good shimming, b), c), d) EPI images with a variety of mis-set shims .....	40
Figure 3-13. Variation in BOLD contrast with TE for different values of T2* .....	41
Figure 3-14. Optimizing TR and Flip Angle .....	42

Figure 4-1. Diffusion of an Extravascular Water Molecule Near Vein and Capillary .....	50
Figure 4-2. Relative Contributions of Extravascular space, Intravascular Capillaries and Intravascular Veins to fMRI signal for Gradient Echo at 1.5T. ....	51
Figure 4-3. Reduction in BOLD signal change as Diffusion-Weighting is Increased .....	52
Figure 4-4. Variation of change in R2* (GE) and change in R2 (SE) as a function of vessel radius for spin echo (SE) and gradient echo (GE) sequences for Extravascular spins .....	52
Figure 4-5. Components of the BOLD fMRI Signal .....	54
Figure 4-6. Cartoon of the Vascular System Showing Delivery of Oxygen and Glucose ..	55
Figure 4-7. Vascular System Model .....	56
Figure 4-8. Hemodynamic response function to brief stimulus and sustained stimulus ...	58
Figure 4-9. Hemodynamic responses in motor cortex for a button press every 16 s: a-b) responses from different subjects, c-d) responses from same subject on different days, e-f) responses of same subject on same day .....	59
Figure 4-10. Dynamic changes in BOLD and its components With Long Stimulus .....	60
Figure 4-11. Sample Block Design Time Course .....	63
Figure 4-12. Comparison of fMRI Experimental Designs .....	66
Figure 4-13. Frequency domain comparison of fMRI Designs .....	67
Figure 4-14. Effects of baseline and number of on-off blocks .....	68
Figure 4-15. Noise Structure .....	70
Figure 4-16. Analysis Steps .....	71
Figure 4-17. Predicted Response Created from Convolution of Boxcar function with Hemodynamic Response and A Measured Response. Colors Show the Variation in Task. ....	74
Figure 5-1. Reaction Time as a Function of Preparatory Interval Showing Patients Who Improved (Solid Lines) and Who Did Not Improve (Dashed Lines) at Regular and Irregular Preparatory Interval. ....	86

Figure 5-2. Results from Naito et al, 2000, showing area correlated with reaction time for different stimulation modality. A auditory, B tactile, C visual .....	87
Figure 5-3. Results from Winterer et al, 2001, showing activation in ACC/SMA from event-related visual 2-choice reaction time task .....	88
Figure 5-4. Functional Subdivisions in Cingulate Cortex of Rhesus Monkey. CMA cingulate motor area, r rostral, v ventral, NCA nociceptive area, AAA attention to action area, VOA vocalization area, VMA visceromotor, VSA visuospatial. ....	88
Figure 5-5. ERP Grand Averages Comparing Healthy Volunteers (black) to individuals with schizophrenia (red). ....	89
Figure 5-6. LORETA Results from ERP Recordings Showing Reduction in Current Amplitude During Auditory Reaction Time Task. ....	89
Figure 5-7. Correlation Between Self-Rated Effort and A) Reaction Time B) ACC/SMA Activity. ....	91
Figure 5-8. Mathematical Models of Reaction Time .....	93
Figure 5-9. Components of fMRI Testing .....	98
Figure 5-10. The 3 Conditions of the Paradigms .....	99
Figure 5-11. Block Design Sequence .....	100
Figure 5-12. Event-Related Design Sequence .....	101
Figure 5-13. Comparison of Reaction Times Between Groups on Block (CRT) and Event-Related (er) Tasks .....	113
Figure 5-14. Gray and White Matter Volumes and Total Volume .....	114
Figure 5-15. VBM Results Gray Matter .....	119
Figure 5-16. VBM Results White Matter .....	120
Figure 5-17. Individual Functional Activation Map (BJ31) .....	121
Figure 5-18. Random Effects Analysis for Groups on Block Design CRT .....	122
Figure 5-19. Group Comparison Maps for Block Design .....	125
Figure 5-20. Individual Functional Activation Map (BJ31) .....	126

Figure 5-21. Right-Only and Left-Only Functional Contrast (BJ31) ..... 126

Figure 5-22. Random Effects Analysis Group Maps for Event-Related Design ..... 127

Figure 5-23. Group Comparisons Maps for Event-Related Design ..... 130

Figure 5-24. Comparison of HV1 RFX Group Maps a)Flashing Checkerboard b) Block Design ..... 136

Figure 5-25. Comparison of HV2 Group RFX Maps a) Choice-Only b) Choice>Watch ... 137

Figure 5-26. RFX Group Maps for Watch-Only Contrast ..... 138

## List of Symbols

$\phi$	phase angle
$\gamma$	gyromagnetic ratio
$\omega$	frequency
$\chi$	magnetic susceptibility
$\sigma$	chemical shift shielding constant
$\tau$	duration of the phase encode gradient
$\mathbf{B}$	magnetic field vector
$\mathbf{B}_0$	static (main) magnetic field
$\mathbf{B}_1$	radio-frequency magnetic field
$\mathbf{G}$	slope of linear gradient magnetic field
$\mathbf{k}$	k-space spatial frequency variable
$\mathbf{M}_0$	available net magnetization moment
$\mathbf{M}_{xy}$	transverse magnetization moment
$\mathbf{R}_2$	transverse relaxation rate
$\mathbf{R}_2^*$	apparent transverse relaxation rate
$t$	time
$T_1$	longitudinal (spin-lattice) relaxation time
$T_2$	transverse (spin-spin) relaxation time (irreversible)
$T_2'$	transverse relaxation time (reversible)
$T_2^*$	apparent transverse relaxation time

## List of Abbreviations

AC	anterior commissure
ACC	anterior cingulate cortex
ADP	adenosine diphosphate
AMPA	alpha-amino-3-hydroxy-5-methyl-4-isoxazolepropionic acid
ATP	adenosine triphosphate
BA	Brodman area
BOLD	blood oxygen level dependent
BVQX	Brain Voyager QX
BW	bandwidth
CBF	cerebral blood flow
CBV	cerebral blood volume
CH	group of people chronically-ill with schizophrenia
CMRO <sub>2</sub>	cerebral metabolic rate of oxygen consumption
CNR	contrast-to-noise ratio
CRT	choice reaction time
CSF	cerebrospinal fluid
DICOM	digital imaging and communications in medicine
DSM-IV	Diagnostic and Statistics Manual IV
erfMRI	event-related functional magnetic resonance imaging
EEG	electroencephalography
EPI	echo planar imaging
ERP	event-related potential

FDR	false detection rate
FFT	fast Fourier transform
fMRI	functional magnetic resonance imaging
FOV	field of view
FR	group of first-degree relatives of someone with schizophrenia
FT	Fourier transform
FWE	family-wise error
FWHM	full width half maximum
GLM	general linear model
HRF	hemodynamic response function
HV	group of healthy volunteers
ICBM	International Consortium for Brain Mapping
IFG	inferior frontal gyrus
ISI	interstimulus interval
ITG	inferior temporal gyrus
MFG	medial frontal gyrus
MIP	maximum intensity projection
MNI	Montreal Neurological Institute
MOG	middle occipital gyrus
MPRAGE	magnetization prepared rapid acquisition gradient echo
MRI	magnetic resonance imaging
MTG	medial temporal gyrus
NMDA	N-methyl-D-aspartic acid

NMR	nuclear magnetic resonance
PC	posterior commissure
PCP	phencyclidine
PET	positron emission tomography
PFC	prefrontal cortex
RFX	random effects analysis
ROI	region of interest
RT	reaction time
SFG	superior frontal gyrus
SNR	signal to noise ratio
SPECT	single photon emission computed tomography
SPM	statistical parametric map
STG	superior temporal gyrus
TE	echo time
TR	repetition time

## Chapter 1 Introduction

Magnetic resonance imaging (MRI) is a relatively new non-invasive imaging technique that has provided a fantastic tool for clinical use in diagnosis of cancers, injuries and disorders in soft tissue in the body. The applications for MRI continue to grow and one of the applications is functional magnetic resonance imaging (fMRI). fMRI is a method of detecting metabolic activity in the brain that is related to neuronal activity.

fMRI has taken over a niche in cognitive neuroscience and psychiatry once filled by positron emission tomography (PET) thanks to advantages such as: being able to be used repeatedly on subjects, higher spatial resolution and coregistration with structural images acquired in the same session. With its spatial resolution of about  $10 \text{ mm}^3$  and time resolution of approximately 20 seconds, it is complementary with other methods such as electroencephalography (EEG), which has millisecond time resolution but poor spatial resolution, and patch clamp and single cell recording which can only be used on animals.

One prime area of study with fMRI is in psychiatry. Disorders such as schizophrenia, depression and bipolar disorder, in which not much progress has been made in understanding using the reductionist techniques of the past, can now be investigated in living, awake patients.

This thesis details a study using fMRI to investigate a particular cognitive deficit in schizophrenia. Chapter 2 provides an overview of schizophrenia and discusses some functional activation studies of the disease. Chapter 3 discusses MRI and in particular, a widely used imaging sequence for fMRI, namely echo planar imaging (EPI).

Chapter 4 discusses several aspects of fMRI. It begins with a discussion of how the neuronal activity results in changes that can be measured by fMRI. There is much that is still unknown in how neuronal activity results in the metabolic changes measured by MRI, but that hasn't stopped fMRI from becoming widely used in cognitive neuroscience and psychiatry. Chapter 4 continues with discussion of the design of paradigms for fMRI and then discusses analysis of the data. This is another area that is evolving rapidly in fMRI with many new techniques being developed.

Chapter 5 is the heart of the thesis. It discusses the background for the study, shows the design of the paradigms, presents the results and discusses the results. Chapter 6 concludes with a summary of the results, discussion of limitations, and future directions.

## **Chapter 2 Schizophrenia**

Schizophrenia is the principal psychotic mental disorder as defined in the DSM-IV (Diagnostic and Statistics Manual of Mental Disorders, 4<sup>th</sup> edition). Schizophrenia has many symptoms that can vary greatly between sufferers, though common symptoms include delusions, hallucinations, thought disorder, avolition and blunt affect. The causes of schizophrenia are unknown and to date no unambiguous biological marker has been found (Heinrichs, 2001).

Schizophrenia brings major direct and indirect costs to its sufferers, their families and society at large as it often strikes people in early adulthood resulting in a significant loss of productivity and potential to society. Treatment for the disease is largely about control of symptoms, thus allowing the sufferers to live in society. However, most are unable to hold more than unskilled jobs, and, with large deficits in social skills, generally have poor relationships, all contributing to a low quality of life (Minzenburg, Yoon & Carter, 2008).

Schizophrenia also has many documented cognitive deficits (Keefe, 2001; Heinrichs & Zakzanis, 1998), which have been directly related to outcome measures such as being able to hold down a job or keep relationships (Green, 1996; Green, Kern, Braff & Mintz 2000). Over the last decade, neuroimaging has become an increasingly important way to probe these cognitive deficits. Neuroimaging methods, including electroencephalography (EEG), positron emission tomography (PET), single photon emission computed tomography (SPECT) and functional magnetic resonance imaging (fMRI), are tools for examining the living, dynamic processes behind cognition and are now widely used in the worlds of psychology, cognitive science, neurology and psychiatry.

There is thus great incentive to use neuroimaging techniques to learn about the cognitive effects of schizophrenia. fMRI applications in particular have mushroomed since about 2000. This chapter will discuss schizophrenia and briefly summarize results of neuroimaging applications to the study of this illness.

### **2.1 Description**

#### **2.1.1 Etiology and Epidemiology**

Schizophrenia has a lifetime prevalence of 0.5% to 1% (Andreasen & Black, 2001). It appears in men and women about equally, it occurs at about the same rate in all populations and ethnic groups, and appears to have been present in human populations throughout history (Jablensky, 2000). Schizophrenia typically strikes young adults, with the mean age of first psychotic episode at 21 years for men and 27 years for women

(Andreasen & Black, 2001, p.230). Nine out of 10 afflicted men have developed the illness by age 30 and 2 out of 3 afflicted women (Andreasen & Black, 2001, p.230). It is also possible, though rare, for children to exhibit the symptoms of schizophrenia. Early-Onset Schizophrenia is characterized as onset from age 13-16 years and Very Early Onset is characterized as before age 13 (Nicolson & Rapoport, 1999). Early-Onset and Very Early-Onset Schizophrenia occur more often in males, and sufferers usually have more severe symptoms and worse prognosis (Nicolson & Rapoport, 1999).

Genetic relatives of persons with schizophrenia have an increased risk of schizophrenia. This ranges from 48% risk for identical twins, 13% risk for children of someone with schizophrenia, and between 2% and 6% for second-degree relatives (Gottesmann, 1991). Despite this clear evidence of a genetic aspect to transmission of schizophrenia, the pattern does not indicate a single major gene carrier and many genes have been linked to schizophrenia (Harrison & Weinberger, 2005). The fact that even monozygotic twins have only a 50% concordance in schizophrenia suggests that environmental factors also play a role.

People with schizophrenia have an increased rate of suicide with approximately 10% dying from suicide (Andreasen & Black, 2001). Also, patients have an increased rate of comorbidity in both physical illness and other psychiatric illnesses, such as addictions and anxiety disorders (Sadock & Sadock, 2005).

Due to its onset in young adults, schizophrenia is a very disabling disease that has high costs for sufferers, their families and society at large. Costs to treat patients and the lost productivity (direct and indirect costs) were estimated at \$6.85 billion CA in Canada in 2004 (Goeree et al, 2005) and \$62.7 billion US in the United States in 2004 (Wu et al, 2005).

The course of schizophrenia varies as much as the symptoms (Jobe & Harrow, 2005). It may vary from a sharp initial stage with almost full recovery and no further episodes, to a gradual and consistent decline in functioning, to a wild swinging between near-normal and psychotic episodes. The course depends very much on the subject's compliance with drug treatment, but in one study, 40% of patients who were followed-up had experienced years of recovery (Jobe & Harrow, 2005).

It is commonly believed that there is (at least) a "two-hit" aspect to the disease. That is, genetic factors make a person vulnerable to the disease, but there may be another factor - such as an obstetric complication, a virus or life events - that result in expression of the disease. Some studies have tried to identify factors, such as prevalence of influenza in

birth month, obstetric complications, birth weight, early childhood diseases, but have not found anything specific to the illness (Sadock & Sadock, 2005).

The neurodevelopmental hypothesis is a hypothesis that attempts to use this “two-hit” aspect to explain the causes and course of schizophrenia. The neurodevelopmental hypothesis can be stated as follows:

Abnormal genetic and/or epigenetic events lead to disruption of early brain development. The resulting neuropathology, interacting with later events of brain development and/or another neuropathological process, causes expression of the symptoms of schizophrenia. (McClure & Weinberger, 2001, p. 28)

A nice summary of the neurodevelopmental theory is shown in Figure 2-1 (Cornblatt, 2001, p. 390). There is an existing genetic risk, likely affecting various processes of brain development. As well, there is some early damage that interacts with the genetic risk to potentially produce schizophrenia later.

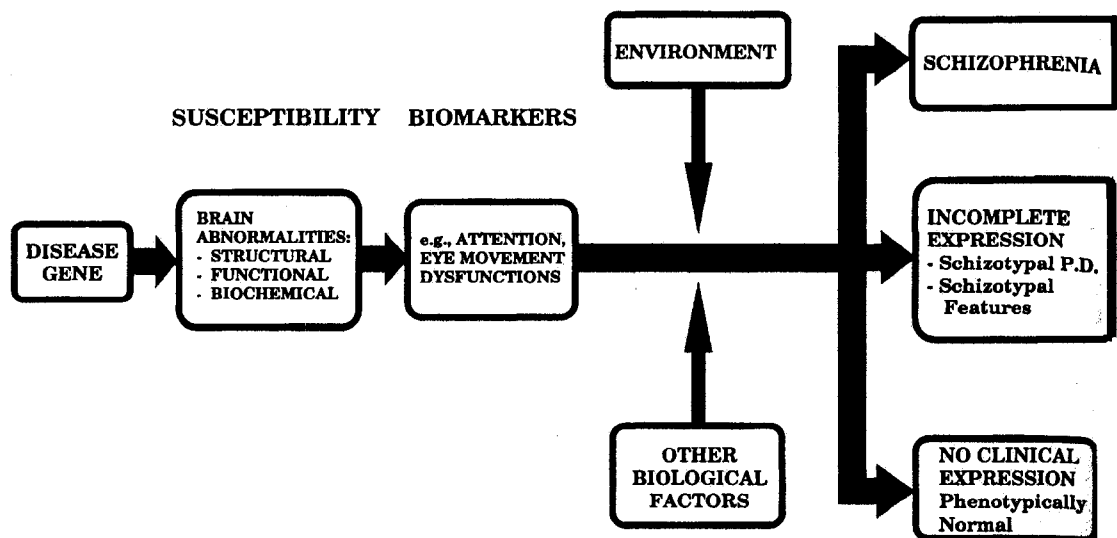


Figure 2-1. Neurodevelopmental Model of Schizophrenia

The neurodevelopmental hypothesis can be contrasted with the neurodegenerative hypothesis, which posits neuron death as the neuropathological process. Evidence for neurodegenerative processes would include longitudinal changes, which have generally not been found in schizophrenia, and evidence of cell death, which also has not been found (Haroutunian & Davis, 2001).

Since the neurodevelopmental theory predicts early damage to brain systems, it would expect some signs and symptoms of that brain damage before the outbreak of

schizophrenia. Reports of motor dysfunction in early childhood in those who later go on to develop schizophrenia (Fish, 1987), and poorer motor coordination, intellectual deficits, and differences in temperament of young adolescents (McClure & Weinberger, 2001) are consistent with this prediction. Further discussion of this issue will appear in section 2.2.1.

The neurodevelopmental hypothesis is rather vague and untestable at this time. Active research programs are seeking to find specific abnormalities and genes. One of the research methods being used is the identification of endophenotypes for schizophrenia. An endophenotype is a quantifiable, measurable characteristic that is linked to schizophrenia and genetics (Braff, 2007). Endophenotypes can help in the search for schizophrenia genes by providing more homogeneous populations for genetic studies.

There are also theories that schizophrenia may not be a single disease (Heinrichs, 2004) and that the range of symptoms and course may be the result of different diseases. Schizophrenia symptoms have been classified in many ways, but have not led to any notable successes in identifying genes. A group from Western Australia has reported on a distinct subtype they are able to identify with neurobehavioural, personality and cognitive tests that they call “cognitively deficient” (Hallmayer et al, 2005).

Some specific brain abnormalities/developmental mechanisms have been proposed. A prime one is the dopamine hypothesis which describes how psychotic symptoms may be induced. The theory is that an excess of dopamine in the mesolimbic pathway stimulates psychotic symptoms (Basile et al, 2001). Supporting evidence comes from different sources (Seeman & Kapur, 2001):

- 1) All antipsychotic drugs block dopamine D2 receptors
- 2) Dopamine D2 receptors are consistently occupied by 60% to 80% by therapeutic doses of antipsychotics, as measured by PET and SPECT in human striatum
- 3) Dopamine D2 receptor density is elevated in schizophrenia patients
- 4) Dopamine D1 receptors, which influence the D2 receptors, are markedly reduced or missing in psychotic patients
- 5) Levels of dopamine in psychotic patients are altered in the extracellular synaptic space
- 6) Dopamine agonists (amphetamine) can induce psychotic symptoms (Carlsson, 2001)

Although this evidence points toward dopamine as a final pathway of psychosis, they are less convincing that dopamine is the primary abnormality in the disorder. Firstly, the data show lots of scatter, so there is not a clear separation between findings in

schizophrenic patients and normal controls. Secondly, the data were found in patients that are stressed by amphetamine and the imaging procedure. Thirdly, the studies were of acute episode patients. (Carlsson, 2001)

There are many interconnections between dopamine and other neurotransmitter systems, as shown by the psychotogenic effect of drugs targeting other neurotransmitters. The prime example is the drug phencyclidine (PCP) which acts as an antagonist on the N-methyl-D-aspartic acid (NMDA) glutamate receptor (Carlsson, 2001).

Glutamatergic and GABAergic neurons are ubiquitous in the brain. These neurotransmitters interact highly with dopamine, being often arranged in complementary braking and accelerating systems (Carlsson, 2001). (See Figure 2-2) Failure of the braking system could lead to enhanced mesolimbic dopamine release and consequent psychotic symptoms.

### Cortical Glutamate/GABA-Mediated Steering of Subcortical Systems

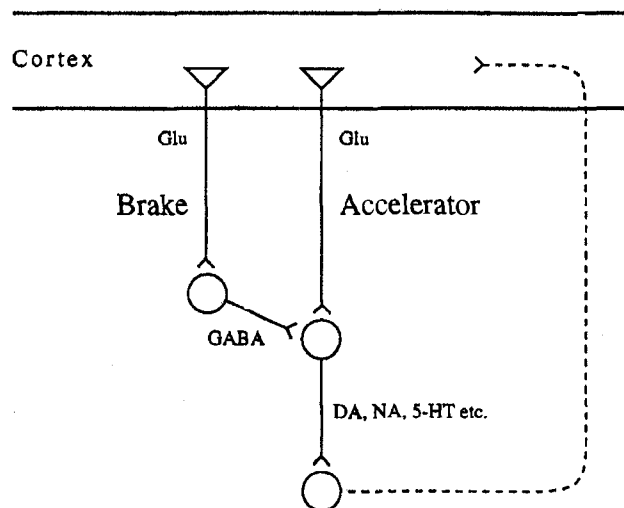


Figure 2-2. Interaction Between Glutamate, GABA and Dopamine Neurotransmitters

### 2.1.2 Symptoms and Signs

Symptoms have been classified in many ways though are now most commonly divided into negative and positive symptoms (Crow, 1980; Andreasen, 1982) or into reality distortion, psychomotor poverty and disorganized syndromes (Liddle, 1989). Positive symptoms are those that are extra to normal function or increased over normal function whereas negative symptoms are deficits of normal function or decreases in normal functioning. Liddle's proposal is from factor analytic studies of symptoms and differs from the positive/negative division mostly by taking some symptoms classified as positive or negative and putting them into a new category of disorganized symptoms.

The DSM-IV uses the positive/negative classification, so the symptoms will be discussed from the positive/negative categorization.

### **2.1.2.1 Positive Symptoms**

Positive symptoms include delusions, hallucinations, thought disorder and disordered behaviours.

Delusions are firmly-held false beliefs and are the most common symptom in schizophrenia, occurring in 90% of cases (Cutting, 2003). Paranoia is a common category of delusions – believing the CIA or FBI is after them, taken by aliens, being watched or talked about by others being common themes. Other categories of delusions are self-reference, persecutory, grandiose, somatic and guilt. A fundamental aspect of delusions is that they are firmly held despite evidence to the contrary; or however far they diverge from normal beliefs of the sufferers' community.

Hallucinations are sensory experiences of things that do not exist. Auditory hallucinations are the most common, occurring in about 50% of patients (Cutting, 2003). Patients often hear voices talking about them, saying negative things. Patients may interpret these voices in ways that depend on, or contribute to, their delusional systems so that a voice may be interpreted as thought broadcasts from people around them, aliens, devils or angels, or even God. Visual, somatic and tactile hallucinations are also found whereas gustatory and olfactory hallucinations are rare (Cutting, 2003).

Thought disorders include disorders of spoken language and may be classified as positive or negative symptoms. Disturbance of thinking includes concrete thinking, overinclusion, illogicality and loosening of associations. Disordered language and speech includes derailment, incoherence, neologisms and poverty of speech or content. Thought disorders are common in schizophrenia, occurring in over 50% of people with schizophrenia (Cutting, 2003).

Disordered behaviour includes catatonia, disorganized behaviour and disorganized affect. Catatonia are involuntary movements of a more complex type than tics, chorea or dyskinesias. Disorganized behaviour can run from odd or careless dress to extreme agitation, shouting or public sexual behaviour. Disorganized affect is expressing of emotions that are clearly at odds with the content of speech. These symptoms are not very common in schizophrenia, estimated as occurring in only 5 to 10% of people with schizophrenia (Cutting, 2003).

### **2.1.2.2 Negative Symptoms**

Negative symptoms, as categorized by Andreasen (1982) include avolition, attentional impairment, anhedonia, alogia and affective flattening. Avolition is a pervasive loss of initiative to begin and persist in goal-directed behaviours and is sometimes called apathy or lack of will. Attentional impairment is an inability to concentrate or possibly an inability to process stimuli leading to a confusion of thoughts. Anhedonia is a loss of pleasure in activities that were previously enjoyed. Depending on the comparison population, from 30% to 45% of people with chronic schizophrenia have anhedonia (Cutting, 2003). Most of this is accounted for by social anhedonia as opposed to physical anhedonia and it may be more present in chronic cases rather than acute. Alogia is an impoverishment in thinking that is shown by lack of speaking or poverty of content. Affective flattening is a lack of emotional expressiveness in body and/or voice and has been observed in about 50% of acute and chronic cases (Cutting, 2003).

### **2.1.2.3 Differential Diagnosis**

Within the DSM-IV grouping of psychotic disorders, there are several disorders that are distinct from schizophrenia yet have to be considered in differential diagnosis. These include schizo-affective disorder, schizophreniform disorder, brief psychotic disorder, delusional disorder and psychotic disorder not otherwise specified (DSM-IV).

Schizo-affective disorder is diagnosed when symptoms of psychosis have occurred outside mood episodes, but mood symptoms are prominent. (Mood episodes include major depressive episode, manic episode and mixed episode.) This is distinct from psychotic mood episode in which psychosis has occurred only within a major depressive episode. Interestingly, there are some studies that suggest schizo-affective disorder has distinct biological effects, and even a different cause, than schizophrenia (Mathalon, Hoffman, Roach, Watson & Ford, 2008).

If there is an existing psychosis that hasn't yet lasted for more than 6 months, schizophreniform disorder is diagnosed, which can be changed to schizophrenia or schizo-affective disorder if symptoms continue longer than 6 months. A psychotic episode that remits within 1 month leaving no other symptoms is diagnosed as brief psychotic disorder. If there are non-bizarre delusions with no mood episodes and no large impact on functioning, delusional disorder can be diagnosed. Psychotic disorder not otherwise specified is a catch-all category if the patient does not fit into any of the existing categories.

Schizophrenia may be mistaken for other mental disorders depending on the symptoms, especially bipolar disorder and major depressive disorder. As there are some overlapping symptoms between schizophrenia and bipolar disorder and the courses can be similar, it

can be difficult to differentiate bipolar disorder from schizophrenia. Similarly, patients with schizophrenia who have mainly negative symptoms can resemble depression. When psychotic symptoms have only occurred during mood episodes, a psychotic mood disorder is diagnosed (DSM-IV).

### **2.1.3 Pharmacotherapy**

Treatment of schizophrenia is usually by antipsychotic medication, which may be supplemented by antidepressant, anxiolytic or other medication to counter side-effects. The clinical effect of antipsychotic drugs is to relieve positive symptoms.

The first antipsychotic medications, called typical antipsychotics, all achieve efficacy by blocking D2 receptors, but their use can result in extrapyramidal symptoms (movement disorders) and even permanent tardive dyskinesia with long-term use (Basile et al, 2001). Typical antipsychotics usually have no effect on negative symptoms and could even make them worse as a result of side-effects (Minzenburg, Yoon & Carter, 2008). The exact method of action of typical antipsychotics is in doubt because the long period between administration of drugs and clinical effect suggests that it is adaptation to the D2 receptor blockade that is leading to the clinical effect (Rosenbaum, Arana, Hyman, Labbate & Fava, 2005).

The next generation of antipsychotics are called atypical antipsychotics. Their method of action is in doubt because they do not block D2 receptors to the same level as typical antipsychotics and yet their efficacy is as great against positive symptoms (Minzenburg, Yoon & Carter, 2008). Two leading theories of their mechanisms are:

- 1) that in blocking serotonergic receptors, they influence dopamine transmission in prefrontal and subcortical areas,
- 2) that they do not bind tightly to D2 receptors (“fast-off”) and can be displaced, though they block enough to cause clinical effects.

They require lower doses than the typical antipsychotics and do not readily cause extrapyramidal symptoms (Rosenbaum, Arana, Hyman, Labbate & Fava, 2005). Atypical antipsychotics are generally as effective as typical antipsychotics on positive symptoms (Rosenbaum, Arana, Hyman, Labbate & Fava, 2005) and are somewhat helpful with negative symptoms (Minzenburg, Yoon & Carter, 2008). Atypical antipsychotics also produce small improvements in cognitive deficits (Harvey & Keefe, 2001; Woodward, Purdon, Meltzer & Zald, 2005).

Individuals respond very differently to the medications. Unfortunately, some individuals become treatment refractory – no treatments work very well for them. Clozapine is a

drug that has been shown to have very good efficacy, but it comes with a potentially fatal side-effect called agranulocytosis so that it is generally prescribed only as a last resort when other drugs have failed (Rosenbaum, Arana, Hyman, Labbate & Fava, 2005).

Current drug treatments are not satisfactory, and research continues to develop new antipsychotic medication.

## 2.2 Cognitive and Neurophysiological Testing

There are many cognitive and neurophysiological tests that have been studied in schizophrenia. This section will review some of the cognitive testing that has been performed in schizophrenia with neuroimaging.

### 2.2.1 Cognitive Tests

People with schizophrenia have been found to score very low on some cognitive domains – lower than their IQ would predict (Keefe, 2001). The domains where schizophrenic patients have the largest deficit include verbal memory, executive functioning, vigilance, motor speed, and verbal fluency (Keefe, 2001). Figure 2-3 shows a profile of cognitive testing results for schizophrenia versus other common mental disorders.

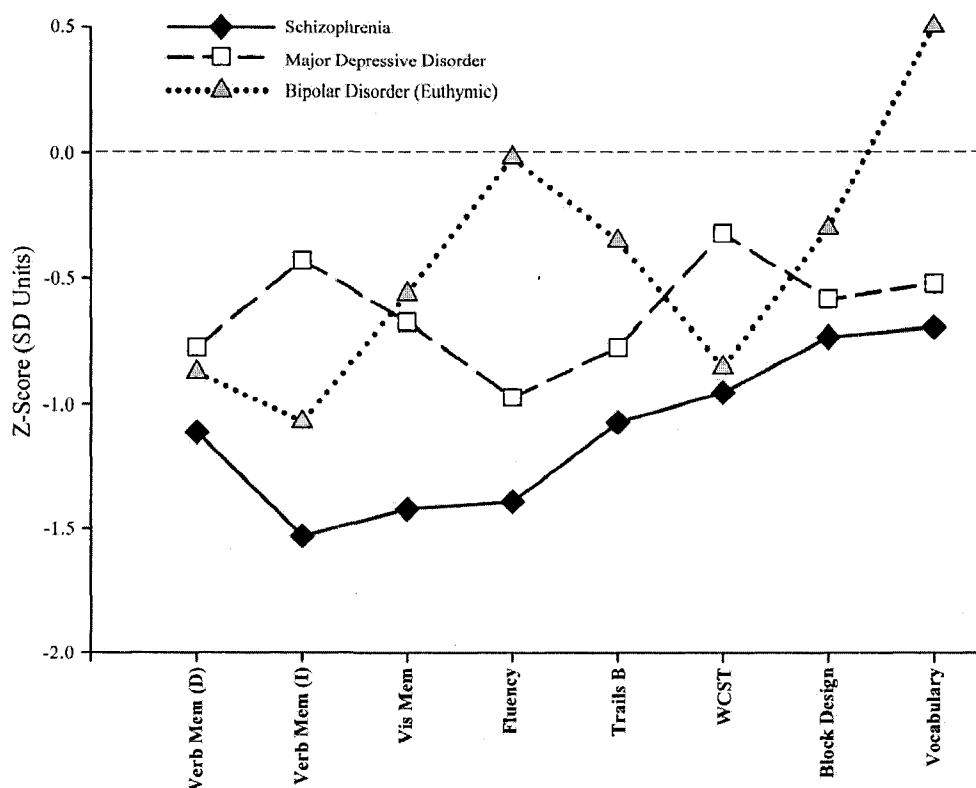


Figure 2-3. Profile of Cognitive Deficit in Schizophrenia Versus Other Disorders (Buchanan et al, 2005)

There has been a lot of interest in cognitive testing recently because of evidence that cognitive performance is linked strongly with functional outcomes (Green, 1996; Green, Kern, Braff & Mintz, 2000). Also, these tests might be usable as markers and predictors of schizophrenia.

Cornblatt and Erlenmeyer-Kimling have been researching cognitive tests as predictors of schizophrenia since the 1970s, largely focused on the continuous performance test (CPT). The optimal predictor was found to be CPT at age 12 with 78.2% accuracy (Cornblatt et al, 1999). Combined with behavioural assessments over early adolescence, the accuracy could be increased to 89.0%.

Table 2-1 displays cognitive tests or domains that are commonly used to identify cognitive deficits in schizophrenia along with their Cohen's *d*, which a measure of the ability of the test to detect a person with schizophrenia out of the normal population. A higher Cohen's *d* signifies an increased separation of the cognitive test scores distribution of the 2 groups. The list is not exhaustive for cognitive tests.

Table 2-1. Cognitive Tests Showing Greatest Ability to Detect Schizophrenia (Heinrichs, 2001)

<i>Cognitive Test</i>	<i>Mean d</i>	<i>N (studies)</i>
General Verbal Memory	1.41	31
Backward Masking	1.27	18
Dichotic Listening	1.16	11
IQ	1.10	35
Word Fluency	1.09	27
Tower problem-solving	1.05	4
Continuous Performance Test	1.04	29
Token Language Comprehension Test	0.98	7
Stroop Effect	0.97	9
Wisconsin Card Sorting Test	0.88	43
Digit span	0.69	29

Cognitive testing can also provide a quantitative and unbiased way to adjudicate drug testing. As a result, an initiative was started to define a standard battery of cognitive testing (MATRICS). First, a set of cognitive domains showing deficits in people with

schizophrenia was chosen and then specific tests in each domain were evaluated to come up with a standard set of tests in each area (Green et al, 2004).

### 2.2.2 Neurophysiological Tests

Neurophysiological tests are at a lower level of processing than the cognitive tests but higher than simple reflexes and they involve central nervous system processing. Neurophysiological testing requires physical measurement such as EEG, eye tracking, EKG, EMG or electrodermal conductance. Table 2-2 presents several common neurophysiological tests with their Cohen's *d* or effect size, which shows that neurophysiological tests are some of the most efficient ways to separate schizophrenia from the rest of the population.

Table 2-2. Effect Sizes of Neurophysiological Tests (Heinrichs, 2001)

<i>Test</i>	<i>Mean d</i>	<i>N</i>
P50 Gating Evoked Potential	1.55	20
Eye Tracking Saccadic Frequency	1.03	14
P300 Evoked Potential Waveform Reduced Amplitude	0.80	56
Eye Tracking Root Mean Squared	0.75	16
P300 Increased Latency	0.70	49

The P50 gating evoked potential is an early (about 50ms post-stimulus) positive deflection of the EEG in response to a stimuli, typically clicks. When a second stimuli is given about 500 ms after the first, the amplitude of the P50 is normally decreased. This reduction in amplitude is not as great in people with schizophrenia.

Eye tracking tests are interesting as they have shown fairly large differences in people with schizophrenia. There are 2 main forms – saccades and anti-saccades, and smooth pursuit eye tracking. Saccadic movements are like jumps, where the eyes move suddenly to another point of focus. Anti-saccades are movements in the opposite direction of a cue and people with schizophrenia have more mistakes on such tests. Smooth pursuit eye movement is tracking a slowly moving object. People with schizophrenia have more trouble tracking without saccadic eye movements. (Kelly & Nuechterlein, 2001)

The P300 is another event-related potential (ERP) component related to sensory processing. Tests use the oddball paradigm, in which occasional different stimuli occur in a train of similar stimuli (Kelly & Nuechterlein, 2001). A reduction of amplitude of the P300 has been observed in people with schizophrenia as well as a prolonged latency (delayed occurrence) of the P300 (Kelly & Nuechterlein, 2001).

Other common measures include startle reflex inhibition, measured by electromyography (EMG), and changes in skin conductance (Kelly & Nuechterlein, 2001). These tests use similar paradigms as the P50 and P300 (paired clicks or oddball detection) and show similar results as those tests in people with schizophrenia.

While neurophysiological tests are important in the understanding of cognition in schizophrenia, the development of fMRI has expanded this field of study.

### **2.2.3 Functional Magnetic Resonance Imaging in Schizophrenia**

Researchers have used fMRI with both cognitive and neurophysiological tests to investigate differences in performance in the brains of people with schizophrenia. This section will present some examples of the studies and results using fMRI to investigate schizophrenia. It is not a comprehensive review but instead touches on important and replicated studies.

Working memory is one of the most-studied cognitive domains in schizophrenia. The most common tasks used to examine working memory are N-back and item recognition (both of which are on the MATRICS test battery). In an N-back test, a subject would be asked to identify a shape, letter, digit, or tone in a display or sequence that was last shown N times back. The task is made more difficult by increasing the N, and performance and activation at N-back can be compared to performance and activation at 0-back. The base state of 0-back includes all the same basic motor movements and decision-making, so it can isolate memory quite well. The stimulus can be visual or auditory. See Walter et al (2003) and Thermenos et al (2005) for examples of studies.

A typical task in an item recognition experiment might be to give a subject a list of digits, let's say 2, 5, 6. Then individual digits would be presented, such as 7, and the subject would have to identify if the digit is one from their initial list. In the rest state, the subject presses the identification button for a digit so that the motor portion can be removed from the activations. Again, the stimulus can be visual or auditory. Examples of studies using this model are Manoach et al (1999) and Callicott et al (2000).

Wager and Smith (Wager & Smith, 2003) produced a meta-analysis of working memory including both PET and fMRI studies. This meta-analysis involved healthy volunteers only. Figure 2-4 shows that many regions of the brain are activated for working memory, but the main finding in schizophrenia involves the dorsolateral prefrontal cortex (DLPFC) (areas 12 and 15 in the following figure) (Wager & Smith, 2003).

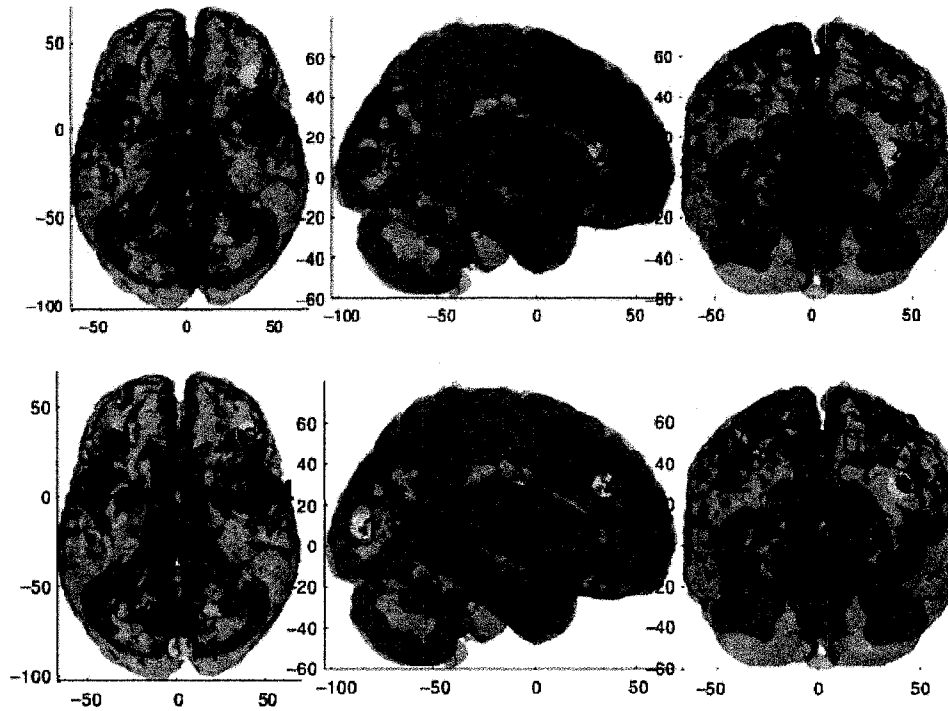


Figure 2-4. Cluster analysis of 15 peak activation areas during working memory tasks. Above: simple storage, Below: executive functions (Wager & Smith, 2003, p.263 and 267).

Earlier PET studies and initial fMRI studies of people with schizophrenia showed hypofrontality (eg. Weinberger et al, 1986; Andreasen et al, 1992). That is, the patients showed less activation of prefrontal cortex. There were some contradictory results, however, and Callicott et al (1999) found that healthy volunteers' activation of the dorsolateral prefrontal cortex is actually U-shaped, with activation rising until a capacity limit is reached, and then dropping as the capacity limit is exceeded (Callicott et al, 1999). A study by Manoach et al (1999) was able to show that the same U-shaped model for DLPFC activation applied to people with schizophrenia, but that the curve was shifted to lower capacity limits for them (Figure 2-5) (Manoach et al, 1999). Manoach (2003) argues that the earlier results showing hypofrontality occurred because the tasks were too difficult for patients and they had exceeded their capacity. Unfortunately, why patients need to put more effort into remembering (increased activation of DLPFC for same memory load) is still in question (Manoach, 2003).

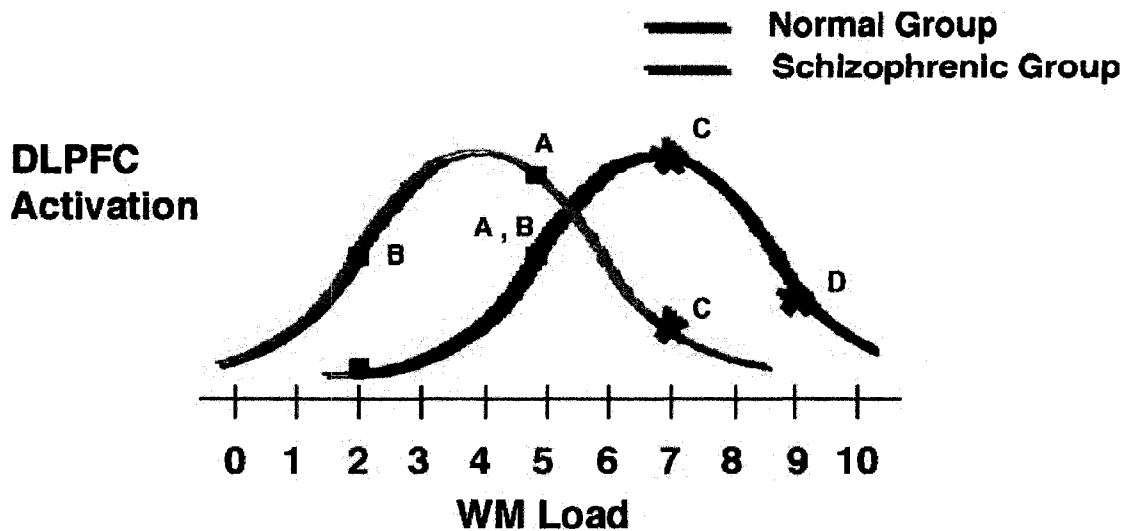


Figure 2-5. Relation of dorsolateral prefrontal cortex (DLPFC) activation to working memory load (squares show measured activation, asterisks are unmeasured) (Manoach, 2003, p. 290)

There are some interesting papers looking at activations due to different stages of working memory (encoding, maintenance and retrieval). A study that concentrates on the encoding process by Cairo, Woodward and Ngan (2006) describes tests using a range of difficulties to show equivalent performance by patients at lower load levels accompanied by increased activation during those lower loads. As difficulty increased, performance began to decline in the people with schizophrenia whereas activation started to increase in the healthy volunteers. Another of their papers suggests the retrieval activity for people with schizophrenia is not load dependent (Cairo, Liddle, Woodward & Ngan, 2004). They suggest that since encoding uses subprocesses in attention and perception and these subprocesses may be present in many other tasks, the observed inefficiency in subprocesses can result in the wide spectrum of deficient cognitive factors in schizophrenia.

At the University of Alberta, a previous functional MRI study of schizophrenia examined procedural learning (Ledkova, Woodward, Harding, Tibbo & Purdon, 2006; Woodward, Tibbo & Purdon, 2007). Procedural learning is learning of movements or unconscious cognitive events. The study looked at procedural learning of a sequence of button pushes in a paradigm similar to another group (Reiss et al, 2006). Another study examining procedural learning used a different paradigm (Kumari et al, 2002). All the studies have found less activity in the basal ganglia in people with schizophrenia despite functional performance that was not significantly different from healthy volunteers.

Several studies using saccadic or smooth pursuit eye movements have been done. In saccadic motion tasks, Raemaekers et al (2001; 2005) and Matsuura et al (2004) found

decreased activation in the striatum during antisaccades in patients and siblings. McDowell et al (2001) found decreased activation during antisaccades compared to saccades in prefrontal cortex. All found that supplementary and frontal eye fields were not affected.

In smooth pursuit eye motion of eye tracking tasks, Lencer et al (2004) found a deficit in patients in the V5 area. Hong et al (2005) found decreased activation in frontal and supplementary eye fields, medial superior temporal cortex and anterior cingulate gyrus in patients but increased activity in medial occipitotemporal cortex for a task in which performance was matched between patients and healthy volunteer groups. Matsuura et al (2004) found reduced activity in fronto-parietal cortex in an attention-enhanced smooth pursuit task. Finally, Tanabe, Tregellas, Martin & Freedman (2006) found an effect of nicotine in smooth pursuit eye motion in which healthy volunteers had a decrease in activity in anterior cingulate gyrus whereas patients had increased activity when on nicotine, suggesting a self-medication effect for patients.

Once the techniques were developed for rapid event-related studies, studies of oddball paradigms became possible in fMRI. One of the earliest was by Kiehl & Liddle (2001). They found schizophrenia patients to have deficit responses in right lateral frontal cortex, thalamus, bilateral anterior superior temporal gyrus, anterior and posterior cingulate, right inferior and superior parietal lobules. Ngan et al (2003), in a study comparing oddball responses to speech or complex nonspeech sounds, found a greater difference in activation in patients in right temporal cortex, left superior frontal cortex and left temporal-parietal junction. Laurens, Kiehl, Ngan & Liddle (2005) found underactivity during novel stimulus processing in right amygdale-hippocampus, rostral anterior and posterior cingulate, right frontal operculum, at right temporo-parietal-occipital junction, bilateral intraparietal sulcus and bilateral dorsal frontal cortex. Kiehl et al (2005) found diffuse hypofunctioning in patients in bilateral frontal, temporal and parietal cortices, amygdala, thalamus and cerebellum.

Appendix A contains a summary of fMRI studies in schizophrenia grouped according to the cognitive or neurophysiological task and the type of subject groups. The summary includes papers published through 2006 but is not comprehensive. It makes a useful summary of the range of cognitive and neurophysiological tasks that have been used in fMRI studies of schizophrenia.

## **2.3 Summary**

Schizophrenia is a disease with large impacts on the sufferers, their families and society as a whole. Many of the most basic aspects of schizophrenia are still unknown, and the vast range of symptoms and course have been puzzling experts since the initial categorization of the disease. There is no biological marker, or series of biological markers for the disease.

Functional neuroimaging, including more recent techniques such as functional MRI, have shown promise in gaining a better understanding of how schizophrenia affects brain function. Following chapters will describe basics of MRI, functional MRI and a study using fMRI to look at a cognitive deficit in schizophrenia.

## References:

- American Psychiatric Association. (1994). *Diagnostic and statistical manual of mental disorders* (4<sup>th</sup> ed.). Washington, DC: American Psychiatric Publishing.
- Andreasen, N.C. & Olsen, S. (1982). Negative v positive schizophrenia. Definition and validation. *Archives of General Psychiatry*, 39, 780-794.
- Andreasen, N.C. & Black, D.W. (2001). Schizophrenia. In *Introductory Textbook of Psychiatry* (3rd ed.) (Chap. 7). Washington, DC: American Psychiatric Publishing.
- Basile, V.S, Masellis, M., Ozdemir, V., Meltzer, H., Macciardi, F.M. & Kennedy, J.L. (2001). Application of pharmacogenetics to schizophrenia: Merging insights. In A. Breier, P.V. Tran, J.M. Herrea, G.D. Tollefson, F.P. Bymaster (Eds.), *Current issues in the psychopharmacology of schizophrenia* (Chap. 6, pp. 85-110). Philadelphia: Lippincott Williams & Wilkins Healthcare.
- Braff, D.L., Freedman, R., Schork, N.J., & Gottesman, I.I. (2007). Deconstructing schizophrenia: An overview of the use of endophenotypes in order to understand a complex disorder, *Schizophrenia Bulletin*, 33(1), 21-32.
- Buchanan, R.W., Davis, M., Goff, D., Green, M.F., Keefe, R.S., Leon, A.C., Nuechterlein, K.H., Laughren, T., Levin, R., Stover, E., Fenton, W., & Marder, S.R. (2005) A summary of the FDA-NIMH-MATRICES workshop on clinical trial design for neurocognitive drugs in schizophrenia. *Schizophrenia Bulletin*, 31(1), 5-19.
- Cairo, T.A., Liddle, P.F., Woodward, T.S., & Ngan, E.T.C. (2004). The influence of working memory load on phase specific patterns of cortical activity. *Cognitive Brain Research*, 21, 3777-3787.
- Cairo, T.A., Woodward, T.S., & Ngan, E.T.C. (2006). Decreased encoding efficiency in schizophrenia. *Biological Psychiatry*, 59(8), 740-746.
- Callicott, J.H., Mattay, V.S., Bertolino, A., Finn, K., Coppola, R., Frank, J.A., et al (1999). Physiological characteristics of capacity in working memory as revealed by functional MRI. *Cerebral Cortex*, 9, 20-26.
- Callicott, J.H., Bertolino, A., Mattay, V.S., Langheim, F.J.P., Duyn, J., Coppola, R., et al (2000). Physiological dysfunction of the dorsolateral prefrontal cortex in schizophrenia revisited. *Cerebral Cortex*, 10, 1078-1092.

Carlsson, A. (2001). Neurotransmitters – Dopamine and beyond. In A. Breier, P.V. Tran, J.M. Herrea, G.D. Tollefson, F.P. Bymaster (Eds.), *Current issues in the psychopharmacology of schizophrenia* (Chap. 1, pp. 3-11). Philadelphia: Lippincott Williams & Wilkins Healthcare.

Cornblatt, B., Obuchowski, M., Roberts, S., Pollack, S., & Erlenmeyer-Kimling, L. (1999). Cognitive and behavioural precursors of schizophrenia. *Developmental Psychopathology*, 11, 487-508.

Crow, T.J. (1980). Molecular pathology of schizophrenia: More than one disease process? *British Medical Journal*, 280, 66-68.

Cutting, J. (2003) Descriptive psychopathology. In S.R. Hirsch & D.R. Weinberger (Eds.) *Schizophrenia*, 2<sup>nd</sup> ed. (Chapter 2, pp 15-24). Malden, Mass: Blackwell Science.

Fish, B. (1987). Infant predictors of the longitudinal course of schizophrenic development. *Schizophrenia Bulletin*, 13, 395-409.

Goeree, R., Farahati, F., Burke, N., Blackhouse, G., O'Reilly, D., Pyne, J., & Tarride, J-E. (2005). The economic burden of schizophrenia in Canada in 2004. *Current Medical Research and Opinion*, 21(12), 2017-2028.

Gottesmann, I.I. (1991). *Schizophrenia Genesis: The Origins of Madness*. New York: W.H. Freeman.

Green, M.F. (1996). What are the functional consequences of neurocognitive deficits in schizophrenia. *American Journal of Psychiatry*, 153(3), 321-330.

Green, M.F., Kern, R.S., Braff, D.L., Mintz, J. (2000). Neurocognitive deficits and functional outcome in schizophrenia: Are we measuring the “right stuff”? *Schizophrenia Bulletin*, 26, 119-136.

Green, M.G., Nuechterlein, K.H., Gold, J.M., Barch, D.M., Cohen, J., Essock, S., et al (2004). Approaching a consensus cognitive battery for clinical trials in schizophrenia: The NIMHS-MATRICES conference to select cognitive domains and test criteria. *Biological Psychiatry*, 56, 301-307.

Hallmayer, J.F., Kalaydjieva, L., Badcock, J., Dragovic, M., Howell, S., Michie, P. et al (2005). Genetic evidence for a distinct subtype of schizophrenia characterized by pervasive cognitive deficit. *American Journal of Human Genetics*, 77, 468-476.

Haroutunian, V. & Davis, K.L. (2001). Neuropathology of schizophrenia. In A. Breier, P.V. Tran, J.M. Herrea, G.D. Tollefson, F.P. Bymaster (Eds.), *Current issues in the psychopharmacology of schizophrenia* (Chap. 4, pp. 57-70). Philadelphia: Lippincott Williams & Wilkins Healthcare.

Harrison, P.J., & Weinberger, D.R. (2005). Schizophrenia genes, gene expression, and neuropathology: On the matter of their convergence. *Molecular Psychiatry*, 10, 40-68.

Harvey, P.D., & Keefe, R.S.E. (2001). Studies of cognitive change in patients with schizophrenia following novel antipsychotic treatment. *American Journal of Psychiatry*, 158:176-184.

Heinrichs, R.W. & Zakzanis, K.K. (1998). Neurocognitive deficit in schizophrenia: A quantitative review of the evidence. *Neuropsychology*, 12, 426-445.

Heinrichs, R.W. (2001). *In search of madness: Schizophrenia and neuroscience*. Cary: Oxford University Press, Inc.

Heinrichs, R.W. (2004). Meta-analysis and the science of schizophrenia: Variant evidence or evidence of variants? *Neuroscience and Biobehavioral Reviews*, 28, 379-394.

Honey, G.D. & Fletcher, P.C. (2006). Investigating principles of human brain function underlying working memory: What insights from schizophrenia? *Neuroscience*, 139(1), 59-71.

Hong, L.E., Tagamets, M., Avila, M., Wonodi, I., Holcomb, H., & Thaker, G.K. (2005). Specific motion processing pathway deficit during eye tracking in schizophrenia: A performance-matched functional magnetic resonance imaging study. *Biological Psychiatry*, 57, 726-732.

Jablensky, A. (2000) Epidemiology of schizophrenia: The global burden of disease and disability. *European Archives of Psychiatry and Clinical Neuroscience*, 250, 274-285.

Jeong, B.S. Kwon, J.S., Kim, S.Y., Lee, C., Youn, T., Moon, C-H. et al (2005). Functional imaging evidence of the relationship between recurrent psychotic episodes and neurodegenerative course. *Psychiatry Research: Neuroimaging*, 139,219-228.

Jobe, T.H. & Harrow, M. (2005). Long-term outcome of patients with schizophrenia: A review. *Canadian Journal of Psychiatry*, 50(14), 892-900.

Keefe, R.S.E. (2001). Neurocognition. In A. Breier, P.V. Tran, J.M. Herrea, G.D. Tollefson, F.P. Bymaster (Eds.), *Current issues in the psychopharmacology of schizophrenia* (Chap. 10, pp. 192-205). Philadelphia: Lippincott Williams & Wilkins Healthcare.

Kelly, K.A. & Nuechterlein, K.H. (2001). Neurophysiology and psychophysiology. In A. Breier, P.V. Tran, J.M. Herrea, G.D. Tollefson, F.P. Bymaster (Eds.), *Current issues in the psychopharmacology of schizophrenia* (Chap. 9, pp. 148-191). Philadelphia: Lippincott Williams & Wilkins Healthcare.

Kiehl, K. & Liddle, P.F. (2001). An event-related functional magnetic resonance imaging study of an auditory oddball task in schizophrenia. *Schizophrenia Research*, 28, 159-171.

Kiehl, K.A., Stevens, M.C., Celone, K., Kurtz, M. & Krystal, J.H. (2005). Abnormal hemodynamics in schizophrenia during an auditory oddball task. *Biological Psychiatry*, 57, 1029-1040.

Kumari, V., Gray, J.A., Honey, G.D., Soni, W., Bullmore, E.T., Williams, S.C.R. et al (2002). Procedural learning in schizophrenia: A functional magnetic resonance imaging investigation. *Schizophrenia Research*, 57, 97-107.

Laurens, K.R., Kiehl, K.A., Ngan, E.T.C. & Liddle, P.F. (2005). Attention orienting dysfunction during salient novel stimulus processing in schizophrenia. *Schizophrenia Research*, 75, 159-171.

Lencer, R., Nagel, M., Sprenger, A., Heide, W. & Binkofski, F. (2005). Reduced Neuronal Activity in the V5 complex underlies smooth-pursuit deficit in schizophrenia: Evidence from an fMRI study. *Neuroimage*, 24, 1256-1259.

Liddle, P.F., Barnes T.R., Morris, D. & Haque, S. (1989). Three syndromes in chronic schizophrenia review. *British Journal of Psychiatry*, Suppl 7, 119-122.

Manoach, D.S., Press, D.Z., Thangaraj, V., Searl, M.M., Goff, D.C., Halpern, E. et al (1999). Schizophrenic subjects activate dorsolateral prefrontal cortex during a working memory task, as measured by fMRI. *Biological Psychiatry*, 45, 1128-1137.

- Manoach, D.S. (2003). Prefrontal cortex dysfunction during working memory performance in schizophrenia: Reconciling discrepant findings. *Schizophrenia Research*, 60, 285-298.
- Mathalon, D.H., Hoffman, R., Roach, B., Watson, T.D. & Ford, J.M. (2008). Neurophysiological distinction between schizophrenia and schizoaffective disorder. *Biological Psychiatry*, 63, 7s, p 229S.
- Matsuura, M., Fukumoto, M., Matshushima, E., Matsuda, T., Ohkubo, T., Ohkubo, H. et al (2005). Functional MRI study on neural network dysfunction in schizophrenia and epileptic psychosis. *International Congress Series*, 1270, 311-314.
- Matza, L., Brewster, J., Revicki, D., Zhao, Y., Purdon, S.E. & Buchanan, R. (2006). Measuring changes in functional status among patients with schizophrenia: The link with cognitive impairment. *Schizophrenia Bulletin*, 32(4), 666-678.
- McClure, R.K. & Weinberger, D.R. (2001). The neurodevelopmental hypothesis of schizophrenia: A review of the evidence, In A. Breier, P.V. Tran, J.M. Herrea, G.D. Tollefson, F.P. Bymaster (Eds.), *Current issues in the psychopharmacology of schizophrenia* (Chap. 3, pp. 27-56). Philadelphia: Lippincott Williams & Wilkins Healthcare.
- McDowell, J.E., Brown, G.G., Paulus, M., Martinez, A., Stewart, S.E., Dubowitz, D.J et al (2001). Neural correlates of refixation saccades and antisaccades in normal and schizophrenia subjects. *Biological Psychiatry*, 51,216-223.
- Minzenburg, M.J., Yoon, J.H. & Carter, C.S. (2008) Schizophrenia. In R.E. Hales, S.C. Yudofsky, and G.O. Gabbard (Eds.) *The American Psychiatric Publishing Textbook of Psychiatry* (5<sup>th</sup> ed., Chap. 10) Washington, DC: American Psychiatric Publishing.
- Ngan , E.T.C., Vouloumanos, A., Cairo, T.A., Laurens, K.R., Bates, A.T., Anderson, C.M. et al (2005). Abnormal processing of speech during oddball target detection in schizophrenia. *Neuroimage*, 20, 889-897.
- Nicolson, R. & Rapoport, J.L. (1999). Childhood-onset schizophrenia: Rare but worth studying. *Biological Psychiatry*, 46, 1418-1428.
- Raemaekers, M., Jansma, J.M., Cahn, W., Van der Geest, J.N., Van der Linden, J.A., Kahn, R.S. et al (2001). Neuronal substrate of the saccadic inhibition deficit in schizophrenia investigated with 3D event-related fMRI. *Neuroimage*, 13, No 6, S1091.

- Raemaekers, M., Ramsey, N.F., Vink, M., van den Heuvel, M.P. & Kahn, R.S. (2005). Brain activation during antisaccades in unaffected relatives of schizophrenic patients. *Biological Psychiatry*,
- Reiss, J.P., Campbell, D.W., Leslie, W.D., Paulus, M.P., Ryner, L.N., Polimeni, J.O. et al (2006). Deficit in schizophrenia to recruit the striatum in implicit learning: A functional magnetic resonance imaging investigation. *Schizophrenia Research*, 87 (1-3), 127-137.
- Rosenbaum, J.F., Arana, G.W., Hyman, S.E., Labbate, L.A. & Fava, M. (2005). Drugs for the treatment of psychiatric disorders. in *Handbook of Psychiatric Drug Therapy* (5<sup>th</sup> ed.). Philadelphia: Lippincott Williams & Wilkins.
- Sadock, B.J., & Sadock, V.A. (2005). Schizophrenia and other psychotic disorders. In *Kaplan & Sadock's Comprehensive Textbook of Psychiatry* (8<sup>th</sup> ed., Chap. 12) Philadelphia : Lippincott Williams & Wilkin.
- Seeman, P. & Kapur, S. (2001). The dopamine receptor basis of psychosis. In A. Breier, P.V. Tran, J.M. Herrea, G.D. Tollefson, F.P. Bymaster (Eds.), *Current issues in the psychopharmacology of schizophrenia* (Chap. 5, pp. 73-84). Philadelphia: Lippincott Williams & Wilkins Healthcare.
- Silverstein, S.M., Schenkel, L.S., Valone, C. & Nuernberger, S.W. (1998). Cognitive deficits and psychiatric rehabilitation outcomes in schizophrenia. *Psychiatric Quarterly*, 69,169-191.
- Schlosser, R., Gesierich, T., Kaufmann, B., Vuvurevic, G., Hunsche, S., Gawehn, J., & Stoeter, P. (2003). Altered effective connectivity during working memory performance in schizophrenia: A study with fMRI and structural equation modeling. *Neuroimage*, 19, 751-763.
- Tanabe, J., Tregellas, J.R., Martin, L.F., Freedman, R. (2006). Effects of nicotine on hippocampal and cingulate activity during smooth pursuit eye movement in schizophrenia. *Biological Psychiatry*, 59(8), 754-761.
- Thermenos, H.W., Seidman, L.J., Breiter, H., Goldstein, J.M., Goodman, J.M., Poldrack, R.A., et al (2004). Functional magnetic resonance imaging during auditory verbal working memory in nonpsychotic relatives of persons with schizophrenia: A pilot study. *Biological Psychiatry*, 55, 490-500.

Thermenos, H.W., Goldstein, J.M., Buka, S.L., Poldrack, R.A., Koch, J.K., Tsuang, M.T. et al (2005). The effect of working memory performance on functional MRI in schizophrenia. *Schizophrenia Research* 74, 179-194.

Wager, T.D. & Smith, E.E. (2003). Neuroimaging studies of working memory: A meta-analysis. *Cognitive, Affective, & Behavioural Neuroscience*, 3, 255-274.

Walter, H., Wunderlich, A.P., Blankenhorn, M., Schafer, S., Tomczak, R., Spitzer, M. et al (2003) No hypofrontality, but absence of prefrontal lateralization comparing verbal and spatial working memory in schizophrenia. *Schizophrenia Research*, 61, 175-184.

Weinberger, D.R., Mattay, V., Callicott, J., Kotrla, K., Santha, A., Gelderen, P.V. et al (1996) fMRI applications in schizophrenia research. *Neuroimage*, 4, S118-S126.

Wu, E.Q., Birnbaum, H.G., Shi, L., Ball, D.E., Kessler, R.C., Moulis, M. et al (2005). The economic burden of schizophrenia in the United States in 2002. *Journal of Clinical Psychiatry*, 66(9), 1122-1129.

Woodward, N, Purdon SE, Meltzer HY, & Zald DH (2005). A meta-analysis of neuropsychological change to clozapine, olanzapine, quetiapine and risperidone in schizophrenia. *International Journal of Neuropsychopharmacology*, 8(3), 457-472.

Woodward, N.D., Tibbo, P.G. & Purdon SE (2007). An fMRI investigation of procedural learning in unaffected siblings of individuals with schizophrenia. *Schizophrenia Research*, 94, 306-316.

Zedkova, L., Woodward, N.D., Harding, I., Tibbo, P.G., & Purdon, S.E. (2006). Procedural learning in schizophrenia investigated with functional magnetic resonance imaging. *Schizophrenia Research*, 88, 198-207.

## Chapter 3 Magnetic Resonance Imaging

Functional magnetic resonance imaging (fMRI) is a subdomain of MRI, so it is not possible to describe fMRI without describing MRI. MRI will be described in this chapter. The basics of nuclear magnetic resonance (NMR) are assumed and the discussion of this chapter will describe the techniques used to make an image using the NMR phenomenon in the human body.

The chapter is divided into 2 sections. The first section will describe imaging basics and the second section will describe in detail a particular imaging sequence, echo-planar imaging (EPI), that is primarily used for fMRI.

### 3.1 Magnetic Resonance Imaging

MRI is based on the NMR phenomenon, which was first discovered in 1939 by Rabi. After Bloch and Purcell independently discovered NMR in liquids and solids (Bloch, Hansen & Packard, 1946; Purcell, Torrey & Pound, 1946), NMR became an important tool in examining chemical and biochemical properties of materials. Up until the first imaging demonstration by Lauterbur (1973), NMR was used with small, homogeneous samples where the signal was derived from the sample as a whole.

The medical applications of MRI were recognized after demonstration of a difference in T1 relaxation rate between cancerous and noncancerous tissue (Damadian, 1971; Weisman, Bennett, Maxwell, Woods & Burk, 1972). The drive was on to develop magnetic resonance imaging and the first whole-body scanner was built by Damadian, Minkoff and Goldsmith. Since those early days, the technology and applications have advanced exponentially until the range of applications today is far beyond the ideas of the initial developers. Technology has drastically improved the quality of images and lowered the time to create them. Although MRI has found many uses in medicine and in sciences such as neuroscience, it is a very expensive technology.

#### 3.1.1 Imaging Stages

A magnetic resonance image is obtained in 3 stages. The stages are preparation, excitation and acquisition.

In preparation, the sample is placed in a homogeneous magnetic field referred to as  $B_0$ .  $B_0$  serves to align the spins inside the sample in the direction of  $B_0$ , producing a magnetic moment referred to as  $M_0$ . The spin elements used in fMRI are hydrogen.

Excitation refers to perturbation of the spins to a non-equilibrium state. The alignment of the spins is disturbed by the transient production of a small magnetic field ( $B_1$ ) at right angles to  $B_0$ .  $B_1$  is produced by a coil driven by an oscillating electrical current that induces a magnetic field around the coil. The field interacts with the spins to tip the magnetic moment of the spins out of alignment with  $B_0$ , producing some component of transverse magnetization, i.e. at right angles to  $B_0$ . In order to perturb the spins, the field must be on resonance with the precession frequency of the spins. The precession frequency is given by the Larmor equation (3-1) and depends on the spin elements and the magnetic field they are exposed to. The frequencies are in the radio-frequency (rf) bands.

$$\omega = \gamma B \quad (3-1)$$

where,  $\omega$  = precession frequency (in rad/s),  $\gamma$  = gyromagnetic constant, a property of an element (in rad/sT or equivalent unit), and  $B$  = magnetic field vector (in T or equivalent unit)

The final stage is acquisition.  $B_1$  is turned off and transverse magnetization is detected by induction of an electrical current in a receiver coil, also at right angles to  $B_0$ . The receiver coil may be the same as the transmission coil (used in the excitation stage).

After  $B_1$  is turned off, the spins return to their equilibrium state with a time constant that depends on the environment of the spins, a process called relaxation. Various tissues have characteristic relaxation rates. There are 2 relaxation rates, referred to as T1 and T2. T1 relaxation is a return of the magnetic moments to their equilibrium state whereas T2 relaxation is a result of dephasing of the spins. Dephasing results from the spins precessing at slightly different rates. That is, when all spins are moving together at the same frequency, they induce a signal in the receiver coil. However, if the spins are moving at slightly different frequencies, they will gradually get out-of-phase with each other, and the net signal is reduced. The main application of MRI, detecting cancers, comes about because of a large change in T1 and T2 in cancerous tissues (Damadian, 1971; Weisman, Bennett, Maxwell, Woods & Burk, 1972).

### **3.1.2 Spatial Encoding**

For imaging the problem is to acquire a signal from small volumes in the sample and to be able to locate from where in the sample the signal is received. MRI encodes spatial location in the precession frequency and phase of spin elements by application of linear magnetic field gradients.

#### **3.1.2.1 Frequency Encoding**

The concept of frequency encoding is illustrated in Figure 3-1, where 3 objects are shown at different locations along a linear magnetic field gradient. Note that the direction of the

magnetic field gradient is in the same direction as the main magnetic field  $B_0$ . Since the precession frequency is given by the Larmor equation (3-1), we can see that the frequency is directly related to the magnetic field experienced by an object. The net magnetic field that an object sees is then given by equation 3-2 for a linear magnetic field gradient, where a linear field gradient can be expressed by a slope,  $G_r$ .

$$B = B_0 + rG_r \quad (3-2)$$

where,  $G_r$  = magnitude of the gradient (slope) (in T/m or equivalent units)  
 $r$  = position of the object (in m or equivalent spatial units)

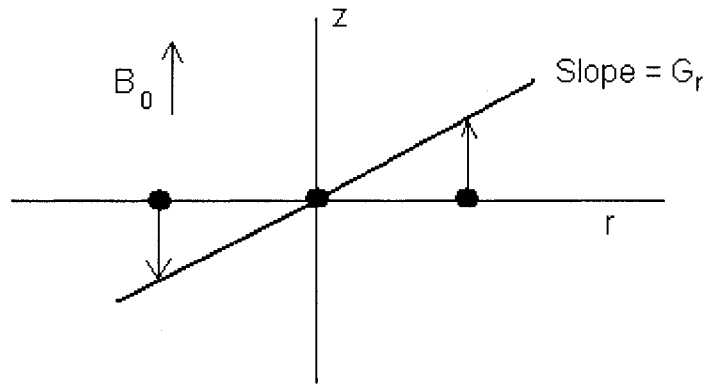


Figure 3-1. Encoding Spatial Information in Frequency Using a Linear Magnetic Field Gradient

Consider a magnetic field gradient ( $G_r$ ) that is small relative to  $B_0$ . The object in the middle position sees no change in the magnetic field, so it precesses at the Larmor frequency ( $\omega_L$ ). The object on the left sees an increased magnetic field, so it will precess at a slightly higher frequency ( $\omega_L + \delta\omega$ ). The object on the right sees a decreased magnetic field, so it will precess at a slightly lower frequency ( $\omega_L - \delta\omega$ ).

### 3.1.2.2 Slice Selection

The frequency encoding idea above is most clearly shown in slice selection. Slice selection is the selective excitation of a thin slice from a volume to reduce a 3-dimensional problem to 2 dimensions. The complete volume can then be imaged by adding up the 2D images of slices over the volume.

Slice selection requires the application of a linear magnetic field gradient during the rf excitation. A slice centered at any position along the gradient can be selected by choosing the appropriate center frequency ( $\omega_0$ ) for the rf excitation pulse.

In addition to the position of the center of the slice ( $z_0$ ), a slice also has a thickness ( $\Delta z$ ). The situation is illustrated in Figure 3-2. The thickness is determined by the bandwidth of the rf excitation pulse as well as the magnitude of the gradient ( $G_z$ ). The relationship

is expressed in equation 3-3. Note that the slice selection gradient must be perpendicular to the desired slice orientation.

$$\begin{aligned} BW = \Delta\omega &= \omega_1 - \omega_2 = \gamma [ B_0 + G_z (z_0 + \Delta z/2) ] - \gamma [ B_0 + G_z (z_0 - \Delta z/2) ] \\ &= \gamma G_z \Delta z \end{aligned} \quad (3-3)$$

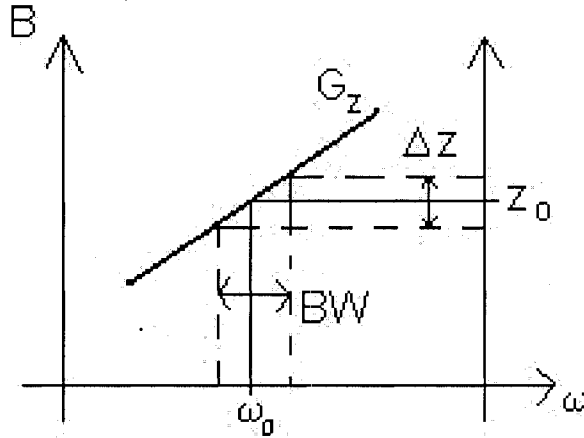


Figure 3-2. Slice Selection

The characteristics of the rf excitation pulse and slice selection gradient determine 3 parameters – slice center, thickness and flip angle. The carrier frequency ( $\omega_0$ ) determines the center of the slice ( $z_0$ ), the bandwidth and gradient determines the thickness of the slice ( $\Delta z$ ), and the flip angle is related to the area of the rf waveform (e.g.  $\gamma B_1 \tau$  for a rectangular waveform).

Ideally, we would like to be able to excite a slice with a perfect rectangular profile. Since we would need an infinitely long rf pulse to excite a perfectly rectangular slice, there will always be some fall-off and ripple in the slice. A double-lobe truncated sinc pulse is often used because it is easy to form and has a relatively good slice excitation profile. See Figure 3-3 for an illustration of a double-lobe truncated sinc pulse and its slice profile compared to a rectangular rf pulse.

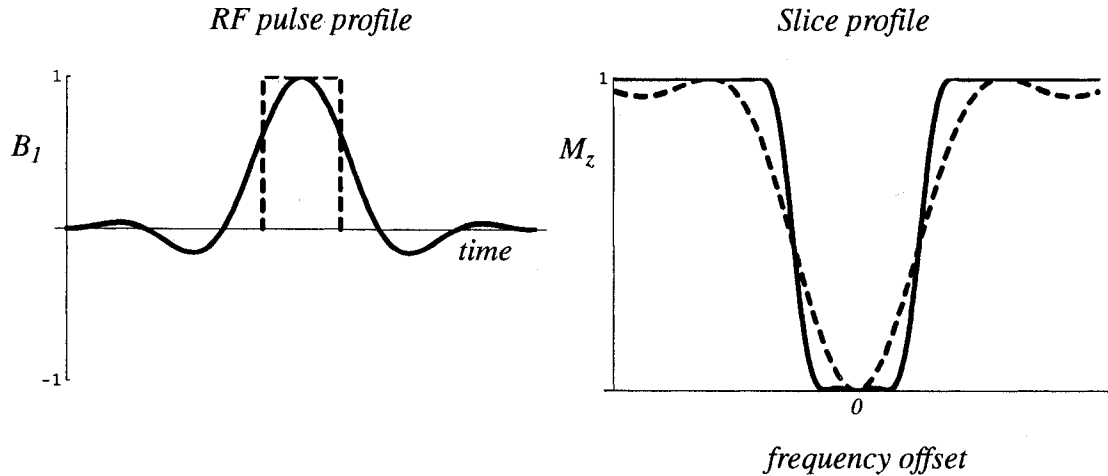


Figure 3-3 Practical rf Pulse and Slice Profile (From Buxton, 2002, p. 145)

### 3.1.2.3 Frequency and Phase Encoding of a Slice

Once the slice is excited, we are only faced with the problem of determining the signal from volumes along 2 dimensions. The frequency encoding method seen previously can be used to find projections along a slice.

It turns out that the signal recovered from a slice during the application of a gradient is the inverse Fourier transform of the projection in the direction of the gradient. Equation 3-4 shows the relationship between the signal as a function of time and the transverse magnetization in the rotating frame, where  $M_{xy}(r)$  = transverse magnetization as a function of position  $r$ .

$$s(t) = \int M_{xy}(r) e^{-i\gamma G_r t} dr \quad (3-4)$$

Thus, the transverse magnetization can be recovered by taking the inverse Fourier transform of the time domain signal and scaling.

This result can give us the spatial distribution along one dimension. An early method to find the image was backprojection, based on techniques from x-ray tomography. The direction of the projections can be varied by the linear magnetic field gradients and reconstruction of many projections could recover the image. However, there is a more elegant solution involving 2-dimensional Fourier transforms and frequency and phase encoding.

For 2-dimensional Fourier transforms, we need another dimension, which can be entered through phase encoding. The idea is to induce a known phase in the spin elements, acquire a signal from the spin elements, then change the phase and acquire another signal

until the whole range of the image has been acquired. The resulting raw data matrix is 2D inverse Fourier transformed to obtain the image.

Phase encoding is done by applying a linear magnetic field gradient in the direction orthogonal to the slice select direction and the frequency encode direction. The phase induced depends on the phase encode gradient and duration of gradient (correctly the area under the gradient curve as a function of time). If we call slice select direction z, frequency encode direction x and phase encode direction y, we can express the relations between frequency and position, for rectangular gradients, with the equations 3-5 and 3-6 respectively. The variables in the equations are illustrated in Figure 3-4.

$$\Phi(x) = \gamma G_x \Delta t \quad (3-5)$$

and  $\Phi(y) = \gamma \Delta G_y \tau \quad (3-6)$

where,

$\Phi(x)$  = phase in frequency encode direction

$\Phi(y)$  = phase in phase encode direction.

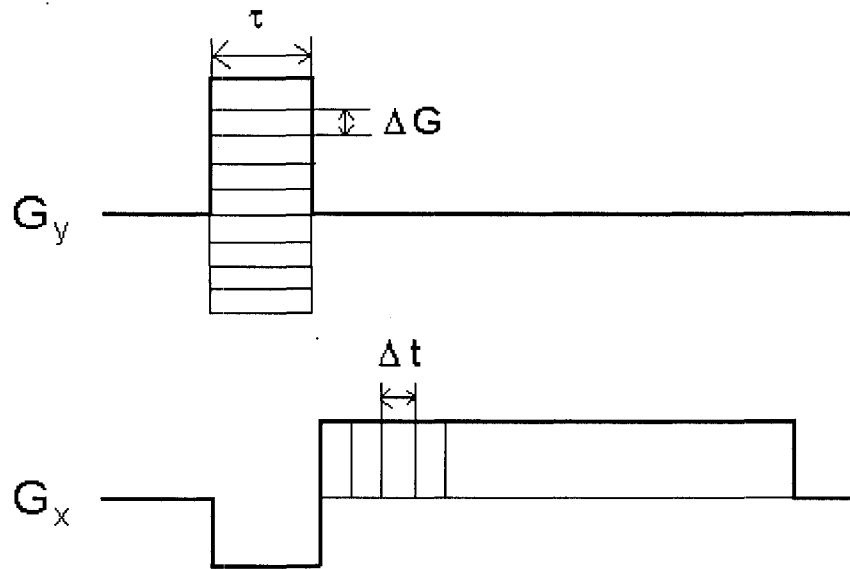


Figure 3-4. Frequency and Phase Encode Steps

### 3.1.2.4 Imaging Sequence

An image is acquired with a specific arrangement of rf pulses and linear magnetic field gradients called a sequence. An example imaging sequence is shown in Figure 3-5. The figure shows the sequence of rf pulses and gradients on separate axes as a function of time. To be complete, the imaging sequence requires that the magnitudes of the gradients, the carrier frequency and waveform of the rf pulse, and the precise timings are specified.

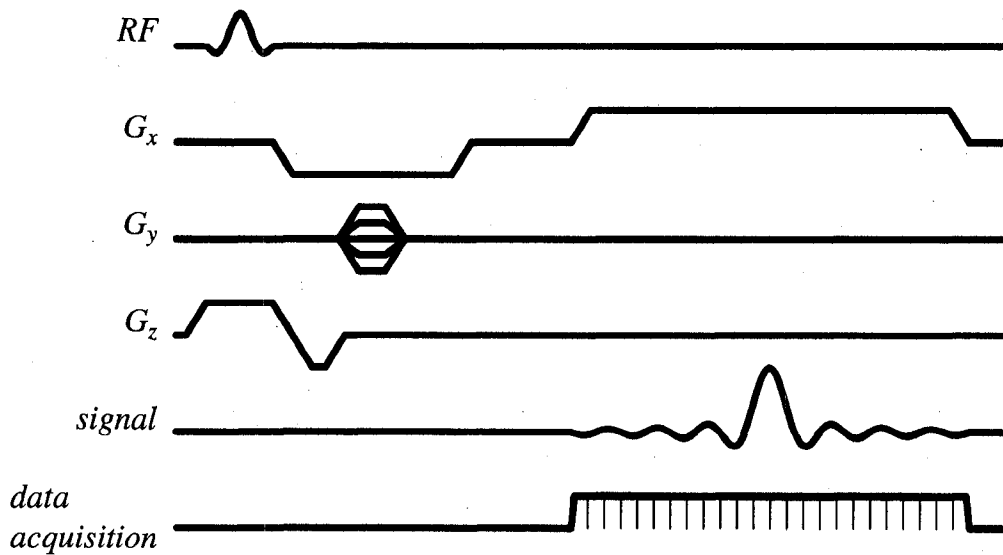


Figure 3-5. Example Sequence (From Buxton, 2002, p.90)

In the example sequence shown, the phase encoding is represented with a hatched box with an understanding that this basic sequence is repeated each time with a different phase encode gradient.

Also note the additional lobes in the slice select and frequency encode gradients. The rephasing lobe in the slice select gradient is required to bring the spins back into phase. The spins are dephased in the slice select gradient during the excitation pulse because of the application of the slice select gradient and the rephasing lobe brings the spins across the slice back into phase. In order to fully refocus the spins, the rephasing lobe should have half the gradient area of the original slice select gradient. At the end of the rephasing lobe, the spins are flipped and in phase and ready to begin their normal relaxation processes.

The dephasing lobe on the frequency gradient acts to shift the location of the peak of the signal to the middle of the data acquisition. This action is more clearly expressed in  $k$ -space, which we will examine next.

Many types of imaging sequences are known. They are broadly categorized into spin echo and gradient echo sequences, where spin echo sequences include a refocusing rf pulse to form an echo. They are given catchy acronyms such as FLASH (Fast Low-Angle SHot). The sequence along with its key parameters, are chosen according to the application, i.e. the purpose of acquiring the image. What makes MRI a truly amazing technique is the huge variety of images it can create suiting many different purposes, all with the same basic hardware.

### 3.1.3 K space

K-space is a transformed domain that represents the raw data. Recall the expression in equation 3-4 which represents the signal in time domain. In the pure frequency domain, we would be dealing with  $\omega$ , as shown in the Fourier transform base shown in equation 3-7.

$$F(\omega) = \int_{-\infty}^{\infty} f(t)e^{-i\omega t} dt \quad (3-7)$$

However, the exponent in equation 3-4 is “ $-i\gamma G_r t$ ”. By a change of variable, we can write equations for  $k_x$  and  $k_y$  (for a rectangular gradient) as:

$$k_x = \gamma G_x t \quad (3-8)$$

$$k_y = \gamma G_y t \quad (3-9)$$

The  $k$  plays the role of  $\omega$  in the Fourier transform equation and has the units of radians/meter, so  $k$  is often referred to as a spatial frequency. The 2D signal equation can then be written:

$$S(k_x, k_y) = \iint M_{xy}(x, y)e^{-ik_x x} e^{-ik_y y} dx dy \quad (3-10)$$

We can then visualize the imaging sequence as sampling k-space where the sampling interval is related to the encoding equations 3-5 and 3-6, namely:

$$\Delta k_x = \gamma G_x \Delta t \quad (3-11)$$

and  $\Delta k_y = \gamma \Delta G_y \tau \quad (3-12)$

The sequence illustrated in Figure 3-5 can then be visualized in k-space as shown in Figure 3-6. Each dot in the coordinate system represents a sample. The sequence is usually chosen to begin sampling at a point given by  $-k_{y\max}$  and  $-k_{x\max}$ , where the dephasing frequency gradient moves the sampling to  $-k_{x\max}$  and the first phase encode gradient moves the sampling to  $-k_{y\max}$ . The sequence samples points along the frequency encode direction in k-space, beginning at  $-k_{x\max}$  and going to  $+k_{x\max}$  by intervals  $\Delta k_x$ . Then the sequence moves into a different phase encode line by the phase encode gradient ( $\Delta k_y$ ) and then sampling across the line. The sequence is repeated until all of k-space is sampled. The image is then obtained by 2D inverse Fourier transform of the k-space data matrix.

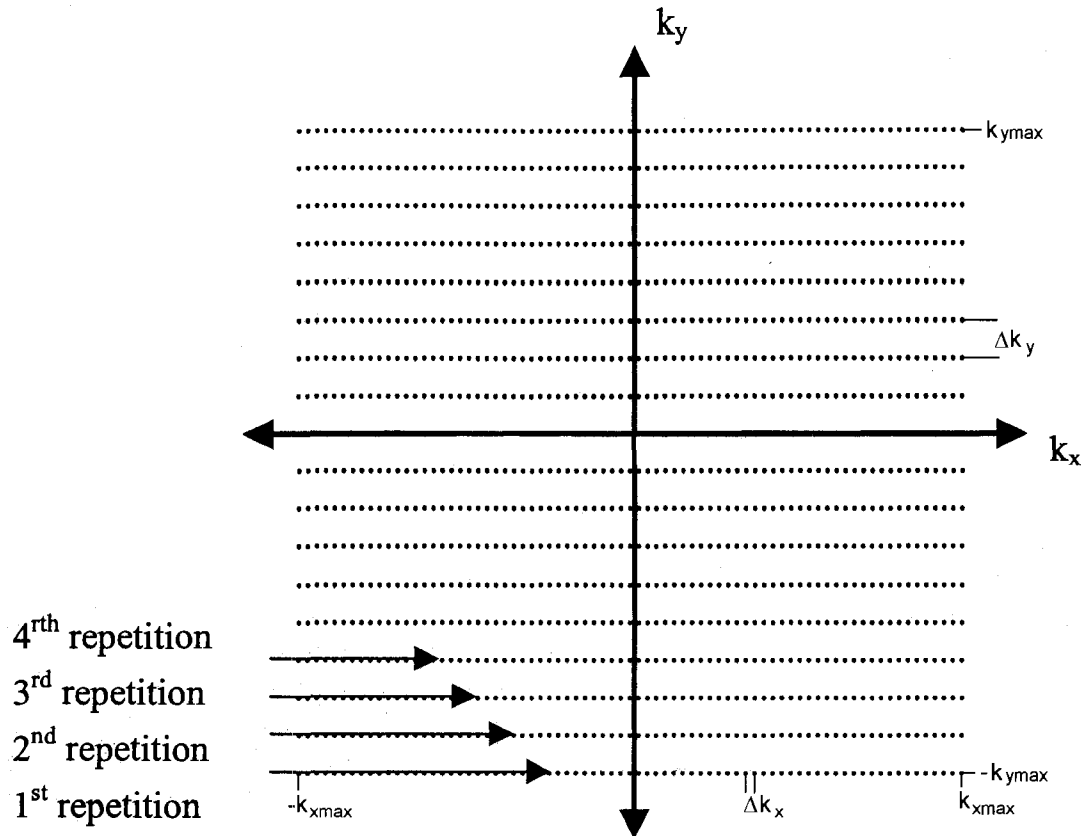


Figure 3-6. K-Space View of Basic Sequence

### 3.1.4 Imaging Parameters

This section will briefly describe some important imaging parameters and how they relate to each other and the image.

TR and TE are very important parameters for defining the contrast of the image. Possible contrasts include T1, T2 and spin density, and other contrasts are derived mainly as a result of these. The specific contrast will show a difference between tissues that differ in the contrast domain in the resulting image.

TR is the repetition time of the imaging sequence and is usually defined as the time between rf pulses. TR allows the longitudinal magnetization  $M_0$  to reform, so that long TRs will allow the magnetization to fully return whereas short TRs will allow only a portion of the total  $M_0$  to return to equilibrium.

TE is the echo time. The definition of TE is easily seen in spin echo sequences, in which a refocusing pulse is used to form an echo. The TE is the time between the initial rf pulse and formation of the first echo. For gradient echo sequences, the TE is defined as the time between the rf pulse and the middle of k-space. Together with the sequence, the

choice of TR and TE will define the contrast so that images can be spoken of as T1-weighted, T2-weighted or spin-density-weighted.

Field of view (FOV) is another important parameter. FOV is the spatial size of the image, such as 240mm x 240mm. It is inversely related to the area under the gradient during the interval between samples and can be expressed as:

$$FOV = \frac{1}{\Delta k} \quad (3-13)$$

where FOV and  $\Delta k$  are for phase encode and frequency encode directions.

Spatial resolution of an image refers to how well two signals can be distinguished when they originate close together in space. In MRI, spatial resolution is defined as the distance  $\Delta x$  such that, for 2 signals separated by  $\Delta x$ , the phase difference in the last data sample is  $180^\circ$ . It is given by the highest values of  $k$  that are sampled and is expressed by the relationship:

$$\Delta x = \frac{1}{2k_{\max}} \quad (3-14)$$

$\Delta x$  is often the pixel size of the image, but does not have to be, as zero-padding can be used to decrease the pixel size of the image. However, this doesn't actually add any more information. The image becomes slightly blurrier if more pixels are added in this way. In order to properly represent the frequency components in a time domain signal, the signal must be sampled at least twice as fast as the maximum frequency expected. This is the Nyquist criterion and produces limits on the combinations of parameters that can be used. The relationship between FOV, gradient strengths and time intervals is given in the following imaging equations, where definitions of symbols are the same as in previous equations (in particular, see Figure 3-4):

$$G_x = \frac{1}{\gamma FOV_x \Delta t} \quad (3-15)$$

$$\Delta G_y = \frac{1}{\gamma FOV_y \tau} \quad (3-16)$$

### 3.2 Echo Planar Imaging

In functional imaging, we normally want to see more than one slice and often the whole brain. The only methods that can image the whole brain in a reasonable time are echo planar imaging (EPI) and spiral imaging. Echo planar imaging places great demands on the scanner hardware and is subject to many artifacts, but despite these problems, EPI is now used almost exclusively for functional imaging. Therefore, it is important to understand the sequence and its limitations.

### 3.2.1 Echo Planar Imaging Sequence

Echo planar imaging was introduced by Mansfield in 1977 (Mansfield, 1977). It can produce a complete image from a single “shot”, that is, a single rf excitation pulse. The sequence can produce a slice of 64x64 samples with a sampling bandwidth of 200 kHz in 20.5 ms. Another advantage is that it can collect a complete image of the brain – 20 or more slices – in about the time required to allow longitudinal magnetization (T1) to recover.

EPI gains its speed from an efficient traverse of k-space. Sequences like fast gradient echo will traverse k-space line by line, always in the same direction, with another excitation after each line. Echo planar imaging reverses direction after each line by reversing the readout gradient. A comparison of the k-spaces trajectories for a conventional gradient echo sequence and EPI is shown in Figure 3-7.

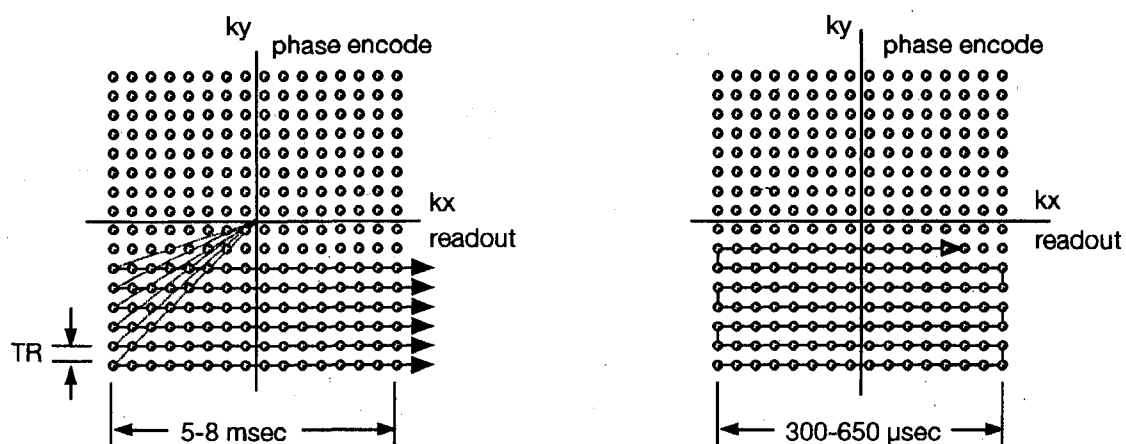


Figure 3-7. Comparison of k-space Traversal for Gradient Echo and Echo Planar Imaging Sequence (From Cohen, 1999, p.139)

Between each readout is a phase gradient to move to the next phase encode line. An idealized gradient echo planar imaging pulse sequence is shown in Figure 3-8. A spin echo sequence would add a  $180^\circ$  refocusing pulse before the readout to refocus dephasing from fixed magnetic field inhomogeneity, but everything else would be the same. A variant is the asymmetric spin echo sequence in which the echo is offset from the centre of k-space. The offset allows the contrast of the images to be closer to a gradient echo sequence.

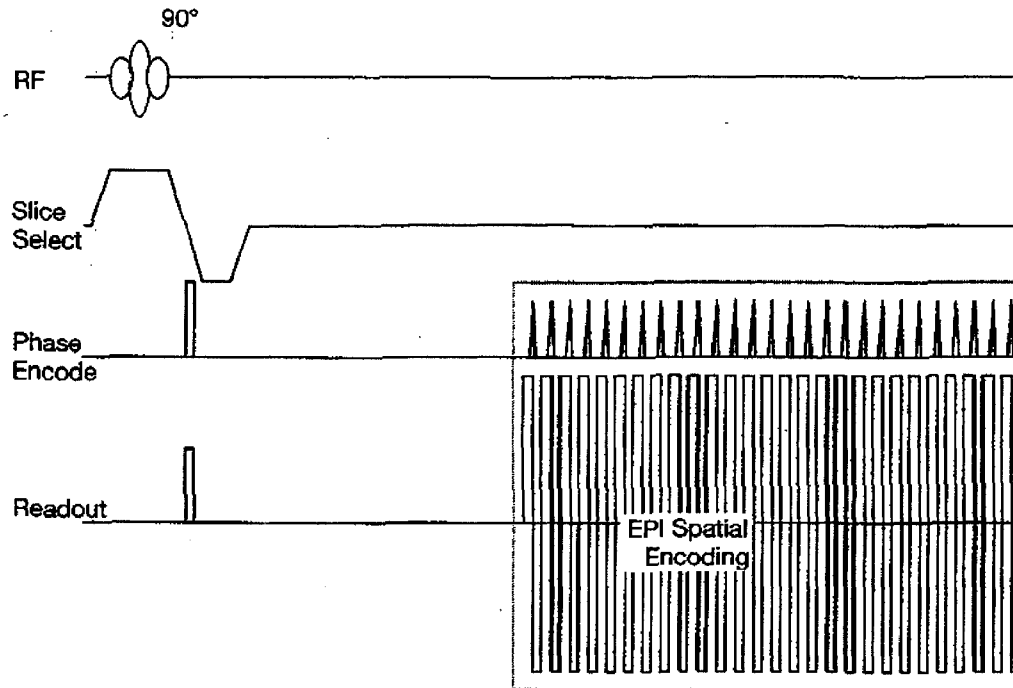


Figure 3-8. Idealized Echo planar imaging pulse sequence (From Cohen, 1999, p.139)

### 3.2.2 Echo Planar Imaging Artifacts

There are 2 main factors that reduce the image quality from EPI. One is the standard trade-offs between speed and image quality. A second is the fact that real hardware has imperfections and this leads to various kinds of artifacts in the image.

An imaging trade-off is in signal-to-noise ratio (SNR). SNR is proportional to the following factors:

- 1) Longitudinal magnetization ( $M_0$ )
- 2) Reception quality of the coil ( $B_T$ )
- 3) Volume of the voxels, and
- 4) Square root of total imaging time.

EPI is so fast that the time spent imaging is much smaller than in multi-shot methods, and this can reduce the SNR by up to two-thirds compared to a conventional gradient echo sequence (Cohen, 1999). However, EPI has the advantage that 90° pulses can usually be used which maximizes the magnetization available. Also, EPI has high efficiency (SNR/unit time) because an image is being acquired for most of the scanning time. The result is that EPI has good SNR so it is other artifacts that cause more problems for imaging.

Another imaging trade-off is with chemical shift. Chemical shift is a change in the local magnetic field seen by a proton because of the chemical environment. Different chemical units, such as  $-\text{CH}$  or  $-\text{CH}_2$ , can “shield” the proton from the applied magnetic field. See equation (3-2).

$$B_{\text{seen}} = B_{\text{applied}} (1-\sigma) \quad \text{chemical shift equation} \quad (3-17)$$

where  $\sigma$  = magnitude of the shielding.

A difference in frequency is equivalent to a difference in position (by imaging equations 3-15 and 3-16), so fat and water that have a frequency shift of 3.35 ppm or about 214 Hz at 1.5T, could experience a shift of 1 mm in a 0.5 G/cm gradient at 1.5T. This is less than a voxel in most fMRI applications.

Note that in the imaging equations, phase offset builds up as frequency times time. In the phase encode direction in EPI, there can be substantial time for a phase offset between fat and water to build up. The effect can be thought of as a lower bandwidth in the phase encode direction. Therefore, a much larger shift in position of the fat is experienced in the phase encode direction. The fat signal is usually eliminated by exciting the fat selectively with an excitation pulse at the fat frequency and dephasing the transverse magnetization with a gradient before the main pulse.

In EPI, the k-space modulation transfer function is poor since there is a long time in between k-space lines at the start of data acquisition versus lines at the end so the signal contrast is changing from one end to the other (see Figure 13-9). The result is distortion in the image.

There are several effects of hardware limitations. One is that no hardware can instantly reverse the gradient. The slew rate is the maximum speed at which the gradient can be changed. If the gradients are not rectangular, but rather have linear slopes (a ramp), the spacing of the readout samples will be changed (see Figure 13-10) which leads to distorted images after the inverse Fourier transform is taken. By taking into account the slower rate of movement through k-space during the ramp, the samples can be put in their correct locations.

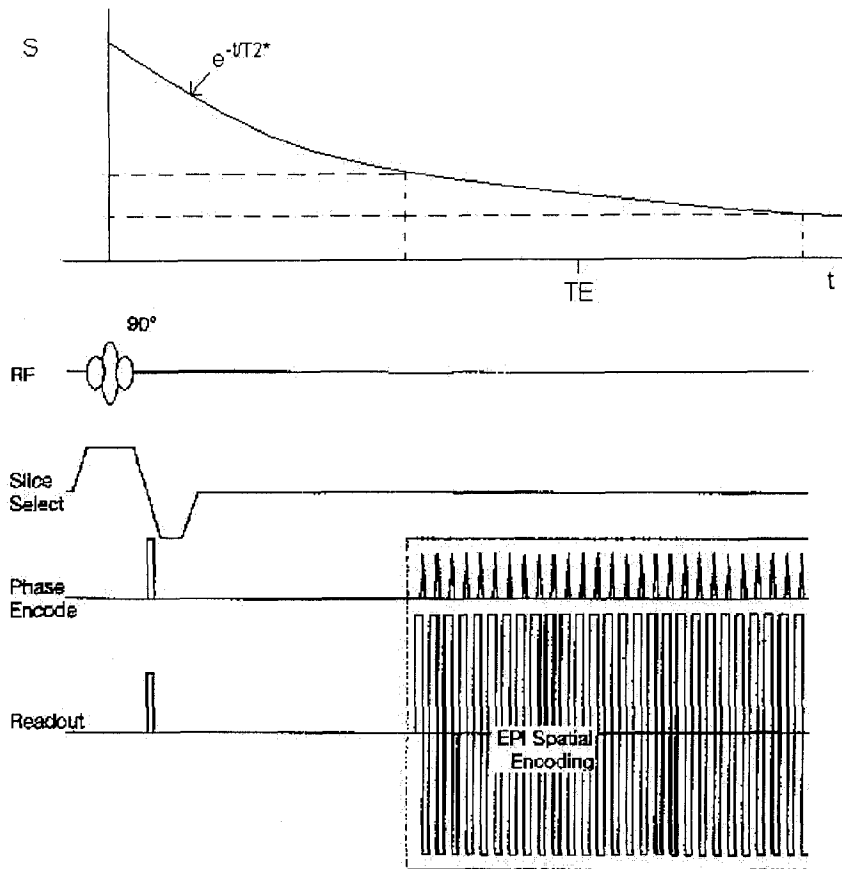


Figure 3-9. Variation in Signal Over Acquisition Time

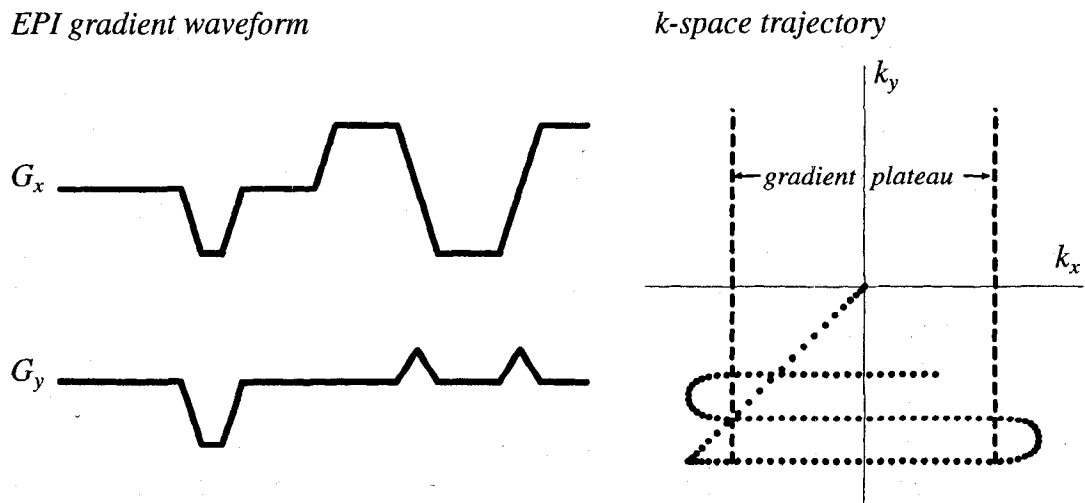


Figure 3-10. Effect of Gradient Ramps on K-Space Sampling (Buxton, 2002, p.268)

Eddy currents are induced in any conducting surfaces by the rapid switching of the gradients and they cause various effects. The size of the eddy currents is proportional to the rate of change of the magnetic fields, and there is no sequence that has more rapid gradients changes than EPI. The eddy currents produce extra magnetic field gradients that oppose the main gradient fields. Since these extra magnetic field gradients will vary with time, they will affect the size of the gradients at any time and thus affect the position of k-space samples. This will cause distortion of the image. The eddy currents also cause the actual gradients to be systematically delayed and shift the center of refocus. The k-space sampling will be shifted in opposite directions on positive and negative gradient readouts and this alternating pattern results in N/2 ghosting (ghosts shifted by half the FOV) (see Figure 3-11 for an example of ghosting; notice that the ghosting in the Figure happens in the phase encode direction).

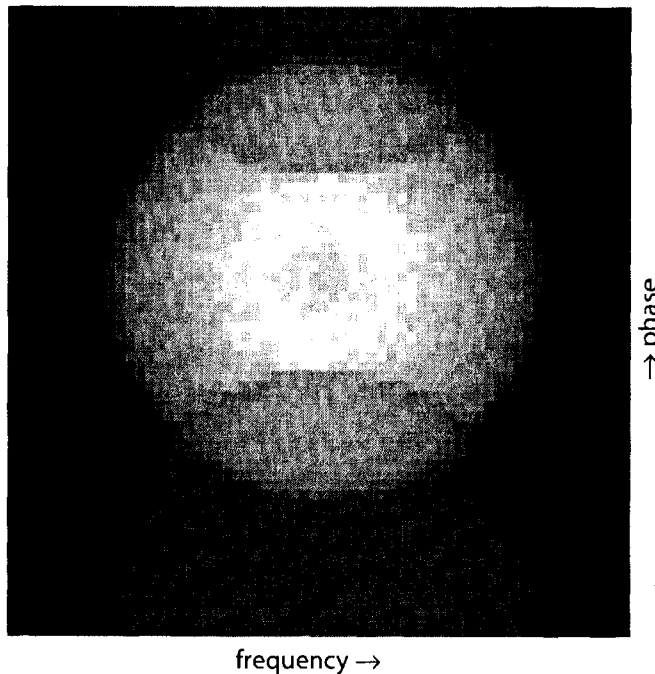


Figure 3-11. Example of Ghosting (From Cohen, 1999, p. 141)

To improve the distortion caused by eddy currents, it is possible to add compensating gradients to achieve constant positive and negative gradient strengths. To improve the ghosting, it is also possible to shift the acquisition of samples so that the sampling will be equalized in the positive and negative gradients. It is also possible to shift the sampled data after collection by adding an appropriate phase shift to the data.

Inhomogeneous magnetic fields cause distortion by a similar process as the chemical shift artifact. Any inhomogeneity in the magnetic field will cause a difference in resonant frequency which will appear as a spatial shift. As was shown earlier with the chemical

shift, the distortion in the frequency encode direction is not much because of its high bandwidth, but there can be lots of distortion in the phase encode direction. See Figure 3-12.

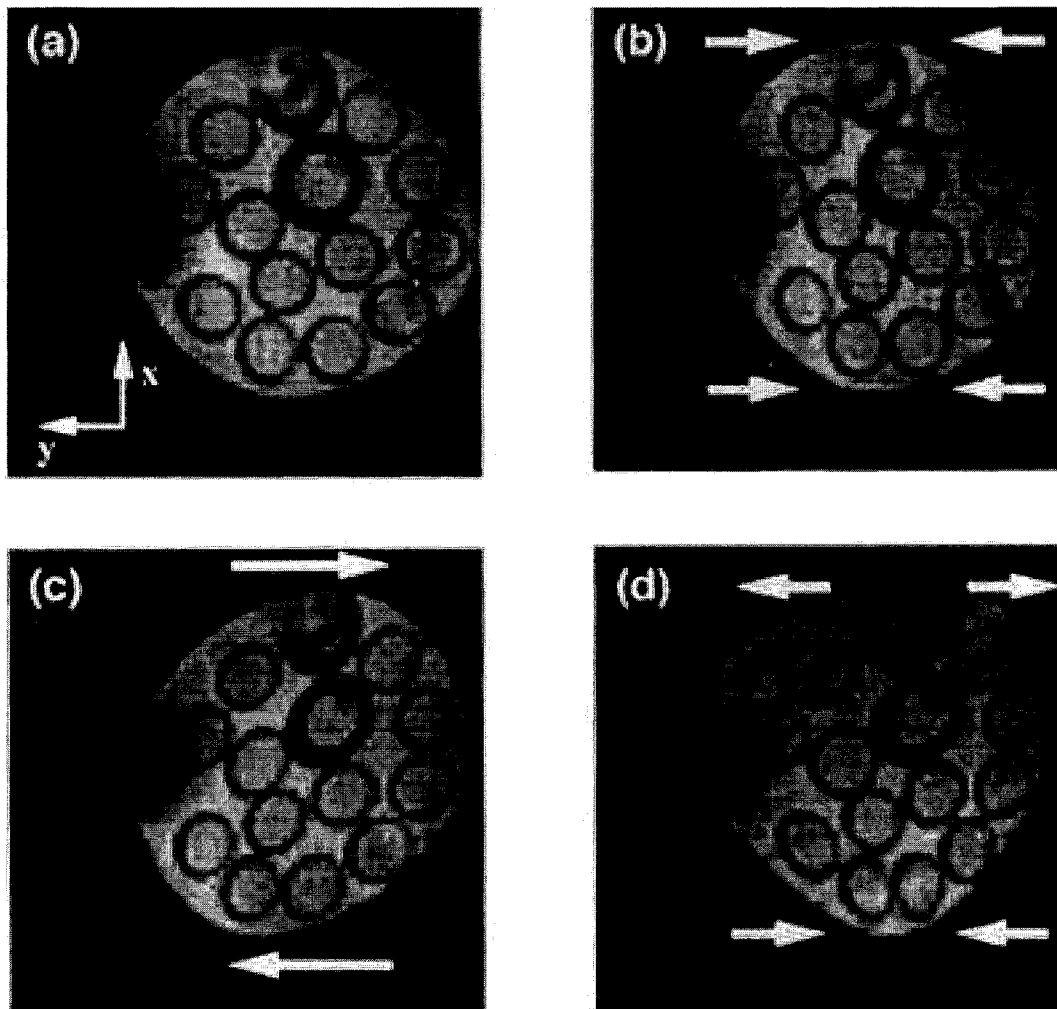


Figure 3-12. Example of Distortion in an EPI Image a) EPI image of phantom with good shimming, b), c), d) EPI images with a variety of mis-set shims. (From Jezzard & Balaban, 1995)

Distortion is minimized by shimming. For any remaining distortion, it is possible to use field mapping techniques to determine the shift at each point, and correct for it (Jezzard & Balaban, 1995). This correction technique will not work if the signal is lost due to dropout or if the signals from 2 or more voxels overlap.

The last artifact discussed here is signal dropout, which results from the large changes in magnetic susceptibility in air/tissue interfaces such as happen around the sinuses in orbital prefrontal cortex. The susceptibility change between deoxygenated air and tissue is much larger than that between hemoglobin and tissue, so the interface creates much

larger decreases in signal. Since there is no signal in such areas, nothing can be said about functional activations in these areas of the brain.

Signal dropout can be improved by reducing the size of the voxel. This will tend to make voxels more homogeneous, and only voxels right on the interface will be lost. More will be stated on voxel size in the next section.

### 3.2.3 Echo Planar Imaging in Practice

In this section, some of the tradeoffs in choosing parameters will be discussed. Generally, parameters are chosen to give the best contrast-to-noise ratio (CNR), but there is often a tradeoff between maximizing the CNR and minimizing artifacts.

An important issue in maximizing the BOLD contrast is the choice of TE. BOLD contrast comes from T2\*-weighting. A rule of thumb is to have  $TE \approx T2^*$  (see Figure 3-13). The T2\* will be different for different scanners, but comes out between 30 and 60 ms typically.

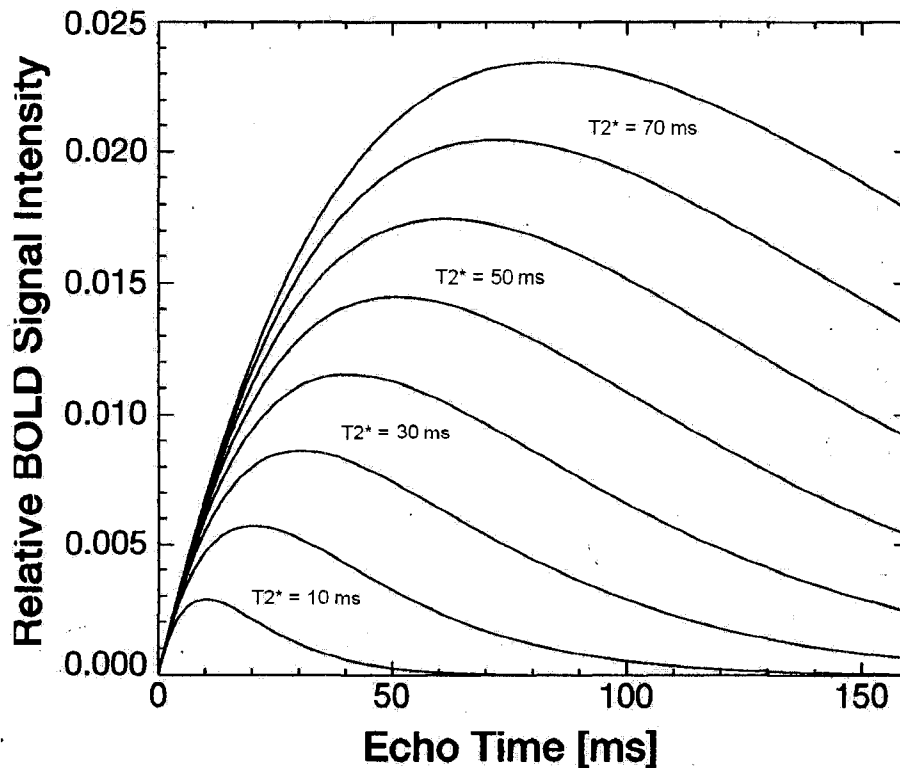


Figure 3-13. Variation in BOLD contrast with TE for different values of T2\* (Adapted from Moonen & Van Gelderen, 1999, p.163)

Another important parameter is the TR. There are many factors to consider in choosing this parameter. The first is the paradigm. Block design paradigms need to have a TR that is an integer dividend of the block length and the paradigm may impose strict limitations

on block length. Also, event-related paradigms may impose some limitations on the TR because there should not be more than one event occurring within a TR.

The choice of TR is also affected by contrast considerations. Maximum contrast can be achieved by allowing the full available magnetization to recover and flipping it by 90°. Thus, TR should be at least 3 times longer than T1. For smaller TRs, the flip angle should be adjusted according to the Ernst equation (3-18) to achieve maximum contrast.

$$\cos(\alpha) = \exp(-TR/T1) \quad \text{Ernst angle equation} \quad (3-18)$$

where  $\alpha$  = Ernst angle (optimum flip angle to maximize transverse magnetization)

With smaller TRs, it is possible to get gains in the efficiency (CNR per unit time) because the faster imaging allows more averaging (assuming noise is not correlated between images). Figure 3-14 shows a variation of SNR with TR/T1 and flip angle.

### *Signal to Noise Ratio*

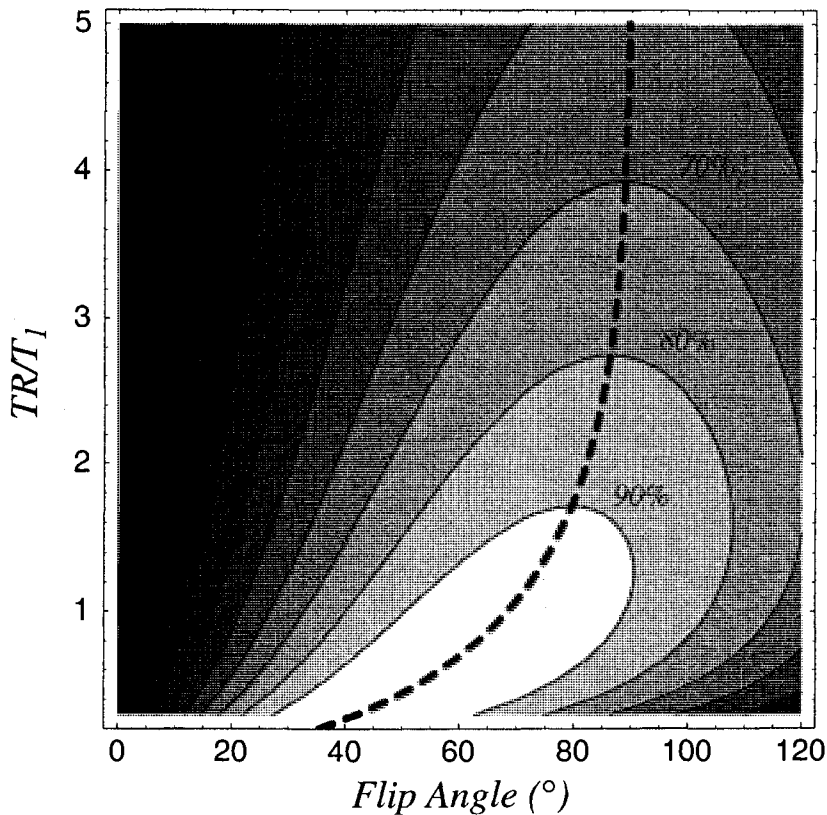


Figure 3-14. Optimizing TR and Flip Angle (Buxton, 2002, p.436)

Voxel size is another important parameter. Larger voxels can have large SNR according to the basic SNR proportions expressed previously. Also, an image with larger voxels

can be taken more quickly, so minimum TRs can be reduced. However, larger voxels can also suffer more from partial volume effects, in which different kinds of tissue are within the voxel. The differing properties of the tissue types lead to loss of signal from the voxel, so reducing voxel size can reduce signal dropout. Common voxel sizes for functional imaging at 1.5T are 3 x 3 mm in-plane and slice thickness of 3 to 7 mm. The number of slices and slice thickness also depend on the size of brain area to be imaged and the TR (especially if TR is small ( $<3$  s)).

### 3.2.4 Variations in Echo Planar Imaging

There are many possible variations in echo-planar imaging. These include multi-shot, partial k-space reconstruction and spiral sequences.

Multi-shot sequences are sequences in which there are more than 1 shot. The advantage of multi-shot sequences over single-shot sequences is in image quality. Because each shot is read out in less time, there is not as much variation in contrast over the length of the readout. The multishot sequences need careful design of the k-space traversals to make the smoothest k-space modulation functions and are obviously slower than single-shot.

Partial k-space reconstruction is a method that takes advantage of real and imaginary data with conjugate symmetry to sample down to half of k-space and thus reduce acquisition times. It is also called partial Fourier encoding. The free induction decays that are sampled are normally set to be symmetric around the echo time by adding a half-length negative gradient in the readout direction (section 3.1.3). By reducing the area of this gradient, we will produce the echo at an earlier time in the readout. By sampling just over half the signal, we should be able to accurately reconstruct the other half. Due to noise, motion, T2 decay and magnetic field inhomogeneity, a fair bit more than half must be acquired to get good images. Around 75% sampling gives good reconstruction. In EPI, partial Fourier encoding is usually done in the phase-encode direction, reducing the number of phase encode steps while leaving the frequency untouched.

Spiral sequences are sequences that traverse k-space in a spiral pattern (Noll, Stenger, Vazquez & Peltier, 1999). After the data acquisition, there is an extra processing step to regrid the sample points so that they can be Fourier-transformed. Spiral sequences offer several advantages, namely they:

- 1) are not as susceptible to distortion
- 2) require lower gradient slew rates
- 3) sample the center of k-space (determines the contrast) when the signal is still high
- 4) have a higher sampling density in the center of k-space.

The tradeoff is that they are more susceptible to blurring, though this can be corrected to some extent (Irrazabal, Meyer, Nishimura & Macovski, 1996; Noll, Pauly, Metzger, Nishimura & Macovski, 1992).

Echo volumar imaging is the dream sequence in which the whole volume is acquired in a single shot (Harvey & Mansfield, 1996). In this case, a single pulse is used to excite the complete volume and then the slice select gradient is stepped to acquire various slices in turn. All the artifacts and demands on hardware become even more severe with such a sequence and so this sequence is not typically used.

## References:

- Bloch, F., Hansen, W.W. & Packard, M. (1946). Nuclear induction. *Physics Review*, 69, 127.
- Buxton, R.B. (2002). *Introduction to functional magnetic resonance imaging: Principles and techniques*. New York: Cambridge University Press.
- Cohen, M.S. (1999). Echo-planar imaging and functional MRI. In C.T.W. Moonen, and P.A. Bandettini (Eds.), *Functional MRI* (Chap. 13). Heidelberg, Germany: Springer-Verlag.
- Damadian, R. (1971). Tumor detection by nuclear magnetic resonance. *Science*, 171, 1151-1153.
- Harvey, P.R. & Mansfield, P. (1996). Echo-volumar imaging (EVI) at 0.5 T: first whole-body volunteer studies. *Magnetic Resonance in Medicine*, 35(1), 80-88.
- Irrazabal, P., Meyer, C.H., Nishimura, D. & Macovski, A. (1996). Inhomogeneity correction using an estimated linear field map. *Magnetic Resonance in Medicine*, 35, 278-282.
- Jezzard, P. & Balaban, R.S. (1995). Correction for geometric distortion in echo planar images From Bo field variations. *Magnetic Resonance in Medicine*, 34(1), 65-73.
- Lauterbur, P.C. (1973). Image formation by induced local interactions: Examples employing nuclear magnetic resonance. *Nature*, 242, 190-191.
- Mansfield, P. (1977). Multi-planar image formation using NMR spin echoes. *Journal of Physics C.*, 10, L55-58.
- Moonen, C.T.W. & van Gelderen, P. (1999). Optimal efficiency of 3D and 2D BOLD gradient echo fMRI methods. In C.T.W. Moonen & P.A. Bandettini (Eds.), *Functional MRI* (Chap. 15). Heidelberg, Germany: Springer-Verlag.
- Noll, D., Pauly, J., Metyer, C., Nishimura, D. & Macovski, A. (1992). Deblurring for non-2D Fourier transform magnetic resonance imaging. *Magnetic Resonance in Medicine*, 25(2), 319-333.

Noll, D.C., Stenger, V.A., Vazquez, A.L. & Peltier, S.J. (1999). Spiral imaging in fMRI. In C.T.W. Moonen & P.A. Bandettini (Eds.), *Functional MRI* (Chap. 14). Heidelberg, Germany: Springer-Verlag.

Purcell, E.M., Torrey, H.C. & Pound, R.V. (1946). Resonance absorption by nuclear magnetic moments in a solid. *Physical Review*, 69, 37-38.

Weisman, I.D., Bennett, L.H., Maxwell, Sr., L.R., Woods, M.W. & Burk, D. (1972). Recognition of cancer in vivo by nuclear magnetic resonance. *Science*, 178, 1288-1290.

## Chapter 4      Functional MRI

Functional neuroimaging refers to methods that allow researchers to image some functional aspect of neural behaviour. It may have had a start with recordings of pulsations of the human cortex following neurosurgical procedures in patients with skull defects by the Italian physiologist Antonio Mosso in 1881. Roy and Sherrington's (1890) experiments on animals suggested a link between brain circulation and metabolism. The first method to measure global cerebral blood flow (CBF) was invented by Kety and Schmidt in 1948 - the nitrous oxide technique (Landau, Freygang, Roland, Sokoloff and Kety, 1955). Then in 1963, Ingvar and Lassen used radioactively inert gas (Krypton-85 and later Xenon-133 (Obrist, Thompson, King & Wang, 1967)) with detectors to measure the decay products and ascertain regional CBF changes (Lassen et al, 1963). They demonstrated that blood flow changes regionally during changes in brain functional activity. Then the deoxyglucose technique for measuring regional glucose metabolism in animals was developed (Sokoloff et al, 1977). Later positron emission tomography (PET) was used to extend the deoxyglucose technique to humans (Reivich et al, 1979) and to measure blood flow by injecting radioactively-labelled water ( $H_2O^{15}$ ) (Raichle, Martin, Herscovitch, Mintun & Markham, 1983). Single photon emission computed tomography (SPECT) is very similar to PET but works with different radioactive tracers (Iodine-132 and Technetium-99 versus Fluorine-18 or Oxygen-15) (Wyper & Montaldi, 2000). The most recent player on the scene is functional magnetic resonance imaging (fMRI).

Functional MRI uses MRI to measure brain function. Although there are several methods that can measure different aspects of function, such as perfusion-weighted imaging using contrast agents or arterial spin labelling (ASL), the BOLD contrast has emerged as the most popular. The BOLD contrast mechanism was used for the study described in this thesis, so only BOLD will be described.

### **4.1    *BOLD contrast mechanism***

BOLD stands for Blood Oxygenation Level Dependent. BOLD uses the changing magnetic properties of blood with and without bound oxygen on its hemoglobin molecules to see a difference in the MRI signal in a region of the brain when its neurons are active versus when they are at rest.

BOLD functional imaging developed from the observation that blood T2 is related to the oxygenation level (Thulborn, Waterton, Matthews & Radda, 1982) and that during neuronal activity, there are local changes in the amount of oxygen in tissue (Fox &

Raichle, 1986). Ogawa was the first to investigate the BOLD effect, with a study in rats using inhaled anaesthetics (Ogawa et al, 1990). Turner demonstrated the use of gradient recalled echo planar imaging with BOLD with an experiment on cats (Turner, LeBihan, Moonen, Despres & Frank, 1991). The first human demonstrations followed shortly (Kwong et al, 1992; Ogawa et al, 1992; Frahm, Bruhm, Merboldt & Hanicke, 1992; Bandettini, Wong, Hinks, Tikofsky & Hyde, 1992).

The BOLD contrast mechanism is very complicated and the mechanisms of the link between neural activity and changes in blood oxygen level are not known in detail. However, the experimental evidence for the link is good and the technique has such great applications in functional human brain mapping that it has become very widely used.

There are 2 parts to the story of how neural activity results in a change in the MRI signal. The first part is how the neural activity causes changes in the blood oxygen level. The second part is how the blood oxygen level changes can be measured with MRI. Since this second part is better known, it will be described first.

#### **4.1.1 Measuring Blood Oxygen Changes with MRI**

Hemoglobin is the molecule of blood that carries oxygen. When blood hemoglobin is carrying oxygen, it is called oxygenated, whereas when it is not carrying oxygen, it is called deoxygenated. The different states have slightly different magnetic properties, measured by the susceptibility (Pauling & Coryell, 1936). Susceptibility is a measure of the component's ability to continue a magnetic field. It is similar to the concept of conductivity in electric systems. Most elements are non-magnetic, meaning they carry a magnetic current poorly. Gases are usually non-magnetic and air has a susceptibility close to 1. This is similar to non-conducting materials. On the other hand, ferromagnetic items such as iron carry a magnetic field very well. Their susceptibility is very high. This is similar to copper or other metals that carry an electric current very easily.

Deoxygenated hemoglobin has a susceptibility that is slightly larger than 1 (paramagnetic), whereas oxygenated hemoglobin reduces the paramagnetic effect (closer to 1) (Pauling & Coryell, 1936). The effect of magnetic susceptibility ( $\chi$ ) is shown in the equation below:

$$B_{\text{seen}} = (1 + \chi) B_{\text{applied}} \quad (4-1)$$

where  $\chi$  for deoxyhemoglobin is 0.3 ppm compared to -8.8 ppm for water and 3.6 ppm for air (Bronskill & Graham, 1992).

Although  $\chi$  is very small, it results in a frequency shift relative to water that is significant for the MRI signal. The important thing is how the susceptibilities compare to typical brain tissue. Brain tissue susceptibility is close to that of oxygenated hemoglobin. The

frequency shift is proportional to the strength of the magnetic field as well as the difference in susceptibility between the materials. At 1.5T, the Larmor frequency is about 64 MHz, so the frequency shift is 20 Hz.

The change in magnetic susceptibility causes a magnetic field gradient. Neighboring magnetic spins in a magnetic field gradient will see slightly different magnetic field strength which results in a different precession frequency and thus a dephasing of spins across the gradient, leading to a loss of signal. This effect is exactly like the dephasing of the T2 relaxation process and the dephasing resulting from  $B_0$  magnetic field inhomogeneity ( $T2'$ ) so it is modeled as a reduction in  $T2^*$ . Therefore, the presence of deoxygenated hemoglobin will lead to loss of signal in  $T2^*$  sensitive sequences, whereas oxygenated hemoglobin will not. Thus, the fMRI signal depends on the state of oxygenation.

As a sidelight, this reduction in  $T2^*$  is also used in bolus tracking. Bolus tracking follows a contrast agent such as Gadolinium that is injected into blood. The contrast agent alters the local magnetic susceptibility, causing a signal decrease as it passes (Rosen, Belliveau, Vevea & Brady, 1990). This effect was used in the first demonstration of brain activation with MRI (Belliveau et al, 1991). Also, in typical gradient recalled echo planar imaging, the susceptibility difference between air and tissue ( $\chi = 10$  ppm) results in signal loss in anterior and orbital parts of the frontal cortex.

Within the blood vessel, the susceptibility difference results in an average frequency shift seen by all protons. Although this average frequency shift is the same for all protons within a single blood vessel, the multitude of blood vessels with different orientations will change the frequency shift and cause dephasing of the protons within the blood vessels.

To spins outside the blood vessels, the size and orientation of the blood vessels will also be important in the results. We will approximate the blood vessels as cylinders with a radius and orientation to  $B_0$ . The cylindrical geometry results in a magnetic dipole field distortion. To spins outside the vessel, the strength of the magnetic field gradient will depend on the radius of the cylinder and the orientation of the line of axis of the cylinder to the magnetic field. The gradient is stronger with a cylinder at a  $90^\circ$  angle to the magnetic field and falls off to zero for a cylinder parallel to the magnetic field because of the shape of the magnetic dipole field distortion around the cylinder. Because there are many blood vessels with different orientations within a voxel, the resulting effect is an exponential signal attenuation that depends on the change in  $T2^*$ .

The extravascular water molecules whose spins are being flipped diffuse within the extravascular tissue. The diffusion within a magnetic field gradient means that a particular molecule will see a varying magnetic field over the course of a measurement, which tends to average out the gradient effects and reduce the dephasing between spin populations (Buxton, 2002).

The effect of diffusion depends on the size of the gradient fields and the average distance travelled by a molecule between the flip pulse and the readout. For small radius vessels, the distance travelled is greater in relation to the gradient fields, and so the molecule can feel the effects of many fields. For large radius vessels, the molecules see less field variation. See Figure 4-1. So gradient-recalled echo sequences see a larger signal change from large vessels. Since veins are larger than capillaries and veins also see a larger change in oxygenation, much of the signal change in gradient echo sequences is caused by veins.

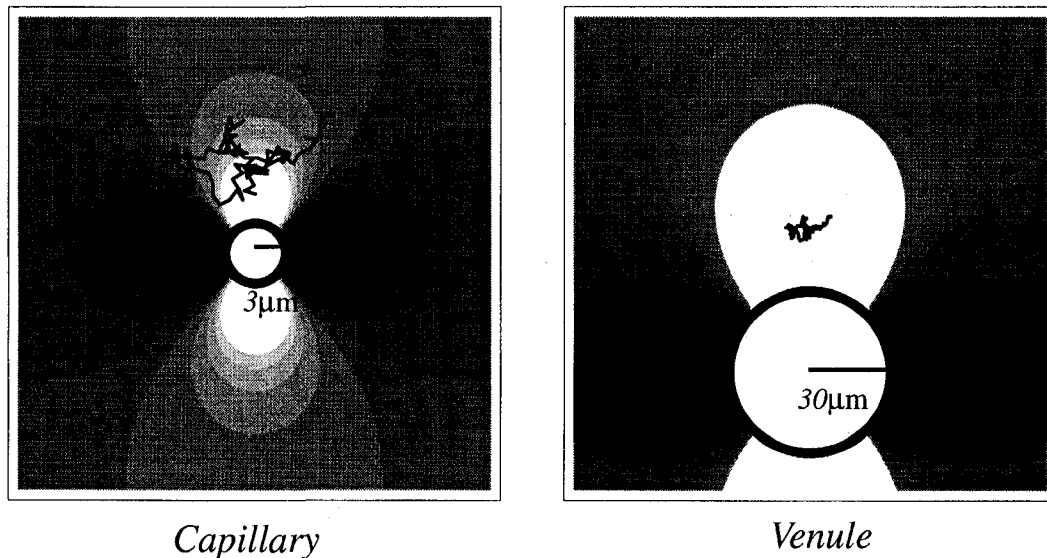


Figure 4-1. Diffusion of an Extravascular Water Molecule Near Vein and Capillary (from Buxton, 2002, p. 403)

Although intravascular space is only a small portion of the total tissue volume in the brain (4-6%), it has an enhanced effect on the signal change. For a gradient echo sequence at 1.5 T, the majority of signal comes from intravascular space (See Figure 4-2; Boxerman et al, 1995). This has been shown by experiment as well as theory.

**Combined EV and IV fMRI Signal Change  
GE TE = 40 ms, 1.5 T**

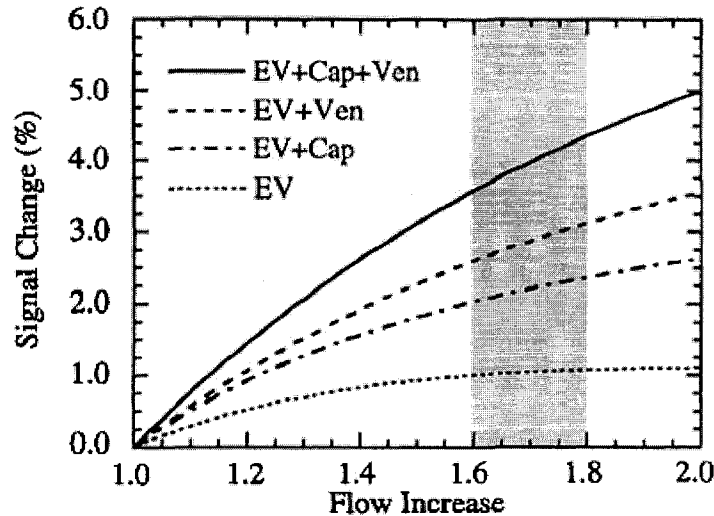


Figure 4-2. Relative Contributions of Extravascular space, Intravascular Capillaries and Intravascular Veins to fMRI signal for Gradient Echo at 1.5T (Boxerman et al, 1995)

Experimentally, one way to reduce the contribution of intravascular spins to the fMRI signal is to add diffusion-weighting (Boxerman et al, 1995; Song, Wong, Tan & Hyde, 1996). Diffusion-weighting is done by adding a bipolar gradient to the sequence. The bipolar gradients will refocus spins that are stationary, whereas spins that move will not refocus properly. Spins in the moving blood will see large changes in their environment, so they can be preferentially eliminated. An example of an experiment in which varying diffusion-weighting factors (b) were applied is shown in Figure 4-3, which confirms that much of the signal at 1.5T is coming from intravascular sources.

Spin echo sequences can also be used for BOLD contrast, though the mechanism of signal change is somewhat different. Spin echo sequences, with a refocusing pulse, eliminate the effect of local field variations, so at first glance are not expected to be sensitive to the blood oxygen level. However, diffusion acts to move the water molecules through individual fields and prevents full refocusing of the signal. Because the spins are partially refocused, the signal change is always less than in a gradient-recalled echo sequence.

Spin-echo sequences produce a different pattern of sensitivity according to vessel size. For larger vessels in which the magnetic field gradients are also spatially larger, the diffusing spins see a more homogeneous magnetic environment so the effect of diffusion is reduced and the signal can mostly refocus. For smaller vessels, diffusion causes

extensive averaging of the fields, so although the spins do not refocus, they show a lot of attenuation just as with gradient echo. (Figure 4-1 is helpful in visualizing the diffusion.)

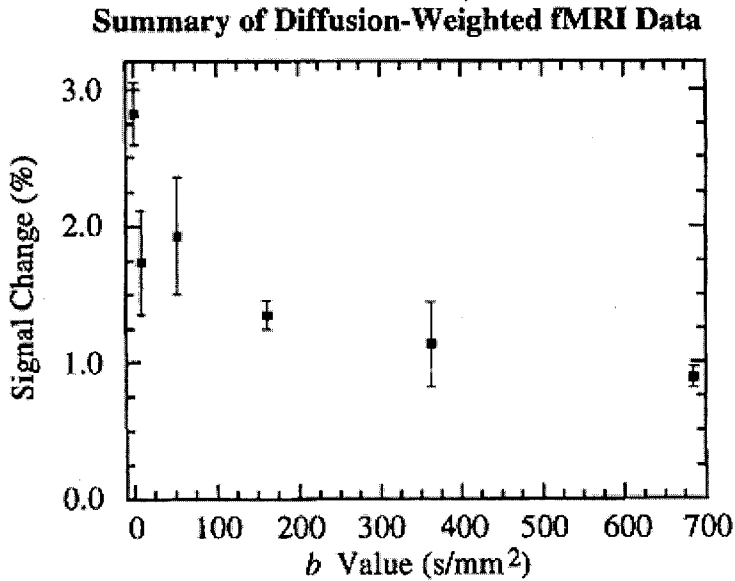


Figure 4-3. Reduction in BOLD signal change as Diffusion-Weighting in Increased (Boxerman et al, 1995)

The signal from spin echo peaks at an intermediate range around the 7  $\mu\text{m}$  in radius (Weisskoff, Zuo, Boxerman & Rosen, 1994). This sensitivity makes the spin echo sequences potentially more sensitive to changes in the tissue rather than veins. Figure 4-4 summarizes these discussions above about SE vs GE sequences and vessel sizes by showing the changes in relaxation rate ( $1/T_2^*$  or  $1/T_2$ ) as a function of vessel radius.

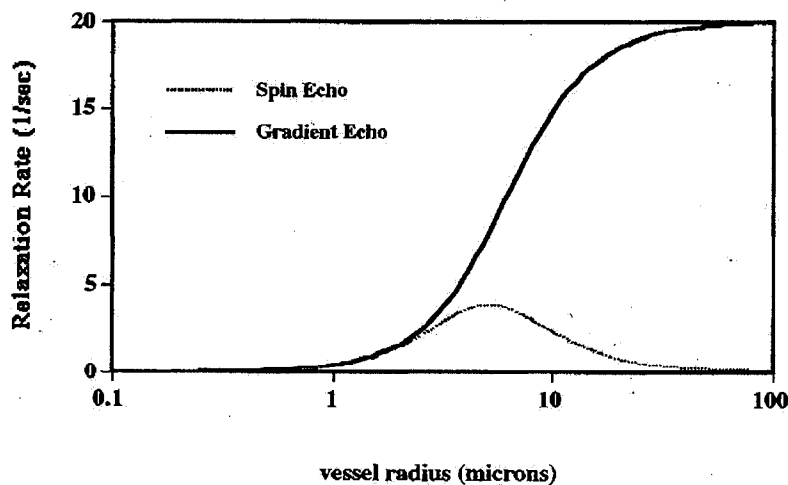


Figure 4-4. Variation of change in  $R_2^*$  (GE) and change in  $R_2$  (SE) as a function of vessel radius for spin echo (SE) and gradient echo (GE) sequences for Extravascular spins (Kennan, 1999, p. 130).

In addition to the effect of changes in  $T2^*$ , blood volume also affects the signal. A cylinder with a larger radius creates a larger pattern of field gradients (proportional to radius squared). Therefore, a single cylinder creates the same total field gradients as 4 cylinders with half the radius. So when considering a volume that can contain many cylinders (blood vessels), the total gradient is proportional to the volume enclosed by all cylinders (Buxton, 2002). This means that the MRI signal is also affected by the cerebral blood volume (CBV), but in a different direction. Increased oxygenation fraction (decreased field gradients) causes a signal increase, whereas increased cerebral blood volume (increased field gradients) causes a signal decrease.

There can also be signal changes caused by changes in  $T1$  from increased blood flowing into the slice. Blood has a longer  $T1$  than tissue at 1.5T (about 1500 ms versus about 900 ms for gray matter and 800 ms for white matter). When TR is in an intermediate range, the blood does not recover longitudinal magnetization but the tissue does. Then when the non-recovered blood flows into the tissue, it will not acquire as strong a magnetization so less signal will be produced. The amount of change depends on the TR.

It's helpful to recap the description to this point. Blood oxygenation changes the susceptibility of the blood. Deoxygenated blood has a susceptibility that is closer to that of tissue than oxygenated blood, so the field gradients will increase with the proportion of deoxygenated blood. The increased field gradients will result in some signal loss. The signal reduction has been calibrated with the blood oxygen level at 1.5T (Davis, Kwong, Weisskoff & Rosen, 1998 among others). For a change in level from 50% oxygenated to 100% oxygenated, the signal is increased by about 8%.

Figure 4-5 summarizes the various components contributing to the MRI signal change from neuronal activity. The discussion so far has described the stages a-g. The next section will discuss the remaining stages.

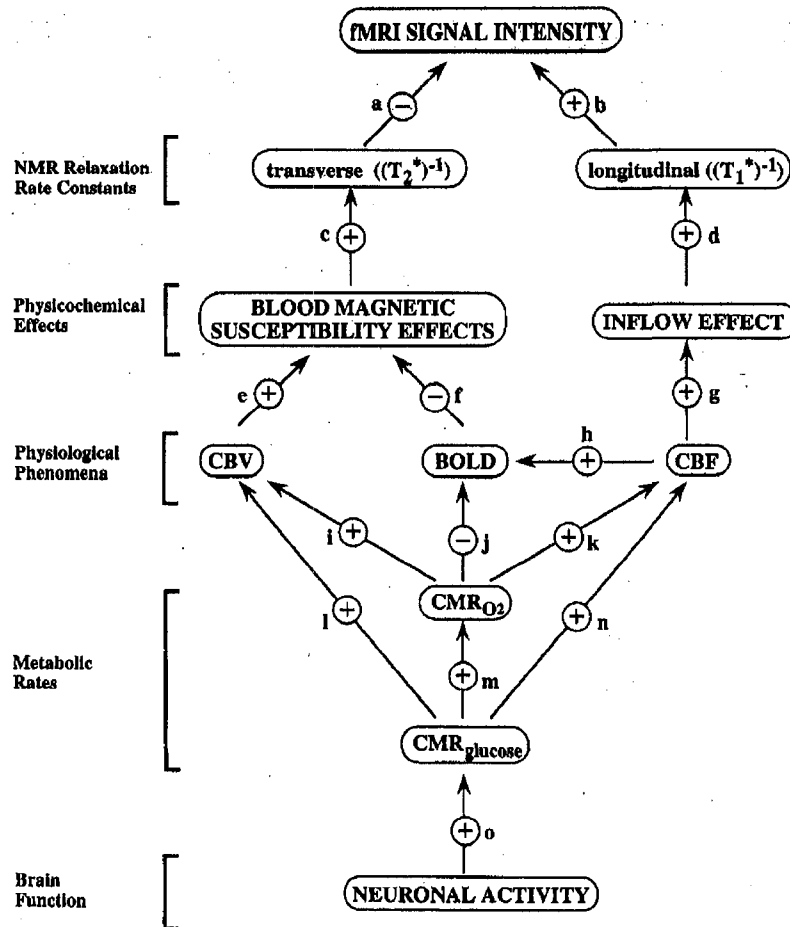


Figure 4-5. Components of the BOLD fMRI Signal (Springer, Patlak, Palyka & Hunag, 1999, p.92)

#### 4.1.2 Physiological Changes

The previous section covered the effect of the blood oxygen level changes on the MRI signal. The next section deals with the link between neuronal activity and the blood oxygen level change. The picture is much less clear because many of the mechanisms are unknown.

Let's start with neuron electrical activity. When a neuron becomes active, it is transmitting electrical signals at a high rate. Each transmission, or firing, requires a transfer of sodium, potassium and calcium between the intraneural and extraneural space. Although firing the neuron uses the chemical and electrical gradient to do its work, the neuron must work against these gradients to recharge itself and be ready for the next fire. This requires energy and the neuron gets its energy from the breakdown of glucose. The first step of this conversion can occur without oxygen (glycolysis) but produces only a small portion of the energy available (2/38). Oxygen is required for the Krebs Cycle and

respiratory chain (Garden & Richardson, 1985) that produces the remainder of the energy available. The processes produce ATP (adenosine triphosphate), which is stored and converted to ADP (adenosine diphosphate) by the cells as energy is needed.

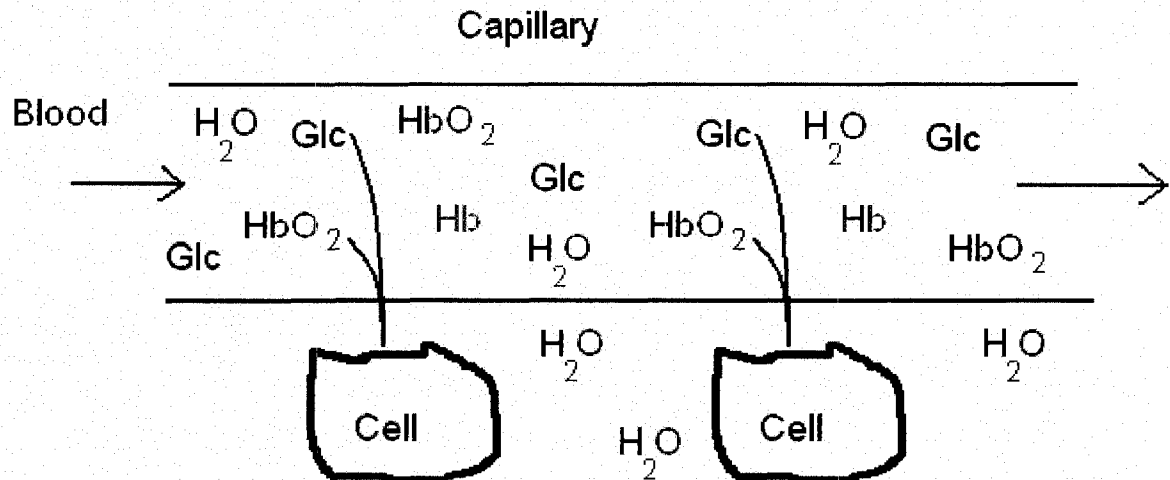


Figure 4-6. Cartoon of the Vascular System Showing Delivery of Oxygen and Glucose

Glucose and oxygen are supplied to the brain through blood as shown in Figure 4-6. It is important to understand the terms used to describe this process. Perfusion is a general term to describe the nutritive delivery of arterial blood to a capillary bed in the tissue. Cerebral blood flow (CBF) is the rate of delivery of arterial blood to the capillary beds of a particular mass of tissue, often expressed as a volume of tissue rather than mass since it is easier to define in imaging. A typical unit is milliliters of blood per 100 grams of tissue per minute and a typical value is 60 ml/100g-min. Cerebral blood volume (CBV) is the fraction of the tissue volume occupied by blood vessels, typically around 4%. Blood velocity is an important physiological parameter that varies depending on the size of the blood vessel. Blood velocity is typically very irregular, due to the heart beat, and because in the capillaries, the size of the vessels is comparable to a red blood cell which restricts blood flow (Villringer, Them, Lindauer, Einhaupl & Dirnagl, 1994). The CBF is related to the CBV through the transit time ( $\tau$ ). Although it is tempting to compare the vascular system to a plumbing system, the vascular system is much more complicated because blood vessels can change in radius. The vascular system and processes that affect blood oxygen level are shown in Figure 4-7.

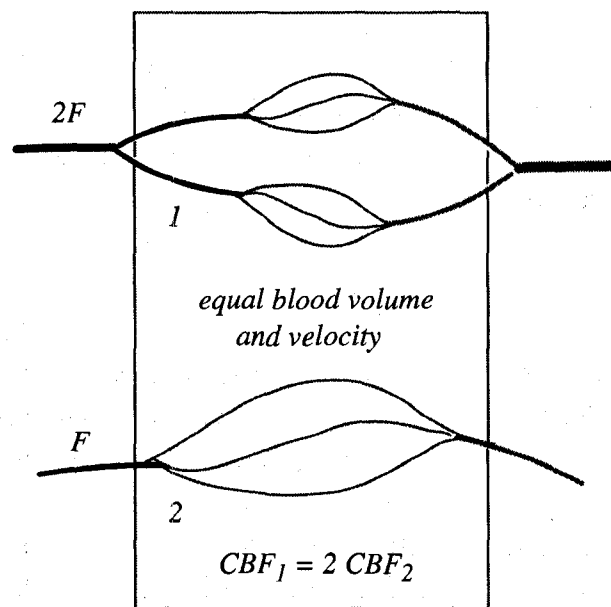
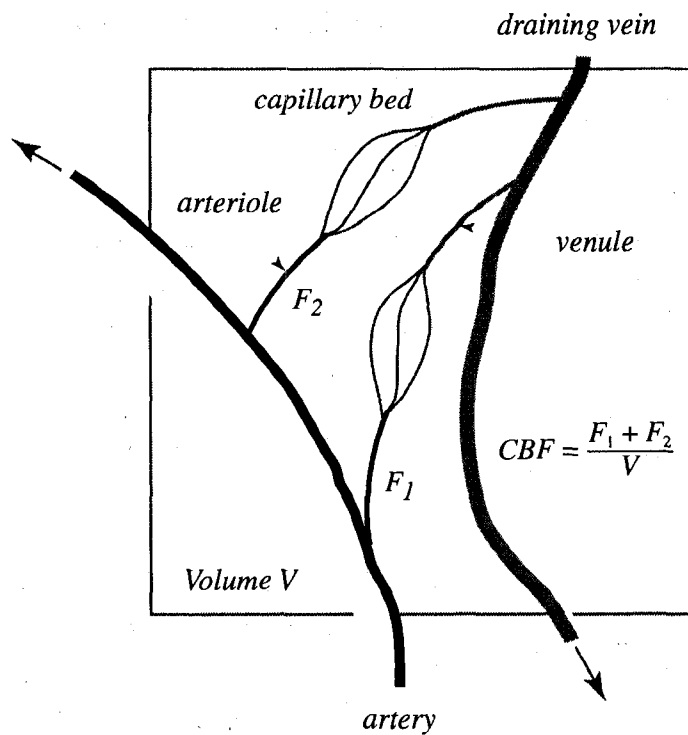


Figure 4-7. Vascular System Model (from Buxton, 2002, p.25)

Blood in the arterioles is close to 100% oxygenated. Arterioles are approximately  $25 \mu\text{m}$  in diameter and make up about 15% of cortical blood volume. Capillaries are typically  $8 \mu\text{m}$  in diameter and make up about 40% of cortical blood volume. Capillaries drain into venules which are approximately  $25\text{-}50 \mu\text{m}$  in diameter and make up about 40% of

cortical blood volume. Oxygenation in capillaries varies linearly along their length so that the average oxygenation can be approximated as the average of the arteriolar and venous oxygenations. Thus the deoxygenation fraction in venules is approximately twice as large as in capillaries, and so venules are twice as magnetic as capillaries. Oxygenation in the venous blood varies between 50 and 75% (at rest, about 40% of the oxygen is extracted – Buxton, 2002, p.115).

In order to supply the increased glucose and oxygen required by an active neuron, blood flow through that area of the brain (regional CBF) will be increased. The increase in blood flow happens to be very large, so although the neurons use more oxygen in total (metabolic rate of oxygen use (CMRO2) increases), the percent of oxygenated blood at the output of the neuron is greater than it was before because of the increased rCBF. As well, the regional cerebral blood volume (rCBV) can increase as veins and capillaries dilate. We have considered in the previous section how changes in the CMRO2, CBF and CBV contribute to the fMRI signal.

There are many unknowns in the process of increasing the blood flow. The mechanism through which this happens is unknown, although there are some candidates including a vasodilatory effect of some product of the energy conversion process. It is also unclear what the spatial extent of the blood flow increase is relative to the neural activity, as it has been shown that the blood flow increases over a wider area than the specific neural activity (Malonek & Grinvald, 1996).

The surprisingly large CBF increase may be required for a small increase in CMRO2 because of the relative rates of oxygen diffusion and binding to haemoglobin (Buxton & Frank, 1997). Alternately, the change in CMRO2 may lag behind the CBF change so that if the process is continued, a new steady-state would be reached (Frahm et al, 1996). The idea of a close coupling between neural activity and rCBF is widely accepted, but the BOLD response is not yet understood in a quantitative way. This is largely due to the lack of a quantitative understanding of the various components contributing to the BOLD response, especially the CMRO2. CMRO2 is much more difficult to measure with PET than CBF because it cannot be measured directly. The measurement requires multiple agents and measurements of several quantities to calculate the CMRO2 (Buxton, 2002). An empirical model has been developed to relate the BOLD signal change ( $\Delta S / S$ ) to changes in CBF, CBV and CMRO2 (Davis et al, 1998).

$$\Delta S / S = S_{\max} (1 - v[m/f]^\beta) \quad (4-2)$$

where,  $S_{\max}$  = maximum BOLD signal change that could be observed

$v = V/V_o$  (activated blood volume normalized to its resting value)

$m = \text{CMRO2}_{\text{act}} / \text{CMRO2}_{\text{rest}}$  (activated state normalized to rest state)

$f = \text{CBF}_{\text{act}} / \text{CBF}_{\text{rest}}$  (activated state normalized to rest state)

From this equation, measuring any 3 variables allows the 4<sup>th</sup> to be calculated, provided  $S_{\max}$  and  $\beta$  are known (or estimable).

Although a quantitative understanding of the BOLD response is unavailable, the experimental results show a good coupling of the local neural activity with BOLD signal, so the BOLD contrast mechanism has become the most widely used technique of functional imaging because of the advantages of MRI versus PET or SPECT (no nuclear medicine facility required).

### 4.1.3 Hemodynamic Response

The hemodynamic response function (HRF) refers to the dynamic response of the BOLD signal to neural activity. Because of the many components involved in the BOLD response, it has a complicated dynamic relationship with the neural events. The general shape is shown in Figure 4-8 and shows a pattern of a small delay (1-3 s) before any response occurs, then a ramp up to a plateau (~6 s), followed by a ramp down and possibly an undershoot for another 20s or so, requiring about 40 s for a full return to baseline (also see Figure 4-9). Also shown in Figure 4-8 is the response to a sustained stimulus, which has the same pattern but includes a plateau of length roughly proportional to the stimulus duration.

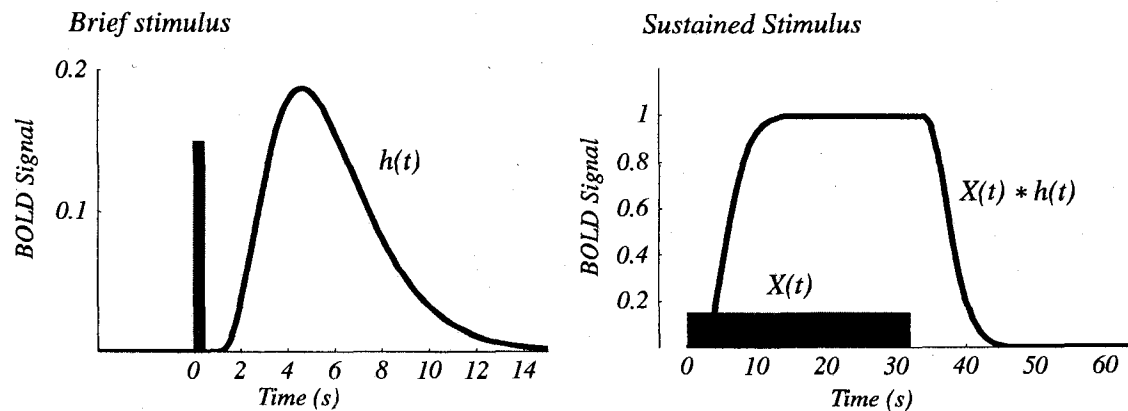


Figure 4-8. Hemodynamic response function to brief stimulus and sustained stimulus (From Buxton, 2002, p. 457)

There is evidence that the HRF varies from person to person, between children and adults, between elderly and adults, between sessions within individuals and even from location to location within an individual (See Figure 4-9) (Aguirre, Zarahn & D'Esposito, 1998; D'Esposito, Zarahn, Aguirre & Rypma, 1999; Richter & Richter, 2003; Neumann, Lohmann, Zysset & von Cramon, 2003).

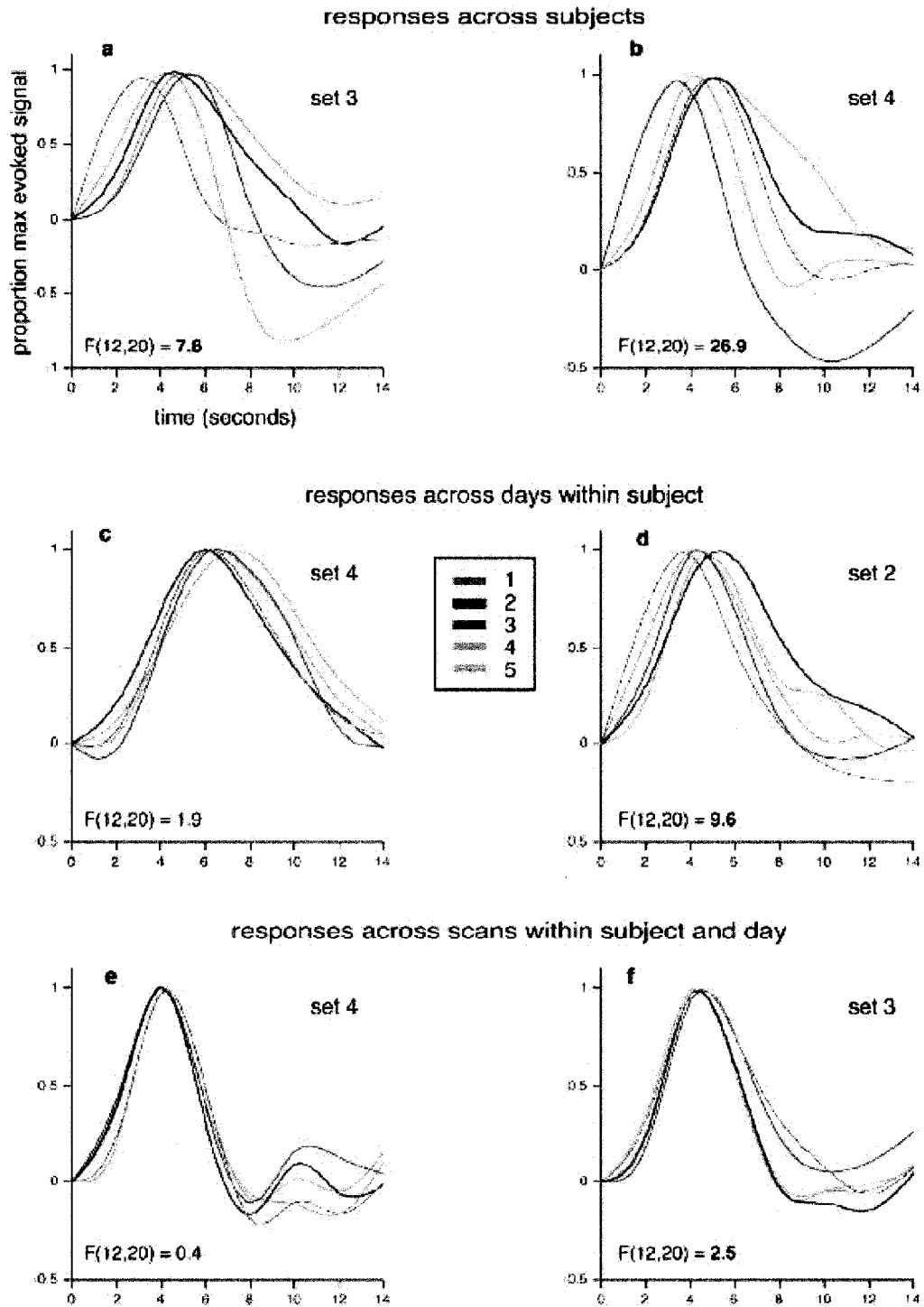


Figure 4-9. Hemodynamic responses in motor cortex for a button press every 16 s: a-b) responses from different subjects, c-d) responses from same subject on different days, e-f) responses of same subject on same day (Aguirre, Zarahn & D’Esposito, 1998, p. 366)

A common feature of the HRF is an undershoot during the return to resting-state. CBF has been measured in tandem with the BOLD response, and does not show undershoot.

However, either a delay in CMRO<sub>2</sub> or CBV could produce the BOLD dynamics (see Figure 4-10), and evidence has been provided for both explanations (Mandeville et al, 1998; Frahm, Kruger, Merboldt & Kleinschmidt, 1996). The debate continues to this day with several presentations on the topic at the 2008 ISMRM Conference (Chen & Pike, 2008; Frahm et al, 2008).

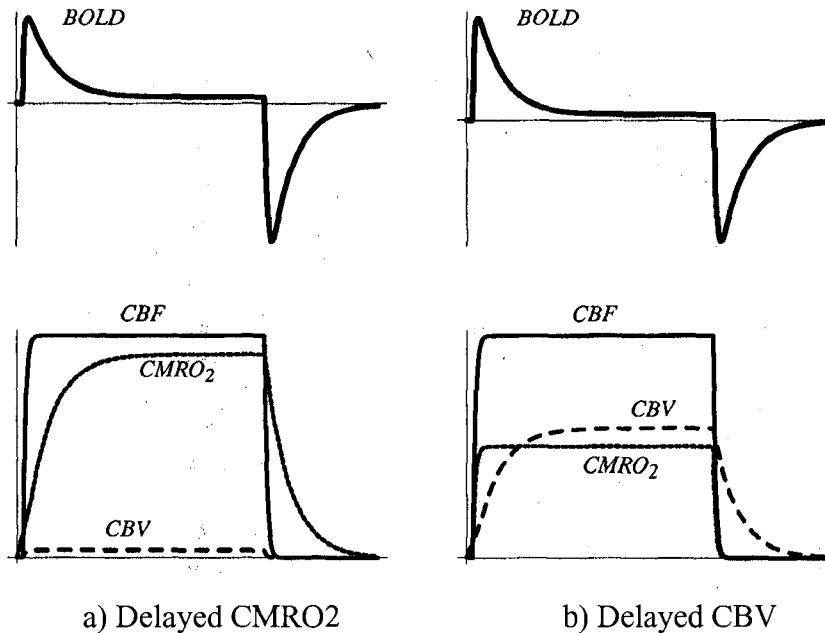


Figure 4-10. Competing models of dynamic changes in BOLD and its components with long stimulus (Buxton, 2002, p.53)

An initial dip has sometimes been observed in the HRF. It was first measured in MRI by Menon and colleagues (Menon et al, 1995) and has received further experimental evidence with optical measurements of an initial decrease in deoxyhemoglobin (Malonek & Grinvald, 1996). The usual interpretation is that the CMRO<sub>2</sub> increases fastest followed by CBF and CBV. However, the initial dip could also be explained by a faster CBV response, similar to how it causes the undershoot. The meaning of the initial dip is still unclear but the optical imaging studies indicate the initial dip may be more spatially localized to the neural activity than the delayed BOLD response (Malonek & Grinvald, 1996).

Another important feature of the HRF is its linearity. Measurements have shown that there is a high degree of linearity in the response (Boynton, Negel, Glover & Heeger, 1996; Dale & Buckner, 1997). Nonlinearity could arise in any of the stages of the BOLD response. The neural activity itself has some nonlinearity since firing rates have been shown to increase to an initial peak followed by a decrease to a plateau level over a few seconds in response to a constant stimulus (Maddess, McCourt, Blakeslee & Cunningham, 1998). Another source of nonlinearity could be the limit of

deoxyhemoglobin, which can't be less than zero. This limit can cause nonlinearity when encountered. The nonlinearities that have been observed are small and thus are generally ignored in analysis.

The HRF has important consequences for experiment design and the limits of temporal resolution. Design of experiments will be discussed later, but for now realize that the most efficient time of stimulus events for block designs and the most efficient spacing for event-related designs is governed by the HRF.

Another important effect of the HRF is on the minimum time resolution that can be measured. Mental chronometry is the study of how long mental events take (Posner, 1978; Posner & Rueda, 2002). For many brain functions, the time between activity in neural regions or the order of activation of regions would be important information. This would require a time measurement on the order of tens of milliseconds. The hemodynamic response suggests that it is impossible to measure neural events with such a time resolution using fMRI. The uncertainty in the exact response, and the variation from person to person and even location to location seemingly makes it impossible. However, the linearity of the time to peak and width of peak have been exploited to make exactly such measurements (Bellgowan, Saad & Bandettini, 2003; Formisano & Goebel, 2003; Menon, Luknowsky & Gati, 1998; Richter et al, 2000).

## **4.2 Design of fMRI Experiments**

Design of fMRI experiments is primarily about having a method that will maximize the chances of finding the effects the experiment is devised to find. The considerations include: the requirements of the desired paradigm, the time sequence of the stimulus (including interstimulus interval), stimulus duration, number of on-off cycles, the number of explanatory variables to include in the design, and the contrasts that will be used for the result. The results are usually a comparison of a stimulus condition to a baseline condition. Explanatory variables may include variables that may confound the results, such as subject movement, or may be extra conditions for which a comparison is required. This section will discuss design from the aspect of paradigms and then move into the 2 main design types – block and event-related. Within event-related designs, there are single-event designs and rapid designs.

### **4.2.1 Paradigms**

The following paragraphs will identify the basic stimulus patterns, comparing them to each other and stating qualitatively how changes in the various factors will affect the design.

A paradigm is the particular task and sequence designed to elicit a desired response in the subject during fMRI scanning. fMRI is useful in many different situations, such as investigating a cognitive or neurophysiological function, investigating the effect of an insult to the brain, or investigating how performance is affected by medication or drugs. The paradigm is chosen according to the demands of the situation, for example, a paradigm may be chosen because it has been shown to activate certain areas that are of interest, or because it uses a cognitive domain that has been shown to be deficient in a certain group of subjects.

Paradigms are usually versions of standard cognitive or neurophysiological tests that have been altered to fit the demands of the fMRI environment. The fMRI environment presents challenges for stimulus presentation and type of response, where auditory stimulus is more difficult to hear and spoken responses can cause movement and signal loss. There are also limitations in the speed and order of presentation, as it takes a certain time to complete the scans (TR, with time between first and last slices). The development of event-related, and especially fast event-related, designs has greatly increased the number of paradigms that can be used in fMRI, but there are still some cognitive tests that are unsuitable. The sequence of the paradigm is an important determinant of the TR. It is also important to take into account effects like habituation, boredom and even motivation.

A standard part of the design of the paradigms is to contrast one or several conditions with a baseline. The idea goes back to Donders (1868) and was called cognitive subtraction. At that time, the idea was to infer the time it took to perform a task by subtraction of the reaction time measurements on 2 separate tasks. The method depends on the assumption of pure insertion which states that adding a component to a task does not change the performance of the original task. Although this assumption may not always hold, the contrast of conditions is still a good idea because there are often subtleties of a task that may not be taken into account during the design. The contrast of a condition with a similar baseline condition helps to remove these other tasks. An example could be having a baseline or control task that requires some of the same input and output functions as the task of interest to remove these uninteresting activations. The danger with trying to refine the task activations is that there could be a major problem during the scan that is not detected because these standard activations are never examined.

An interesting question in paradigm design for group comparisons is whether the task itself should show similar or different group behavioural performance. Earlier in chapter 2, some studies on working memory that exemplify this confound were presented. Interpretation of results seems clearer if the behavioural performance is similar, as was

shown for higher activation of dorso-lateral prefrontal cortex in people with schizophrenia with equivalent behavioural performance.

A desirable addition to paradigm design is to make parametric designs, or designs that have different levels of difficulty. This kind of paradigm is useful for showing how neural activation can change across task difficulty.

#### 4.2.2 Block Design

The block design is a natural design type arising from how studies were designed for PET and takes advantage of the statistical methods that had been developed for PET (Friston et al, 1995). An example time course for a block design is shown in Figure 4-11. Block design applies a constant stimulus (ideally), or multiple stimuli applied with a short interval between them, for a duration of 20s to a minute in an on-off pattern with a baseline situation.

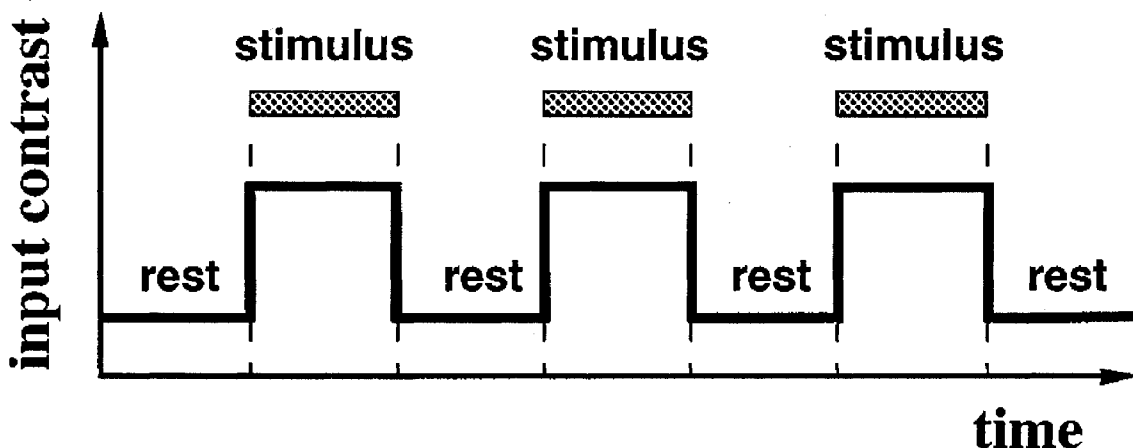


Figure 4-11. Sample Block Design Time Course

The constant or multiple stimuli should result in a smooth hemodynamic response that reaches a plateau and stays there for some time. The pattern can create a large variance in response to the stimuli.

More than one type of stimulus can be included in the design and then contrast between various conditions are possible. It is often useful to have a baseline condition, such as a fixation cross, as well as the 2 conditions to be compared. The fixation baseline allows a contrast between individual conditions and the baseline to be seen and may help to verify that expected common activations are in fact being seen.

Strengths of the block design include: greater activation detection than event-related design, less dependence on HRF and ease of design and analysis.

### 4.2.3 Event-Related

The limitations of block design were felt by researchers interested in applying ERP-type paradigms to fMRI. Paradigms such as oddballs and memory tests that could be wrong or right could not be done with a blocked design. Thus, there was impetus to develop event-related methods that could accommodate these paradigm limitations.

Event-related designs are of 2 main types and were introduced for 2 main reasons. The first reason is to accommodate psychological tasks that cannot be done as a block design. The second is to measure the HRF. The 2 main types are the single-trial and the rapid.

Initial event-related experimental designs used the single trial design (Buckner et al, 1998). In this design, a stimulus instigates a response and the response is allowed some 14-20 s to play out. Because of the small fMRI signal changes within a lot of noise, many single trials must be done and averaged together, as is done with event-related potentials (ERP) measured using electroencephalography (EEG). The time course of the HRF can be calculated from the average of many single trials. Critical questions are how many single trials are required to achieve the accuracy desired, and how much time is required between trials. Bandettini and Cox showed that the optimal interstimulus interval for this type of study depends on the stimulus duration and is 12-14 s for short (50 ms) stimuli (Bandettini & Cox, 2000). This design takes a long time with reasonable numbers of trials and trials lengths. Because of the increased signal changes at high fields, such experiments are usually only done at 4T and above, and historically have involved simple visual, auditory or motor activation paradigms where the expected response is well known and the only uncertainty is the shape of the HRF (eg. Aguirre, Zarahn & D'Esposito, 1998; see Figure 4-9).

As single-trial experiments continued, researchers discovered that rapid event-related paradigms could be done by randomizing the stimulus intervals (Burock, Buckner, Woldorff, Rosen & Dale, 1998; Buckner et al, 1998). Rapid event-related paradigms do not space out the trials so that the hemodynamic responses can be fully separated. Instead, the randomized responses can create enough variance in the BOLD response to be measured and detected in spite of the noise. Rapid event-related paradigms have multiplied and many studies have been published using this design.

Advantages of event-related designs include (Henson, 2000):

1. Ability to randomly intermix events of different types. This prevents predictability and keeps a subject honest.
2. Events can be categorised post-hoc based on the subjects' behaviour. For example, correct and error responses can be separated.

3. The occurrence of events can be initiated by the subject, such as when their perception of a visually ambiguous figure changes (eg. Vase-faces illusion).
4. Treating stimuli as discrete events provides a potentially more accurate model, especially if the interstimulus interval is more than a few seconds. Then the HRF may not be a straightforward delay, ramp up, plateau, ramp down, but something with more variability, eg. No plateau.

#### 4.2.4 Comparison of Designs

The detection of activation depends on the intrinsic activation amplitude 'a', the noise variance  $\sigma$  and the design matrix M. The intrinsic activation amplitude depends on the type of task that is being done and the brain physiology. The noise variance is set by the scanner hardware, the pulse sequence used and the individual subject. So the amplitude and the noise variance are either fixed for a particular paradigm and scanner or, in the case of noise, are not controllable. M, however, is set by the design of the paradigm, so it is the main factor that can be varied to change the sensitivity of the experiment and is the best way to compare different designs.

The various designs are compared in Figure 4-12 (Buxton, 2002, p. 475). The comparison is strictly on the basis of the design matrix resulting from the experimental design. The M values are calculated from a mathematical HRF and the time sequence of each design. The figure compares 3 different designs with 2 different numbers of stimuli. The results show that the blocked design is the most efficient at detecting an activation (Friston, 1999). It also shows that more events improve the detection of activation, but with a diminishing returns pattern, exactly as would be expected from a SNR calculation (SNR increases by square root of number of trials). The results also show that event-related designs are best for estimating the shape of the HRF (Dale, 1999; Birn, Cox & Bandettini, 2002).

The results can also be understood by considering a frequency analysis (See Figure 4-13). The hemodynamic response acts as a smoothing function. The frequency content of each design can be determined and plotted against the hemodynamic response. The sensitivity is then proportional to the area under the combined frequency spectrum. A longer block increases the frequency content under the hemodynamic response and so increases the sensitivity. The same occurs by increasing the number of events in a rapid event-related design, but a single-trial design has a frequency spectrum in which the frequency difference between peaks increases as the interval between stimuli decreases with the result that there is an optimum duration between events of about 12-15 s (Buxton, 2002, p. 476).

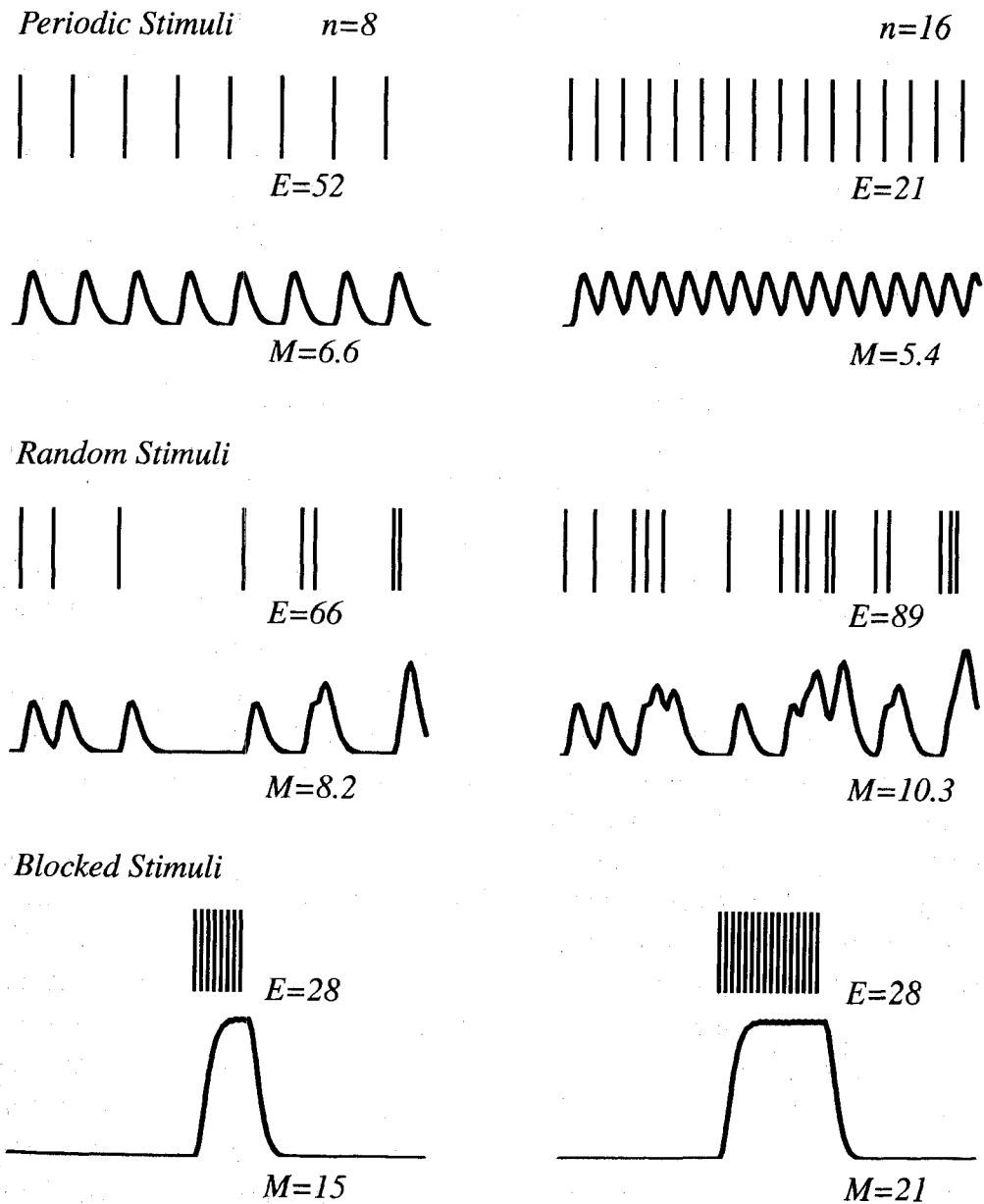


Figure 4-12. Comparison of fMRI Experimental Designs (From Buxton, 2002, p. 475)

A final way to look at the comparison is shown in Figure 4-14. This figure shows that block designs with only 2 blocks are most efficient in comparing activations between 2 conditions (as shown by the highest value of  $1/\sigma_{1,2}$ ). Designs with a baseline between the conditions are most efficient at detecting activations in each condition (highest value of  $1/\sigma_1$ ). Fast event-related designs are less efficient in either case.

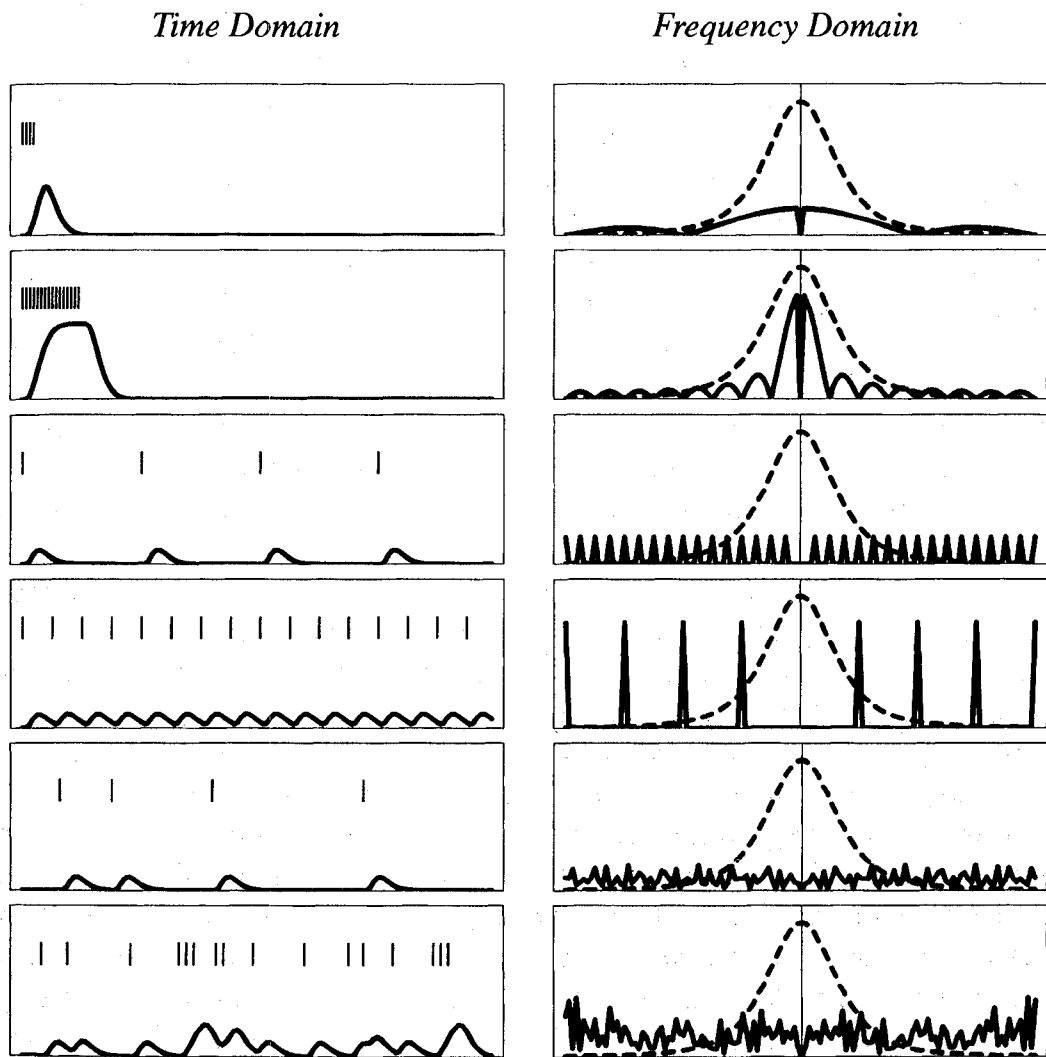


Figure 4-13. Frequency domain comparison of fMRI Designs (From Buxton, 2002, p.477)

The results shown in Figure 4-12 make it clear that a rapid event-related design is less efficient at detecting activation than a comparable block design. A rapid event-related design model needs additional trials to increase its sensitivity to that of a block design. However, rapid event-related designs have an advantage if the desire is to estimate the shape of the HRF. Of course, some designs are not possible to do with block design even if the desire is to find activations. Considering these results, the purpose of the study and the paradigm must be kept in mind in choosing the most efficient design.

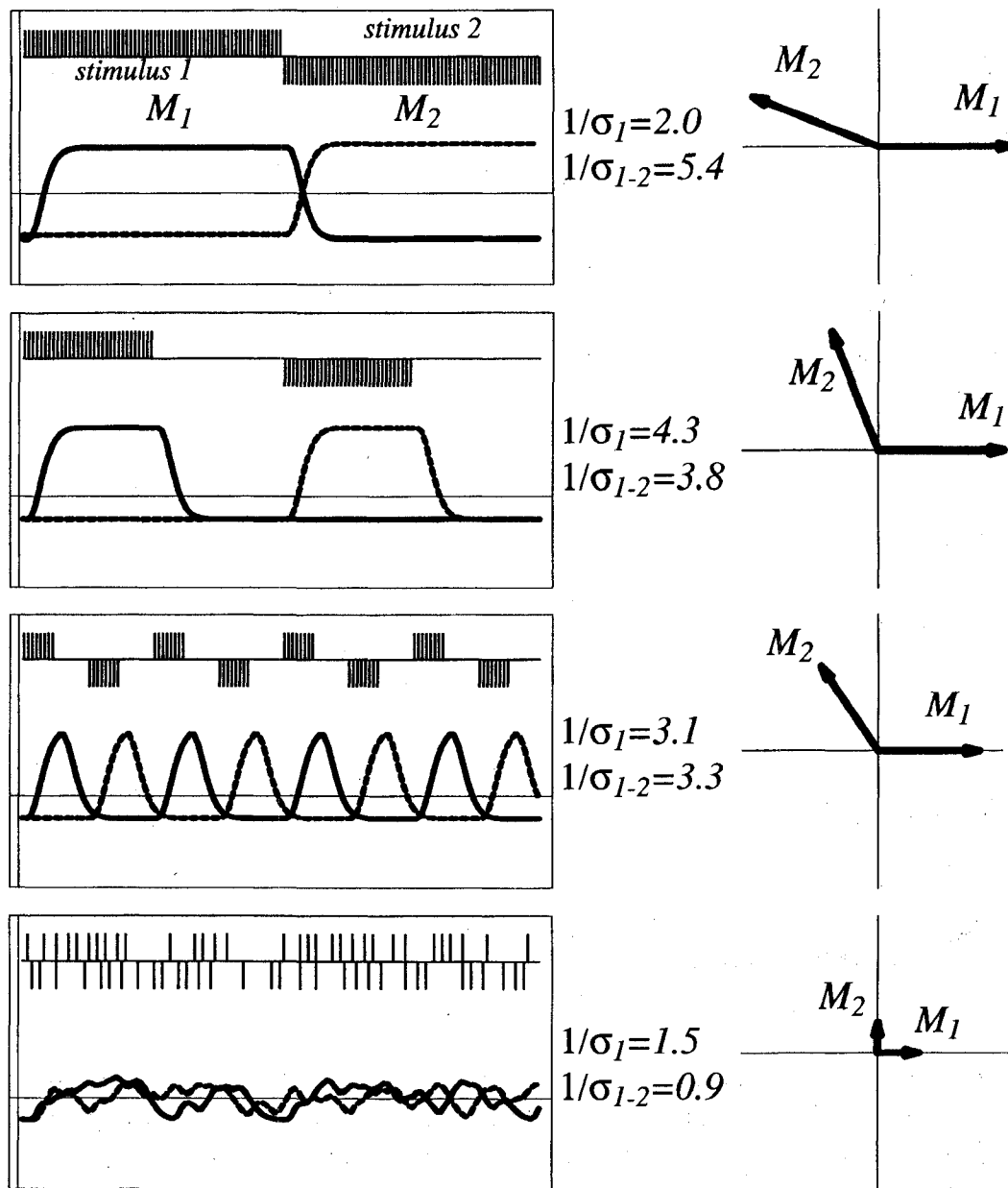


Figure 4-14. Effects of baseline and number of on-off blocks (From Buxton, 2002, p.484)

A final factor is how many explanatory variables to choose. More explanatory variables should be able to increase the variance the model can account for, but at a cost. Each additional explanatory variable reduces the degrees of freedom of the test and potentially makes it more difficult to get a statistically significant result. The loss in sensitivity is directly related to the angle between the explanatory variables. Orthogonal variables cause only a minor loss of sensitivity, whereas explanatory variables in nearly the same

direction cause a large reduction in sensitivity. There is a tradeoff between the number of explanatory variables and the number of on-off cycles. A single cycle with a long block is potentially more sensitive, but also more sensitive to low-frequency drifts and other unmodelled effects, so that in practice, usually 4 to 8 cycles are chosen.

### **4.3 Analysis of fMRI Experiments**

In chapter 5, the detailed use of SPM5 and BrainVoyager QX to analyze functional imaging data will be discussed, but this section will examine the analysis in theory.

We have seen in the previous sections that the signal change from the BOLD response is quite small and has a complicated dynamic relationship to the neural events. A reliable identification of activation, therefore, requires statistical methods and also requires knowledge of the noise in the measurement.

#### **4.3.1 Noise**

The noise in an fMRI signal has 2 main sources: thermal noise and physiological noise. Thermal noise is produced by random stray currents in the body. The noise is spread throughout the raw acquired data so that when the image is reconstructed, the noise is spread through all the voxels. It is common to all MRI measurements and it fits the definition of uniform random Gaussian noise having a constant standard deviation for each voxel, and being independent of the noise in other voxels.

Physiological noise, however, has temporal and spatial structure. Two important sources are cardiac and respiratory (Jezzard, 1999). There are also very low-frequency drifts in signal caused by scanner hardware and slow physiological pulsations. The physiological noise has distinct frequency bands that may be aliased into lower frequencies depending on the sampling rate (TR) (See Figure 4-15). The physiological noise also has a spatial structure so that the noise variance in different voxels is not the same. It, therefore, becomes difficult to separate a weak signal change from a true activation from a larger signal change due to noise without having a separate measure of the noise in each voxel.

Differing noise variability affects the interpretation of activation for different voxels. If 2 voxels have similar changes in BOLD signal but differing noise levels, the analysis might identify the first voxel, with lower noise, as activated but not the second voxel. This approach is primarily concerned with eliminating false positives but does not estimate the likelihood of a voxel being a false negative. That is, it does not state that a voxel that has not been identified as activated is in fact not activated.

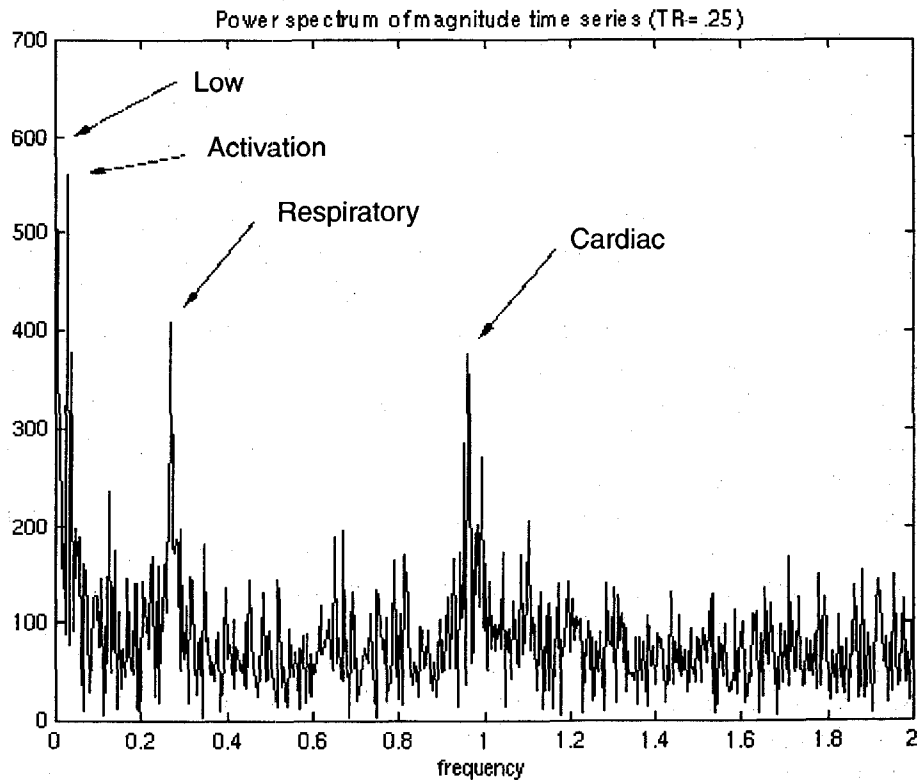


Figure 4-15. Noise Structure (From Buxton, 2002, p.448)

The physiological noise has spatial as well as temporal structure. Pulsatile motion or head motion will affect neighboring voxels in substantially the same way. The temporal and spatial correlation of noise creates problems for the analysis because the analysis requires assumptions about the independence and distribution of the noise.

There are a couple of options that can help to reduce the physiological noise components and bring the remaining noise to a closer approximation of normally distributed random Gaussian noise. The first of these is removing low frequency drifts, which can be accomplished using a high-pass filter. This removes both low-frequency drifts and any physiological noise that was aliased into the low-frequency range. The second is spatial smoothing. This can spread out the spatial structure of physiological noise so that it is closer to being normally distributed random Gaussian noise on a spatial level.

### 4.3.2 Pre-Processing

Figure 4-16 shows an overview of the analysis steps. At a high level of description, the flow is pre-processing, 1<sup>st</sup>-level or individual analysis, and then 2<sup>nd</sup>-level or group-level analysis.

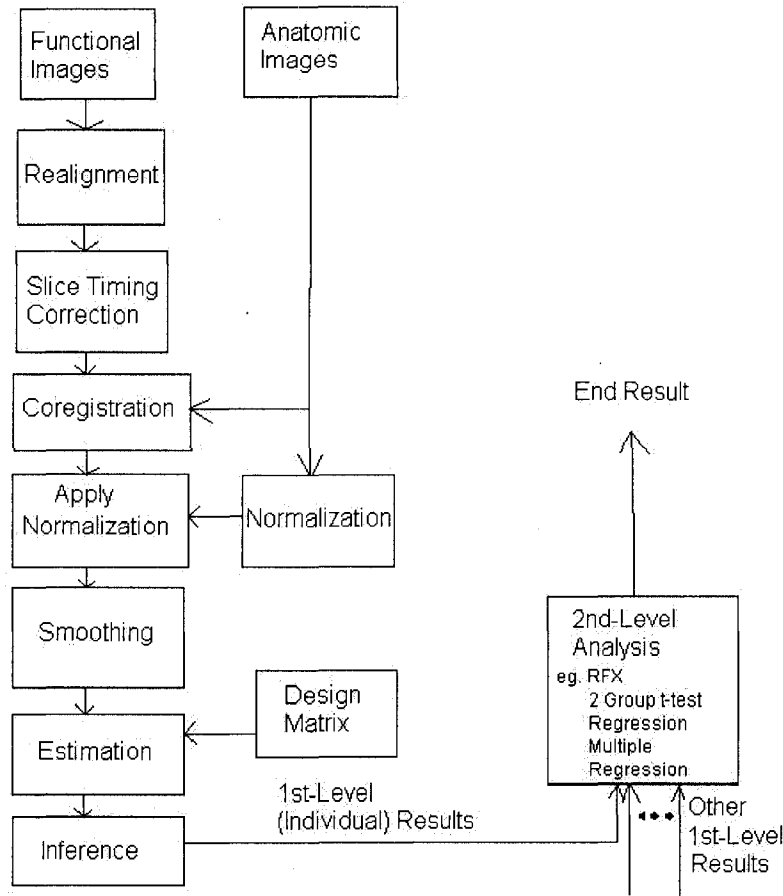


Figure 4-16. Analysis Steps

There are several processing steps that are usually done before the statistical analysis of activation takes place. These steps are done for a multitude of reasons including improving the data for later analysis and matching the voxels to an anatomical location. Not all of these steps will be required depending on the design.

#### 4.3.2.1 Motion Correction

The first step that is normally done is motion correction. A 6 parameter affine rigid body model is used with 3 translations and 3 rotations. Motion correction is done to correct for movement that might carry the signal from one voxel into a neighboring voxel on subsequent images.

Motion correction can be done in 2 ways:

- 1) determine the motions and use these as regressors in the general linear model later on, or
- 2) correct the images slice-by-slice to maintain each voxel in the same place.

#### **4.3.2.2 Slice Timing Correction**

Slice timing correction is required for event-related designs to compensate for the difference in time between acquisitions. Even with echo planar imaging, it takes a significant amount of time to collect all the slices to create an image. Event-related design analysis is very sensitive to the timing of the events, so the data are corrected to make it appear as if all slices are acquired at the same time. A Fourier model of the signal is used to make the corrections. Since the time when each slice is acquired is known, the phase offset can be calculated and used to adjust each slice.

#### **4.3.2.3 Alignment to Anatomical Image**

In looking at the results, we are usually interested to know what anatomical area is being activated. Functional MRI typically provides spatial resolution around 3mm x 3mm x 3mm. Although it is possible to get an idea of the anatomical area from the raw EPI images, it is far better to align the functional images with an anatomical image, which can be high resolution.

Alignment uses a 6 parameter affine rigid body model that uses the 3 translations and 3 rotations to best align the functional images to the anatomical. Automated algorithms may struggle to deal with areas in the functional images that have signal loss – especially the orbital frontal cortex – and distortions in the functional images (see 3.2.2).

#### **4.3.2.4 Normalization**

People do not all have the same size and shape of brain. It is, therefore, difficult to directly compare functional results between individuals. In order to make comparison more valid, each person's brain can be warped into a standard template brain. The neurological standard is the Talairach and Tournoux brain (Talairach & Tournoux, 1988). In neuroimaging, the standard is the ICBM-152 (International Consortium for Brain Mapping) which is based on the Montreal Neurological Institute (MNI) average of 351 MRI images of normal brains.

Normalization uses a 12-parameter affine registration to initially align the brain with the standard. Following that, nonlinear deformations are determined to warp each individual's brain to the standard. Once the transformation is determined for the anatomical images, the same transformation is applied to the functional images.

#### **4.3.2.5 Smoothing**

Smoothing can be in the spatial and temporal domains. As discussed earlier in section 4.3.1, physiological noise contaminates the signal. High-pass filtering in time can remove aliased noise sources, such as the heart rate, and remove any low-frequency drifts in the signal caused by scanner hardware.

Spatial smoothing is required to spread out the spatial structure of physiological noise so that it is closer to being normally distributed random Gaussian noise on a spatial level. This can improve the signal-to-noise ratio and the validity of the statistical analysis. Spatial smoothing also helps to minimize remaining differences in individual brains from the standard.

### 4.3.3 Conventional Statistical Analysis

#### 4.3.3.1 General Linear Model for Single-Subject Designs

The general linear model (GLM) is the standard mathematical tool for estimating the likelihood of activation, and it can be applied to any experimental design. The GLM can be applied to a system with any number of explanatory variables and is expressed in the equation below.

$$Y = X\beta + \varepsilon \quad (4-3)$$

where  $Y(t)$  = Measured Response

$X(t)$  = Design matrix (matrix of conditions hypothesized to cause signal change)

$\beta$  = Parameter estimates

$\varepsilon$  = Residual error ( $Y_{\text{actual}}(t) - Y(t)$ )

In general the model works by using the explanatory variables ( $X(t)$ , which can be a convolution of the time course with a HRF as in Figure 4-17) to create an expected signal at each voxel by adjusting the parameters ( $\beta$ ) of each explanatory variable to minimize the residual error ( $\varepsilon$ ). Then the parameters are compared to the variance to determine its statistic. The results are used to create an image (a statistical parameter map or SPM) by showing voxels with parameters above a statistically significant threshold.

The significance of the explained variance is assessed in the general case of multiple explanatory variables by the F-statistic, which becomes the t-statistic for the special case of 1 explanatory variable. Under the assumption of normally distributed random Gaussian noise, the significance of the F or t-statistic is known.

It is important to note that the value of the F or t-statistic is a measure of probability or likelihood that the voxel in question is activated. This is not the same as the strength of the activation, which must be assessed by looking at the percent signal change.

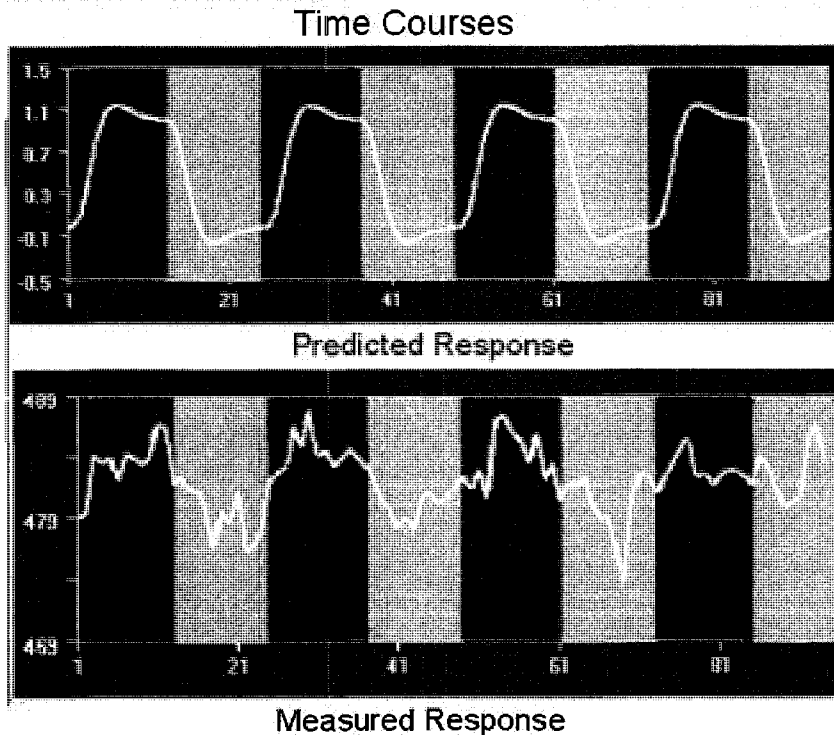


Figure 4-17. Predicted Response Created from Convolution of Boxcar function with Hemodynamic Response and A Measured Response. Colors Show the Variation in Task.

#### 4.4.2.2 General Linear Model in 2<sup>nd</sup>-Level (Group) Analysis

Group analysis can be performed to compose an activation map of a single group, or to determine differences in the activations between 2 or more groups. The group maps can be made in 2 ways, fixed effects or random effects.

Fixed effects analysis is applicable only to the subjects actually studied. It does not take into account the variance at each voxel, but instead is like adding each subject's time course to the next in one great long string. Fixed effects analysis can produce very high activations and is useful for small sample sizes, but the results are not extendible to populations.

Random effects (RFX) analysis method analyzes the individuals in a way that is extendible to populations. The results of each subject are used to obtain a mean and variance at each voxel. Then a statistical test is performed, such as a t-test, to determine whether the activation is significant or, when comparing different groups, whether the difference in activation is significant.

### **4.3.4 Event-Related Analysis Options**

The analysis methods discussed above are developed from PET studies and are generally applicable to block designs (Friston et al, 1995). Event-related designs have some complications in the basic method, mainly because of the hemodynamic response (HRF).

We have seen how the HRF can vary between individuals, and even between an individual on different days, or different regions in same brain. The method described previously depends on creating an expected signal by convolving the HRF with the sequence of tasks. Although the HRF did not make much difference for the block design, it makes a lot of difference for event-related designs.

There are a few methods to compensate for differing HRF. The SPM5 analysis program includes options to vary the timing of the hemodynamic response as well as the amplitude, so a canonical hemodynamic shape is used, but the amplitude, the time to peak response and the width of the response can be varied to best match the data.

Another method to deal with the issue is to use a separate functional test to measure the HRF in individuals, and then fit the measured HRF to make the best estimates for each individual. This can produce improvement on an average basis and substantial improvements in individuals (64% improvement in one example; Hollmann et al, 2008).

To determine hemodynamic shapes, we can use single-event studies or we can analyze the designs using a method much like ERPs using selective averaging. Since we know the time at which each stimulus occurs, we can take the time course around each of these times and add them all together to create an averaged HRF (Dale & Buckner, 1997).

### **4.3.5 Other Analysis Options**

Recently, many other methods of analysis have become more widely used. One of these is Independent Component Analysis (ICA) (Bell & Sejnowski, 1995; McKeown et al, 1998).

ICA can be done on temporal or spatial domain. An algorithm goes through the data and separates it into independent components – up to as many components as there are data points. The spatial map of components and the time course of the components are individually examined to identify useful components, i.e. related to the task. The method is finding more and more applications (e.g. Calhoun, 2006; Jagannathan et al, 2008).

Resting state analysis is another technique which is gaining acceptance. Resting state analysis looks at the correlations in low-frequency physiological noise between brain areas (Biswal, Yetkin, Haughton & Hyde, 1995). The data are acquired with the subject

in the scanner but performing no particular task during the scan. The data are analyzed by choosing a starting region-of-interest (ROI) and then correlating the averaged time sequence of this ROI across the brain. By choosing different ROIs, different networks can be identified. Resting state analysis is being used more and more in schizophrenia (Oh, Shenton, Westin & Kubicki, 2008; Camchong, Bell, Fried, Muller & MacDonald, 2008). Resting state analysis can also be done with ICA (Greicius, Srivasta, Reiss & Menon, 2004).

This chapter has dealt with the theory of fMRI. The next section will go into detail in the application of fMRI to a study to identify differences in brain activation in people with schizophrenia.

## References:

Aguirre, G.K., Zarahn, E. & D'Esposito, M. (1998). The variability of human, BOLD hemodynamic responses. *Neuroimage*, 8,360-369.

Bandettini, P.A., Wong, E.C., Hinks, R.S., Tikofsky, R.S. & Hyde, J.S. (1992). Time course EPI of human brain function during task activation. *Magnetic Resonance in Medicine*, 25, 390-397.

Bandettini, P.A. & Cox, R.W. (2000). Event-Related fMRI contrast when using constant interstimulus interval: Theory and experiment. *Magnetic Resonance in Medicine*, 43, 540-548.

Bell, A.J. & Sejnowski, T.J. (1995). An information-maximization approach to blind separation and blind deconvolution. *Neural Computation*, 7, 1129-1159.

Bellgowan, P.S.F, Saad, Z.S. & Bandettini, P.A. (2003). Understanding neural system dynamics through task modulation and measurement of functional MRI amplitude, latency and width. *Proceedings of the National Academy of Science USA*, 100(3), 1415-1419.

Belliveau, J.W., Kennedy, D.N., McKinstry, R.C., Buchbinder, B.R., Weisskoff, R.M., Cohen, M.S., Vevea, J.M., Brady, T.J. & Rosen, B.R. (1991) Functional mapping of the human visual cortex by magnetic resonance imaging. *Science*, 254, 716-719.

Birn, R.M., Cox, R.W. & Bandettini, P.A. (2002). Detection versus estimation in event-related fMRI: Choosing the optimal stimulus timing. *Neuroimage*, 15, 252-264.

Biswal, B., Yetkin, F.Z., Haughton, V.M. & Hyde, J.S. (1995). Functional connectivity in the motor cortex of resting human brain using echo-planar MRI. *Magnetic Resonance in Medicine*, 34, 537-541.

Boynton, G.M., Negel, S.A., Glover, G.H. & Heeger, D.J. (1996). Linear systems analysis of functional magnetic resonance imaging in human V1. *Journal of Neuroscience*, 16, 4207-4221.

Boxerman, J.L., Bandettini, P., Kwong, K., Baker, J., Davis, T., Rosen, B & Weisskoff, R. (1995). The intravascular contribution to fMRI signal change: Monte carlo modeling and diffusion-weighted studies in vivo. *Magnetic Resonance in Medicine*, 34, 4-10.

Bronskill, M.J., & Graham, S.J. (1992). NMR characteristics of tissue. In *The Physics of MRI 1992 AAPM Summer School Proceedings*. Woodbury, NY: American Institute of Physics Inc.

Buckner, R.L., Goodman, J., Burock, M., Rotte, M., Koutstaal, W., Schacter, D., Rosen, B.R., & Dale, A.M. (1998). Functional-anatomic correlates of object priming in humans revealed by rapid presentation event-related fMRI. *Neuron*, 20, 285-296.

Burock, M.A., Buckner, R.L., Woldorff, M.G., Rosen, B.R. & Dale, A.M. (1998). Randomized event-related experimental designs allow for extremely rapid presentation rates using functional MRI. *Neuroreport*, 9, 3735-3739.

Buxton, R.B. & Frank, L. (1997). A model for the coupling between cerebral blood flow and oxygen metabolism during neural stimulation. *Journal of Cerebral Blood Flow Metabolism*, 14, 365-372.

Buxton, R.B. (2002). *Introduction to functional magnetic resonance imaging: Principles and techniques*. New York: Cambridge University Press.

Calhoun, V.D., Adali, T., Giuliani, N.R., Pekar, J.J., Kiehl, K.A. & Pearlson, G.D. (2006). Method for multimodal analysis of independent source differences in schizophrenia: Combining gray matter structural and auditory oddball functional data. *Human Brain Mapping*, 27, 47-62.

Camchong, J., Bell, C., Fried, P., Muller, B. & MacDonald, A. (2008). Functional connectivity abnormalities in schizophrenia during rest. *Biological Psychiatry*, 63, 251S.

Chen, J.J. & Pike, G.B. (2008). Origins of the BOLD post-stimulus undershoot. 18<sup>th</sup> Conference of the International Society for Magnetic Resonance in Medicine, 3-9 May, 2008, Toronto, Canada.

Dale, A.M. & Buckner, R.L (1997). Selective averaging of rapidly presented individual trials using fMRI. *Human Brain Mapping*, 5, 329-340.

Dale, A.M. (1999). Optimal experimental design for event-related fMRI. *Human Brain Mapping*, 8(2-3), 109-114.

Davis, T.L., Kwong, K.K., Weisskoff, R.M. & Rosen, B.R. (1998). Calibrated functional MRI: Mapping the dynamics of oxidative metabolism. *Proceedings of the National Academy of Sciences USA*, 95, 1834-1839.

D'Esposito, M., Zarahn, E., Aguirre, G.K. & Rypma, B. (1999). The effect of normal aging on the coupling of neural activity to the BOLD hemodynamic response. *Neuroimage* 10, 6-14.

Donders, F.C. (1868; 1969). On the speed of mental processes. *Acta Psychologica*, 30, 412-431.

Formisano, E. & Goebel, R. (2003). Tracking cognitive processes with functional MRI mental chronometry. *Current Opinion in Neurobiology*, 13, 174-181.

Fox, P.T. & Raichle, M.E. (1986). Focal physiological uncoupling of cerebral blood flow and oxidative metabolism during somatosensory stimulation in human subjects. *Proceedings of the National Academy of Sciences USA*, 83(4), 1140-1144.

Frahm, J., Bruhm, H., Merboldt, K.D. & Hanicke, W. (1992). Dynamic MR imaging of human brain oxygenation during rest and photic stimulation. *Journal of Magnetic Resonance Imaging*, 2(5), 501-505.

Frahm, J., Kruger, G., Merboldt, K-D. & Kleinschmidt, A. (1996). Dynamic uncoupling and recoupling of perfusion and oxidative metabolism during focal activation in man. *Magnetic Resonance in Medicine*, 35, 143-148.

Frahm, J., Baudewig, J., Kallenberg, K., Kastrup, A., Merboldt, D. & Dechent, P. (2008). The post-stimulation undershoot in BOLD fMRI of human brain is not caused by elevated cerebral blood volume. 18<sup>th</sup> Conference of the International Society for Magnetic Resonance in Medicine, 3-9 May, 2008, Toronto, Canada.

Friston, K.J., Holmes, A.P., Worsley, K.J., Poline, J.-B., Frith, C.D. & Frackowiak, R.S.J. (1995) Statistical parametric maps in functional imaging: A general linear approach. *Human Brain Mapping*, 2, 189-210.

Friston, K.J., Zarahn, E., Josephs, O., Henson, R.N. & Dale, A.M. (1999). Stochastic designs in event-related fMRI. *Neuroimage*, 10(5), 607-619.

Garden, J.E. & Richardson, R.A. (1985). *Chemistry of the body*. Toronto, Canada: John Wiley & Sons Canada Limited.

Greicius, M.D., Srivastava, G., Reiss, A.L. & Menon, V. (2004). Default-mode network activity distinguishes alzheimer's disease from healthy aging: Evidence from functional MRI. *Proceedings of the National Academy of Sciences USA*, 101(7), 4637-4642.

Henson, R. (2000), Event-related fMRI: Introduction, statistical modelling, design optimisation and examples. 5<sup>th</sup> Congress of the Cognitive Neuroscience Society of Japan.

Hollmann, M., Moench, T., Baecke, S., Luchtman, M., Tempelmann, C., Stadler, J., & Bernarding, J. (2008). Increased statistical power in event-related real-time fMRI (erfMRI) using individual hemodynamic response function: First results at 3T and 7T. *Proceedings of the International Society for Magnetic Resonance in Medicine*, 16, p 3624. Toronto, Canada.

Jagannathan, K., Pearlson, G.D., Calhoun, V.D., Kraut, M.A., Hart, J. & Assaf, M. (2008). Functional network connectivity in schizophrenia during semantic memory task. *Biological Psychiatry*, 63, 54S.

Jezzard, P. (1999) Physiological noise: Strategies for correction in functional MRI. In C.T.W. Moonen & P.A. Bandettini (Eds.) *Functional MRI* (Chap. 16). Heidelberg, Germany: Springer-Verlag.

Kennan, R.P. (1999). Gradient echo and spin echo methods for functional MRI in functional MRI. In C.T.W. Moonen & P.A. Bandettini (Eds.) *Functional MRI* (Chap. 12). Heidelberg, Germany: Springer-Verlag.

Kwong, K.K., Belliveau, J.W., Chesler, D.A., Goldberg, I.E., Weisskoff, R.M., Poncelet, B.P., Kennedy, D.N., Hoppel, B.E., Cohen, M.S., Turner, R., Cheng, H-M., Brady, T.J., & Rosen, B.R. (1992). Dynamic magnetic resonance imaging of human brain activity during primary sensory stimulation. *Proceedings of the National Academy of Science USA*, 89, 5675-5679.

Landau, W.M., Freygang, W.H.J., Roland, L.P., Sokoloff, L, & Kety, S.S. (1955). The local circulation of the living brain: Values in unanesthetized and anesthetized cat. *Transactions of the American Neurology Association*, 80, 125-129.

Lassen, N.A., Hoedt-Rasmussen, K., Sorensen, S.C., Skinhoj, E., Cronquist, S., Bodfors, B. & Ingvar, D.H. (1963). Regional cerebral blood flow in man determined by krypton-85. *Neurology*, 13, 719-727.

- Maddess, T., McCourt, M.E., Blakeslee, B. & Cunningham, R.B. (1988). Factors governing the adaptation of cells in area 17 of the cat visual cortex. *Biological Cybernetics*, 59, 229-236.
- Malonek, D. & Grinvald, A. (1996). Interactions between electrical activity and cortical microcirculation revealed by imaging spectroscopy: Implications for functional brain mapping. *Science*, 272, 551-554.
- Mandeville, J.B., Marota, J.J.A., Kosofsky, B.E., Keltner, J.R., Weissleder, R., Rosen, B.R. & Weisskoff, R.M. (1998). Dynamic functional imaging of relative cerebral blood volume during rat forepaw stimulation. *Magnetic Resonance in Medicine*, 39, 615-624.
- Mandeville, J.B., Marota, J.J.A., Ayata, C., Moskowitz, M.A., Weisskoff, R.M. & Rosen, B.R. (1999). MRI measurement of the temporal evolution of relative CMRO2 during rat forepaw stimulation. *Magnetic Resonance in Medicine*, 42, 944-951.
- McKeown, M.J., Makeig, S., Brown, G.G., Jung, T-P., Kindermann, S.S., Bell, A.J., & Sejnowski, T.J. (1998). Analysis of fMRI data by blind separation into independent spatial components. *Human Brain Mapping*, 6, 160-188.
- Menon, R.S., Ogawa, S., Hu, X., Strupp, J.S., Andersoen, P., & Ugurbil, K. (1995) BOLD based functional MRI at 4 Tesla includes a capillary bed contribution: Echo-planar imaging mirrors previous optical imaging using intrinsic signals. *Magnetic Resonance in Medicine*, 33, 453-459.
- Menon, R.S., Luknowsky, D.C. & Gati, J.S. (1998). Mental chronometry using latency-resolved functional MRI. *Proceedings of the National Academy of Sciences USA*, 95, 10902-10907.
- Neumann, J., Lohmann, G., Zysset, S. & von Cramon, D.Y. (2003). Within-subject variability of BOLD response dynamics. *Neuroimage*, 19, 784-796.
- Obrist, W.D., Thompson, H.K., King, C.H. & Wang, H.S. (1967). Determination of regional cerebral blood flow by inhalation of 133-Xenon. *Circulation Research*, 20, 124-135.
- Ogawa, S., Lee, T.M., Kay, A.R. & Tank D.W. (1990). Brain magnetic resonance imaging with contrast dependent on blood oxygenation. *Proceedings of the National Academy of Sciences USA*, 87, 9868-9872.

- Ogawa, S. Tank, D.W., Menon, R., Ellermann, J.M., Kim, S-G. Merkle, H. & Ugurbil, K. (1992). Intrinsic signal changes accompanying sensory stimulation: Functional brain mapping with magnetic resonance imaging. *Proceedings of the National Academy of Sciences USA*, 89, 5951-5955.
- Oh, J.S., Shenton, M.E., Westin, C-F. & Kubicki, M. (2008). Decreased resting-state functional connectivity in schizophrenia. *Biological Psychiatry*, 63, 55S.
- Pauling, L. & Coryell, C.D. (1936). The magnetic properties and structure of hemoglobin, oxyhemoglobin and caonmonoxyhemoglobin. *Proceedings of the National Academy of Sciences USA*, 22, 210-216.
- Posner, M.I. (1978). *Chronometric explorations of mind*. London: Oxford University Press.
- Posner, M.I. & Rueda, M.R. (2002). Mental chronometry in the study of individual and group differences. *Journal of Clinical and Experimental Neuropsychology*, 24(7), 968-976.
- Raichle, M.E., Martin, W.R.W., Herscovitch, P., Mintun, M.A. & Markham, J. (1983). Brain blood flow measured with intravenous H<sub>2</sub>O<sup>15</sup>. II. Implementation and validation. *Journal of Nuclear Medicine*, 24, 790-798.
- Raichle, M.E. (1987). Circulatory and metabolic correlates of brain function in normal humans. In F. Plum (Ed.), *Handbook of physiology: The nervous system Vol.5 Higher functions of the brain* (pp. 643-674). Bethesda, MD: American Physiological Society.
- Reivich, M., Kuhl,, D., Wolf, A., Greenberg, J. Phelps, M., Ido, T., Casella, V., Hoffman, E., Alavi, A. & Sokoloff, L. (1979). The [<sup>18</sup>F] fluorodeoxyglucose method for the measurement of local cerebral glucose utilization in man. *Circulation Research*, 44, 127-137.
- Richter, W., Somorjai, R., Summers, R., Jarmasz, M., Menon, R.S., Gati, J.S., Georgopoulos, A.P., Tegeler, C., Ugurbil, K., & Kim, S-G. (2000). Motor area activity during mental rotation studied by time-resolved single-trial fMRI. *Journal of Cognitive Neuroscience*, 12(2), 310-320.
- Richter, W. & Richter, M. (2003). The shape of the fMRI BOLD response in children and adults changes systematically with age. *Neuroimage*, 20, 1122-1131.

Rosen, B.R., Belliveau, J.W., Vevea, J.M., & Brady, T.J. (1990). Perfusion imaging with NMR contrast agents. *Magnetic Resonance in Medicine*, 14, 249-265.

Sokoloff, L., Reivich, M., Kennedy, C., Des Rosiers, M.H., Patlak, C.S., Pettigrew, K.D., Sakurada, O., & Shinohara, M. (1977). The [14C]deoxyglucose method for the measurement of local glucose utilization: Theory, procedure and normal values in the conscious and anesthetized albino rat. *Journal of Neurochemistry*, 28, 897-916.

Song, A.W., Wong, E.C., Tan, S.G., & Hyde, J.S. (1996). Diffusion weighted fMRI at 1.5T. *Magnetic Resonance in Medicine*, 35, 155-158.

Springer, Jr, C.S., Patlak, C.S., Palyka, I., & Hunag, W. (1999). Principles of susceptibility contrast-based functional MRI: The sign of the functional MRI response. In C.T.W. Moonen & P.A. Bandettini (Eds.), *Functional MRI* (Chap. 9). Heidelberg, Germany: Springer-Verlag.

Talairach, P. & Tournoux, J. (1988). *A stereotaxic coplanar atlas of the human brain*. Stuttgart, Germany: Thieme.

Thulborn, K.R., Waterton, J.C., Matthews, P.M., & Radda, G.K. (1982). Oxygenation dependence of the transverse relaxation time of water protons in whole blood at high field. *Biochim. Biophys Acta (G)*, 714(2), 265-270.

Turner, R., LeBihan, D., Moonen, C.T.W., Despres, D., & Frank, J. (1991). Echo-planar time course of MRI of cat brain oxygenation changes. *Magnetic Resonance in Medicine*, 22, 159-166.

Villringer, A., Them, A., Lindauer, U., Einhaupl, K., & Dirnagl, U. (1994). Capillary perfusion of the rat brain cortex: An in vivo confocal microscopic study. *Circulation Research*, 75, 55-62.

Weisskoff, R.M., Zuo, C.S., Boxerman, J.L. & Rosen, B.R. (1994). Microscopic susceptibility variation and transverse relaxation: Theory and experiment. *Magnetic Resonance in Medicine*, 31, 601-610.

Wyper, D.J. & Montaldi, D. (2000). Applications of SPECT in cognitive neuroscience. *Neurology and psychiatry. Behavioural Neuroscience*, 12, 1-2.

Yacoub, E., Ugurbil, K., & Harel, N. (2006). The spatial dependence of the poststimulus undershoot as revealed by high-resolution BOLD- and CBV-weighted fMRI. *Journal of Cerebral Blood Flow & Metabolism*, 26, 634-644.

## **Chapter 5: Investigation of Functional and Structural Abnormalities in the Anterior Cingulate Cortex in Recent-Onset and Chronic Schizophrenia**

An earlier chapter (chapter 2) described schizophrenia and some of the previous fMRI studies of schizophrenia. This chapter opens with the background and motivation for this current study, followed by the methods, results and discussion.

### **5.1 Background/Motivation**

Cognitive deficits are an important symptom to investigate in schizophrenia. Although positive symptoms can often be controlled by antipsychotic drugs, residual negative symptoms and cognitive deficits persistently undermine the quality of life of sufferers and are associated with poorer long-term outcome (Jobe & Harrow, 2005; Green, 1996; Green, Kern, Braff & Mintz, 2000). Improvement in cognitive skills may thus produce gains in emotional, physical, social, and vocational adaptation (Matza et al, 2006). A wide spectrum of relatively treatment resistant neuropsychological deficits is apparent in schizophrenia (Woodward, Purdon, Meltzer & Zald, 2005), but the cerebral basis of this pathology remains speculative. One limitation in the articulation of cerebral pathology related to the cognitive deficits in schizophrenia is that most of the tests used to measure cognitive impairment are too complicated for examination within functional imaging paradigms of cerebral pathology in schizophrenia. It is thus extremely important to return to more basic cognitive tasks that allow a more precise delineation of relevant cerebral structure and function.

#### **5.1.1 Reaction Time in Schizophrenia**

A reaction time task is perhaps the simplest method for demonstrating cognitive limitations in schizophrenia, and it is well suited to functional neuroimaging paradigms. In schizophrenia, visual or auditory reaction time is a well-established measure dating to the 1920s and 1930s (Wells & Kelley, 1922; Huston, Shakow & Riggs, 1937).

Simple reaction time tasks require a single response to the stimulus, whereas choice reaction time (CRT) requires a decision among several possible responses that depends on the stimulus. The modality (auditory, visual, tactile) makes a difference in the reaction time, with auditory being faster than visual (Naito et al, 2000). As well, the preparatory interval (period of time before the stimulus) affects reaction time with a longer reaction time resulting from a longer preparatory interval. Variables of interest

include median reaction time, interquartile range (25% to 75%), mistakes (incorrect response to stimulus), errors of omission (no response to a stimulus) and errors of commission (responding without a stimulus).

Similar to measures of more complex cognitive functions, the reaction time deficits in schizophrenia are related to poor outcome. Studies by Zahn and Carpenter and Cancro et al in the 1970s correlated longer RT with increased hospitalization for schizophrenia (Zahn & Carpenter 1978; Cancro, Sutton, Kerr & Sugarman, 1971). In particular, patients who would improve versus who would not improve with treatment had different average profiles on the basis of their admission RT tests (See Figure 5-1).

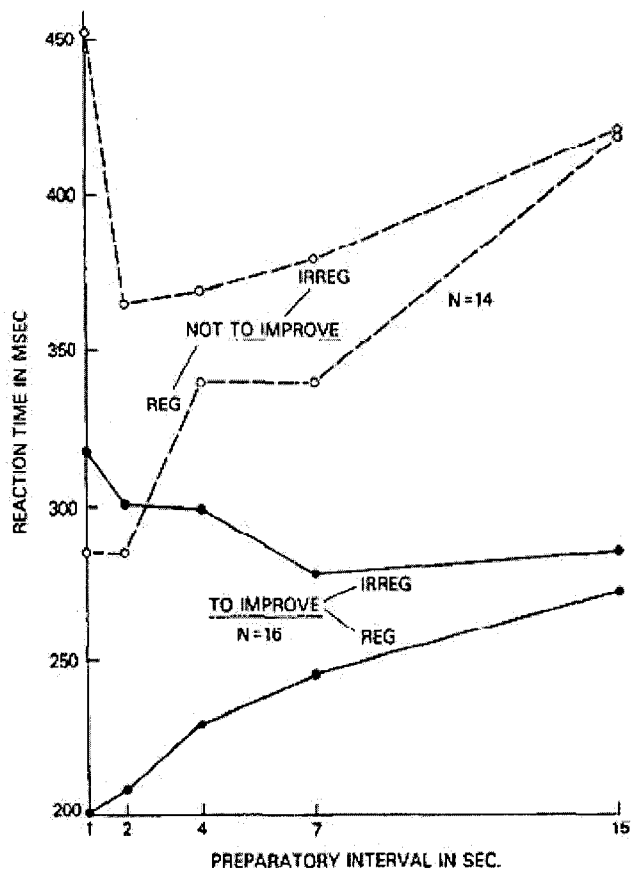


Figure 5-1. Reaction Time as a Function of Preparatory Interval Showing Patients Who Improved (Solid Lines) and Who Did Not Improve (Dashed Lines) at Regular and Irregular Preparatory Interval. From Zahn & Carpenter (1978)

Silverstein et al included auditory simple reaction time in a study involving several other common neurocognitive tests (Silverstein, Schenkel, Valone & Nuernberger, 1998). They found that the presence of an error of commission predicted reduced performance at the end of vocational training of individuals with schizophrenia. Ngan and Liddle (2000) studied reaction times in populations with schizophrenia and found negative correlation between disorganization symptoms and negative symptoms and simple reaction times in

persistent illness populations, and negative correlation between disorganization symptoms and choice reaction time in the same population.

### 5.1.2 Neuroimaging Studies of Reaction Time

Neuroimaging studies of reaction time have been done using all different functional neuroimaging techniques (Naito et al, 2000; Mulert et al, 2001; Jansma, Ramsey, Slagter & Kahn, 2001; Winterer, Adams, Jones & Knutson, 2002; Gallinat et al, 2002; Mulert, Gallinat, Herrmann, Dorn & Winterer, 2003; Mulert, Menzinger, Leicht, Pogarell & Hegerl, 2005). A PET study (Naito et al, 2000) identified a negative correlation between reaction time and activation of the anterior cingulate cortex (ACC) and activation of ACC has been found in all the neuroimaging studies.

Naito et al (2000) looked at simple reaction time to stimuli in various modalities in healthy volunteers using positron emission tomography (PET) (See Figure 5-2). Mulert et al (2001) looked at choice reaction time to an auditory stimulus using electroencephalography (EEG) and low resolution electromagnetic tomography (LORETA) and found reduced activation in anterior cingulate cortex in people with schizophrenia compared to healthy volunteers. Jansma et al's study (2000), which was intended to look at learning, included choice reaction time to a visual stimulus in healthy volunteers using functional magnetic resonance imaging (fMRI) and found ACC activity, although they did not attempt to correlate reaction time to degree of ACC activation. Winterer et al's study (2002), which looked at choice reaction time to a visual stimulus in healthy volunteers using event-related fMRI, found negative correlation between activity in ACC and reaction time (see Figure 5-3). The fact that ACC activation has been consistently found by different researchers using different imaging techniques and different paradigms based on reaction time makes it a robust finding.

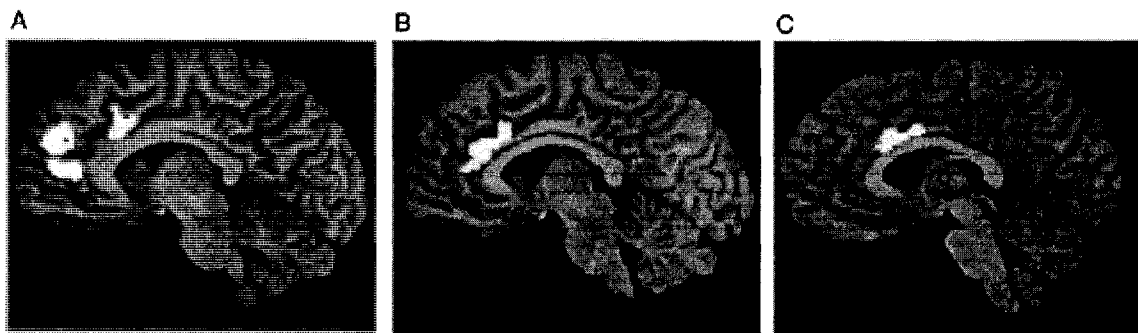


Figure 5-2. Results from Naito et al, 2000, showing area correlated with reaction time for different stimulation modality in healthy volunteers. A auditory, B tactile, C visual

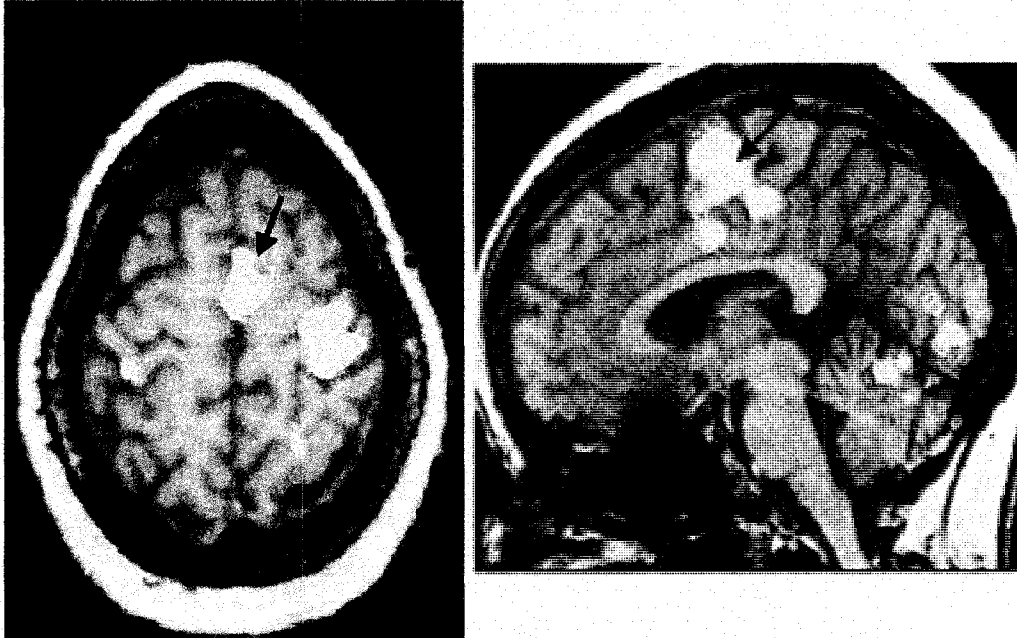


Figure 5-3. Results from Winterer et al, 2002, showing activation in ACC/SMA from event-related visual 2-choice reaction time task from healthy volunteers.

The ACC is located in the anterior portion of the cingulate gyrus, a medial structure that sits superior to the corpus callosum. The anterior and posterior portions of the cingulate gyrus are distinct cytoarchitectonically and functionally, and are postulated to be the home of many varied functions (Vogt, Finch & Olson, 1995) (see Figure 5-4). In humans, a review of PET studies identified distinct regions of functional control in cingulate motor areas (Picard & Strick, 1996), with distinct areas for simple or complex movements and within these divisions for face and arm movements.

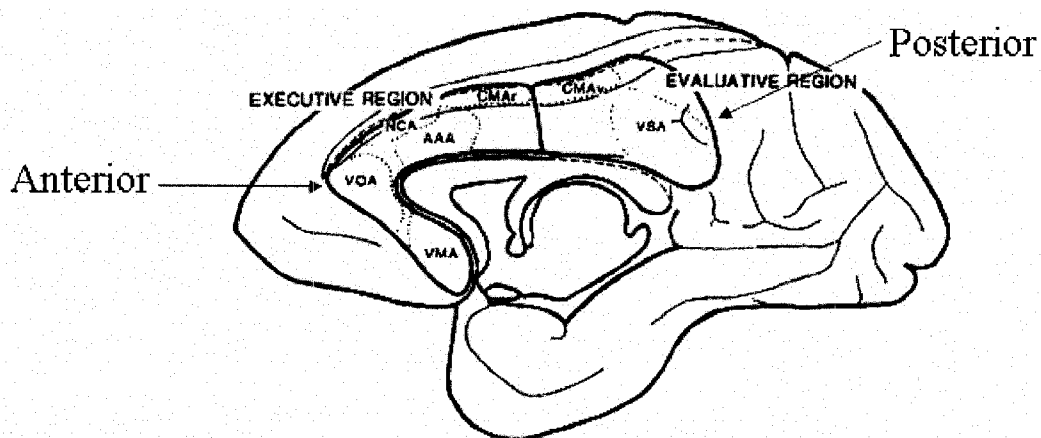


Figure 5-4. Functional Subdivisions in Cingulate Cortex of Rhesus Monkey. CMA – cingulate motor area, r – rostral, v – ventral, NCA – nociceptive area, AAA – attention to action area, VOA – vocalization area, VMA – visceromotor, VSA – visuospatial. From Vogt, Finch & Olson, 1995

Several neurophysiology studies have also looked specifically at individuals with schizophrenia and have shown reduced ACC activation compared to healthy volunteers using a reaction time test (Mulert et al, 2001; Gallinat et al, 2002) (See Figures 5-5 and 5-6). These studies used EEG and an auditory 2-choice reaction time task. Mulert et al (2001) looked at a group of people with chronic schizophrenia at admission to hospital, but before they had received treatment. Most of these subjects were drug-free at the time. Gallinat et al (2002) looked at mostly first-episode, drug-naïve patients. Both studies showed a deficit in activity in a central region identified as ACC. It should be noted that these EEG studies concentrated on a time about 100 ms post-stimulus that may be a different function than activation at a later time. With fMRI, there is no way to separate out components by time as in EEG.

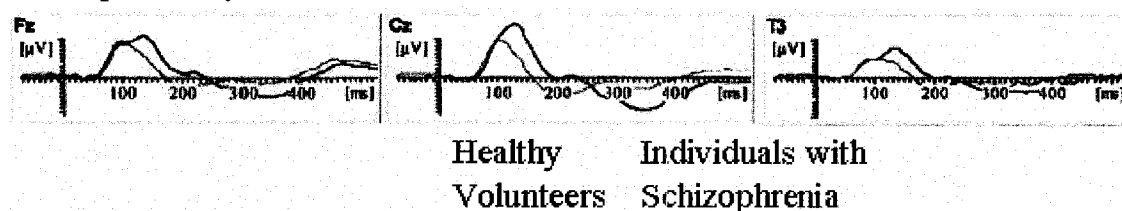


Figure 5-5. Selected ERP Grand Averages Comparing Healthy Volunteers (black) to Individuals with Schizophrenia (red). From Mulert et al, 2001. (Grand Average is average of all subjects' recordings, where subject's recording is already the average of their individual event recordings.)

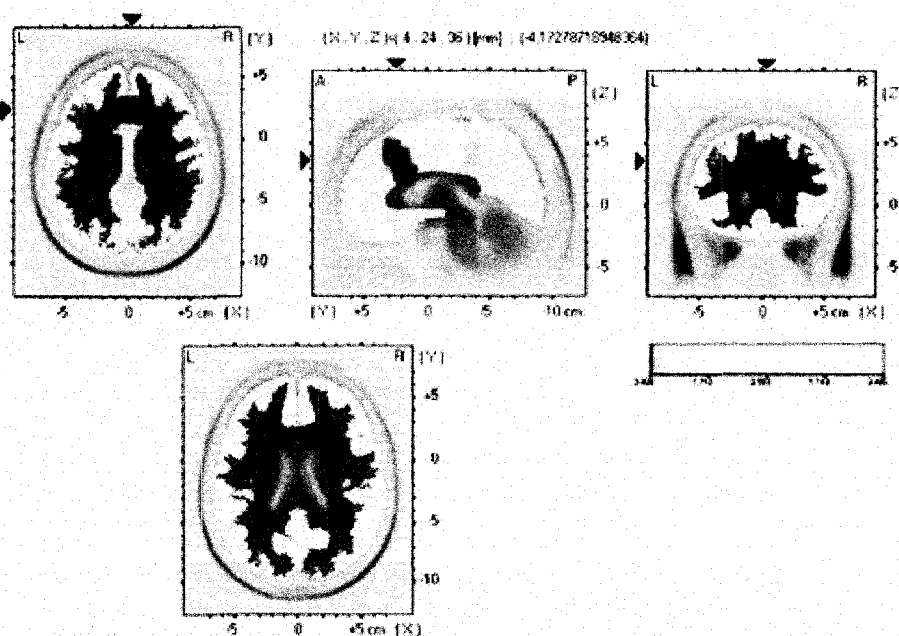


Figure 5-6. LORETA Results from ERP Recordings Showing Reduction in Current Amplitude During Auditory Reaction Time Task. From Gallinat et al, 2002.

The finding of a deficit in functional activation of ACC in individuals with schizophrenia has been investigated with other paradigms. Early PET studies of individuals with schizophrenia at rest showed higher regional cerebral blood flow (rCBF) in the anterior cingulate cortex of individuals with schizophrenia than in healthy volunteers (Liddle et al, 1992; Yuasa et al, 1995) and correlated the degree of rCBF with disorganization symptoms.<sup>1</sup>

Many task-oriented neuroimaging studies have also found ACC activation deficits. Experiments using Go-NoGo Inhibition tasks also show ACC activation deficits in individuals with schizophrenia (Ford et al, 2004; Rubia et al, 2001). Ashton, Barnes, Livingston and Wyper (2000) investigated verbal fluency in drug-naive individuals with schizophrenia using PET and found decreased rCBF correlated with PANSS (positive and negative syndrome scale) negative symptom scores. Carter, Mintun, Nichols and Cohen (1997) using the Stroop task and PET found reduced ACC activation. Carter, MacDonald III, Ross and Stenger (2001) used a continuous performance test with stimulus degradation to increase error rates with event-related fMRI and again found lower activity in ACC in individuals with schizophrenia. Fan, McCandliss, Fossella, Flombaum and Posner (2005) used the attention network task (ANT) and event-related fMRI with healthy volunteers and identified ACC activation only during the executive portion of the task. Since the ANT includes a choice reaction time task which previous results have shown activated the ACC (Jansma et al, 2001), the finding of no activity of this region means that the ACC activation is common in the different tasks of the ANT. Based on the evidence from Fan's study and the EEG studies, this common, early activation of the ACC on simple and choice reaction time tasks may be a different function than the activation shown by the executive-type tasks.

A possible explanation for the function of this early, non-executive activation of ACC is effort or degree of engagement with the task. This theory was investigated by Mulert et al (2005) who were able to correlate ACC activation and reaction time with the self-reported effort on the task (See Figure 5-7). This is an interesting explanation since a major confound with cognitive tasks on individuals with schizophrenia is whether the results are biased by their involvement with the task. The early ACC activity may be a neural sign of the degree of engagement in a task by people.

---

<sup>1</sup> It is possible that the increased activity of ACC in the rest state has led to apparent deficiency during other studies (i.e. ACC is differentially activated to a lesser extent, though absolute activation may be the same).

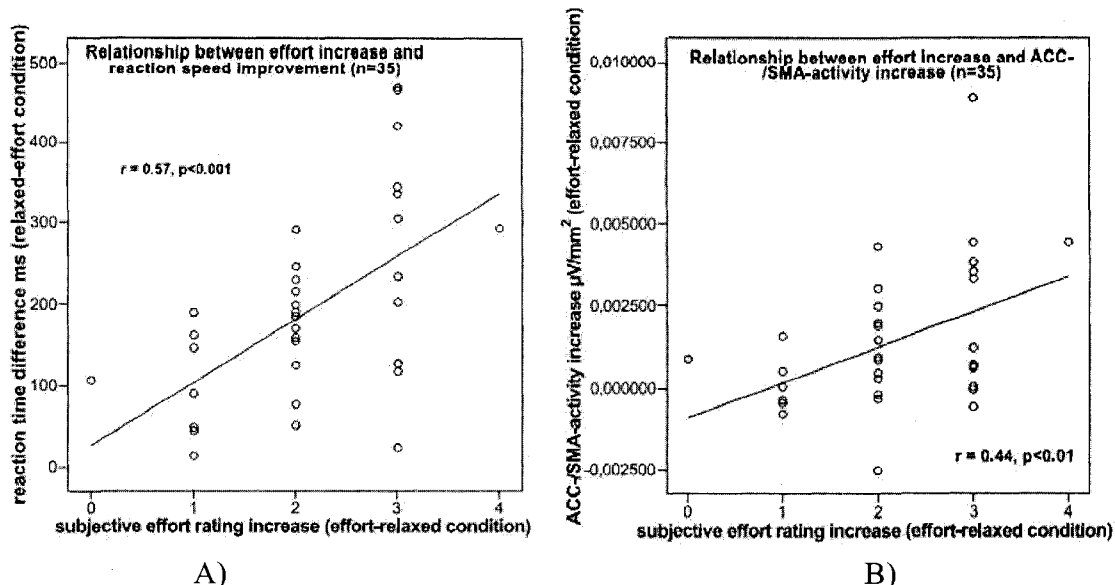


Figure 5-7. Correlation Between Self-Rated Effort and A) Reaction Time B) ACC/SMA Activity. From Mulert et al, 2005.

### 5.1.3 Heritability of Reaction Time

Reaction time has been shown to be one of the most heritable cognitive tasks. A study of twins looking at both simple and choice reaction time found 64% and 62% heritability respectively at 16 years of age (Rijsdijk, Vernon & Boomsma, 1998). Another study of twins also found 64% heritability for choice reaction time (Wright et al, 2001). This is higher than working memory tasks (below 50% in Wright et al, 2001).

In addition, reaction time has been shown to be slightly but reliably correlated with IQ, with estimates of between -0.2 and -0.4 (Rijsdijk et al, 1998; Wright et al, 2001) (where the negative sign shows that shorter reaction time correlates with higher IQ).

The heritability of reaction time could be important if we can show a difference in activation between people with schizophrenia, first-degree relatives of schizophrenia and healthy volunteers. Schizophrenia has a sizable genetic loading, but there has been limited progress in identifying suspect genes for schizophrenia. One reason may be that schizophrenia may not be a single disease (Heinrichs, 2004; Hallmayer et al, 2005) and as a result, identifying endophenotypes is an active research area (Braff, 2007). Where phenotypes are the outward, visible expression of the genotype, endophenotypes are an intermediate expression of the genotype that must be measured as they are not obviously visible. Endophenotypes are regarded as closer to the genetic variation than the phenotype. The theory is that endophenotypes of schizophrenia may be more amenable to genetic analysis than the phenotype. Endophenotypes should show measurable differences between people with schizophrenia and healthy volunteers, as well as being

heritable. Reaction time is thus a good candidate for an endophenotype, as it is heritable and measurably different.

### **5.1.4 Structural Abnormalities**

Structural abnormalities in ACC have been found in individuals with schizophrenia. Sigmundsson et al (2001) identified a volumetric deficit in ACC of negative-symptomatic individuals with schizophrenia using MRI at 1.5T (Sigmundsson et al, 2001). Benes et al (1992) found increased density of vertical fibers during post-mortem examinations of brains of individuals with schizophrenia (Benes, Sorensen, Vincent, Bird & Sathi, 1992). Functionally, this could result in increased excitatory associative inputs and fewer inhibitory interneurons, resulting in altered flow of activity to prefrontal cortex and hippocampus.

As reaction time tests have been found to be focused functionally at the ACC, it would be important to not only measure function but structure of the ACC as well. Since brain structure was being imaged as part of the study, volumetric differences could also be tested. As well as identifying volumetric deficiencies in ACC, correlation of structural abnormalities with the performance on reaction time, activation from the fMRI task, and symptoms could be done.

### **5.1.5 Models of Reaction Time**

Models for reaction time have been developed by mathematical psychology. An early model that explained the dependence of reaction time on number of choices was Hick's Law, which is:

$$\text{Mean RT} = K \log_2(n+1) \tag{5-1}$$

where, K is a constant that changes for each individual, and  
n is the number of choices

Note that the log function is a log base 2. 'n+1' indicates that not-responding is also a choice. Various additions to the basic Hick's Law can account for the effect of frequency, the effect of sequence, the effect of discriminability and the effect of errors.

The most successful modern models are the Ornstein-Uhlenbeck diffusion model and the leaky competing accumulator model (Smith & Ratcliff, 2004.) Both models are for a 2-choice reaction time task and can predict most aspects of the RT distributions, including errors with fast RTs. In the leaky, competing accumulator model, 2 connected leaky accumulators gather evidence for their related response from the stimulus (see Figure 5-8). The accumulation is a stochastic process so that there is variability in the RT results

even when the stimulus is exactly the same, and mistakes can sometimes occur.

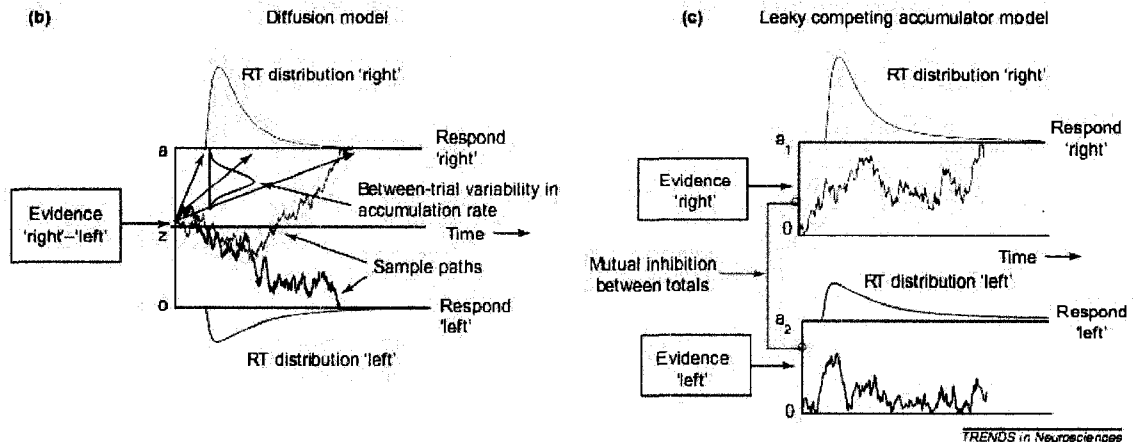


Figure 5-8 Mathematical Models of Reaction Time (from Smith and Ratcliff, 2004)

In recent years, single-cell recording of awake monkeys performing a visual discrimination task has identified areas that may be involved in their decisions (Roitman & Schadlen, 2002; Schall, 2002). This work has identified areas in the middle temporal lobe, lateral intraparietal (LIP) area in extrastriate cortex, the frontal eye field and superior colliculus. The rate of rise of activity in these areas has been correlated with the behavioural decision time.

Based on what has been discovered about the neurophysiology of the visual saccade task in monkeys, biophysically plausible neuronal simulations have been built that replicate real behavioural reaction time results (Wong & Wang, 2006; Lo & Wang, 2006). Wong's work modelled the basic task which could be used to show that the time integration in LIP neurons must be mediated by NMDA receptors (N-methyl-D-aspartic acid) rather than AMPA (alpha-amino-3-hydroxy-5-methyl-4-isoxazolepropionic acid) receptors. Lo and Wang's work specifically attempted to answer questions about the decision threshold in reaction time tasks, and whether variability in the threshold could be modelled with a biophysically-based model. They found that a network including neocortex, basal ganglia and superior colliculus could perform the task, and that the basal ganglia was primarily responsible for the decision threshold. Although the work is specific to the visual saccade task, one can imagine a similar network being developed for a reaction time task involving finger movements.

Lo and Wang's work is very suggestive for reaction time results in schizophrenia because of the connections of mid-brain dopamine neurons with neurons in the caudate. If a circuit involving the caudate is involved in setting decision threshold, it could be influenced by dopamine levels (Kiana, Shanks & Shadlen, 2006). Dopamine has a well-known connection to schizophrenia, and Lo's model results suggest a mechanism for how

abnormal dopamine levels could affect reaction times.

## **5.2 Objectives and Hypotheses:**

The objectives of the study are to verify the finding of a deficit in anterior cingulate cortex (ACC) activation in individuals with schizophrenia during choice reaction time tasks and to investigate the deficiency in a genetically high-risk group (first-degree relatives of someone with schizophrenia) to study choice reaction time as an endophenotype.

The hypotheses of the study are:

1. relative to healthy subjects with no family history of schizophrenia, chronically-ill individuals with schizophrenia and first-degree relatives will have slower and more variable reaction times on choice reaction time tasks.
2. relative to healthy subjects with no family history of schizophrenia, chronically-ill individuals with schizophrenia and first-degree relatives will show a deficit in the activation of the ACC during performance of simple and choice reaction tasks, and the amount of ACC activation will be negatively correlated with reaction time.
3. relative to healthy subjects with no family history of schizophrenia, chronically-ill individuals with schizophrenia and first-degree relatives will have volumetric deficits in the ACC.

## **5.3 Research Procedures**

This section will describe the methods used in the research, including the recruitment of subjects, subject symptom ratings and IQ estimates, and paradigm design.

### **5.3.1 Recruitment**

For chronically-ill individuals with schizophrenia, recruitment posters were placed in outpatient mental health and schizophrenia clinics in Edmonton and some group sessions were attended to discuss the study. The first-degree relative group was recruited through posters and advertisement in the Schizophrenia Society of Alberta newsletter. Healthy volunteers were recruited from the general community by posters in libraries and recreation centres, advertisements in free weekly entertainment magazines, and Schizophrenia Society of Alberta displays.

First contact with subjects was usually by telephone, except for some chronically-ill schizophrenia patients recruited from group sessions. In the telephone contact, the study was briefly explained and a preliminary screening, based on the exclusion criteria listed in §5.3.1.1 Methods of Sampling, was completed. Those who passed the screening were invited to the University of Alberta for an interview.

### **5.3.1.1 Method of Sampling and Justification of Sampling Size**

The following subject groups were recruited:

- A. 25 healthy volunteers (HV1 and HV2)
- B. 15 chronically-ill individuals with schizophrenia (CH)
- C. 11 individuals who have first-degree relatives with schizophrenia (FR)

For experiments of this type, between 10 and 15 subjects in a group is a typical sample size eg. Jansma et al, 2001; Carter et al, 2001. It was expected that data from a few patients would have to be discarded due to excessive movement or other artefacts. A previous fMRI study at University of Alberta used 10 individuals with schizophrenia and 15 healthy volunteers and found significant differences in brain activation between groups (Zedkova, Woodward, Harding, Tibbo & Purdon, 2006). The 25 healthy volunteers can be broken down into 2 groups (HV1 and HV2) to match groups B (CH) and C (FR) for age and IQ. Additionally, the 2 HV groups can be compared to each other as a controls test.

Inclusion and Exclusion Criteria:

#### A. Healthy volunteers:

Exclusion criteria

1. Female
2. Current or past history of psychiatric illness or drug abuse
3. Family history of psychotic illness
4. Left-handed
5. Poor vision
6. Serious head injury including a significant time unconscious
7. Metal objects in the body (unable to have MRI).
8. Over 50 years of age or younger than 18.

#### B. Individuals with chronic schizophrenia:

Inclusion Criteria:

1. More than 10 years of illness.
2. Stable dose of atypical antipsychotic drugs.
3. History of clinically stable symptoms since treatment was begun.
4. Between 18 and 50 years of age.

Exclusion criteria:

1. Female
2. Left-handed
3. Poor vision
4. Metal objects in the body.

C. First-Degree Relatives of Someone With Schizophrenia:

Inclusion Criteria:

1. First-degree relative of an individual with schizophrenia
2. No history of psychiatric disorders
3. Between 18 and 50 years of age

Exclusion criteria:

1. Female
2. Left-handed
3. Poor vision
4. Metal objects in the body.

The above conditions help to reduce confounds of handedness, drug use, age, IQ and gender (women are slightly slower on reaction time although at the sample size used in the study, the difference was not significant (Zahn & Carpenter, 1978)).

#### **5.3.1.2 Interview**

Once informed consent was obtained, the SCID (Structured Clinical Interview for DSM IV) (First et al, 1997) was used to determine medical and family history, current diagnosis, if any, and past psychiatric history, if any. An estimate of IQ was obtained using the Peabody Picture Vocabulary Test, 3<sup>rd</sup> Edition, Form IIIA (American Guidance Service Inc.). This was required to match subjects for IQ, since reaction time has been shown to be correlated with IQ (Jensen & Munro, 1979; Rijdsik, Vernon & Boomsma, 1998). For individuals with schizophrenia, the Structured Clinical Interview for the Positive and Negative Syndrome Scale (SCI-PANSS) (Kay, Fiszbein & Opler, 1987) was used to rate symptoms to enable correlations between symptoms and other measures to be calculated. The interview took approximately 1 hour for healthy volunteers and 2 hours for individuals with schizophrenia.

#### **5.3.1.3 Scanning**

Acceptable subjects were scheduled for scanning at the University of Alberta In Vivo Nuclear Magnetic Resonance Centre. Scanning took approximately an hour in total - from the description of the task and preparation to enter the scanner, through scanning

and debriefing. A final screen for MRI was completed before patients entered the scanner room. Patients spent about 30 minutes in the Siemens Sonata 1.5T scanner for fMRI tests.

EPI parameters were as follows:

TR: 2s

TE: 50 ms

Flip angle: 90°

FOV: 240mm x 240mm

Matrix: 64 x 64

In-plane resolution: 3.75mm x 3.75mm

Number of slices: 23

Slice thickness: 4mm + 1mm gap

Slice order: descending (top to bottom), non-interleaved

Hz/pixel: 2604

Partial Fourier: none

A fat saturation pulse was used to remove the fat signal. The scanner EPI sequence automatically did 2 dummy scans and 5 additional dummy scans were added to ensure the signal reached steady-state and any startle effect was dissipated before the paradigm began. A short TR (2s) was chosen because the paradigm is best run with as many events in a block as possible. The matrix size (64x64) was chosen instead of a higher resolution in order to gain SNR, as discussed in section 3.2.2 and 3.2.3, and to make a short TR possible. The number of slices chosen was the maximum that could be accommodated with the given sequence, TR, matrix size and sampling bandwidth. The slice thickness was chosen to cover the whole brain, including most of the cerebellum, for most subjects. Adding partial Fourier encoding did not allow for more slices so it was not included in the sequence. The flip angle was chosen to give best SNR. (According to the Ernst angle relationship for a T1 of 920 ms for gray matter at 1.5T, an angle of 84° is ideal.)

Following the localizer scan, the block design task was done and then an anatomical scan based on an MPRAGE (Magnetization Prepared Rapid Acquisition Gradient Echo) sequence. Parameters for the MPRAGE sequence were:

TR: 1.87 s

TE: 4.4 ms

TI: 1.1 s

Flip Angle: 15°

FOV: 192 mm x 256 mm

Matrix: 384x512 (interpolated x2)

In-plane resolution: 0.5 mm x 0.5 mm (interpolated x2)

Number of slices: 144  
Slice thickness: 1mm, no gap

Occasionally, a subject would not be able to continue (1 person with schizophrenia because of anxiety and another because of elbow pain from being squeezed into the scanner). For those who were able to continue, the event-related design was performed and finally an optional flashing checkerboard was run as a QA check.

### 5.3.2 Paradigm

The paradigm was presented to subjects in the scanner using a paradigm computer whose display was communicated visually to the subject within the scanner, as in previous fMRI studies at the U of A (Zedkova et al, 2006). The paradigm computer output was sent to a projector in the equipment room behind the scanner. The projector displayed the visuals through a wave guide in the scanner room wall. A screen was hung from velcro on the back of the scanner, and a mirror was placed on the head coil for the subject to view the screen. Behavioural data (reaction times) were recorded using the paradigm computer and fibre-optic buttons that were used for previous fMRI studies. The fibre-optic buttons connected to interface hardware inside the scanner control room. The set-up is summarized in Figure 5-9.

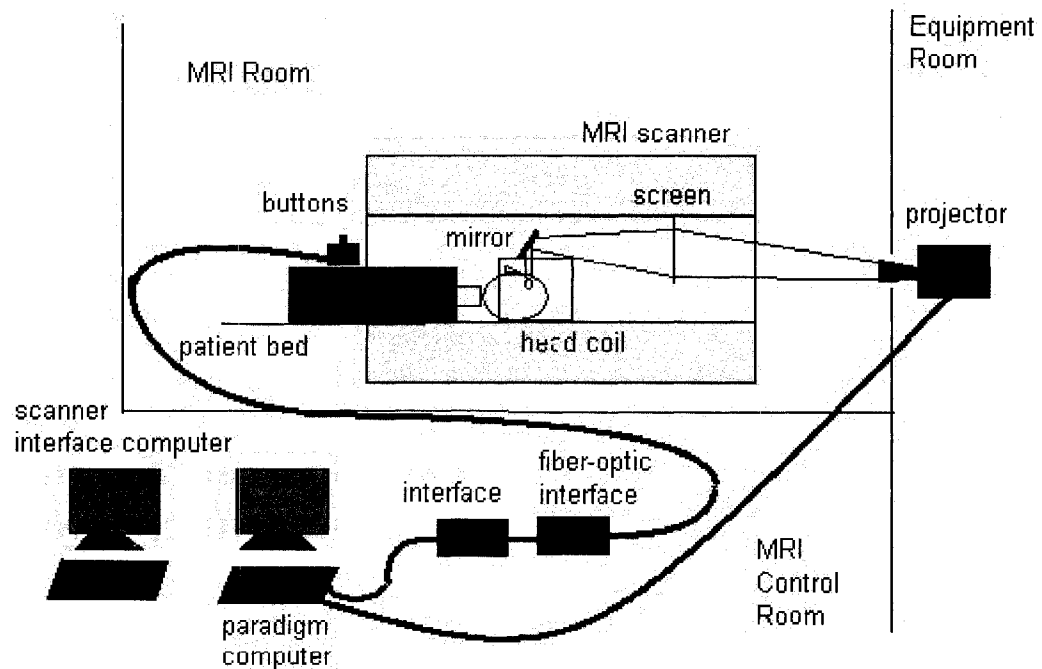


Figure 5-9. Components of fMRI Testing

The paradigm used was based on the visual 2-choice reaction time task. Two paradigms were designed and used - a block design and an event-related design. The block design was used to examine the major hypothesis of this study. The event-related design was

included to gain experience with event-related designs, and to make possible a wide variety of alternate contrasts that could be examined. The designs will be explained in the next paragraphs.

Both designs use a similar basic display and differ only in timing and sequence. Two boxes are arranged horizontally across the screen. A black target circle appears in one box at varying intervals. The designs include 3 conditions - choice, watch and fixation, as shown in Figure 5-10. Conditions in which the subject presses a button in response to the stimulus are called choice. Conditions in which the subject just watches the stimulus are called watch. The difference between choice and watch conditions is indicated by the color of the border of the boxes – red for choice and black for watch.



Figure 5-10. The 3 Conditions of the Paradigms

The watch condition is included to provide a better comparison for the choice condition rather than a fixation block. The watch condition helps to focus the subject's mind on the task, and comparison of choice with watch removes most direct visual activation, confounds of timing, and any other implicit processes. Fixation conditions, consisting of a black cross in the center of the display, are used after a sequence of watch and choice blocks. Fixation blocks are a neutral block that serves to give time for neural activity caused by watch or choice conditions to die away. The order of watch and choice blocks is varied to prevent order-induced activation.

To ensure the subject responds with a pure choice reaction each time, the time between appearances of the targets (preparation time) is varied. For the block design, the time is varied using 4 basic intervals. Stimulus duration was chosen to be 800 ms and the average preparation time was 1200 ms, giving an average duration for one complete

stimulus of 2 s. Watch and Choice blocks have 4 events with 4 preparation times each, giving 16 events in each block, which requires 32 seconds. Right and left stimuli are displayed equally in each block. Fixation blocks are 24 s long, as this is sufficiently long for activations to die away. They are kept short to reduce subject fatigue. The sequence for the block design is shown in Figure 5-11. Although the actual set of stimuli with left and right and varying preparation times is different for each block, the sequence is programmed and is the same for each subject (pseudo-random).

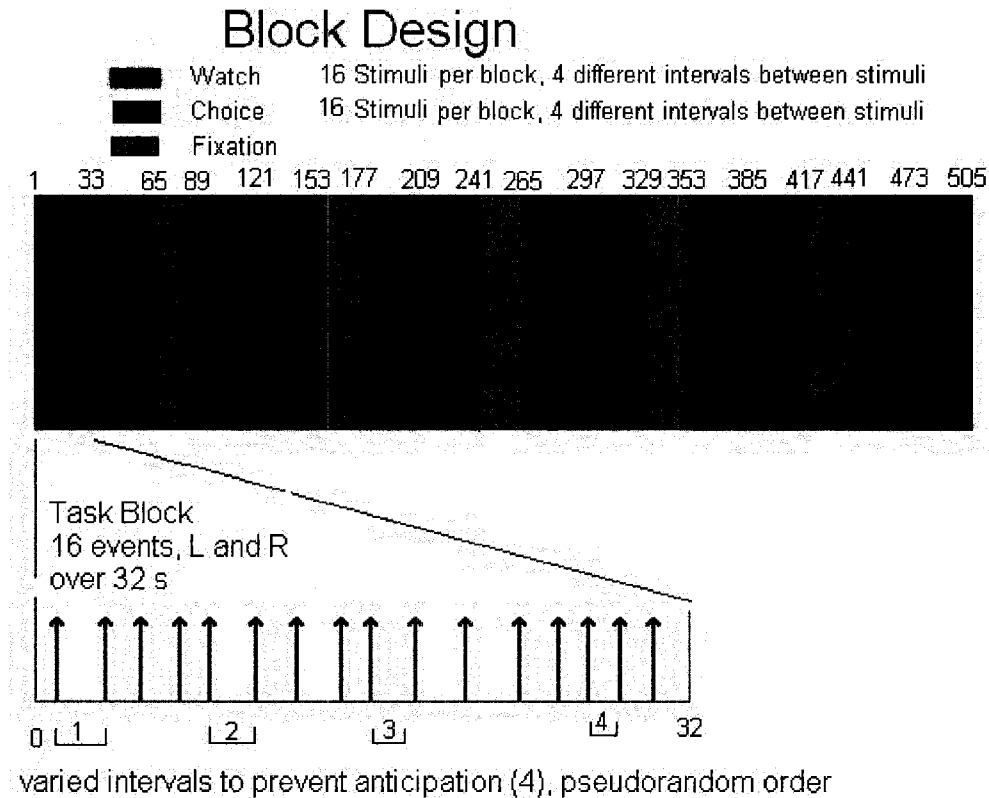


Figure 5-11. Block Design Sequence

The event-related design has 90 events of each condition, giving 180 events in all (see Figure 5-12). The events are pseudo-randomly presented to meet the conditions that the the appearance of the stimuli fall either on, or halfway between, TRs. This condition is required because the measurements of each slice must be shifted in time to model the measurements occurring at the same time (i.e. there cannot be 2 events within one TR). Events fall on or halfway between to reduce sampling bias (Price, Veltman, Ashburner, Josephs & Friston, 1999). This follows the study using event-related fMRI by Winterer (Winterer, Adams, Jones & Knutson, 2002). The event-related design has 3 time intervals to achieve variation: 2s, 3s and 4s. The average is 3s, so the total time for the 180 events is 540 s or 9 minutes. Including the fixation blocks at the beginning and end, the total test takes 9 minutes, 32 seconds. As much as possible, events are balanced so

that left and right, and each condition, are equally divided between falling on or halfway between TRs and the different choice and watch events follow each other equally often.

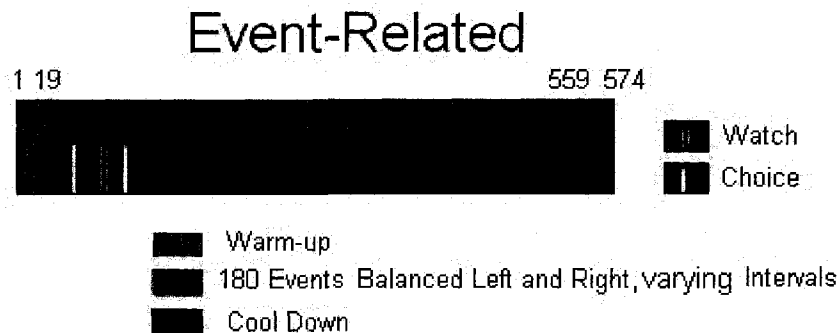


Figure 5-12. Event-Related Design Sequence

The paradigm was programmed in E-Prime (Psychology Software Tools, Inc., Pittsburgh). E-Prime provides an ideal software environment for developing paradigms, whether for fMRI or psychological testing. It has an object-oriented GUI for preparing the displays, various settings for controlling the timing of displays, and built-in interfaces for controlling and reading input/output devices.

Since we used E-Prime on a computer running Windows XP, E-Prime couldn't guarantee to present the display at exactly the time requested. Since it is more important in the fMRI paradigm design that the displays appear at the right time rather than last for the right duration, E-Prime was set to keep the cumulative time. E-Prime records the actual delay time (time between when the display was actually presented versus the time when the display should be presented) in the data file. No display was delayed by more than 14 ms and this was felt to not be important for the analysis.

The paradigm and scanner computers ran independently and the only synchronization was that they were started at the same time. Over the 9 minutes of the paradigm, both computers run very precisely and the scanner and paradigm were always observed to end at the same time within limits of the observation.

A method in which the paradigm computer triggered the scanner computer for each volume scan was attempted by connecting a signal from the paradigm computer parallel port to the scanner bed trigger in port. The trigger signal initiated a volume scan. The E-Prime event-related design scheme was adjusted to write a trigger signal to the port as each display was initiated. Only the event-related design paradigm was changed this way as timing is not so critical to the block design paradigm. 2 subjects were scanned with the triggered event-related scan and the free-run event-related scan. Although activations

were achieved with the free-run, no activations were achieved with the triggered scan, so the triggered scan was dropped.

As well as the complete 2-choice visual reaction time tasks in block design and event-related design, short training tasks were also developed. They contained the second fixation, watch and choice blocks of the block design test, and the first fixation and 10 events for the event-related test. These training tasks were used to introduce the task to the subject before entering the scanner. The subject performed the test using a keyboard and could clarify any uncertainty with the interviewer directly. The subject's reaction times could be viewed.

A flashing checkerboard design was often run at the end of the scans. This paradigm alternated a blue-and-yellow reversing checkerboard with a fixation cross. During the flashing checkerboard, subjects were asked to alternately press their left and right buttons. There were 4 blocks of each type and blocks were 24 s long resulting in a total of 3 minutes and 26 seconds including dummy scans. The Siemens console was set to perform a simple voxel-by-voxel correlation analysis of the data for immediate display. Also, results of this scan could be used to validate results from the other functional scans. See Appendix E for results from the flashing checkerboard scans.

## **5.4 Method of Data Analysis**

In this section, the method of data analysis is specified. It includes behavioural, structural and fMRI analysis.

### **5.4.1 Behavioural Data**

Reaction times were recorded to within 1 ms by E-Prime. The E-Prime Data-Aid program was used to view the data and reduce it to a subset needed for later analysis. The subset was written to a comma-separated variable file. A program written in MATLAB was used to find the maximum and minimum reaction times, calculate the median reaction time (with and without errors) and interquartile range (25% to 75%), and count 3 types of errors – errors of response (pressing left button when stimulus was for right), errors of omission (no response to a stimulus) and errors of commission (responding to a watch stimulus). The program also plotted the reaction time distributions.

The calculated median reaction times were analyzed by comparing groups using 2-sample t-tests for each combination of groups, including HV1 to HV2. Since reaction times are not normally distributed (the distribution is skewed with a long tail for longer

times and a minimum reaction time on the other end), median RTs were used instead of means, and interquartile ranges instead of standard deviation. However, once the median and range data were obtained, standard parametric tests were used.

The behavioural data for each group were correlated with age and IQ using Pearson's correlation coefficient.

### **5.4.2 fMRI Data**

Brain activation was analyzed using Brain Voyager QX v1.9 (Brain Innovations, Maastricht, Netherlands) and SPM5 (Wellcome Department of Imaging Neuroscience, London, UK). These two programs use a different data flow and different algorithms to accomplish the analysis. Results that were consistent between the two gave confidence in the results.

The manual for SPM5 was not much use and contains the same text present in the graphics window when running an operation in SPM5. The manual for SPM99 contains much more information about files, the operations and choosing parameters.

Brain Voyager QX comes with a getting started guide and online help. While both of these are useful, a better source for help is found in the help files for Brain Voyager 2000.

#### **5.4.2.1 Data Conversion**

fMRI data must be presented to the data analysis programs in a specific format. Brain Voyager QX and SPM5 contained data converters to convert the data files from the Siemens 1.5T scanner into the correct format. Note that for Brain Voyager, files must be processed with the IMAtool first to name files correctly. Otherwise, Brain Voyager will follow Windows conventions and sort files as "XX1", "XX11", "XX12", ... "XX2" etc.

SPM5 uses analyze or nifti file format. It has a converter that will convert DICOM images into analyze format and the conversion can be easily batched. Brain Voyager QX will read files in DICOM, analyze or a few other formats particular to the major MRI manufacturers (GE, Philips, Siemens).

Anatomical image data in the DICOM format comes in different files for each slice. SPM5 converts these multiple files into one analyze format file. For SPM5, the images must be in the expected orientation; that is, anterior at the top and left on left. Note that the default for L-R can be changed within the SPM5 program. Brain Voyager QX (BVQX) converts the images into one vmr file. The images are then converted to isovoxel, which makes images better for viewing since the number of pixels in the slice encode direction is so much less, and then to BVQX's standard sagittal views.

Functional images from the Siemens come in DICOM Mosaic images; that is, each file contains the set of slices taken during one TR. The SPM5 DICOM converter converts these into analyze format, with each file still representing the set of slices taken at one TR. BVQX converts the DICOM mosaic files into files particular for each slice (slice time course or .stc), so each file represents the time course over that slice.

SPM5 always names the design and results files SPM.mat. Therefore, a new directory must be created for every different analysis. On the other hand, BVQX allows the user to name every analysis file. It is more flexible, but it also easy to get confused.

One feature of BVQX that is good for comparing maps is overlay maps. The result of any analysis can be saved as an overlay mask and then loaded back in again so that flipping between 2 maps requires only one mouse click.

#### **5.4.2.2 Preprocessing in SPM5**

Pre-processing of data in SPM5 proceeds according to a standard sequence that lends itself to batching. The sequence is:

Realignment (motion correction) (prefix 'r')

Slice Timing Correction (for event-related data only) (prefix 'a')

Coregistration (writes transformation files)

Normalisation (Standardization) (prefix 'w')

Spatial Smoothing (prefix 's')

At each step, new files are written with a unique prefix as listed. The initial analyze files have either prefix 's' for structural or 'f' for functional. The final files then have a list of prefixes identifying what has been done to them (e.g. swrf or swarf files are analyzed according to whether it is block design or event-related design respectively).

For this study, realignment is set to rewrite the files (estimate and reslice option) so that motion regressors are not included in the design matrix. Default options are used. All images are resliced, plus a mean image is created that is later used for the coregistration.

Slice timing correction is used only for the event-related design. The number of slices is 23, TR is 2 and TA is calculated with the standard formula:  $TR - TR/nslices$ , which is not exactly right because the sequence does not fill the whole TR period. Since the slice order is descending, the first (top) slice is chosen as the reference slice (to which all others are corrected). The slice timing correction could be done before or after the realignment. There are disadvantages both ways because correction before realignment will be affected by head movement and could interpolate signals from different brain

regions, especially at edges. On the other hand, realignment may shift some voxels to adjacent slices, resulting in an incorrect time shift when slice time correction is done after realignment. The SPM99 manual recommends doing slice timing correction after realignment for ascending or descending sequences, so slice time correction is done after realignment in this study.

The coregistration results in the structural image being adjusted. The estimation only option is used. The mean image created in the realignment step is used as the reference image. The default estimation options are used.

The normalise estimate and write option is used with no source weighting image and the output voxel size is set to be 3 mm x 3 mm x 3 mm.

The spatial smoothing size is recommended to be 2-3 times the voxel size. A large size smooths each voxel across a larger volume. For this study with voxel sizes of 3 mm, 6 mm was chosen. Analyses with a smoothing size of 8 mm were also done, but didn't result in any group level changes.

The pre-processing sequence in SPM5 is fixed and automatic, and so suitable for batching. 2 basic preprocessing batches were set up: one for the block design and the other for the event-related. Not only is batching convenient for processing, it also provides a record of exactly what was done in each case.

#### **5.4.2.3 Preprocessing in Brain Voyager QX**

BVQX takes quite a different approach to the data analysis than SPM5. Comparing the results of the 2 programs provides confidence in the analysis.

Pre-processing in BVQX consists of only 2 or 3 steps: motion correction (called realignment in SPM5), slice timing correction (for event-related data only), and high-pass filtering. Motion correction and slice timing correction accomplish the same goals as in SPM5, but for motion correction, BVQX uses the first image as the base image. High pass filtering occurs at a later stage in SPM5 (at analysis), but the goal is the same: to remove low frequency, physiologically-based signals from the measured time courses. All these preprocessing steps result in new slice time course (.stc) files.

Coregistration is done somewhat differently as well. BVQX does coregistration as 2 steps. For the first step, it aligns the functional images and structural image using the data from the headers (DICOM only). This is a rough alignment mainly to get the orientation correct. Following that, BVQX offers a manual and an automatic option. The automatic option seems to produce poor results, so the images are aligned manually. The

6 alignment parameters (translation and rotation) are written into 2 files, called `_IA` and `_FA` for initial and final alignment respectively. The actual transformation of the files is done when creating the volume time course (`.vtc`) files.

Normalisation is also different. In BVQX, the user locates the AC and PC (written into a `_AC_PC` file for later use) and the program then aligns the images according to the AC-PC axis with the AC at the origin. Following that orientation, the user is prompted to identify the most anterior, most posterior, most superior, most inferior, right-most and left-most planes of the brain. The points are written into a `.TAL` file. This follows the Talairach and Tournoux brain atlas system (Talairach and Tournoux, 1998). The data are written into a file and then the structural image is transformed into a single 3D file.

Following the preprocessing, coregistration and normalisation, the functional images are transformed into a 3D file (`.vtc`) with specification of the coregistration (`_IA`, `_FA`) and normalization (`AC_PC` and `TAL`) transformation files.

#### **5.4.2.4 First-Level Analysis in SPM5**

First-level analysis (individual subject analysis) in SPM5 consists of four stages: specifying the design, reviewing the design, estimating the design and viewing the results.

The most important stage is the specification. In the specification, the directory in which to write the output data, the files to be used for the analysis, the sequence and timing of the blocks or events, the duration of blocks (0 for events) and the high pass filter parameter are all specified. One more important setting is the autoregressive correction. The statistical analysis requires the data to be independent, but the data are somewhat correlated in time. The autoregressive correction sets a first-order correction for the correlation. Another important setting is the base function. Usually, a canonical HRF is convolved with the basic boxcar setup by the design matrix, but there are other possibilities. For block analysis, the canonical HRF with no time derivatives was always used. For event-related analysis, adding time derivatives was tried, but the group-level results presented use only the canonical HRF.

The review stage provides various ways of looking at the design, including the design matrix, covariate matrix, and time and frequency charts. Here, one can check the frequency chart to see that the highpass filter setting is not set too high, and check that the design matrix and files are correctly specified.

The estimate stage is where the statistics are calculated. The results are placed in the `SPM.mat` file and several other files are written – `beta`, `.Res` and `.RPV`. Beta files are

written for each predictor in the model, plus the mean, and contain the beta parameter estimates (see GLM model in section 4.3.3.1) at each voxel. Res contains an image of the estimated residual variance and RPV contains an image of the estimated resolution elements per voxel.

The final stage is to view the results. In this stage, a contrast and a threshold are specified, and the results are viewed in different ways. Contrasts are a specification of the conditions to be compared. The MIPs (maximum intensity projection), one for each dimension, appear automatically and a table of activations can be constructed by pressing the volume button. It is also possible to view sections with the statistical results superimposed on the structural glass brains with medial and lateral views, define ROIs, and show time courses for a specified voxel or ROI. For each specified contrast, a .con file and a .spmT file are written. spmT files are image files with the value of the t-statistic at each voxel. Con files are statistical files used in the second-level analysis. This means that the second-level analysis is done for specific contrasts.

Tables of activation volumes can be output easily. SPM gives all coordinates in MNI format, and these should be converted to Talairach coordinates for best comparison to other experiments. A MATLAB function called mni2tal does the conversion, and a modification to the existing spm\_list.m program converts the coordinates and writes them to a text file when the right mouse button is pressed with the cursor on the table.

For the specific contrast, the threshold for the maps can be chosen in various ways. These include maximum p, maximum family-wise error (FWE), or maximum false detection rate (FDR).  $FWE < 0.05$  or  $p < 0.001$  are most commonly used. Also, a cluster size can be defined, using the idea that an isolated voxel can be activated by random processes, but a cluster of a certain size is unlikely to be randomly activated.

In the table of activations, 3 levels of statistics are reported. The first is the set-level which expresses the probability of finding the number of found clusters or greater in the search volume under the null hypothesis (that there is no functional activation in the search volume). The second is the cluster level, which includes the size of the cluster in calculating p – the probability of finding this size of a cluster in the search volume under the null hypothesis. The third is the voxel-level. The voxel with the highest t-statistic in each cluster is reported including the t-statistic coordinates uncorrected p-value and corrected p-value. The p-value is corrected for both FWE and FDR.

Multiple corrections is a major problem when reporting on so many comparisons as a  $p < 0.05$  for 4096 voxels would report 205 voxels as activated on average, strictly from noise. The corrected FWE p-value uses the Bonferroni correction, which is very

conservative. FDR is another correction that is based on controlling the number of false-positive voxels. It is an adaptive routine that depends on how many activated voxels are identified. It is applicable without spatial smoothing and has high sensitivity to detect activations, provided some true activation is present.

The coordinates can be labelled with anatomical areas using various programs. The Talairach Demon client program (Lancaster et al, 1997) was used in this study to obtain anatomical labels. The program provides options for searching. It can search a cube around the specified coordinate or find the nearest GM coordinate. A 3mm cube search was generally used, but the nearest GM search was used if no GM area was found in the cube. Sometimes the nearest GM area was too far away from the coordinate to include any part of the GM in the activation cluster identified. The same program labels WM but not according to fascicule. For WM, only lobe, corpus callosum, sub-lobar, or brainstem are reported.

#### **5.4.3.4 First-Level Analysis in Brain Voyager QX**

Analysis in BVQX proceeds along more graphical lines than SPM5. The specification of the stimulation protocol (design matrix) can be done graphically, if it is fairly simple, or with a text file for the more complicated event-related designs. The protocol is then shown as a horizontal chart with the type of block or event shown in color in the appropriate time sequence.

The general linear model option is used to analyse the data. To run the GLM option, a structural image must be selected, which can be either 2D slices or a 3D volume. The stimulation protocol is shown, and predictors can be added, specified, and convolved with a specified HRF if desired. For event-related designs, it is best to set the events using a click of the right mouse button on the color tag to the left of the stimulation protocol. The actual HRF function used can be set as 2-gamma functions, Boynton function or simple delay, all with various parameters. There is no canonical HRF.

Upon clicking Go, BVQX calculates the statistics for the specified general linear model. It immediately displays a default contrast on the 3D structural image. The statistical threshold value can be changed directly by clicking the increase or decrease threshold buttons. Clicking on the image changes the view, and the beta values for the selected voxels are shown on a chart. The Talairach coordinates of the selected voxel are also shown and contrasts can be easily set. Unfortunately, it is more difficult to get a tabulation of activations as in SPM5.

BVQX is a fast and easy-to-use option for looking at brain activities, but SPM5 was used for reporting the results. Using 2 different analysis programs has helped to give

confidence in the results. The methods the programs use are very different, so the fact that most of the results come out similar gives a lot of confidence in the analysis portion of the study.

#### **5.4.3.5 Second-Level Analysis in SPM5**

Second-level analysis in SPM5 is straightforward. There is a menu to select the type of analysis. Possibilities include: 1-sample t-test, 2-sample t-test, paired t-test, multiple regression, full factorial and flexible factorial. 1-sample t-test was used to do random effects analysis of each group and 2-sample t-test was used to compare group-by-group.

Covariates can be specified for any of these designs. In particular, 1-sample t-test was used with log(RT), Age and IQ separately as covariates to test whether any of these factors influenced the activations. Based on the previous results with PET and EEG, a negative correlation between log(RT) and activation in ACC was expected. Log(RT) was used because that was the function identified in the PET testing.

All of the scans used for second-level analysis in SPM5 are the con output files from contrast specifications in first-level analysis.

#### **5.4.3.6 Second-Level Analysis in Brain Voyager QX**

Second-level analysis in BVQX is quite different from that in SPM5. Second-level analysis in BVQX does not depend on individual analyses. The pre-processed, co-registered and normalized individual files (.vtc) and individual GLM definitions (.prt) are first defined. The analysis has options for doing fixed effects analysis and random effects analysis, though it expresses these differently. Fixed Effects Analysis is the default option. For random effects analysis (RFX), the RFX option can be selected. Other options are to use z-transform or %-transform for mean extraction and to use separate subject and/or study predictors.

Following that analysis, the model can be calculated in 2 different ways. The first and easiest way is to use the overlay GLM contrasts menu. If the model has been set up for RFX analysis, the overlay GLM contrasts will automatically set the RFX analysis option and allow specification of the group for each of the individual scans (for group analysis or group comparison, as desired). The contrast is specified in the same way as for individual scans. This method is adequate for 1-sample t-tests (RFX analysis of a group) and for comparisons of 2 groups, but does not allow covariate analysis.

The second way is more complete and suited for analysis of variance (ANOVA) designs and multivariate regression. It is entered using the ANCOVA Random Effects Analysis menu. It offers full flexibility in designs including specifying numbers of between-

subjects factors, within-subjects factors and multiple covariates.

#### **5.4.3.7 ROI Analysis**

As a hypothesis involving the activation of a specific cortical area is made, it is appropriate to do a region-of-interest (ROI) analysis of the cortical area.

ROIs can be functionally or anatomically defined. Two approaches are usually used for defining a functional ROI: 1) using one fixed ROI for all subjects, or 2) using individually-defined ROIs. The problem is to define the ROIs without biasing the results. To be most correct, an additional test should be used specifically to identify the ROI and the analysis proceeds on a different set of data.

Because there is great variety in the individual results around the areas showing activation, individual ROIs are defined as the area showing statistical activation that is closest to the region of the ACC. The percent change in signal in the ROI is measured using the program MARSBAR (Brett, Anton, Valabregue, & Poline, 2002). Since the study contrasts the choice and watch conditions, the percent signal change should be measured using the same contrast. The individual percent signal changes in watch and choice conditions were estimated and the difference between them was used in the correlation analysis. As with the second-level correlation analyses, the log of the median RTs was used to correlate with the percent signal change in the ROI.

#### **5.4.3.8 Voxel-Based Morphometry**

Volumetric data was analyzed using voxel-based morphometry (VBM) (Ashburner & Friston, 2000). VBM is an automated technique that does not depend on manual tracing of boundaries. It is suited to analyzing the whole brain with no bias as to where differences in structure might be found. The ACC is an area with a varying boundary because of variations between individuals in the cingulate patterns. Besides a callosal sulcus, cingulate gyrus and cingulate sulcus, many people also have a paracingulate gyrus and sulcus (Yucel et al, 2001), and this additional component can extend to varying lengths of the full ACC. It is unclear what the functional consequence of this variation in structure is, and also unclear how to account for this variation in manual tracing techniques. Therefore, VBM is more suited for finding differences in the ACC.

Voxel-Based Morphometry consists of the following sequence of steps:

1. normalise the individual brains to the standard space,
2. segment individual structural files into grey matter (GM), white matter (WM) and cerebrospinal fluid (CSF),
3. smooth the individual segmented files,
4. specify a second-level analysis,

5. estimate the design, and
6. view the results.

Normalization is the same operation as discussed in the pre-processing steps.

Segmentation creates 3 files, one for each tissue type. The files are an image of the probability that the voxel at that location contains the particular tissue type. The probability is normally 0 or 1, but may be intermediate around tissue borders. The various types of tissue are then compared individually in the estimation, and the results are separate for each tissue type. The structural data files must be in the correct orientation prior to being segmented.

Smoothing convolves the tissue files with a Gaussian kernel of specified size. Smoothing is required to meet assumptions of the statistical analysis and also helps normalize structures for comparison between subjects. 4-12 mm smoothing is common. Various sizes of smoothing can be tried to determine the effects. 6 mm, 8 mm and 12 mm smoothing were tried and 8 mm smoothing was chosen.

The second-level analysis is usually a 2-sample t-test to compare the volumetric probability maps for each tissue type, if comparing 2 groups, or ANOVA for more than 2 groups. Covariates such as age can be included. The files specified are the individual smoothed tissue type files, with separate analysis of each tissue type.

Estimation proceeds similarly to the 2<sup>nd</sup> level analysis of functional data. Viewing the results is the same as with the fMRI second-level analysis.

VBM was not done on BVQX.

As well as the VBM, gray and white matter volumes were calculated from the segmented images using the spm program “spm\_get\_volumes.m”. This program adds up the number of voxels included in an image and multiplies by the volume per voxel to arrive at an estimate of the volume.

## **5.5 Results**

In this section, the results of the study are described.

### **5.5.1 Demographic Data**

Table 5-1 shows the demographic data of each group in the study. The healthy volunteers are divided into 2 groups, called HV1 and HV2, to match the first-degree

relative (FR) and chronic schizophrenia (CH) respectively in N, Age and IQ. In addition to these main comparisons, FR is compared to CH and HV1 is compared to HV2, although these groups have statistically significant differences in N and IQ. PANSS – T is the total PANSS symptom scores, which applies only to the chronic schizophrenia group (see section 5.3.1.2).

Of the people with schizophrenia, 2 were on trifluoperazine of which 1 was on both trifluoperazine and clozapine. Another subject was on an anxiolytic only (fluoxetine). Others were evenly split between risperidone, quetiapine and olanzapine.

Table 5-1 Demographic Data

Group	N	Avg Age (years)	Avg IQ	Avg PANSS - T
HV1	11	36.36 ± 9.75	116.54 ± 5.45	N/A
FR	11	34.73 ± 12.19	116.00 ± 9.73	N/A
HV2	14	38.79 ± 10.90	105.78 ± 8.10	N/A
CH	15	37.4 ± 9.00	101.50 ± 9.53*	71.7 ± 10.0

\* The CH group is statistically significantly different from HV1 and FR groups in IQ (p<0.05)

### 5.5.2 Behavioural Data

Behavioural data are shown in Table 5-2 and in Figure 5-13. A statistically significant difference in RT is shown between the CH and all other groups on both the block design (CRT) and event-related design (er) paradigms. No other group shows any statistically significant difference with another group on RT. Regarding variability in reaction times (50% quartile range, shown only for the block design), the CH group has a statistically significant difference with all the other groups, but no other groups have a statistically significant difference.

Table 5-2 Behavioural Data Summary

Group	N	Avg Median RT (ms) on CRT	Avg 50% Quartile Range (ms)	Avg Median RT (ms) on er
HV1	11	300.27 ± 56.35	59.46 ± 21.00	336.65 ± 75.84
FR	11	294.54 ± 27.13	52.56 ± 19.22	325.51 ± 42.24
HV2	14	298.93 ± 27.45	60.88 ± 21.91	343.45 ± 50.53
CH	15	335.73 ± 44.64*	85.2 ± 23.19*	394.64 ± 63.71*

\* - statistically significant difference with other groups (p<0.05)

The correlations of Median RT on the block design paradigm (CRT) with IQ are negative

for each group except CH. Also, the correlation of Median RT with Age is strong for each group except CH. This is the expected correlation identified in section 5.1.3 (Rijsdijk et al, 1998; Wright et al, 2001). The correlation of Age with RT is strong for all groups except CH. Again, this is the expected decrease in RT with age (Deary & Der, 2005). The correlation between RT and range is strong for all groups including CH.

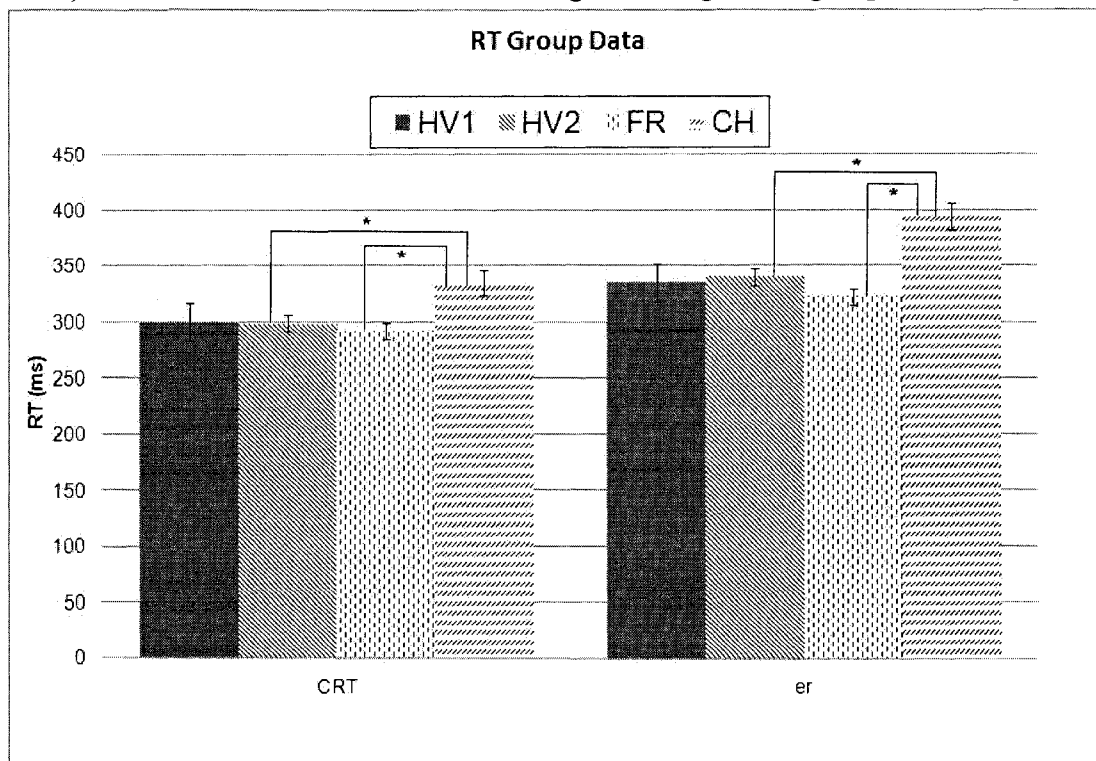


Figure 5-13 Comparison of Reaction Times Between Groups on Block (CRT) and Event-Related (er) Tasks. Asterisks show statistically significant differences between groups.

Some additional correlations were also run between Age and IQ, and Age and Range. These results are shown in Table 5-3. HV2 has a significant negative correlation of Age with IQ (meaning as Age increases, IQ decreases). This is likely to be an anomaly of this particular group since the other HV group has a nonsignificant relation. All groups have quite significant correlations between Age and Range except the CH, in which even the sign is different. HV1, HV2 and FR show that as age increases, the variability in response (range) also increases. This is as expected from other studies (Deary & Der, 2005).

Table 5-3 Correlation Coefficients

Group	N	Correlation Between Age and:		Correlation of CRT With:		
		IQ	Range	Age	Range	IQ
HV1	11	-0.12	0.84*	0.53	0.87*	-0.32

Group	N	Correlation Between Age and:		Correlation of CRT With:		
		IQ	Range	Age	Range	IQ
FR	11	0.29	0.79*	0.40	0.57	-0.27
HV2	14	-0.62*	0.51	0.40	0.62*	-0.18
CH	15	0.29	-0.20	0.14	0.47	0.36

\* - statistically significant correlation ( $p < 0.05$ )

### 5.5.3 Volumetric Data

Table 5-4 and Figure 5-14 show results of total gray matter (GM) and white matter (WM) volumes in the different groups. The only significant differences ( $p < 0.05$ ) are for the comparison of HV2 to CH GM and HV2 to CH total. Several others are verging on significance including HV1 to CH GM, HV2 to CH WM, and all groups compared to CH total volume.

Table 5-4 Gray and White Matter Volumes in Litres

	Gray Matter	White Matter	Total
HV1	0.717 $\pm$ 0.045	0.527 $\pm$ 0.053	1.244 $\pm$ 0.092
FR	0.716 $\pm$ 0.060	0.542 $\pm$ 0.060	1.258 $\pm$ 0.106
HV2	0.741 $\pm$ 0.097	0.531 $\pm$ 0.052	1.272 $\pm$ 0.141
CH	0.666 $\pm$ 0.068*	0.489 $\pm$ 0.066	1.155 $\pm$ 0.121*

\* The CH group is statistically significantly different ( $p < 0.05$ ) from HV2 group on the indicated measures

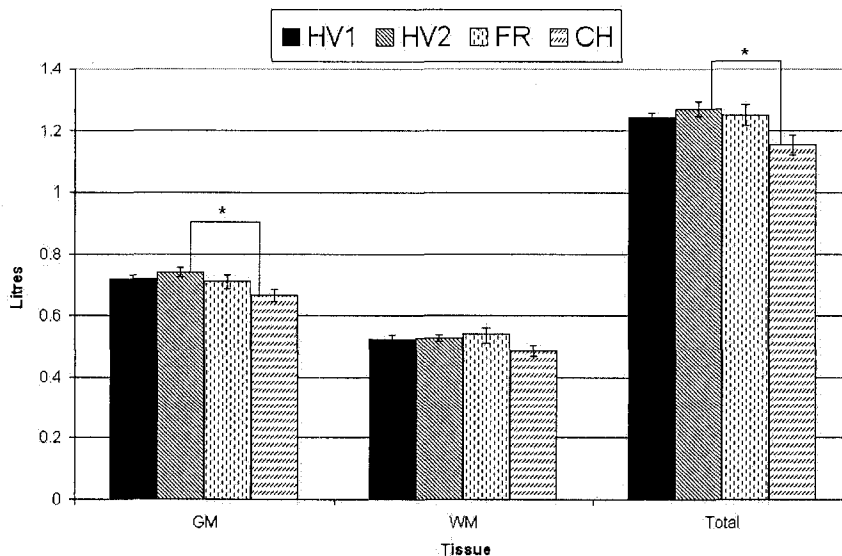


Figure 5-14 Gray and White Matter Volumes and Total Volume. Asterisks show statistically significant differences between groups ( $p < 0.05$ ).

Tables 5-5, 5-6 and Figures 5-15 and 5-16 show the results of VBM analysis for the gray and white matter respectively. No comparison has a set-level  $p < 0.05$  and most were close to 1.00. Some clusters were found with  $p_{\text{corrected}} < 0.05$ . For completeness, results are reported for all clusters showing an uncorrected  $p < 0.05$ .

Figures 5-15 and 5-16 are maximum intensity projections (MIPs) along the 3 orthogonal axes (coronal, sagittal and transverse). For each 2D representation of the brain, any activation along a projection will show up as shading, with darker shading indicating likelier activations or multiple activations along the projection. To determine the location of activation, it is necessary to compare the positions of the shading in all 3 pictures. For example, consider the position of the red arrow in Figure 5-16a. The sagittal view shows that the difference is in the anterior/middle (not superior or inferior), the coronal view shows that it is in the left medial/middle, and the transverse view shows that it is in the left medial/anterior part of the brain. The result is that we know the activation is in anterior/medial/middle of the brain, likely part of the anterior cingulate cortex or possibly medial frontal gyrus. The remainder of the figures will also be MIPs because they are the best for showing all activations (or differences for group comparisons). In all the MIPs, left and right are the natural left and right side of the images respectively.

Note that anatomical abbreviations such as superior temporal gyrus are abbreviated as STG and similar for all superior, middle, and inferior gyri. Other gyri names are written out.

Table 5-5 Summary of VBM Results – Gray Matter

T-statistic – highest voxel	Highest Voxel (Talairach coordinates)	Highest voxel anatomical label	# voxels in cluster	p uncorrected
HV2>CH				
6.38	(-8, 49, 5)	L MFG BA 10	916	<0.000
4.62	(-2, 25, -16)	L MFG BA 25	848	<0.000
4.26	(17, -14, -14)	R Parahippocampal Gyrus BA 28	922	<0.000
4.25	(50, 14, -27)	R STG BA38	179	0.049
4.18	(-46, -20, 61)	L PostCentral Gyrus	674	0.001
4.09	(5, -60, 14)	R Posterior Cingulate BA 23/30	207	0.036
4.01	(-46, -56, 27)	L STG BA 39	283	0.017
3.98	(1, -70, 3)	R Lingual Gyrus BA 30	275	0.018

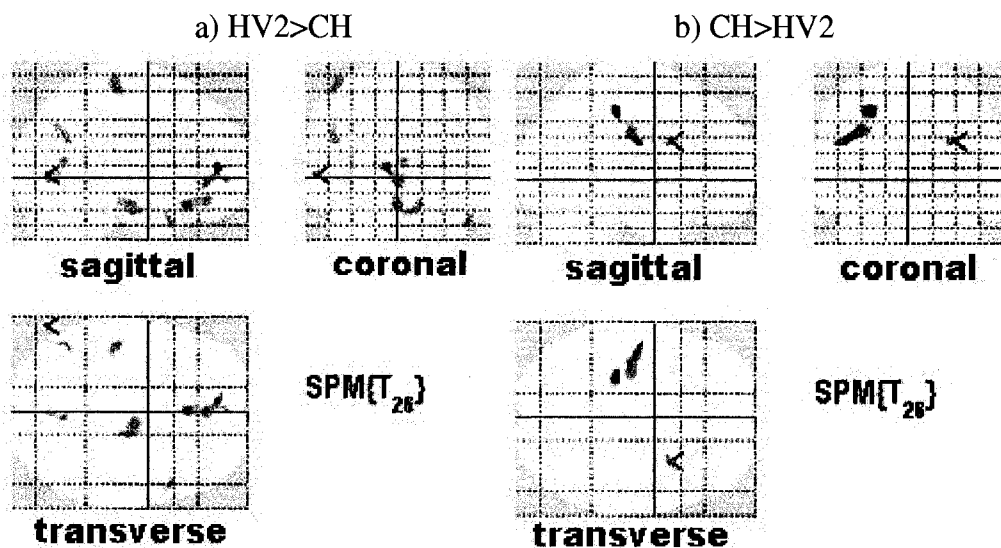
T-statistic – highest voxel	Highest Voxel (Talairach coordinates)	Highest voxel anatomical label	# voxels in cluster	p uncorrected
3.80	(-60, -73, 6)	L MOG BA37	229	0.029
CH>HV2				
5.82	(-29, -26, 46)	L PreCentral Gyrus BA4	568	0.001
5.55	(-48, -10, 24)	L PreCentral gyrus (BA 4/6)	1111	<0.000
4.09	(31, 11, 24)	R IFG BA 9	241	0.025
HV1>FR				
5.91	(28, 28, 14)	R Insula BA 13	262	0.012
5.68	(-6, 72, -17)	L SFG BA 11	542	0.001
5.19	(26, 50, 10)	R SFG BA 10	179	0.033
4.99	(75, -48, -2)	No data	175	0.034
4.49	(-31, -91, 24)	L Superior Occipital Gyrus BA 19	213	0.021
4.42	(55, -26, -5)	R MTG BA 21	267	0.011
FR>HV1				
5.13	(48, 13, -13)	R STG BA 38	352	0.005
4.77	(-18, -71, -9)	L Lingual Gyrus BA 18	448	0.002
4.45	(51, 28, 44)	R MFG BA 8	313	0.007
FR>CH				
5.90	(-53, 13, 4)	L PreCentral Gyrus BA 44	540	0.002
5.81	(-3, 58, -15)	L MFG BA 11	501	0.002
4.92	(32, 70, 8)	R MFG BA 10	855	<0.000
4.77	(-27, 53, 39)	L SFG BA 9	229	0.027
4.56	(60, 23, 36)	R MFG BA 9	302	0.013
4.30	(-25, -49, -24)	L Cerebellum, Culmen	458	0.003
4.21	(47, 12, -7)	R STG BA 38	222	0.029
4.10	(-60, 6, 43)	L MFG BA 6	240	0.024
CH>FR				
4.81	((-41, -42, 31)	L Supramarginal Gyrus BA 40	234	0.025
4.44	(24, 51, 10)	R MFG BA 10	174	0.049
HV2>HV1				
5.58	(-6, -42, 63)	L PostCentral Gyrus BA 5	939	<0.000
4.84	(-7, -69, 42)	L Precuneus BA 7	554	0.001

T-statistic – highest voxel	Highest Voxel (Talairach coordinates)	Highest voxel anatomical label	# voxels in cluster	p uncorrected
4.79	(16, -78, 44)	R Precuneus BA 7	556	0.001
4.74	(-49, -61, 37)	L Inferior Parietal Lobe BA39/40	316	0.008
4.73	(-50, 23, -14)	L IFG BA 47	205	0.026
4.63	(-4, 8, 31)	L Cingulate Gyrus BA 24	292	0.010
4.15	(-15, -84, 35)	L Cuneus BA 19	211	0.024
3.86	(2, -83, 35)	R Cuneus BA 19	203	0.026
HV1>HV2				
No significant differences				

Table 5-6 Summary of VBM Results – White Matter

T-statistic – highest voxel	Highest Voxel (Talairach coordinates)	Highest voxel anatomical label	# voxels in cluster	p uncorrected
HV2>CH				
5.74	(-29, -26, 46)	L Parietal Lobe WM	634	0.001
5.53	(-49, -10, 24)	L Frontal Lobe WM	1496	<0.000
5.12	(-60, -32, -7)	L MTG WM	166	0.048
4.59	(3, -21, 11)	R sub-lobar WM	251	0.018
4.46	(16, -79, 41)	R Precuneus WM	211	0.028
4.42	(-18, 65, -1)	L Frontal Lobe WM	238	0.021
4.37	(10, -34, 9)	R Sub-lobar WM	1854	<0.000
4.36	(52, -30, 48)	R Parietal Lobe WM	243	0.020
4.13	(31, 11, 24)	R Frontal Lobe WM	286	0.013
CH>HV2				
No significant differences				
FR>HV1				
6.30	(-22, 47, 33)	L Frontal Lobe WM	368	0.004
6.20	(27, 52, 10)	R Frontal Lobe WM	533	0.001
5.03	(14, -18, -22)	R Brainstem	609	0.001
4.28	(56, -25, -5)	R Temporal Lobe WM	333	0.006
4.12	(2, 17, -11)	R Frontal Lobe/Limbic Lobe WM	233	0.018
4.11	(2, -32, 68)	R Frontal Lobe WM	235	0.018

T-statistic – highest voxel	Highest Voxel (Talairach coordinates)	Highest voxel anatomical label	# voxels in cluster	p uncorrected
HV1>FR				
No significant differences				
FR>CH				
5.06	(-43, -42, 32)	L Parietal Lobe WM	449	0.002
4.97	(26, 53, 10)	R Frontal Lobe WM	591	0.001
CH>FR				
No significant differences				
HV2>HV1				
5.92	(-55, -34, 27)	L Parietal Lobe WM	403	0.004
4.67	(-7, -33, 2)	L Sub-lobar WM	347	0.007
4.06	(4, 16, -15)	R MFG WM	184	0.037
3.92	(15, -24, 21)	R Corpus Callosum	395	0.004
HV1>HV2				
No significant differences				



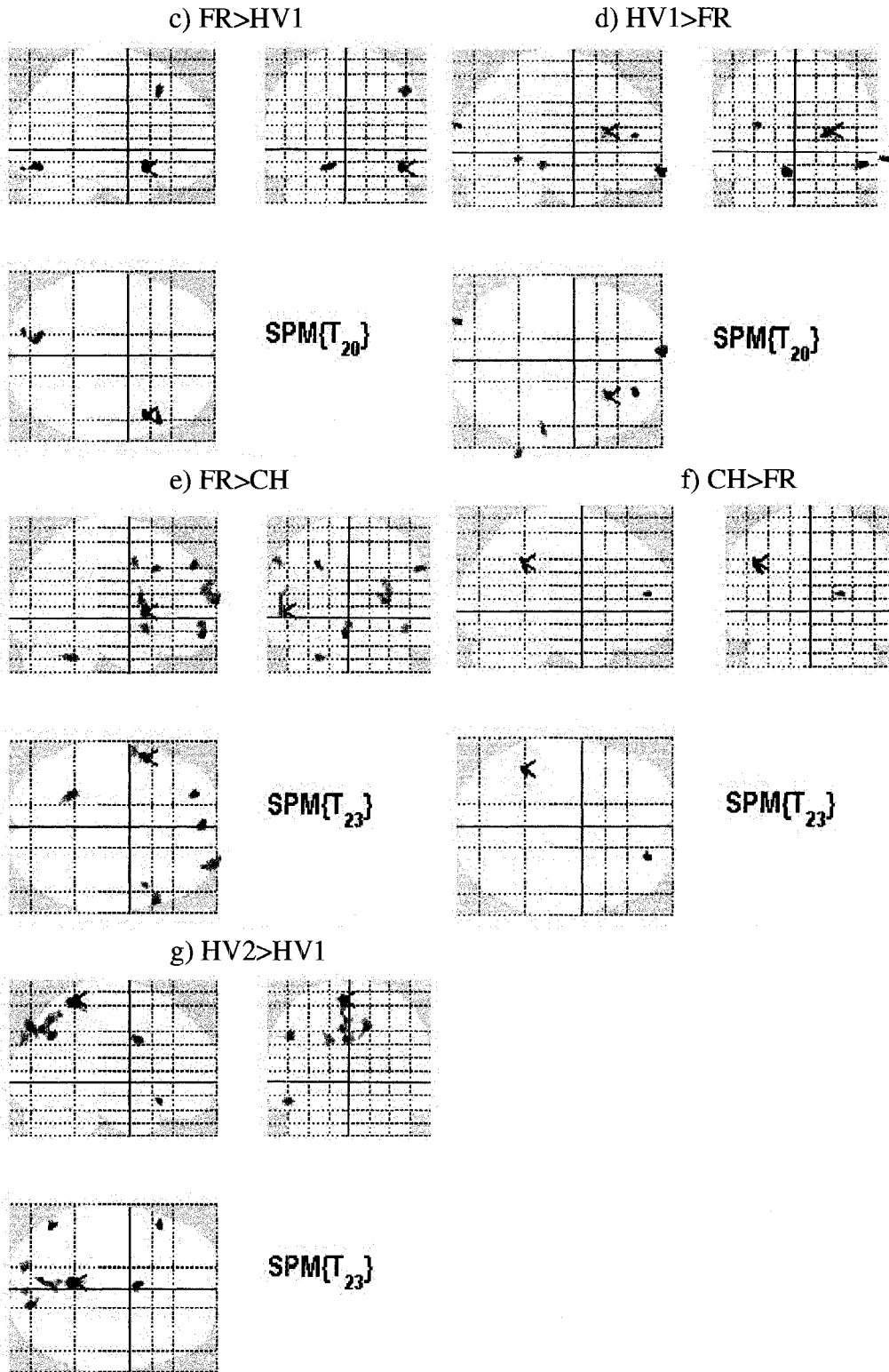


Figure 5-15. VBM Results Gray Matter

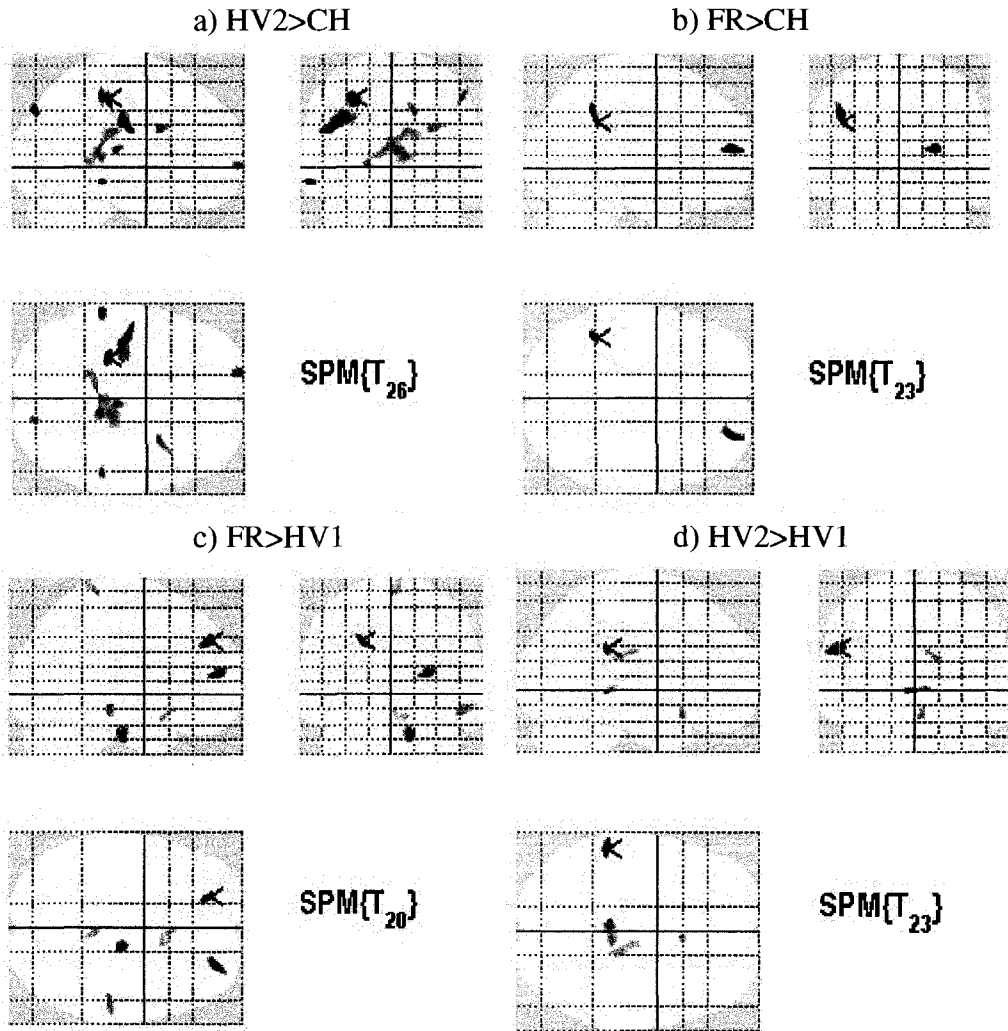


Figure 5-16. VBM Results White Matter

### 5.5.4 Functional Data for Block Design

An example of an individual functional activation map is given in Figure 5-17. The map shows typical activations in ACC, SMA, bilateral PMC and bilateral cerebellum. The red arrow shows activation in left STG, another area that was often activated. The individual maps have a lot of variation, especially in terms of the statistics, where the statistical threshold to obtain a reasonable-looking map varies considerably between individuals.

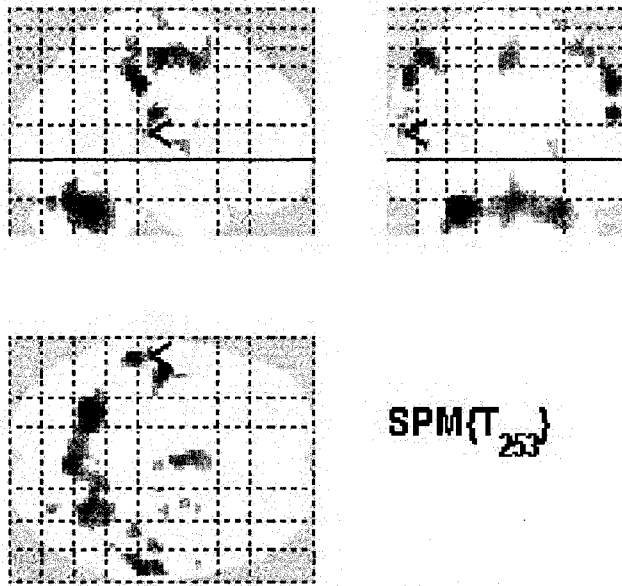


Figure 5-17. Individual Functional Activation Map (BJ31)

A summary of the random effects analysis for each group is given in Figure 5-18. The analyses show a similar main pattern for each group involving ACC/SMA, bilateral PMC, bilateral cerebellum, and bilateral caudate. There are also differences. The FR group is lacking cerebellum activation. The CH group has activation in bilateral occipital lobe that is not seen in other groups.

Correlation analyses of each group (healthy volunteers as one large group) with the log(RT) are summarized in Table 5-7. Only negative correlations are seen. Two areas are identified with the HV group. They include a cingulate area we expect from the PET results (Naito et al, 2000), although the correlation is not very strong. The results for the FR and CH groups, however, identify very different areas – CH in L inferior parietal lobule and FR in R precentral gyrus.

An ROI analysis of activation for correlation was also done as described in section 5.4.3.7. Table 5-8 shows the results for 2 measures: choice and choice-watch. The standard deviations are quite high relative to values, so no statistically significant differences are seen. The correlations have the right sign (a negative sign means increased activation correlates with lower reaction time) but are not statistically significant.

The results of the group comparison analyses are summarized in Tables 5-9, 5-10, 5-11, and 5-12 and shown in Figure 5-19. Note that only group comparisons identifying significant differences are shown in the tables. The HV1 to HV2 comparison revealed no significant differences, as expected.

Significant differences are seen in the comparisons HV2>CH, CH>HV2, FR>HV1, and FR>CH. The comparison HV2 >CH is to be expected and the areas identified seem reasonable with bilateral putamen and R cingulate gyrus. The cingulate gyrus agrees with the previous EEG study comparing HV and CH on a reaction time task. The R insula is an interesting result. The FR>HV1 is a surprising result. The expected result is activations in the FR group between those of HVs and CHs, but instead there are more. The FR>CH comparison is generally consistent with the other 2 comparisons, where some areas of the HV2>CH are present, and the areas in FR>HV1 also. One of the areas identified in the CH>HV2 comparison is a WM area. That is, it is too far from any GM areas for them to be included in its cluster of activations.

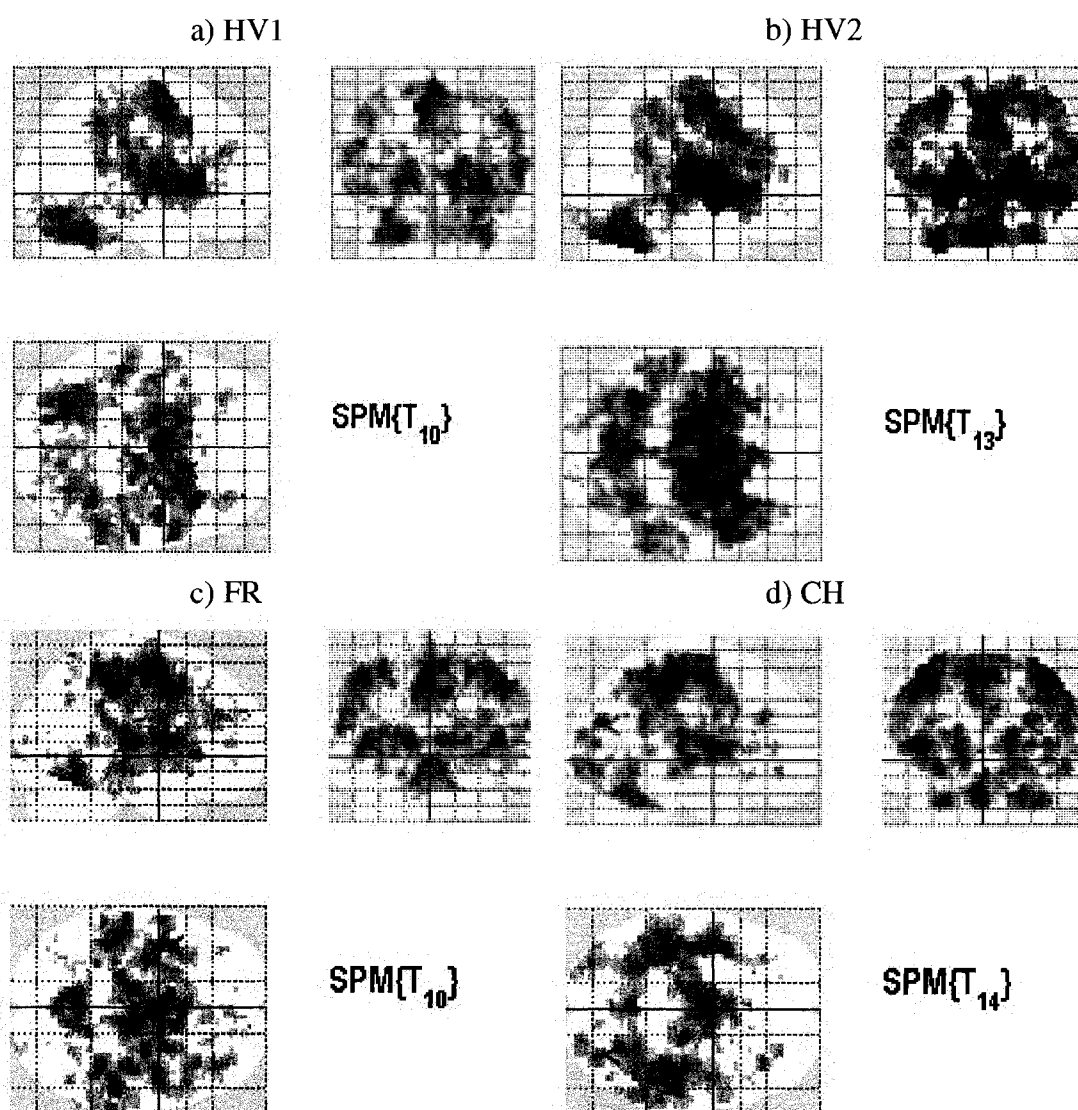


Figure 5-18. Random Effects Analysis for Groups on Block Design CRT

Table 5-7 Correlation of Activation With Median RT

Group	Neg or Pos	T-statistic – highest voxel	Highest Voxel (Talairach coordinates)	Cluster center description	# voxels in cluster	Puncorrected (cluster)
CH	-	5.08	(-56, -25, 34)	L Inferior Parietal Lobule BA 40	9	0.039
FR	-	5.90	(59, -2, 28)	R Precentral Gyrus BA 10	8	0.042
HV1	-	4.73	(-12, 19, 32)	L Cingulate Gyrus BA 32	10	0.067
HV2	-	4.17	(-3, 47, 11)	L Middle Frontal Gyrus BA 10	16	0.025

Table 5-8 ACC ROI Analysis Summary

Groups	%sc <sup>+</sup> Choice	Correlation* With RT	%sc <sup>+</sup> Choice- Watch	Correlation* With RT
HV1	0.760 ± 0.196	0.12	0.877 ± 0.306	-0.47
FR	0.971 ± 0.516	-0.21	0.974 ± 0.421	-0.54
HV2	0.898 ± 0.467	-0.27	0.790 ± 0.377	-0.18
CH	0.906 ± 0.446	-0.11	0.807 ± 0.318	-0.16

<sup>+</sup>%sc is percent signal change

\* Pearson correlation coefficient

Table 5-9 HV2 > CH Group Comparison Results

T-statistic – highest voxel	Highest Voxel (Talairach coordinates)	Cluster center description	# voxels in cluster	puncorrected (cluster)
4.88	(0, -5, 9)	Thalamus	9	0.081
4.86	(-27, 0, 0)	L Putamen	45	0.001
4.74	(27, 0, -5)	R Putamen	15	0.029
4.38	(27, 20, -6)	R Insula (BA47/13)	10	0.067
4.34	(3, 33, 26)	R Cingulate Gyrus (BA32)	9	0.081

Table 5-10 CH&gt;HV2 Group Comparison Results

T-statistic – highest voxel	Highest Voxel (Talairach coordinates)	Cluster center description	# voxels in cluster	puncorrected
4.87	(-45, -56, -9)	L Fusiform Gyrus BA37	12	0.047
4.62	(39, -16, 23)	R Insula	10	0.067

Table 5-11 FR &gt; HV1 Group Comparison Results

T-statistic – highest voxel	Highest Voxel (Talairach coordinates)	Cluster center description	# voxels in cluster	puncorrected
4.60	(48, -56, 36)	R Inferior Parietal Lobule BA 40	24	0.010
3.98	(21, 34, 40)	R Middle Frontal Gyrus (BA8)	13	0.047
3.78	(-3, -16, 34)	L Cingulate Gyrus (BA 24/23)	10	0.076
3.70	(6, 50, 6)	R Medial Frontal Gyrus (BA10)	21	0.015
3.68	(9, -48, 33)	R Precuneus (BA31)	26	0.008
3.54	(56, -15, -17)	R Inferior Temporal Gyrus (BA21)	9	0.091

Table 5-12 FR &gt; CH Group Comparison Results

T-statistic – highest voxel	Highest Voxel (Talairach coordinates)	Cluster center description	# voxels in cluster	puncorrected
5.69	(3, -13, 34)	R Cingulate Gyrus (BA24/23)	48	0.001
4.97	(24, 31, 40)	R Middle Frontal Gyrus (BA8)	20	0.018
4.44	(53, -13, -17)	R Middle Temporal Gyrus (BA21)	33	0.004
4.43	(3, 33, 26)	R Cingulate Gyrus (BA32)	15	0.037
4.08	(-56, 4, 22)	L IFG (BA9/44)	9	0.095
4.03	(-27, 0, 6)	L Putamen	25	0.010
3.88	(0, 47, 6))	Anterior Cingulate (BA32)	18	0.024

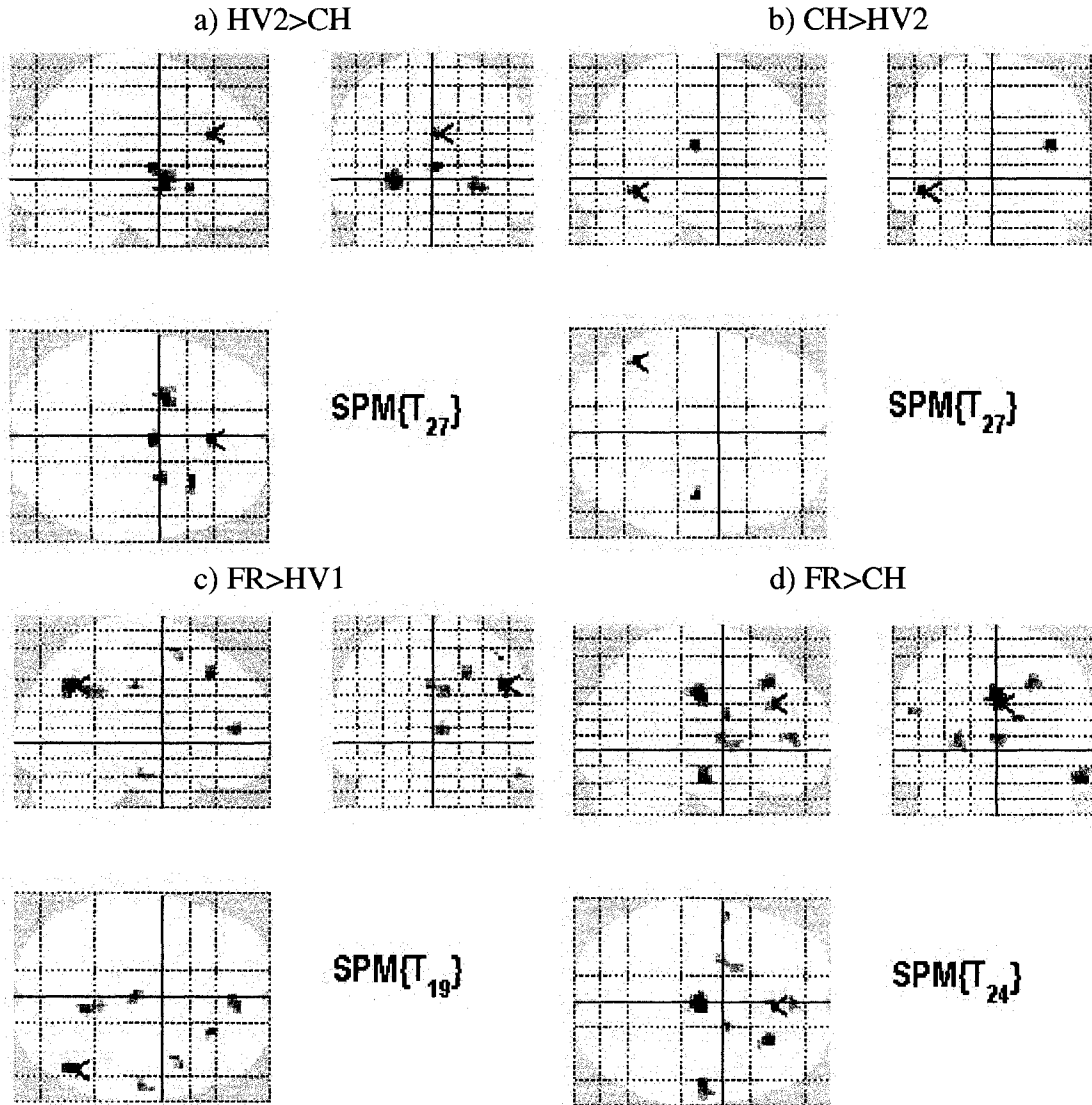


Figure 5-19. Group Comparison Maps for Block Design

### 5.5.5 Functional Data for Event-Related Design

An example of an individual functional activation map using the event-related design is given in Figure 5-20. The map shows typical activations in ACC, SMA, bilateral PMC and bilateral cerebellum. Other areas also show activation such as the right occipital lobe and the left superior temporal gyrus. This is the same individual as was shown in the individual activation map for the block design, so it is interesting to compare.



ACC/SMA, bilateral PMC, bilateral cerebellum, and bilateral caudate.

No correlation with RT, Age or IQ was done for the event-related design results.

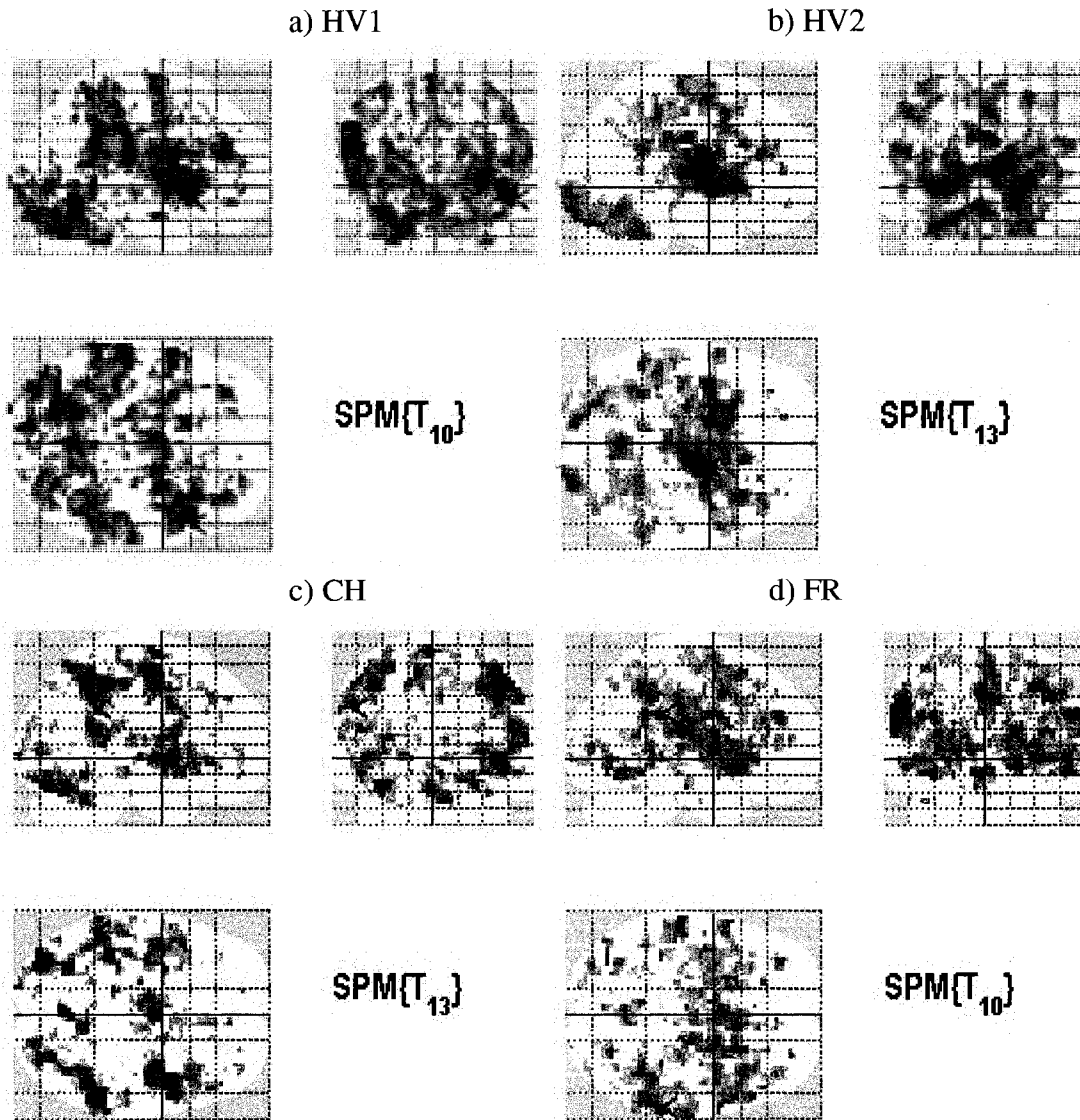


Figure 5-22. Random Effect Analysis Group Maps for Event-Related Design

The results of the group comparison analyses are summarized in Tables 5-13, 5-14, 5-15, 5-16 and 5-17 and Figure 5-23. Note that only group comparisons identifying significant differences are shown in the tables. Since the HV1 to HV2 comparison revealed some significant differences, the results of the event-related analysis are in question.

Table 5-13 HV2 > CH Event-Related Group Comparison Results

T-statistic – highest voxel	Highest Voxel (Talairach coordinates)	Cluster center description	# voxels in cluster	puncorrected
5.85	(18, 1, 22)	R Caudate Body	42	0.001
4.95	(-18, 47, 9)	L MFG/Anterior Cingulate (BA10)	11	0.045
4.89	(-24, -13, 23)	L Claustrum	9	0.067
4.01	(-30, 0, 3)	L Putamen	11	0.045
3.99	(-24, 17, -1)	L Putamen	7	0.101

Table 5-14 CH > HV2 Event-Related Group Comparison Results

T-statistic – highest voxel	Highest Voxel (Talairach coordinates)	Cluster center description	# voxels in cluster	puncorrected
4.27	(-12, -83, 26)	L Cuneus (BA 18/19)	11	0.045
4.06	(6, -50, -3)	R Cerebellum Culmen	9	0.067
3.85	(-48, -9, -7)	L Superior Temporal Gyrus (BA22)	8	0.082

Table 5-15 FR > HV1 Event-Related Group Comparison Results

T-statistic – highest voxel	Highest Voxel (Talairach coordinates)	Cluster center description	# voxels in cluster	puncorrected
5.18	(-48, -9, -10)	L STG (BA 21)	8	0.058
4.80	(33, -35, 5)	R Caudate Tail	8	0.058

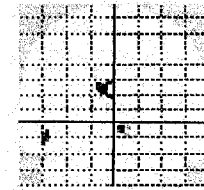
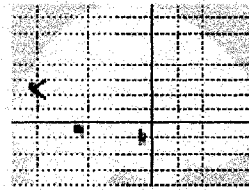
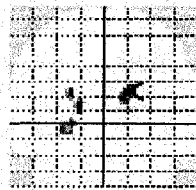
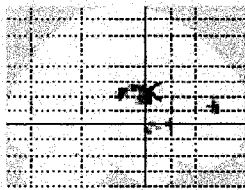
Table 5-16 HV1 > FR Event-Related Group Comparison Results

T-statistic – highest voxel	Highest Voxel (Talairach coordinates)	Cluster center description	# voxels in cluster	puncorrected
4.42	(36, 18, 18)	R Frontal Lobe Subgyral WM	6	0.095

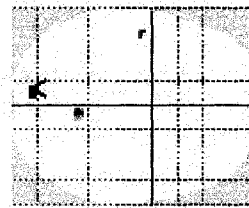
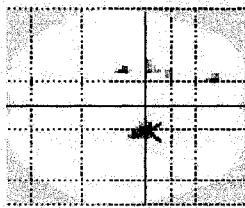
Table 5-17 HV1>HV2 Event-Related Group Comparison Results

T-statistic – highest voxel	Highest Voxel (Talairach coordinates)	Cluster center description	# voxels in cluster	puncorrected
5.52	(9, -52, 3)	R Cerebellum Culmen	72	0.000
5.00	(-21, 40, -10)	L Middle Frontal Gyrus (BA11)	8	0.088
4.67	(24, -67, 6)	R Posterior Cingulate (BA30)	11	0.049
4.20	(-15, -58, -2)	L Lingual Gyrus (BA19)	7	0.108
4.17	(-30, -70, 6)	L Lingual Gyrus (BA19)	11	0.049
4.06	(6, -76, -6)	R Lingual Gyrus (BA18)	39	0.001
3.91	(3, -83, 29)	R Cuneus BA 19	9	0.072

a) HV2>CH



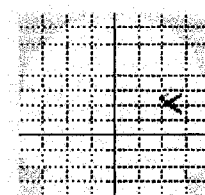
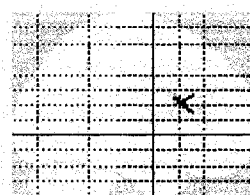
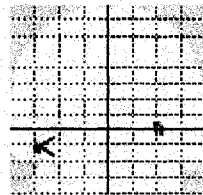
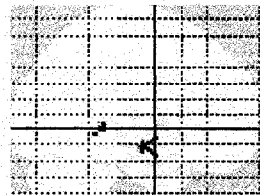
b) CH>HV2



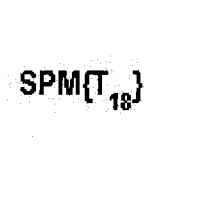
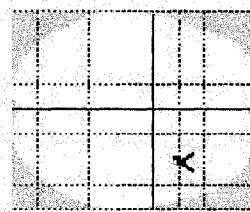
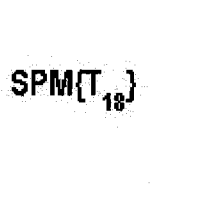
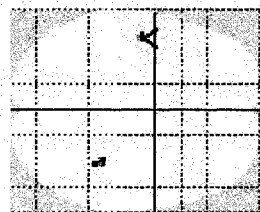
SPM{T<sub>25</sub>}

SPM{T<sub>25</sub>}

c) FR>HV1



d) HV1>FR



SPM{T<sub>18</sub>}

SPM{T<sub>18</sub>}

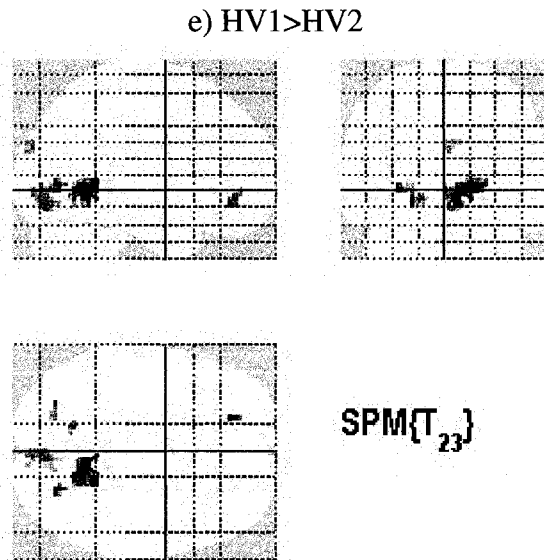


Figure 5-23. Group Comparison Maps for Event-Related Design

The group comparisons from the event-related design create a very different pattern than the results from the block design. Comparisons not reported yielded no significant differences, meaning no significant differences were observed for FR>HV, the most interesting result from the block design comparison. As well, significant differences were observed for HV1>HV2, where differences are not expected. At least the comparison of HV2>CH identifies some familiar areas from the block design contrast, such as medial frontal gyrus and anterior cingulate. As well, some areas are identified in the CH>HV2 comparison, including R cerebellum and L cuneus.

## 5.6 Discussion

### 5.6.1 Behavioural Results

The behavioural results show longer reaction times for people with chronic schizophrenia. This finding is fully anticipated by the literature described in §5.1.1 and meets hypothesis 1.

The reaction times for the event-related design are longer than for the block design because of the longer interstimulus interval in the event-related design (Welford, 1980), and possibly because of the rapid switching of subject set in the event-related design, in which the subject has to pay attention to the color of boxes on each trial.

RT is also correlated with Age and IQ to varying degrees, although the CH group does not show the same patterns as the other groups. The weak, negative correlation of RT

and IQ is anticipated by section 5.1.3. RT has a positive correlation with age, as was shown in the study by Deary and Der (2005).

The strongest correlation identified is that between Age and 50% interquartile range, achieving a Pearson correlation coefficient of 0.84 for HV1 group. This result, implying that variability in RT increases with age, is also shown in the study by Deary and Der (2005).

## **5.6.2 Volumetric and VBM Results**

The volumetric results show lower GM and WM volumes in the people with chronic schizophrenia. How does this compare with other studies?

Whole brain volumes (which includes ventricles and central canal) are reported by 2 meta-analyses as slightly lower in patients (Ward et al, 1996; Wright et al, 2000). Since increased ventricle size is a well-known finding in people with schizophrenia, going back as far as 1964 (Huber, 1964) and confirmed many times since (Johnstone et al, 1976; Raz & Raz, 1990; Shenton et al, 2001), the whole brain volume finding would suggest that GM or WM, or both, must be reduced in people with schizophrenia.

Of the studies that examined grey and white matter compartments separately, more have found reduction in GM than WM (Liddle & Pantelis, 2002).

Sigmundsson et al (2001) found whole gray matter deficits and white matter deficits of 5-6%, which was verging on significance. Their study had 27 subjects in each group and all patients were characterized as “with prominent negative symptoms”. This is consistent with the results found in this study.

The VBM results show deficits in GM and WM in localized regions of the brain. The most significant findings here show deficit in CH relative to HV2 in L MFG (BA 10 and 25), R parahippocampal gyrus (BA 28), R STG (BA 38), L STG (BA39), L postcentral gyrus and R posterior cingulate (BA 23/30). The ACC is not included in these areas so hypothesis 3) has evidence against it. There were also increases in GM in CH versus HV2 in L precentral gyrus, L parietal lobe WM and R IFG.

The fact that significant differences were shown in this method between the 2 HV groups (specifically HV2>HV1) does create questions in the significance of the results with people with schizophrenia and first-degree relatives.

A review of structural MRI findings in schizophrenia was conducted by Shenton et al (2001). The findings included chronic and first-episode patients groups. Brain areas,

excluding ventricles, that were more consistently reported to have differences included the medial temporal lobe (hippocampus, amygdala, parahippocampal gyrus), STG (GM), cavum septi pellucidi, and to a lesser extent basal ganglia and cerebellum. These findings would correspond with findings here showing deficit in R parahippocampal gyrus and bilateral STG.

A meta-analysis of 15 VBM studies of schizophrenia was reported by Honea (Honea, Crow, Passingham & Mackay, 2005). The most common findings were deficits in people with schizophrenia in left MTL and left STG, reported in 69% and 57% of studies respectively. Their meta-analysis considered size of smoothing kernel to be an important variable in the methods that affected the size of the region that could be distinguished. The studies included mostly groups of people with chronic schizophrenia, but some first-episode groups were included.

A study at the University of Alberta found enlarged caudate volumes in first-episode patients but not people with chronic schizophrenia (Kostov, Valiakayil, Seres & Tibbo, 2007).

A meta-analysis of brain volumes in first-degree relatives was recently published by Boos et al (2007). The meta-analysis considered 25 studies and found greatest deficit in relatives in the hippocampus relative to healthy volunteers. Differences were also found in overall GM (deficit in relatives) and third ventricle (increased in relatives). The current study did not find decreased GM in hippocampus in first-degree relatives.

More recent studies of first-degree relative brain structure have been completed by Honea et al, (2008) Gruber et al, (2008) Goldman et al (2008) and Mitelman et al (2008). Honea found no significant decreases in GM in the first-degree relatives. Gruber correlated lower levels of a neurotransmitter called neuregulin-1 haplotype (HAP<sub>ICE</sub>) with lower hippocampal volume in people with schizophrenia and their family members. Goldman compared people with schizophrenia and their relatives and found no differences in relatives. They suggest that brain structure is under genetic control but is not an endophenotype for schizophrenia. Mitelman tried to relate functional outcome with volumes and found regions of GM loss in frontal and temporal regions bilaterally were correlated. For WM, they found volumes in frontal, parietal and temporal lobes bilaterally were correlated.

### **5.6.3 Functional Results**

The block design finds areas of greater functional activation in healthy volunteers than people with chronic schizophrenia in thalamus, bilateral putamen, R insula and R

cingulate gyrus; whereas L inferior temporal gyrus and an area in R insula are greater in CH than HV2. This finding is consistent with the prediction of greater activation in ACC in healthy volunteers than people with chronic schizophrenia (hypothesis 2). The cingulate gyrus region identified is in the ACC. The thalamus and putamen regions also identified as hypoactive in people with chronic schizophrenia seem reasonable because these regions have been shown activated in other studies (Jansma, Ramsey, Slagter & Kahn, 2001; Winterer, Adams, Jones & Knutson, 2002). The fact that areas of cingulate gyrus and L putamen are also identified in the FR>CH comparison is a reassuring verification of the HV2>CH results.

The most interesting result is the hyperactivity in activation in the first-degree relatives compared to healthy volunteers. This hyperactivity corresponds reasonably well with the results of the FR>CH comparison to lend confidence in the results. In comparing a first-degree relatives group to a healthy volunteer group and a schizophrenia group, activity in the first-degree relative group is expected to be mid-way between the healthy volunteers and people with chronic schizophrenia so the diverse result of hyperactivity in first-degree relatives compared to hypoactivity in chronic schizophrenia is unexpected.

The hyperactivity especially in R MFG (BA 8 and 10) and L cingulate gyrus (BA24/23) in the first-degree relatives is suggestive of a burn-out process where these areas are hyperactive in people with a genetic susceptibility to schizophrenia. As schizophrenia develops, the hyperactivity may lead to apoptosis or changes in receptor density and lead to hypoactivity. However, this study found no volumetric changes in the areas identified in the functional differences.

A recent review of functional imaging results in first-degree relatives was reviewed to see if any similar results have been obtained in other functional neuroimaging studies (MacDonald, III, Thermenos, Barch & Seidman, 2008). The report points to 20 studies in diverse cognitive domains. The studies are summarized by reporting the comparisons of first-degree relatives to healthy volunteers in 8 broad areas. Each paper was examined individually for evidence of a diverse response in FR and CH groups, but no evidence was found.

Increased functional activation with similar performance on a task may be evidence of lower efficiency of the structure in performing the task, or it may represent compensatory activity when the usual network of areas is unavailable for some reason.

Is there any candidate for a neurotransmitter or receptor that could show a burnout? The dopamine system has long been considered altered in schizophrenia and may be a source of positive symptoms. Could the dopamine system provide any candidates for burnout?

The dopamine system consists of cell bodies that concentrate in the substantia nigra and ventral tegmental area and that project in 4 main connections: nigro-frontal, nigro-limbic, nigro-striatal and tubero-infundibular pathways. The last is a specific pathway relating the hypothalamus to pituitary gland and affects the sympathetic and parasympathetic nervous systems. The first is a projection to the nucleus accumbens in the frontal cortex and is implicated in triggering feelings of pleasure and reward behaviour. The nigro-limbic projection is a general projection throughout the limbic cortex, which includes cingulate cortex, amygdala and hippocampus, and appears to influence general states of excitability. The 3<sup>rd</sup> pathway is a projection to striatum and is implicated in movement. Loss of dopaminergic cell bodies is responsible for the movement disorders in Parkinson's disease. Loss of striatal cell bodies is implicated in Huntington's disease which also has movement disorders.

The nigro-limbic and nigro-striatal pathways may have something to do with the higher-order behaviour. Striatum is known to play a role in inhibition of movement, such as in Go/NoGo tasks, or the stop movement task (Vink et al, 2006). It also plays a role in procedural learning (Zedkova et al, 2007; Woodward et al, 2007; Reiss et al, 2006) and appears to be disordered in people with schizophrenia (Zedkova et al, 2007; Reiss et al, 2006) and first-degree relatives (Woodward et al, 2007). Striatum has also been shown to potentially play a role in decision threshold adaptation in a computational cognitive model (Lo & Wang, 2006).

ACC is a part of the limbic system and presumably receives dopaminergic projections and thus could be affected by abnormalities in the dopaminergic system. A normal effect of aging of the ACC and slow down in RT is known. An effect of aging on activity in the ACC was shown in a PET study by Pardo et al (2007) where clusters of negative correlation of brain activity with age were found. This is consistent with the other evidence that shows increasing RT with age (Deary & Der, 2005) and activation of ACC correlating with RT (Naito et al, 2000). So a degeneration of ACC and corresponding effect on RT is known from normal aging. The reason for the degeneration and how it affects RT is not known, but a similar process could impact people with schizophrenia.

However, dopamine may not be the only neurotransmitter system affected, or even the primary neurotransmitter responsible for the RT deficit in schizophrenia.

Glutamate and GABA are neurotransmitters that interact with the dopamine system, and glutamate antagonists such as PCP can induce a psychotic condition mimicking schizophrenia (refer to section 2.1.1). Glutamate affects both accelerator and brake so the actual outcome of a glutamate deficiency or overactivity depends on the actual conditions

(refer to Figure 2-2). Glutamatergic cells can be killed by excitotoxicity, which is an excess activation of glutamate receptors, and which is suggestive of a burnout process. This is the mechanism that could be proposed for the overactivity and eventual burnout seen in this functional imaging study.

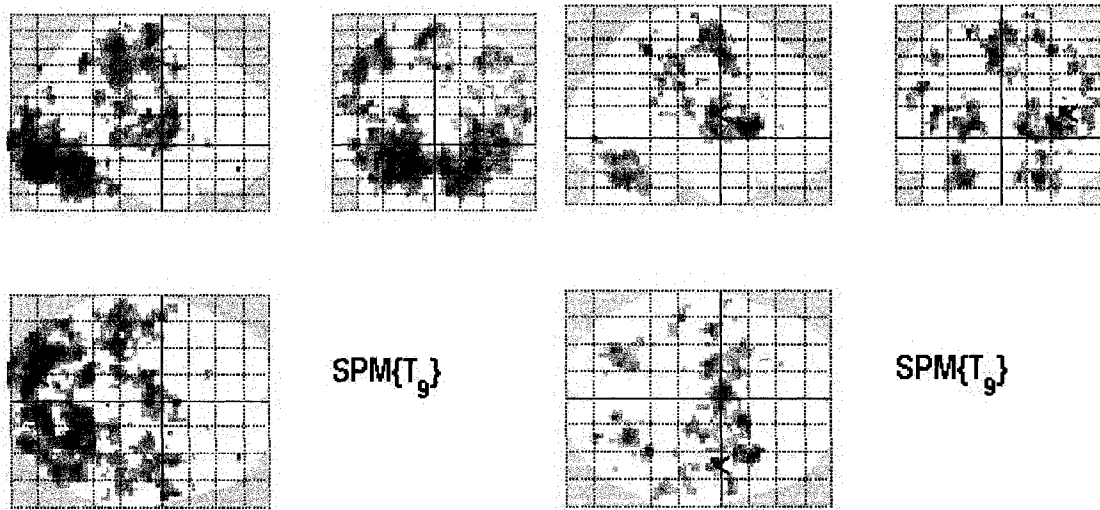
Computational biologically-based models would be useful tools to test the plausibility of this idea. A biologically-based model to simulate the CRT task could be developed, similar to the connectionist model developed for the CPT (Braver, Barch & Cohen, 1999) or the visual discrimination task (Lo & Wang, 2006). The impact of glutamate overactivity and glutamatergic cell death on the model could be evaluated to determine the effects and see if they can simulate the pattern of responses seen in this study.

A final caution is that the ACC is a diverse area that impacts many different parts of functioning of the brain, as shown by an analysis of resting state networks (Margulies et al, 2007). This fact must be considered carefully in reviewing functional studies of the ACC, as different areas of the ACC are involved with different functions. Even timing of the activation may be different, as seen by suggested involvement of ACC at different time scales in the ERP studies (Winterer et al, 2001).

#### **5.6.4 Other Functional Results**

There are several other potentially useful contrasts, at least for enhancing confidence in the results. Because the results are surprising, there is need for other analyses to enhance confidence. The additional analyses considered are flashing checkerboard, choice-only contrast, and watch-only contrast.

The flashing checkerboard is an additional functional task that was done at the end of scanning sessions. The membership in the groups was a little different for this task, as not everyone completed it. The areas involved in the flashing checkerboard are similar to those involved in the choice reaction time tasks – visual areas, primary motor and somatosensory areas, cerebellum, supplementary motor area and cingulate cortex. Thus, the RFX group maps for this task look very similar to those of the choice reaction time task (see Figure 5-24). However, the group comparisons are quite different. HV1 was greater than HV2 in R cuneus; whereas HV2 was greater than HV1 in frontal areas including MFG, SFG and cingulate gyrus. There were no significant differences between CH and HV2, and a few differences between HV1>FR and CH>FR.



a) HV1 Flashing Checkerboard

b) HV1 Block Design

Figure 5-24. Comparison of HV1 RFX Group Maps a) Flashing Checkerboard b) Block Design

The choice-only and watch-only contrasts can be done with block design and event-related design data. Since there are 3 conditions, a comparison can be made between any combination of the 3, and potentially interesting contrasts include the choice-only and watch-only, in which the condition named is compared to the fixation condition.

Choice-only contrast is expected to be similar to the choice vs watch contrast, but includes visual area activation and other activations that may be related to implicit timing, pattern recognition or others implicit tasks. Since these are inconsistent from individual to individual, the group level comparisons could be expected to be similar to choice > watch, except for the visual area activations. The group RFX maps are actually very busy (see Figure 5-25). The group comparison result are quite different from the choice > watch, and the most significant differences are found between the HV1 and HV2 groups, mostly in visual areas (occipital lobe, lingual gyrus, cuneus) but also L cerebellum. No significant differences were found in the HV2>CH and FR>HV1 comparisons.

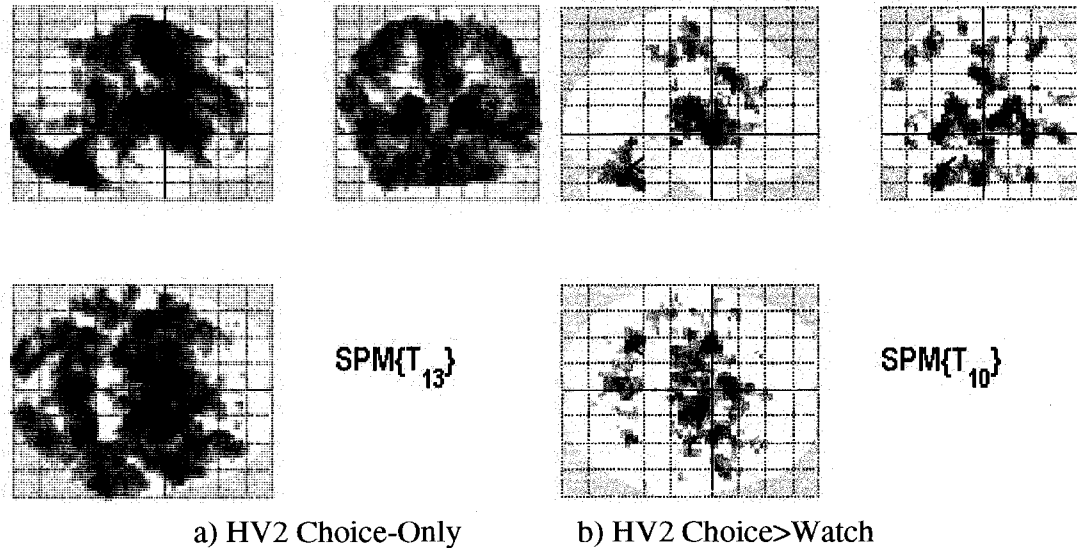


Figure 5-25. Comparison of HV2 Group RFX Maps a) Choice-Only b) Choice>Watch

Watch-only contrast is expected to produce activation mostly in visual areas, although implicit timing, pattern recognition and others may also be active. The maps are shown in Figure 5-26. The RFX group map for the FR group shows only 1 small area of activation in occipital lobe, but outside the primary visual areas. The RFX group map for the CH group shows strong activation in L primary visual areas, but very small on the right side. The HV1 RFX group map shows the expected bilateral activation in primary visual areas, as does the HV2 RFX group map, which also shows activation in bilateral cerebellum and R STG. These results are not as enlightening as we would hope. The group comparisons of the watch only show significant differences only for HV1>HV2, HV2>HV1 and HV1>FR. For HV1>HV2, the areas are R cuneus and L lingual gyrus. The HV2 is greater than HV1 in the corpus callosum. The HV1 is greater than FR in R SFG. Except for the HV1>HV2 in R cuneus, the other differences barely sneak under the 0.10 cluster level cutoff that has been used, suggesting the R cuneus in HV1>HV2 is the only real difference in activation between any of the groups in the watch-only test, which is a good result. This overactivity in R cuneus in the HV1 group was also seen in the flashing checkerboard analysis, which is a satisfying confirmation of the result.

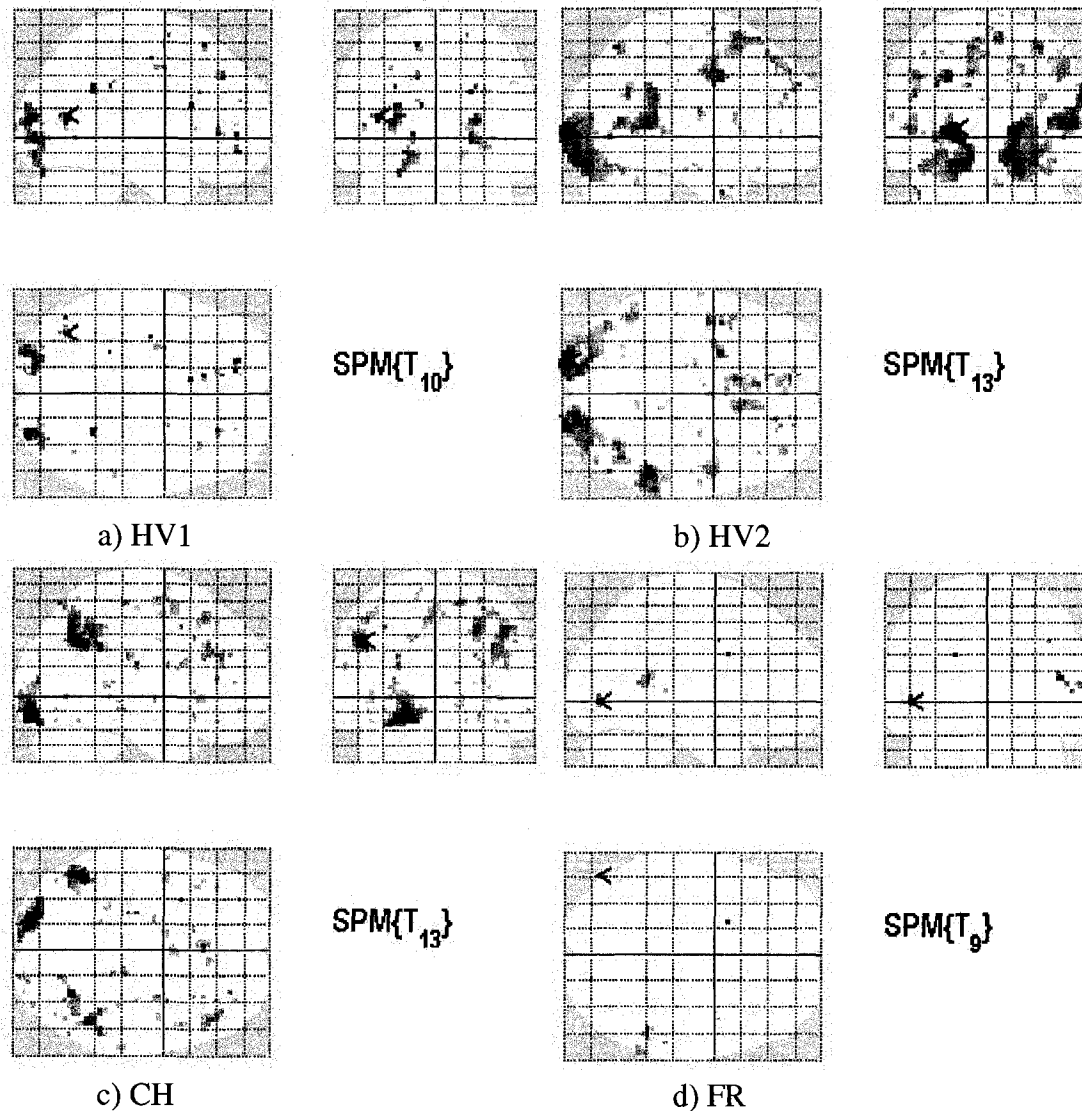


Figure 5-26. RFX Group Maps for Watch-Only Contrast

As well, the expected correlation of ACC activity to reaction time (Naito et al, 2000; Winterer, Adams, Jones & Knutson, 2002) does not hold for this study. This is another factor that leads to questioning of the study results. On the whole, no additional confidence in the results is gained by looking at these other analyses.

It is curious the differences found between HV1 and HV2 in the other tests. Since much of the differences are in visual areas, and the direction is HV1>HV2, it would suggest that subjects in the HV1 group have stronger activation, possibly because of differences in eyesight. The one member of the HV1 group that had very slow RT was removed and the watch-only analysis redone. The R cuneus was still overactive in the HV1 group.

## References:

- Ashburner, J., & Friston, K.J. (2000). Voxel-Based Morphometry – The Methods. *Neuroimage*, 11, 805-821.
- Ashton, L., Barnes, A., Livingston, M. & Wyper, D. (2000). Cingulate abnormalities associated with PANSS negative scores in first episode schizophrenia. *Behavioural Neurology*, 12, 93-101.
- Benes, F.M., Sorensen, I., Vincent, S.L., Bird, E.D. & Sathi, M. (1992). Increased density of glutamate-immunoreactive vertical processes in superficial laminae in cingulate cortex of schizophrenic brain. *Cerebral Cortex*, 2, 503-512.
- Boos, H.B., Aleman, A., Cahn, W., Pol, H.H., & Kahn, R.S. (2007). Brain volumes in relatives of patients with schizophrenia: A meta-analysis. *Archives of General Psychiatry*, 64(3), 297-304.
- Braff, D.L., Freedman, R., Schork, N.J., & Gottesman, I.I. (2007). Deconstructing schizophrenia: An overview of the use of endophenotypes in order to understand a complex disorder. *Schizophrenia Bulletin*, 33(1), 21-32.
- Brett, M., Anton, J-L., Valabregue, R., & Poline, J-B. (2002). Region of interest analysis using an SPM toolbox. 8<sup>th</sup> International Conference on Functional Mapping of the Human Brain, June 2-6, 2002, Sendai, Japan. Available on CD-ROM in *NeuroImage*, 16(2).
- Cancro, R. Sutton, S., Kerr, J. & Sugarman, A.A. (1971). Reaction time and prognosis in acute schizophrenia. *Journal of Nervous and Mental Disorders*, 153, 351-359.
- Carlsson, A. (2001). Neurotransmitters – Dopamine and beyond. In A. Breier, P.V. Tran, J.M. Herrea, G.D. Tollefson, F.P. Bymaster (Eds.), *Current issues in the psychopharmacology of schizophrenia* (Chap. 1, pp. 3-11). Philadelphia: Lippincott Williams & Wilkins Healthcare.
- Carter, C.S., Mintun, M., Nichols, T. & Cohen, J.D. (1997). Anterior cingulate gyrus dysfunction and selective attention deficits in schizophrenia: An <sup>15</sup>O H<sub>2</sub>O PET study during single trial stroop task performance. *American Journal of Psychiatry*, 154, 1670-1675.

- Carter, C.S., MacDonald III, A.W., Ross, L.L. & Stenger, V.A. (2001). Anterior cingulate cortex activity and impaired self-monitoring of performance in patients with schizophrenia: An event-related fMRI study. *American Journal of Psychiatry*, 158(9), 1423-1428.
- Deary, I.J. & Der, G. (2005). Reaction time, age and cognitive ability: Longitudinal findings from age 16 to 63 years in representative population samples. *Aging, Neuropsychology and Cognition*, 12, 187-215.
- Fan, J., McCandliss, B.D., Fossella, J., Flombaum, J.I. & Posner, M.I. (2005). The activation of attentional networks. *Neuroimage*, 26, 471-479.
- First, M.B., Spitzer, R.L., Gibbon, M., & Williams, J.B.W. (1995). *Structured clinical interview for DSM-IV axis I disorders – Patient edition (SCID-I/P, v2.0)*, New York, Biometrics Research Department, New York State Psychiatric Institute.
- Ford, JM, Gray, M., Whitfield, S.L., Turken, A.U., Glover, G., Faustman, W.O. et al (2004). Acquiring and inhibiting prepotent responses in schizophrenia. *Archives of General Psychiatry*, 61, 119-129.
- Gallinat, J., Mulert, C., Bajbouj, M., Herrmann, W.M., Schunter, J., Senkowski, D. et al (2002). Frontal and temporal dysfunction of auditory stimulus processing schizophrenia. *Neuroimage*, 17, 110-127.
- Gati, J.S., Menon, R.S., Ugurbil, K., & Rutt, B.K. (1997) Experimental determination of BOLD field strength dependence on vessels and tissue. *Magnetic Resonance in Medicine*, 38, 296-302.
- Goldman, A.L., Pazawas, L., Mattay, V.S., Fischl, B., Verchinski, B., Zolnick, B., Weinberger, D.R., & Meyer-Lindenberg, A. (2008). Heritability of brain morphology related to schizophrenia: A large-scale automated magnetic resonance imaging segmentation study. *Biological Psychiatry*, 63, 475-483.
- Green, M.F. (1996). What are the functional consequences of neurocognitive deficits in schizophrenia. *American Journal of Psychiatry*, 153(3), 321-330.
- Green, M.F., Kern, R.S., Braff, D.L., & Mintz, J. (2000). Neurocognitive deficits and functional outcome in schizophrenia: Are we measuring the "Right Stuff"? *Schizophrenia Bulletin*, 26, 119-136.

- Gruber, O., Falkai, P., Schneider-Axmann, T., Schwab, S.G., Wagner, M. & Maier, W. (2008). Neuregulain-1 haplotype HAP<sub>ICE</sub> is associated with lower hippocampal volumes in schizophrenic patients and in non-affected family members. *Journal of Psychiatric Research*, article in press, available 2 Jan, 2008.
- Hallmayer, J.F., Kalaydjieva, L., Badcock, J., Dragovic, M., Howell, S., Michie, P. et al (2005). Genetic evidence for a distinct subtype of schizophrenia characterized by pervasive cognitive deficit. *American Journal of Human Genetics*, 77, 468-476.
- Heinrichs, R.W. (2004). Meta-analysis and the science of schizophrenia: Variant evidence or evidence of variants? *Neuroscience and Biobehavioral Reviews*, 28, 379-394.
- Holden, A. A. (2004). *Functional magnetic resonance imaging: Determination of its feasibility at 4.7T and applications in parkinson's disease research at 1.5T* (Chapter 9). M.Sc. Thesis, Department of Biomedical Engineering, University of Alberta, Edmonton, AB.
- Honea, R., Crow, T.J., Passingham, D., & Mackay, C.E. (2005). Regional deficits in brain volume in schizophrenia: A meta-analysis of voxel-based morphometry studies. *American Journal of Psychiatry*, 162, 2233-2245.
- Honea, R.A., Meyer-Lindenberg, A., Hobbs, K.B., Pazawas, L., Mattay, V.S., Egan, M.F, Verchinski, B., Passingham, R.E., Weinberger, D.R., & Callicott, J.H. (2008). Is gray matter volume an intermediate phenotype for schizophrenia? A voxel-based morphometry study of patients with schizophrenia and their healthy siblings. *Biological Psychiatry*, 63, 465-474.
- Huber, G. (1964) Neuroradiologie und Psychiatrie. In H.W. Gruhle, R.Jung, W. Mayer-Gross & M.Muller (Eds.) *Psychiatrie der Gegenwart, Forschung und Praxis, Vol. 1 Grundlagenforschung Zur Psychiatrie* (Part B., pp. 253-290). Berlin: Springer-Verlag.
- Huston, P.E., Shakow, D., & Riggs, L.A. (1937). Studies of motor function in schizophrenia: II. Reaction time. *Journal of General Psychology*, 16, 39-82.
- Jansma, J.M., Ramsey, N.F., Slagter, H.A. & Kahn, R.S. (2001). Functional anatomical correlates of controlled and automatic processing. *Journal of Cognitive Neuroscience*, 13(6), 730-743.
- Jensen, A. & Munro, E. (1979). Reaction time, movement time and intelligence. *Intelligence*, 3, 121-126.

- Jobe, T.H. & Harrow, M. (2005). Long-term outcome of patients with schizophrenia: A review. *Canadian Journal of Psychiatry*, 50(14), 892-900.
- Johnstone, E.C., Crow, T.J., Frith, C.D., Husband, J. & Kreel, L. (1976). Cerebral ventricular size and cognitive impairment in chronic schizophrenia. *Lancet*, 2, 924-926.
- Kay, S.R., Fiszbein, A. & Opler, L.A. (1987). The positive and negative syndrome scale (PANSS) for schizophrenia. *Schizophrenia Bulletin*, 13, 261-276.
- Kiana, R., Shanks, T.D. & Shadlen, M.N. (2006). When is enough enough? *Nature Neuroscience*, 9(7), 861-863.
- Khosrow-Khavar, F. (2007) *Evaluation of functional MRI at 4.7T* (Chapter 6). M.Sc. Thesis, Department of Biomedical Engineering, University of Alberta, Edmonton, AB.
- Kostov, S., Valiakayil, A., Seres, P. & Tibbo, P. (2007). A volumetric MRI study of the caudate nuclei in first-episode and chronic patients with schizophrenia. *Schizophrenia Bulletin*, 33(2), 339.
- Lancaster, J.L., Rainey, L.H., Summerlin, J.L., Freitas, C.S., Fox, P.T., Evans, A.C., Toga, A.W. & Mazziotta, J.C. (1997). Automated labeling of the human brain: A preliminary report on the development and evaluation of a forward-transform method. *Human Brain Mapping*, 5(4), 238-242.
- Liddle, P.F., Friston, K.J., Frith, C.D. Hirsch, S.R., Jones, T. & Frackowiak, R.S. (1992). Patterns of cerebral blood flow in schizophrenia. *British Journal of Psychiatry*, 160, 179-186.
- Liddle, P. & Pantelis, C. (2003) Brain imaging in schizophrenia. In S.R. Hirsch & D.R. Weinberger (Eds.) *Schizophrenia*, 2<sup>nd</sup> ed (Chap. 22, pp. 403-417). Malden, Mass: Blackwell Science.
- Lo, C-C. & Wang, X-J. (2006). Cortico-basal ganglia circuit mechanism for a decision threshold in reaction time tasks. *Nature Neuroscience*, 9(7), 956- 963.
- Luciano, M., Wright, M.J., Geffen, G.M., Geffen, L.B., Smith, G.A. & Martin, N G. (2004). A genetic investigation of the covariation among inspection time, choice reaction time, and IQ subtest scores. *Behavior Genetics*, 34(1), 41-50.

- MacDonald, III, A.W., Thermenos, H.W., Barch, D.M., & Seidman, L.J. (2008). Imaging genetic susceptibility to schizophrenia: Systematic review of fMRI studies of patients' nonpsychotic relatives. *Schizophrenia Bulletin*, Advance access published June 12, 2008.
- Margulies, D.S., Kelly, A.M.C., Uddin, L.Q., Biswal, B.B., Castellanos, F.X., & Milham, M.P. (2007). Mapping the functional connectivity of anterior cingulate cortex. *NeuroImage*, 37, 579-588.
- Matza, L., Buchanan, R., Purdon, S.E., Brewster-Jordan, J., Zhao, Y., Purdon, S.E. & Revicki, D. (2006). Measuring changes in functional status among patients with schizophrenia: The link with cognitive impairment. *Schizophrenia Bulletin*, 32(4). 666-678.
- Mitelman, S.A., Brickman, A.M., Shihabuddin, L., Newmark, R.E., Hazlett, E.A., Haznedar, M.M. & Buchsbaum, M.S. (2007). A comprehensive assessment of gray and white matter volumes and their relationship to outcome and severity in schizophrenia. *NeuroImage*, 37, 449-462.
- Mulert, C., Gallinat, J., Pacual-Marqui, R., Dorn, H., Frick, K., Schlattmann, P. et al (2001). Reduced event-related current density in the anterior cingulate cortex in schizophrenia. *Neuroimage*, 13, 589-600.
- Mulert, C., Gallinat, J., Dorn, H., Herrmann, W.M. & Winterer, G. (2003). The relationship between reaction time, error rate and anterior cingulate cortex activity. *International Journal of Psychophysiology*, 47, 175-183.
- Mulert, C., Menzinger, E., Leicht, G., Pogarell, O. & Hegerl, U. (2005). Evidence for a close relationship between conscious effort and anterior cingulate activity. *International Journal of Psychophysiology*, 56, 65-80.
- Naito, E., Kinomura, S., Geyer, S., Kawashima, R., Roland, P.E. & Zilles, K., (2000). Fast reaction to different sensory modalities activates common fields in the motor areas, but the anterior cingulate cortex is involved in the speed of reaction. *Journal of Neurophysiology*, 83, 1701-1709.
- Ngan, E.T.C. & Liddle, P.F., (2000). Reaction time, symptom profiles and course of illness in schizophrenia. *Schizophrenia Research*, 46,195-201.
- Pardo, J.V., Lee, L.T., Sheikh, S.A., Surerus-Johnson, C., Shah, H., Munch, K.R., Carlis, J.V., Lewis, S.M., Kuskowski, M.A., & Dysken, M.W. (2007). Where the brain grows

old: Decline in anterior cingulate and medial prefrontal function with normal aging. *NeuroImage*, 35, 1231-1237.

Picard, N. & Strick, P.L. (1996). Motor areas of the medial wall: A review of their location and functional activation. *Cerebral Cortex*, 6, 342-353.

Price, C.J., Veltman, D.J., Ashburner, J., Josephs, O. & Friston, K.J. (1999). The critical relationship between the timing of stimulus presentation and data acquisition in blocked designs with fMRI. *Neuroimage*, 10, 36-44.

Raz, S. & Raz, N. (1990) Structural brain abnormalities in the major pcyhoses:A quantitative review of the evidence from computerized imaging. *Psychological Bulletin*, 108, 93-108.

Rijsdijk, F.V., Vernon, P.A. & Boomsma, D.I. (1998). The genetic basis of the relation between speed-of-information-processing and IQ. *Behavioural Brain Research*, 95, 77-84.

Roitman, J.D. & Shadlen, M.N. (2001). Response of neurons in the lateral intraparietal area during a combined visual discrimination reaction time task. *Journal of Neuroscience*, 22, 9475-9489.

Rubia, K., Russell, T., Bullmore, E.T., Soni, W., Brammer, M.J., Simmons, A. et al (2001). An fMRI study of reduced left prefrontal activation in schizophrenia during normal inhibitory function. *Schizophrenia Research*, 52, 47-55.

Schall, J.D. (2002). The neural selection and control of saccades by the frontal eye field. *Philosophical Transactions of the Royal Society of London B Biological Sciences*, 357, 1073-1082.

Shenton, M.E., Dickey, C.C., Frumin, M. & McCarley, R.W. (2001). A review of MRI findings in schizophrenia. *Schizophrenia Research*, 49, 1-52.

Sigmundsson, T, Suckling, J., Maier, M., Williams, S.C.R., Bullmore, E.T., Greenwood, K.E. et al (2001). Structural abnormalities in frontal, temporal and limbic regions and interconnecting white matter tracts in schizophrenic patients with prominent negative symptoms. *American Journal of Psychiatry*, 158(2), 234-243.

- Silverstein, S.M., Schenkel, L.S., Valone, C. & Nuernberger, S.W. (1998). Cognitive deficits and psychiatric rehabilitation outcomes in schizophrenia. *Psychiatric Quarterly*, 69,169-191.
- Smith, P.L. & Ratcliff, R. (2004). Psychology and neurobiology of simple decisions. *Trends in Neuroscience*, 27(3), 161-168.
- Vink, M., Ramsey, N.F., Raemaekers, M., Kahn, R.S. (2006). Striatal dysfunction in schizophrenia and unaffected relatives. *Biological Psychiatry*, 60, 32-39.
- Vogt, B.A., Finch, D.M. & Olson, C.R. (1995). Functional heterogeneity in cingulate cortex: The anterior executive and posterior evaluative regions. *Cerebral Cortex*, 2, 435-443.
- Ward, K.E., Friedman, L., Wise, A. & Schultz, S.C. (1996) Meta-analysis of brain and cranial size in schizophrenia. *Schizophrenia Research*, 22, 197-213.
- Welford, A.T. (1980). Choice reaction time: Basic concepts. In A.T. Welford (Ed.) *Reaction Times* (Chap. 3). New York: Academic Press.
- Wells & Kelley, (1922). The simple reaction time in psychosis. *American Journal of Psychiatry*, 2, 53-59.
- Winterer, G., Mulert, C., Mientus, S., Gallinat, J., Schlattmann, P., Dorn, H. et al (2001). P300 and LORETA: Comparison of normal subjects and schizophrenic patients. *Brain Topography*, 13(4), 299-313.
- Winterer, G., Adams, C.M., Jones, D.W. & Knutson, B. (2002). Volition to action – An event-related fMRI study. *Neuroimage*, 17, 851-858.
- Wong, K-F. & Wang, X-J. (2006). A recurrent network mechanism of time integration in perceptual decision. *Journal of Neuroscience*, 26(4), 1314-1328.
- Woodward N, Purdon SE, Meltzer HY, & Zald DH (2005). A meta-analysis of neuropsychological change to clozapine, olanzapine, quetiapine and risperidone in schizophrenia. *International Journal of Neuropsychopharmacology*, 8, 1-16.
- Wright, M., De Geus, E., Ando, J., Luciano, M., Posthuma, D., Ono, Y. et al (2001). Genetics of cognition: Outline of a collaborative twin study. *Twin Research*, 4(1), 48-56.

Wright, I.C., Rabe-Hesketh, S., Woodruff, P.W.R., David, A.S., Murray, R.M. & Bullmore, E.T. (2000). Meta-analysis of regional brain volumes in schizophrenia. *American Journal of Psychiatry*, 157, 16-25.

Yuasa, S., Kurachi, M., Suzuki, M., Kadono, Y., Matsui, M., Saitoh, O. et al (1995). Clinical symptoms and regional cerebral blood flow in schizophrenia. *European Archives of Psychiatry and Clinical Neuroscience*, 246, 7-12.

Yucel, M., Stuart, G.W., Maruff, P., Velakoulis, D., Crowe, S.F., Savage, G., & Pantelis, C. (2001). Hemispheric and gender-related differences in the gross morphology of the anterior cingulate/paracingulate cortex in normal volunteers: An MRI morphometric study. *Cerebral Cortex*, 11, 17-25.

Yucel, M., Stuart, G.W., Maruff, P., Wood, S.J., Savage, G.R., Smith, D.J., Crowe, S.F., Copolov, D.L., Velakoulis, D. & Pantelis, C. (2002). Paracingulate morphologic differences in males with established schizophrenia: A magnetic resonance imaging morphometric study. *Biological Psychiatry*, 52, 15-23.

Zahn, T.P., & Carpenter, W.T., (1978). Effects of short term outcome and clinical improvement on RT in acute schizophrenia. *Journal of Psychiatric Research*, 14, 59-68.

Zedkova, L., Woodward, N.D., Harding, I., Tibbo, P.G. & Purdon, S.E. (2006). Procedural learning in schizophrenia investigated with functional magnetic resonance imaging. *Schizophrenia Research*, 88, 198-207.

## Chapter 6: Conclusions

### 6.1 Summary

The important results of each part of the study will be briefly summarized here.

#### 6.1.1 Behavioural Results

The group average of each median RT was compared. HV1, HV2 and FR groups had very comparable RTs for the block and event-related designs. The chronic schizophrenia group had a significantly longer RT in both designs. Times on the event-related design of the study were longer than on the block design. These results match the expectations and confirm hypothesis 1.

#### 6.1.2 Volumetric and VBM Results

The average gray and white matter volumes of the groups were compared. GM was similar for HV1, HV2 and FR groups. GM in the CH group was about 10% lower than the HV2 group and met statistical significance, but was not significantly lower than the HV1 or FR groups. WM was a bit larger in the FR group, but not significantly. HV1 and HV2 groups had similar WM volumes. The CH group had a lower WM volume, but not meeting statistical significance. The CH group was about 9% lower than HV2 group in WM plus GM volume and met statistical significance. These results match expectations.

The VBM analysis identified many differences between the groups. For GM, HV2 showed greater than CH in some areas identified in other studies, namely bilateral STG and R parahippocampal gyrus. Other areas identified in the study with HV2>CH included L MFG, L postcentral gyrus and R posterior cingulate gyrus. On the other hand, CH were greater than HV2 in L precentral gyrus, L parietal lobe and R IFG. FR group had areas greater than the HV1 group in R STG, L lingual gyrus and R MFG. On the other hand, HV1 had greater than FR in R insula, L and R SFG, L superior occipital gyrus and R MTG. FR is greater than CH in L precentral gyrus, L and R MFG, L SFG, L cerebellum and R STG. CH is greater than FR in L supramarginal gyrus and R MFG. HV2 is greater than HV1 in L postcentral gyrus, L and R precuneus, L inferior parietal lobule, L IFG, L cingulate gyrus, and L and R cuneus. HV1 had no areas significantly larger than HV2.

For WM, HV2 was greater than CH in WM areas in L and R parietal lobe, L and R frontal lobe, L MTG, R sublobar, and R precuneus. No areas were larger for CH than HV2. FR was larger than HV1 in WM areas in L and R frontal lobe, R brainstem, R temporal lobe, and R frontal/limbic lobe. No areas were larger for HV1 than FR. FR was greater than CH in WM areas in L parietal lobe and R frontal lobe whereas no areas were larger in CH than FR. HV2 was larger than HV1 in WM areas in L parietal lobe, L sublobar, R MFG and R corpus callosum, whereas no areas were larger in HV1 than HV2.

The main findings in the literature are for deficits in schizophrenia in L STG and areas of L medial temporal lobe (hippocampus, amygdala, entorhinal cortex). The current study results do not confirm the hypothesis of a GM deficit in ACC for people with chronic schizophrenia or first-degree relatives.

### **6.1.3 Block Design Results**

The block design results are for group comparisons and correlations with RT. HV2 group had increased functional activation than CH group in thalamus, bilateral putamen, R insula and R cingulate gyrus, whereas CH has greater activation than HV2 in L IFG and R insula WM. This finding is consistent with the hypothesis of greater activation in ACC in healthy volunteers than people with chronic schizophrenia.

FR had larger activation than HV1 and CH. FR was greater than HV1 in R inferior parietal lobule, R MFG, L cingulate gyrus, R precuneus and R ITG. FR was greater than CH in 2 areas of R cingulate gyrus, R MFG, R MTG, L putamen and R anterior cingulate gyrus. The finding of hyperactivity in FR versus HV1 is surprising, especially since the hyperactivity includes cingulate gyrus.

Correlation between functional activation and RT was weak. Some correlation was shown in a cingulate gyrus area, but much weaker than results in the literature (Naito et al, 2000; Winterer, Adams, Jones & Knutson, 2002).

### **6.1.4 Event-Related Design Results**

The event-related design results are for group comparisons only. HV2 group had greater activation than CH group in L MFG/anterior cingulate gyrus, R caudate, L putamen and L claustrum. CH had greater than HV2 in areas of L cuneus, R cerebellum and L STG. These results are only consistent with the block design results in the L putamen. FR and CH groups had no significant activation differences. FR had greater activation than HV1 in L STG and R caudate tail. HV1 had greater than FR in R frontal lobe subgyral WM.

HV1 had greater than HV2 in R cerebellum, L MFG, R posterior cingulate gyrus, L lingual gyrus, L lingual gyrus and R lingual gyrus. The results are not consistent with the block design results and the differences between HV1 and HV2 suggest that results for the event-related design are not reliable.

## **6.2 Limitations**

The study as performed has some weaknesses and limitations. They will be discussed in accord with each section of the study.

### **6.2.1 Paradigm Design**

The watch condition is in the design to make a good contrast for the choice condition. There are many possible subtle effects that could influence the activations if comparing choice to a fixation or other “rest” condition. These include implicit timing, implicit pattern seeking, visual response, attention and possibly other cognitive tasks that haven’t been considered. As one example of these effects, the subjects will notice that some targets have a longer or shorter duration than others. This is implicit timing - a non-conscious routine that times the duration between targets (Praagstra, Kourtis, Kwok & Oostenveld, 2006).

The watch condition in theory should do away with a lot of these effects, but the big question mark is attention. Since no response is required in the watch condition, attention may not be the same as in the choice condition, and attention can affect everything else.

### **6.2.2 Behavioural**

The methods gave the expected results, but there were a couple of factors that might have affected the results. One is that the scanner can make some people sleepy, and this is even worse for those coming in at the end of their work day. 2 of the HVs in particular had trouble with the event-related design after lying sleepily in the scanner during the 5 minute structural scan. This may have affected some event-related results, but it is not likely to have affected the block design results.

Also, there were 2 subjects – 1 HV and 1 CH – who were very large and fit into the scanner only with difficulty. The CH subject complained on pain in his left elbow after the scans and this may have affected his performance as his RTs were high compared to the average CH.

One HV who had a good IQ score had very slow RT. Perhaps he didn’t remember the instruction that he should be pressing the buttons as soon as possible and instead was being a bit cautious.

Statistically, a median of the group RTs might be a fairer measure of the group RTs than the average because of the possibility of skewed results from the factors listed above. A comparison of median and average RTs for the groups is given below. Most groups show a small reduction in RT using the median as opposed to the average, but the difference is small.

Table 6-1 Median Versus Average Group RTs

Group	Median RT (ms)	Average RT (ms)	Direction of Change
HV1	287.95	290.70	-
HV2	297.75	300.37	-
FR	296.00	294.54	+
CH	332.00	339.73	-

### 6.2.3 Volumetric and VBM Study

There are several possible difficulties with the method used in the volumetric and VBM study. The first is with the segmentation. Although the procedure is pretty good when determining partial volumes in areas between GM and WM and GM and CSF/other, there is an artifact that can occur in partial volumes of WM and CSF. Since the signal intensity is largest for WM and smallest for CSF/other, partial volumes of these 2 tissue types, such as around the ventricles, can result in these voxels being specified as GM (Honea, Crow, Passingham & Mackay, 2005). This did in fact occur in some of the segmentations. No correction for this was attempted. There is no bias in this effect towards one group or the other, so it should have no bearing on the group comparison results.

A second method difficulty is with the choice of the spatial smoothing kernel. The smoothing helps to match intersubject variations in brain size and shape and has a large effect on what areas might eventually be found. Small smoothing kernels are required to find difference in small tissue areas such as hippocampus or amygdale. On the other hand, more false positive results occur for smaller smoothing kernels (Honea et al, 2005). The method used in this study for choosing a smoothing kernel was quite subjective. Quite different results were obtained with other smoothing kernels and the decision is based on limited experience with what might be expected.

Another problem specific to the volumetric calculation is in the routine used to calculate the volumes. This routine counts each voxel that has a non-zero number equally, so voxels that are partial-volumed will be counted as complete voxels for each tissue type. As this problem is again completely unbiased as to the group, it should not cause any

differences in the group comparisons, although the absolute values of the volumes are slightly larger than they really are.

#### **6.2.4 Functional Results**

There are a lot of contentious issues in fMRI analysis and interpretation. A few issues that affect the results of this study will be highlighted.

A first issue is with the intersubject comparison. Nonlinear warping of the individual's brain to a template is meant to standardize the subject's size and shape; however, many individuals have a recognizable shape even after the normalization. Spatial smoothing is also meant to help to minimize intersubject differences. Even leaving aside the issue of the effectiveness of the normalization and smoothing to minimize differences, there is evidence that individual's functional areas don't all map to exactly the same places relative to structures such as gyri and sulci (Brett, Johnsrude & Owen, 2002), although the relation for primary functional sensory and motor areas are well-related to gyral and sulcal anatomy (Brett, Johnsrude & Owen, 2002). In addition, there are structures such as the anterior cingulate gyrus that have anatomical variations between individuals (paracingulate gyrus and sulcus) (Yucel et al, 2001).

An alternate possibility is to use a standard test to locate a desired functional area in an individual and use that identification in other tests. This approach has been used by Kanwisher (Kanwisher, McDermott & Chun, 1997) and works very well for single subjects. (Note that the ROI analysis of correlation with log(RT) essentially used this method).

Another alternate approach is to match cortical locations, called cortex-based alignment (Fischl et al, 1999; Goebel, 2002; Goebel, 2004). In this method, after normalization of the subject brain to get approximate locations, the cortex-based alignment morphs the subject brain in trying to match the curvature of the subject brain to a target brain.

Although the issue described above affects the anatomical labelling of structures, there is a more immediate issue in the labelling. Labelling can be done according to macroanatomy (gyri and sulci), microanatomy (Brodmann's Areas) or functional areas. Labelling depends on the relation between different domains like Talairach space and Brodmann's cytoarchitectonic analysis which are not done on the same brain. Manual labelling is somewhat subjective and automated labelling such as the Talairach Demon (Lancaster et al, 1997) depends on someone's manual labelling.

In practice, often the peak voxel location is not identified as a GM area and the Talairach

Demon has a setting to find the closest gray matter area (Lancaster et al, 2000). Does this mean that spatial resolution of fMRI is not actually as good as expected? The reality is that the resolution in group-level analysis is not as good as in individual analysis. The spatial smoothing and normalization must affect the ability to accurately locate activation voxels. As a result, locating voxels in group level analyses involves some subjective judgement as well as non-ideal translation from individuals.

An issue with interpreting the results is with how to interpret negative activation. BVQX automatically identifies all voxels with statistical correlation with the defined model, whether these correlations are positive or negative, so that it is easy to see the negative activations but it is still a mystery what negative activations really mean. 2 theories for the negative BOLD effect are: i) the vascular blood steal, and ii) actual lowering of neural activity due to inhibitory connections (Kennerley et al, 2008). The vascular blood steal theory is a rerouting of blood flow from an inactive area to an active one, but this seems unlikely as there is lots of capacity in the system. The 2<sup>nd</sup> possibility has been investigated and seems to have some truth for at least some negative bold responses (Shmuel et al, 2002).

In general, the individual activation maps from the event-related design are weaker than in the block design. Although it was shown in Chapter 4 that event-related design is less effective than block design at detecting functional activation, I believe there are 2 additional reasons for the weak responses.

The first reason is the analysis which assumes the shape of HRF. Numerous studies have shown that the shape of the HRF varies a lot between individuals (Aguirre, Zarahn & D'Esposito, 1998; D'Esposito et al, 1999; Richter & Richter, 2003; Neumann et al, 2003). One study showed that using individual HRFs increased the power of the activation by (Hollmann et al, 2008). This is also the reason that the analysis of the event-related design with BVQX sometimes did not show as much activation as the SPM5 analysis. Whereas SPM5 uses the canonical HRF shape (note that I have been unable to find the exact specification of this canonical HRF), BVQX uses different HRF shapes based on mathematical models such as gamma variate functions. It is possible to obtain maps similar to those obtained by SPM5 by varying the HRF parameters in BVQX. Presumably it would also be possible to continue to vary the parameters until an optimum activation map was achieved, but this would be very time-consuming.

A second reason that the activations with event-related design may not match the block design is the strength of the magnet. Many studies have shown that the contrast-to-noise ratio (CNR) improves with higher magnet strength (Gati, 1997; Holden, 2004; Khosrow-Khavar, 2007). Most event-related studies have been done with 3T magnets. 1.5T may

have barely enough CNR for optimal conditions, and under sub-optimal conditions such as subject movement, it fails. The event-related design is much more dependent on the CNR because the event-related pattern does not produce as high a change in signal as the block design.

The weaker individual responses likely mean that the group comparisons are less reliable than in the block design.

### **6.2.5 Homogeneity of Groups**

In this study that was designed to identify an endophenotype, a surprising result was found that the first-degree relatives group had increased activity compared to healthy volunteers whereas the people with chronic schizophrenia had decreased activity. The finding is surprising in light of other studies with first-degree relative groups that found activity in first-degree relatives to be generally between the levels of activity in control groups and schizophrenia groups (MacDonald, III, et al, 2008). The finding may be explained as a burn-out phenomenon, but something similar would be expected to be seen in other studies if burn-out is the case. There may be an issue in the study with the recruitment of the groups.

There are 3 main groups recruited for the study and there could be people who do not meet the criteria in any of the groups (i.e. people with mental health issues such as addiction in the healthy volunteer group). The healthy volunteer group is divided into 2 separate groups which were then compared to each other and no significant differences were found (for the block-design paradigm). Thus one expects that these groups are good, although it is possible that both groups are equally contaminated by people who don't fit the healthy volunteer description. Other comparisons did find differences between the healthy volunteer groups.

There is certainly a difference in the chronic schizophrenia group of the current study compared to the baseline studies. The study by Mulert examined people with chronic schizophrenia who were mostly drug-free (Mulert et al, 2001) and the study by Gallinat examined mostly first-episode patients (Gallinat et al, 2002). So there is certainly a difference in drug use between the studies. It is possible that antipsychotic drug use could affect the results. However, the result with the chronic schizophrenia group is showing a deficit the same as the studies by Mulert and Gallinat. So it seems more likely that the first-degree relative group might have problems.

The comparison of the groups is predicated on the first-degree relative group having a genetic vulnerability to schizophrenia without having schizophrenia. It is possible that

some of these people might develop schizophrenia in the future. We might expect, however, that if people who later develop schizophrenia would already show the activity deficit of the chronic schizophrenia group, then that should bring the group activity level down in accord with the expectation. Alternately, if the hypothesized burnout process has not yet happened, those relatives who would go on to develop schizophrenia in the future would presumably experience the burnout process and the results of the current analysis would not change whatever the later status of the relatives.

The antipsychotic drug use could be affecting the chronic schizophrenia group so that the chronic schizophrenia group would be similar to the first-degree relatives without the drugs. However, this would be inconsistent with the results of the Mulert and Gallinat studies.

It is also possible that the genetic vulnerability may be present in some relatives and not others. However, that situation would be expected to result in the moving of the group activation closer to the activation of the healthy volunteer group, which would suggest that first-degree relatives with the genetic vulnerability may be even more extreme than the current study found.

Another factor that could affect the chronic schizophrenia group is addictive drug use as the people with drug-induced psychosis can be expected to have different genetics and different performance and activity on the RT test. If patients have drug-induced psychosis and are given antipsychotics as well as ceasing from drug use, then it is not clear whether the antipsychotics or the cessation of drug use are responsible for amelioration of the symptoms. As well, the accuracy of the SCID depends on the answers to the interview questions. However, the people with chronic schizophrenia often don't have good memories of what was happening at the time of their first break or are reluctant to talk about it, so a study that depends only an interview with the patients cannot be expected to give the most accurate diagnosis.

Of course there is always the issue of schizophrenia being potentially many different diseases with differing etiology and effects (Heinrichs, 2005). A measure of this might be the symptom scale or the family inheritance. The people with schizophrenia who have family histories might have different genetics than those who do not have anyone else in their family with the illness. Since this factor would be expected to affect other studies as well, so it is hard to see how that could explain the current study results.

### **6.3 Future Directions**

Despite the weaknesses and limitations of the existing methods, functional MRI is still a useful tool that will continue to be used and developed for all kinds of cognitive neuroscience, psychology, and psychiatry applications. Improvements to the methods will continue.

In particular for this study, there are numerous points of discussion. There is a weakness in the paradigm design in the watch condition and there may be some changes to the condition that could make it a better contrast condition to the choice, such as adding a button-pressing component.

Analysis methods will continue to improve and particularly in the 2 areas identified – the inter-subject comparisons and the GLM analysis of the event-related design – improvements are needed. There are already potential candidates to resolve these difficulties, and future projects could try to apply the alternate methods.

Despite all the issues, there are some exciting results from the study. The identification of a hyper-activity in the first-degree relatives is very surprising and unique. It points to a genetic vulnerability that could lead to a disease process. More scanning to determine when the burn-out may occur would be very interesting. Obvious candidates for inclusion are first-episode subjects (to address possible confounds of drugs, and to address disease progression) and ultra-high-risk subjects (teenagers who have risk factors as well as some prodromal-type symptoms, to address progression).

If the burnout process is related to neurotransmitter levels or receptors, scanning techniques such as magnetic resonance spectroscopy and PET on the same subjects could be very informative, as could diffusion tensor imaging (DTI) to measure white matter connections directly.

Computational models such as those used to model the visual discrimination task in monkeys (Lo & Wang, 2006) or to model the CPT (Braver, Barch & Cohen, 1999) could be developed to test any specific hypotheses of disorders and processes, such as glutamatergic overactivity and excitotoxicity.

The paradigm can be easily modified for many other interesting studies. Possible modifications to the paradigm include making it parametric (varying numbers of choice between simple, 2 and 4-choice) to examine different levels of activity in the same subject. Using the paradigm to look at the impact of smoking or the impact of different antipsychotic drugs is also possible.

In general, psychiatric investigations are progressing towards studies in which testing with all different techniques (neurocognitive, neurophysiological, electrophysiological, structural MRI, functional MRI) are done on the same subjects as part of long-term projects. The use of this paradigm could be extended into the Edmonton Early Psychosis Intervention Clinic which already includes many of these measures.

## References:

Braver, T.S., Barch, D.M., & Cohen, J.D. (1999). Cognition and control in schizophrenia: A computational model of dopamine and prefrontal function. *Biological Psychiatry*, 46, 312-328.

Brett, M., Johnsrude, I.S., & Owen, A.M. (2002). The problem of functional localization in the human brain. *Nature Reviews Neuroscience*, 3, 243-249.

D'Esposito, M., Zarahn, E., Aguirre, G.K. & Rypma, B. (1999). The effect of normal aging on the coupling of neural activity to the BOLD hemodynamic response. *Neuroimage* 10, 6-14.

Fischl, B., Sereno, M.I. & Dale, A.M. (1999). Cortical surface-based analysis. II: Inflation, flattening, and a surface-based coordinate system. *NeuroImage*, 9, 195-207.

Gallinat, J., Mulert, C., Bajbouj, M., Herrmann, W.M., Schunter, J., Senkowski, D. et al (2002). Frontal and temporal dysfunction of auditory stimulus processing schizophrenia. *Neuroimage*, 17, 110-127.

Gati, J.S., Menon, R.S., Ugurbil, K., & Rutt, B.K. (1997) Experimental determination of BOLD field strength dependence on vessels and tissue. *Magnetic Resonance in Medicine*, 38, 296-302.

Goebel, R., Staedtler, E., Munk, M.H.J., & Muckli, L. (2002). Cortex-based alignment using functional and structural constraints. *Neuroimage Supplement*.

Holden, A. A. (2004). *Functional magnetic resonance imaging: Determination of its feasibility at 4.7T and applications in parkinson's disease research at 1.5T* (Chapter 9). M.Sc. Thesis, Department of Biomedical Engineering, University of Alberta, Edmonton, AB.

Hollmann, M., Moench, T., Baecke, S., Luchtman, M., Tempelmann, C., Stadler, J., & Bernarding, J. (2008). Increased statistical power in event-related real-time fMRI (erfMRI) using individual hemodynamic response function: First results at 3T and 7T. *Proceedings of the International Society for Magnetic Resonance in Medicine*, 16, p 3624. Toronto, Canada.

- Honea, R., Crow, T.J., Passingham, D., & Mackay, C.E. (2005). Regional deficits in brain volume in schizophrenia: A meta-analysis of voxel-based morphometry studies. *American Journal of Psychiatry*, 162, 2233-2245.
- Kanwisher, N., McDermott, J. & Chun, M.M. (1997). The fusiform face area: A module in human extra-striate cortex specialized for face perception. *Journal of Neuroscience*, 17, 4302-4311.
- Kennerley, A.J., Boorman, L., Johnston, D., Zheng, Y., Redgrave, P., Mayhew, J.E., & Berwick, J. (2008). The negative BOLD effect in the rodent barrel cortex model: Investigation using multimodal imaging and electrophysiology. *Proceedings of the 18<sup>th</sup> Annual Conference of the International Society for Magnetic Resonance in Medicine*, Program 222.
- Khosrow-Khavar, F. (2007) *Evaluation of functional MRI at 4.7T* (Chapter 6). M.Sc. Thesis, Department of Biomedical Engineering, University of Alberta, Edmonton, AB.
- Lancaster, J.L., Rainey, L.H., Summerlin, J.L., Freitas, C.S., Fox, P.T., Evans, A.C., Toga, A.W. & Mazziotta, J.C. (1997). Automated labeling of the human brain: A preliminary report on the development and evaluation of a forward-transform method. *Human Brain Mapping*, 5(4), 238-242.
- Lancaster, J.L., Woldorff, M.G., Parsons, L.M., Liotti, M., Freitas, C.S., Rainey, L., Kochunov, P.V., Nickerson, D., Mikiten, S.A. & Fox, P.T. (2000). Automated talairach atlas labels for functional brain mapping. *Human Brain Mapping*, 10, 120-131.
- Lo, C-C. & Wang, X-J. (2006). Cortico-basal ganglia circuit mechanism for a decision threshold in reaction time tasks, *Nature Neuroscience*, 9(7), 956- 963.
- MacDonald, III, A.W., Thermenos, H.W., Barch, D.M., & Seidman, L.J. (2008). Imaging genetic susceptibility to schizophrenia: Systematic review of fMRI studies of patients' nonpsychotic relatives. *Schizophrenia Bulletin*, Advance access published June 12, 2008.
- Mulert, C., Gallinat, J., Pacual-Marqui, R., Dorn, H., Frick, K., Schlattmann, P. et al (2001). Reduced event-related current density in the anterior cingulate cortex in schizophrenia. *Neuroimage*, 13, 589-600.
- Naito, E., Kinomura, S., Geyer, S., Kawashima, R., Roland, P.E. & Zilles, K., (2000). Fast reaction to different sensory modalities activates common fields in the motor areas,

but the anterior cingulate cortex is involved in the speed of reaction. *Journal of Neurophysiology*, 83, 1701-1709.

Neumann, J., Lohmann, G., Zysset, S. & von Cramon, D.Y. (2003). Within-subject variability of BOLD response dynamics. *Neuroimage*, 19, 784-796.

Praamstra, P., Kourtis, D., Kwok, H.F., & Oostenveld, R. (2006). Neurophysiology of Implicit Timing in Serial Choice Reaction-Time Performance. *The Journal of Neuroscience*, 26(20), 5448-5455.

Richter, W. & Richter, M. (2003). The shape of the fMRI BOLD response in children and adults changes systematically with age. *Neuroimage*, 20, 1122-1131.

Shmuel, A., Yacoub, E., Pfeuffer, J., Van de Moortele, P-F., Adriany, G., Hu, X., & Ugurbil, K. (2002). Sustained negative BOLD, blood flow and oxygen consumption response and its coupling to the positive response in the human brain. *Neuron*, 36, 1195-1210.

Winterer, G., Adams, C.M., Jones, D.W. & Knutson, B. (2002). Volition to action – An event-related fMRI study. *Neuroimage*, 17, 851-858.

Yucel, M., Stuart, G.W., Maruff, P., Velakoulis, D., Crowe, S.F., Savage, G., & Pantelis, C. (2001). Hemispheric and gender-related differences in the gross morphology of the anterior cingulate/paracingulate cortex in normal volunteers: An MRI morphometric study. *Cerebral Cortex*, 11, 17-25.

## APPENDIX A SUMMARY of fMRI PAPERS in SCHIZOPHRENIA

During my first summer, I collected many papers that dealt with schizophrenia and fMRI and created a summary. Papers were collected initially from a review article on imaging in schizophrenia (Liddle & Pantelis, 2003). Additional papers were collected from searches of the journals Biological Psychiatry, Schizophrenia Research and Neuroimage.

Summary information for the papers was collected in an Excel spreadsheet. The papers were additionally summarized in a table showing papers according to a grid of the cognitive test used and subject groups. The summary is presented in Table A-1.

Table A-1

Patients/ Cognitive Deficit	Sub-Domain	Test	HVs	Chronic	First-episode, drug-naive	typical antipsychotics	atypical antipsychotics	relatives/high risk
Working Memory	Visuospatial	N-Back	Callicott (1999), Honey (2000)	Schlosser (2000), Fox (2005), Walter (2003), Barch (2003), Meyer-Lindberg (2001) PET	Lund (2002) LTE		Kumari (2006) rivastigmine, Jansma (2004)	
		Sternberg Item Recognition	Cairo (2004)	Cairo (2005), Manoach (2000), Manoach (2001)				
		Continuous Processing Test		Holmes (2005) + MD, Fukuta (2004) er	Barch (2001)			
		Ordering or Maintaining List	D'Esposito (1999) er, D'Esposito (2000) er					

Patients/ Cognitive Deficit	Sub-Domain	Test	HVs	Chronic	First-episode, drug-naive	typical antipsychotics	atypical antipsychotics	relatives/ high risk
		Counting Multiple Sets (attention-shift)	Li (2004)					
	Auditory (Letters unless otherwise specified)	N-Back	Honey (2002)	Walter (2003), Barch (2003), Schlosser (2003), Thermenos (2005), Callicott (2000), Callicott (2003), Menon (2001) (presented by sound), Perlstein (2003)	Mendrek (2000)	Honey (2002),	Jacobsen (2004) nicotine	Callicott (2003)
		Sternberg Item Recognition	Rypma (1999)	Wolf (2005), Manoach (1998)				
		Continuous Processing Test		Perlstein (2003)	Barch (2001)			Thermenos (2004)
		Word and Tone Serial Position		Stevens (1998) (presented by sound)				
	Visual Cue/Choice			Kindermann (2004)			Quintana (2003)	
	Levels of Processing of Words for Memory			Kubicki (2003)				

Patients/ Cognitive Deficit	Sub-Domain	Test	HVs	Chronic	First-episode, drug-naive	typical antipsychotics	atypical antipsychotics	relatives/ high risk
Verbal Learning and Memory	verbal fluency				Boksmann (2005)		Jones (2004) quetiapine, Weiss (2004), Yurgelun-Todd (2005) D-cycloserine	Picchioni (2001) twins
	Hayling Sentence Completion/ Cloze Probability			Lawrie (2002), Arcuri (2001), Sommer (2003) female			Sommer (2001) clozapine,	Whalley (2005)
	semantic categorization and subvocal rehearsal		Krant (2002, 2003) Assaf (2006)	Welchew (2002)				
	Discourse coherence			Caplan (2001) (children and epileptics)				
	Auditory Hallucinations		Sokhi (2005) er	Shergill (2000) er, van de Ven (2005)				
	Lexical Decision and Retrieval			Foucher (2005)				
	Synonym Judgment						Tendolkar (2004)	
	Sentence Formation using Two Words			Stone (2005)				

Patients/ Cognitive Deficit	Sub-Domain	Test	HVs	Chronic	First-episode, drug-naive	typical antipsychotics	atypical antipsychotics	relatives/ high risk
Visual Learning and Memory	Saccade/Anti-saccade			Matsuura (2004) also SPEM, McDowell (2001), Raemaekers (2001) er				Raemaekers et al (2005)
	Smooth Pursuit Eye Movement			Hong (2005), Lencer (2005)			Tanabe (2005) nicotine	
	Episodic Memory			Bonner-Jackson (2005), Leube (2003), Zorrilla (2002)			Northoff (2005) ketamine	
	Face Recognition		Landau (2004) (learning) er					
Attention / Vigilance	Single Finger Opposition - Paced or Non-Paced			Buckley (1996), Ganesan (2005) er	Lencz (2000)		Bertolino (2004) olanzapine	
	Sequential Finger Opposition			Braus (1999)				
	Auditory Oddball		Schall (2003)	Kiehl (2005) er, Laurens (2005) er, Winterer (2003) EEG			Kiehl (2001), mostly olanzapine, Ngan (2003) er	Winterer (2003) EEG
	Visual Oddball			Ford (2005), Morey (2005)				

Patients/ Cognitive Deficit	Sub-Domain	Test	HVs	Chronic	First-episode, drug-naive	typical antipsychotics	atypical antipsychotics	relatives/ high risk
	Learned Irrelevance/ Latent Inhibition		Young (2005)					
	Oculomotor Delayed Response			Camchong (2005)				
	Motor Go No-Go Inhibition			Ford (2005) mostly atypical Arce (2006)			Rubia (2001)	
	Startle Reflex Inhibition			Swerdlow (2001)				
Reasoning and Problem Solving	Two-choice prediction and response task?			Paulus (2002)	Juckel (2006)			
	Wisconsin Card Sorting				Riehemann (2000)			
	Tower of London			Ward (2001)				
	Paper-Stone- Scissors Game			Omori (2000)				
Speed of Processing	Pronation/ Supination			Schroder (1999)				
	Stroop Color Word Interference			Jeong (2005) et al				

Patients/ Cognitive Deficit	Sub-Domain	Test	HVs	Chronic	First-episode, drug-naive	typical antipsychotics	atypical antipsychotics	relatives/ high risk
	Monitoring Self-Motion		Leube (2003)					Artiges (2003)
	Number comparison			Artiges (2005) er, Dehaene (2003) er				
Social Cognition	Viewing Affective Pictures			Takahashi et al (2004), Fahim (2005), Northoff (catatonia)				
	Face Emotion Processing			Holt (2005), Kosaka (2002), Holt (2005), Suzuki (2004), Schneider (1998)				
	Viewing Sad Films					Stip (2005) quetiapine		
	Comic Strip Stories		Vollm (2006)					
Procedural Learning	Blocked Periodic Sequence Learning	Serial Reaction Time Task (SRTT)	Reiss (2005)	Kumari (2002) mostly typical Ledkova (2006)			Reiss (2006)	Woodward (2007)

References:

Liddle, P & Pantelis, C. (2003) Brain Imaging in Schizophrenia. In J.R. Hirsch & D.R. Weinberger (Eds.), *Schizophrenia*, 2<sup>nd</sup> ed (Chap. 22). Malden, Mass.:Blackwell Science.

## **APPENDIX B DEVELOPMENT OF HTML VERSION OF THE SCID**

The SCID is a document on paper with 9 modules, an overview, and a summary section. Pages generally follow a 3-column pattern where headings and questions to ask are down the first column, information from the DSM-IV is in the second column, and the third column has a place to record the judgement. Many questions will result in skipping to another module or another page in the same module. As well, after the SCID is finished, the interviewer must transfer the judgements onto a summary page at the end.

A set of video tapes is available for training on the SCID. The tapes contain a detailed discussion of each module of the SCID and sample interviews and are available from EEPIC – the Edmonton Early Psychosis Intervention Clinic. After the video training, I practiced a few times with my wife and fellow students.

The SCID can be obtained in a computer version, however I decided to create my own computer version of the SCID as it seemed a perfect web-style application and I had some experience with web pages.

All the pages of the SCID were scanned into a gif format, a picture format that is quite compressed to minimize the file sizes. Our computer expert, Beau Sapach, wrote a Java script that would save the judgements as they are made into a window on the screen. The following recording elements were used: checkbox, radio button, and text box. The pages were created using FrontPage since the facilities for editing and viewing web pages and holding together all the files and pictures as a project are very helpful.

The display is formatted in 3 sections. The first section displays the first 2 columns of the SCID page. The second section is the third column of the SCID transformed into the 3 kinds of Java input objects. This section also contains the links that enable the user to skip directly to the desired page where called for in the SCID. The 3rd section is a small text box at the bottom of the page that records all the inputs with a numeric code that identifies precisely which question is being answered. The numeric code is taken from the SCID where possible, though not everything is numbered in the SCID.

Finally, the application was tested by going through every page using sample interviews, and checking that all the input objects and links performed correctly. The whole process was performed through February and March 2006. Now, to perform an interview, the html SCID is used with no pages to photocopy or store. Each interview file is backed up

onto a memory stick and a version of the html SCID is also kept on memory stick as well, in case something should happen to the version at work.

All-in-all, the html SCID has been a very useful tool that saves a lot of time, paper and administration.

## APPENDIX C CHOICE vs SIMPLE PARADIGM RESULTS

The paradigm initially tested was a contrast of choice vs simple reaction time. Simple reaction time is when there is only 1 motor response, versus 2 or more in choice reaction time. The simple versus choice contrast was suggested as being likely to activate areas such as the ACC. The paradigm was tested on students and other people I knew to check that reasonable results could be obtained. However, initial results with the simple versus choice reaction time contrast resulted in nothing – no areas activated more in one task than the other. From looking at the individual tasks versus the fixation cross, some expected areas were being activated so it wasn't a problem with the data. As a result, the paradigm was changed to choice vs watch and then substantial ACC activations were observed.

This appendix documents results from these initial tests with simple versus choice contrast.

The choice condition has already been discussed in the body of the thesis. The simple condition used the same basic display, but turned only one box outline red to show the subject which button to press. For most of the paradigms, an equal number of left and right buttons were used in the simple condition. In case the switching between left and right within a simple block approximated the choice, a second paradigm was set up in which within a simple block, all responses were the same. This paradigm was called the finger block paradigm compared to the other one which was called, for historical reasons, the long CRT, which contained 6 of each fixation, choice and simple block with each block being 24 seconds long.

Examples of results on the subjects are shown in the figures below.

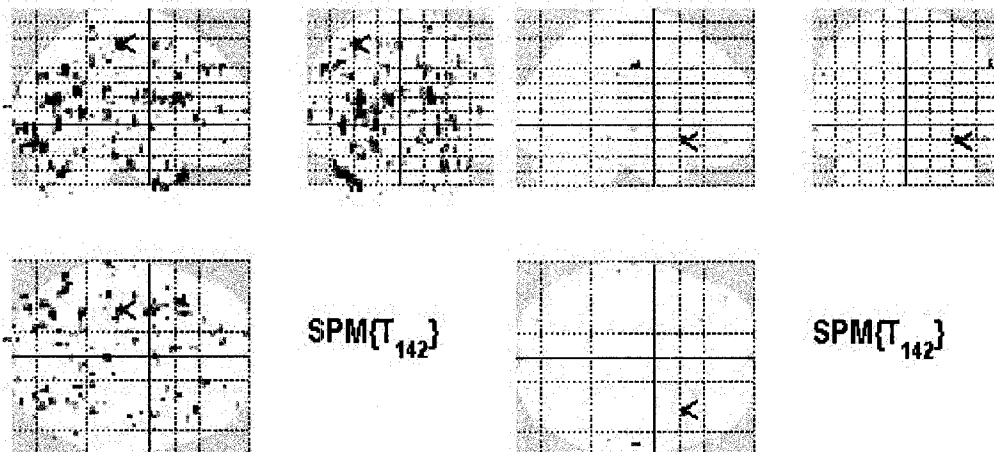


Figure C-1 a) Choice>Simple b) Simple > Choice with  $p < 0.001$  – Subject 1

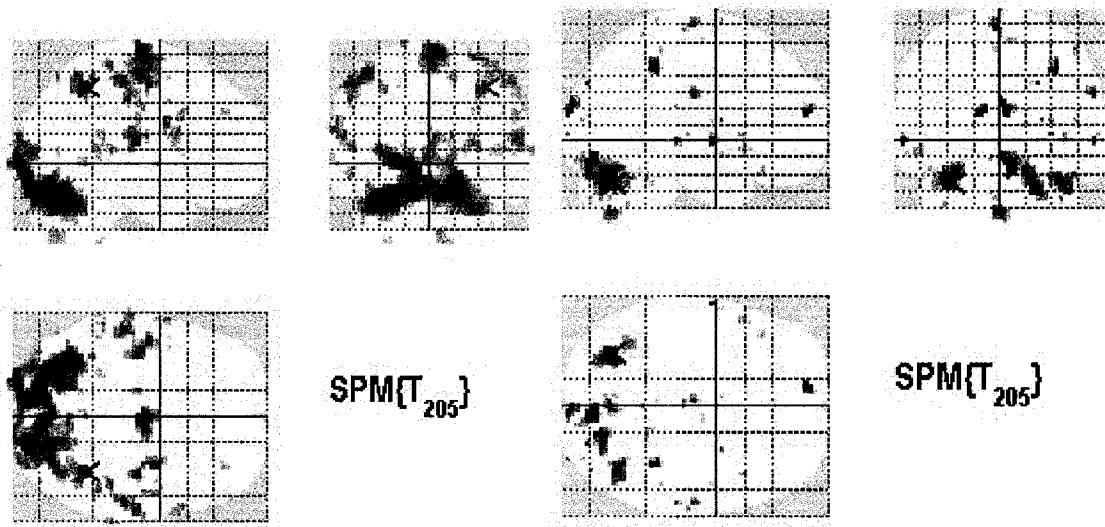


Figure C-2 a) Choice>Fixation b) Choice>Simple with  $p < 0.001$  – Subject 2 Finger Blocks

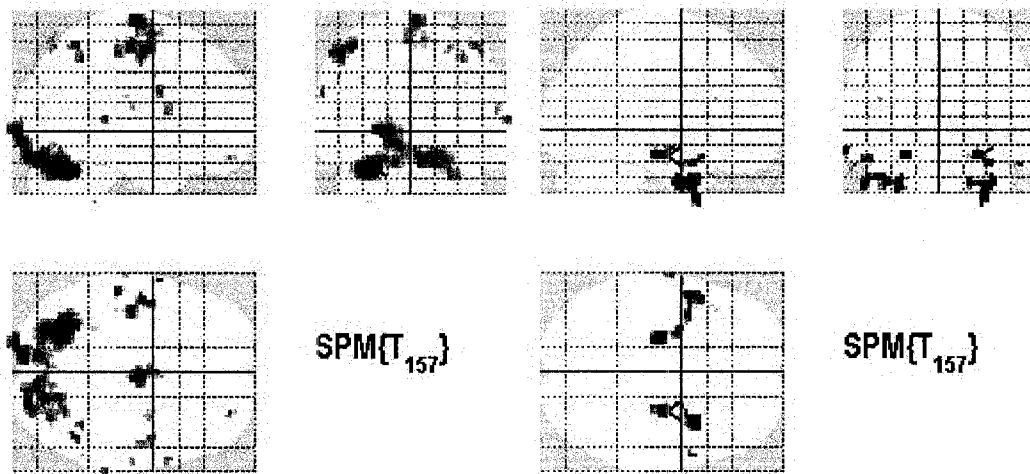


Figure C-3 a) Choice>Fixation b) Choice>Simple with  $FWE < 0.05$  – Subject 2

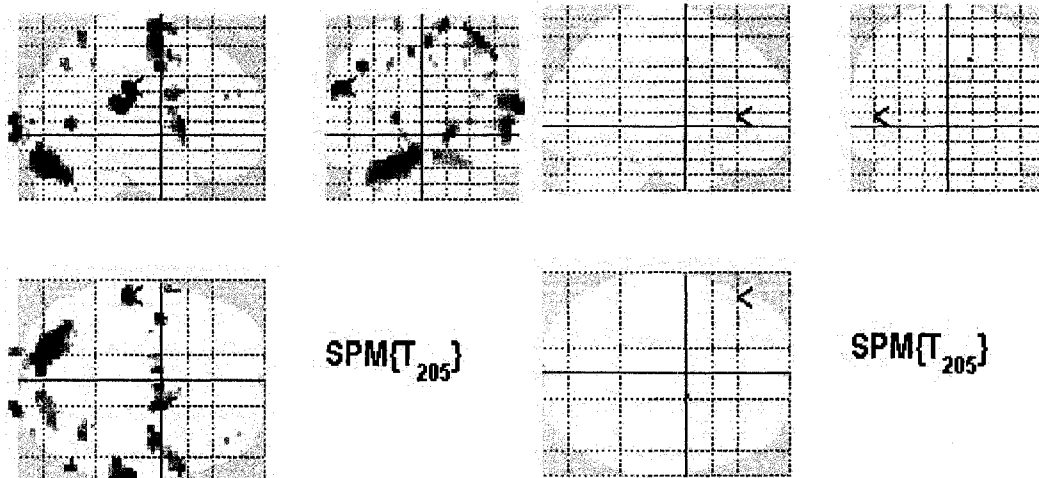


Figure C-4 a) Choice>Fixation b) Choice>Simple with  $p < 0.001$  – Subject 3

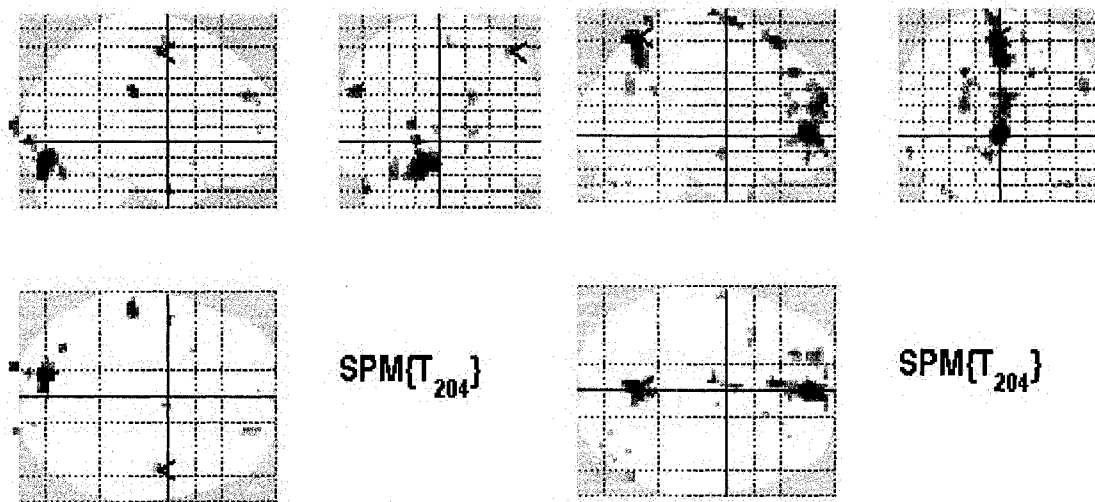


Figure C-5 a) Choice>Fixation b) Choice>Simple with  $FWE < 0.05$  – Subject 3 Finger Blocks

## **APPENDIX D EVENT-RELATED ANALYSIS of FAST versus SLOW RESPONSES**

Event-related design gives many options for analysis. One of the most interesting is to use the subjects own behaviour to separate responses. A nice example is left and right responses.

We would expect that a contrast of left only choice vs watch would show activation in only right primary motor cortex and left cerebellum rather than bilateral in these areas. In at least of the subjects, this is what is seen, though the limits of the event-related design at 1.5T prevent seeing this pattern in all subjects. Some examples of these results are given below.

Another very interesting possibility is to compare the fast and slow responses of a subject versus each other. Since we have some results that show that activity in the anterior cingulate cortex is negatively correlated with reaction time, we might expect to see some activation in anterior cingulate cortex as a result of a comparison of a subject's fast versus slow reaction time. If we could see this, it would be an elegant verification of the correlation.

To perform the contrast, a MATLAB program was written to divide each subject's responses into fast, middle and slow, using 30%, 40% and 30% quartiles, and output a file with a vector of event times for each condition. These vectors of event times were used to create a separate design matrix for each individual. A contrast of fast>slow (1 0 - 1) was used.

Results from the analysis were inconsistent and no activations of anterior cingulate cortex were seen. Examples of the results are shown below. A group fixed effects analysis of 8 healthy volunteers showed only 2 significant areas (cluster  $p < 0.10$ ): R MFG BA 11 and L globus pallidus. So this analysis is not achieving anything.

Figure F-1 a) through show examples of individual results with the fast-slow dichotomy. Figure F-2 shows a group map from a fixed effects fast-slow analysis with 8 HVs.

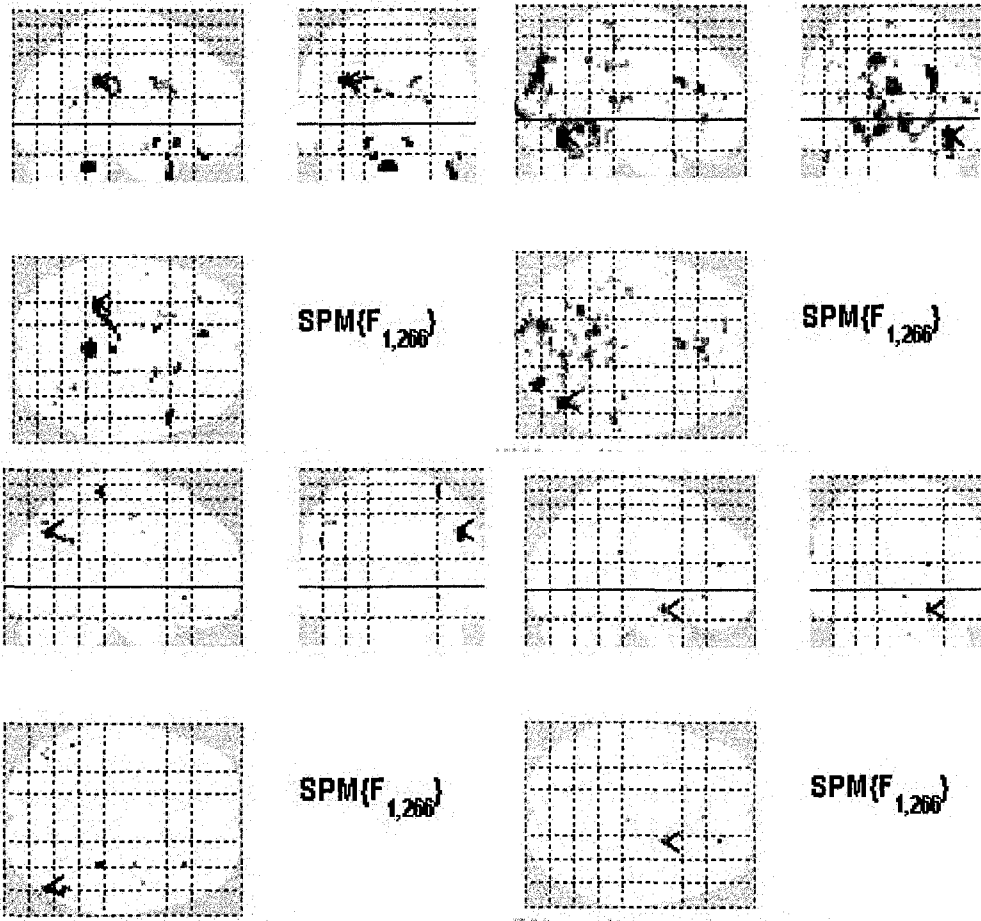


Figure F-1 Fast-Slow Individual Results a) BD42 b) BJ1 c) BJ31 d) BK24

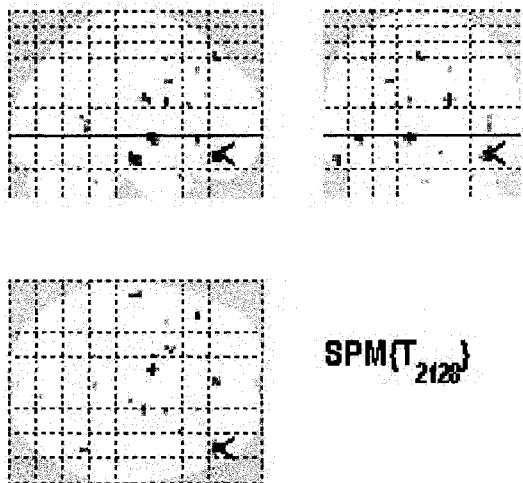


Figure F-2 Fast-Slow Fixed Effects Analysis Group Map (N=8)

## **APPENDIX E ANALYSIS of FLASHING CHECKERBOARD**

The flashing checkerboard was a paradigm run at the end of scans as a quality check on the subjects. The design is block with all blocks 24s. A blue-and-yellow reversing diagonal checkerboard flickering at 8Hz was contrasted with a fixation cross. There were 4 blocks of each condition, beginning with the checkerboard.

While subjects were viewing the flashing checkerboard, they also pressed the left and right buttons alternately, at speeds that varied from individual to individual. A few subjects instead were instructed to press just the right button repeatedly during the first checkerboard, followed by only the left, then right, then left.

The paradigm was simple enough that it could be entered into the Siemens console sequence for functional-activation correlation-analysis display immediately after the completion of the sequence. Results were reasonable, varying with the amount of motion of each individual. Better results were of course obtained from the motion-corrected analysis but the immediate results helped to confirm that results could be expected.

Additionally, the analysis of the paradigm allowed comparison with the individual analysis results from the block and event-related paradigms since some of the areas activated – visual and motor – should be the same as in those other paradigms. In practice, only a few subjects showed a very close correspondence, though every one that showed activations in motor areas had them in similar areas between the block design and flashing checkerboard paradigms.

This Appendix shows results of analysis of the flashing checkerboard group results. Figures E-1 a) to d) show group RFX results. Keep in mind that CH and HV2 groups have more members than FR and HV1. This accounts in some part for the apparently greater activations in CH and HV2 groups.

Figure E-2 a) to d) show group differences wherever significant (ones not shown are not significant). These data show an odd pattern in which the greatest differences are between HV1 and HV2, leading to the result that there is no difference between healthy volunteers and people with schizophrenia on the flashing checkerboard task.

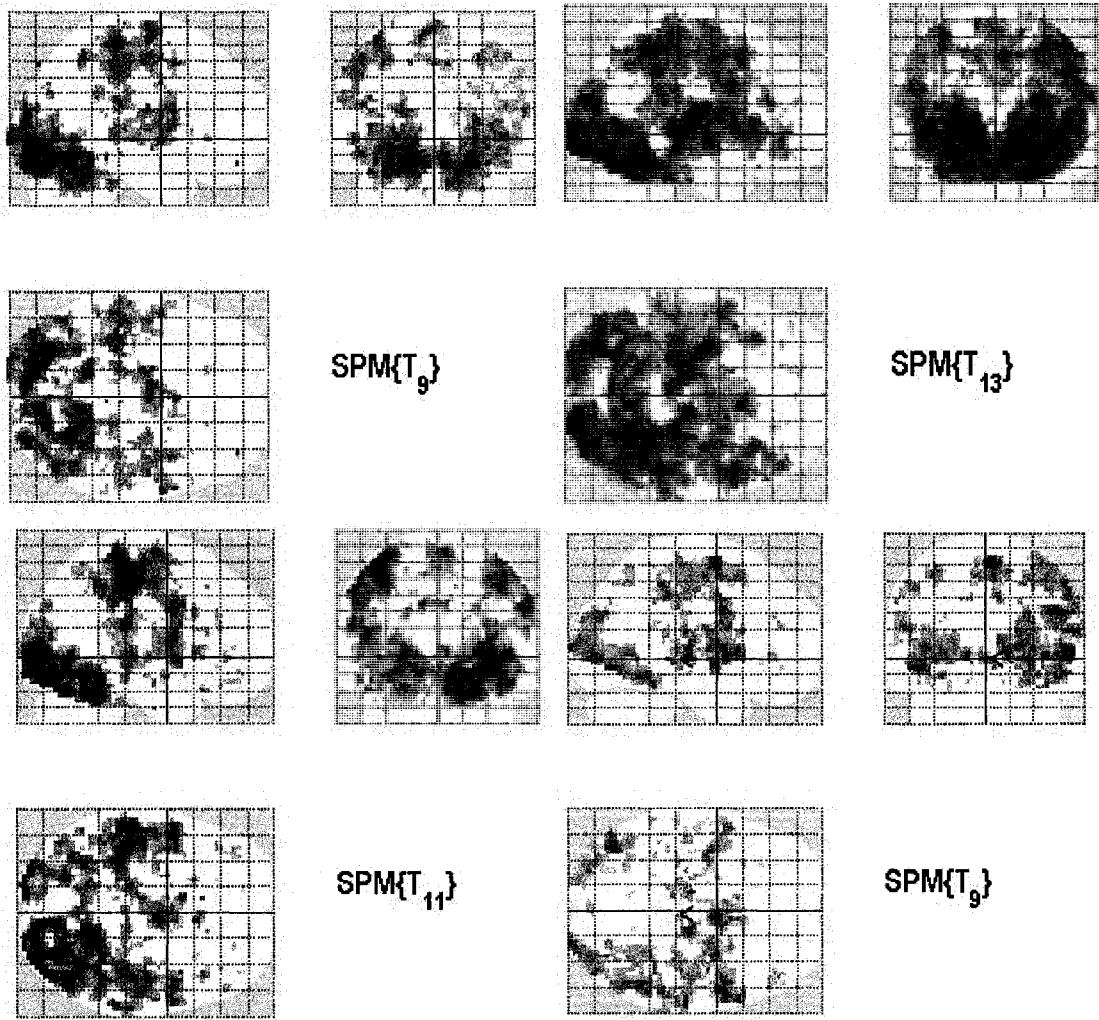
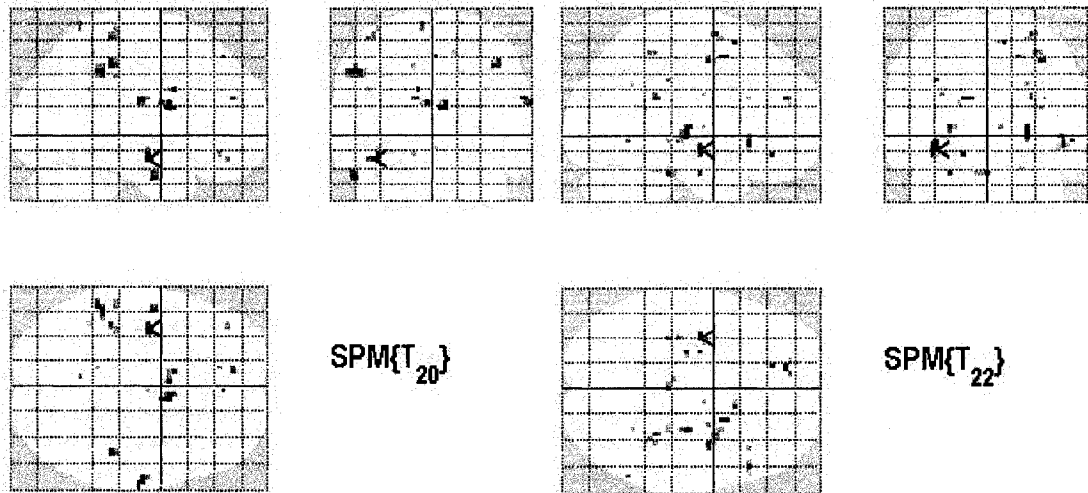


Figure E-1 Group RFX Maps for Flashing Checkerboard a) HV1 b) HV2 c) CH d) FR



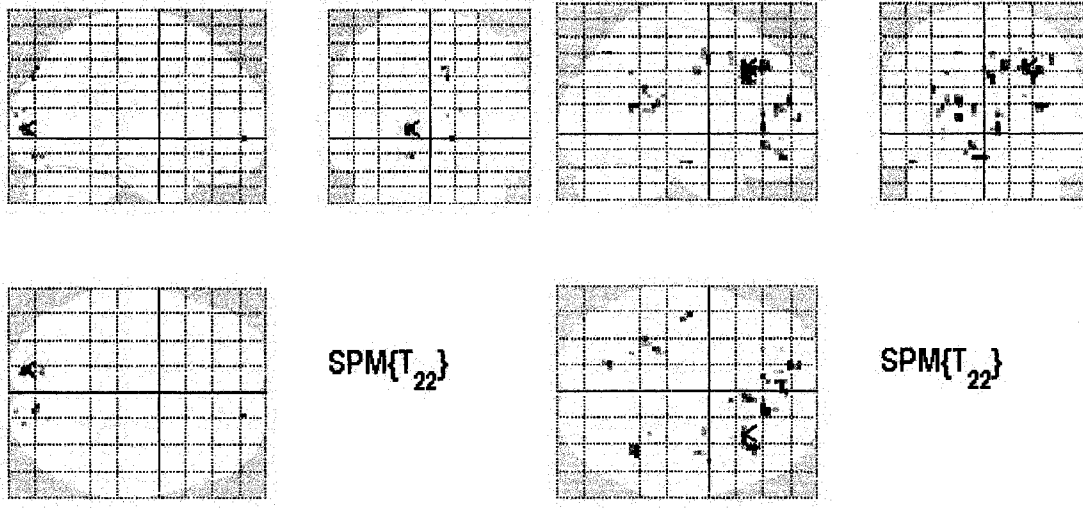


Figure E-2 Group Differences in Flashing Checkerboard a) CH>FR b) HV>FR c) HV1>HV2 d) HV2>HV1